APPLICATION OF NATIVE AND MUTANT THREONINE ALDOLASES TO CHEMICAL SYNTHESIS

By

SARAH FRANZ BEAUDOIN

A DISSERTATION PRESENTED TO THE GRADUATE SCHOOL
OF THE UNIVERSITY OF FLORIDA IN PARTIAL FULFILLMENT
OF THE REQUIREMENTS FOR THE DEGREE OF
DOCTOR OF PHILOSOPHY

UNIVERSITY OF FLORIDA

2017

To my family

ACKNOWLEDGMENTS

First of all, I would like to acknowledge and express my ultimate gratitude to my advisor and mentor Dr. Jon Stewart for this support and guidance over the past four and a half years. It was a pleasure to work with him and his inspiration and compassionate teaching style has been invaluable to me. I would also like to thank Dr. Brent Feske for his leadership and encouragement through my first years of research as an undergraduate and leading up to my decision to attend graduate school. I thank Dr. Matthew Burg for his patience and instruction towards solving the crystal structure of threonine aldolase.

I am very thankful for current and past group members of the Stewart group, in particular, Michael Hanna for working alongside me during the mutagenesis studies as my undergraduate assistant. Dr. Robert Powell III, Dr. Louis Mouterde, Hyunjun Choe, Richard Watkins, Thinh Nguyen, Kevin Fisher, Cristina Iturrey and others have been invaluable coworkers and friends. Their support, combined expertise and friendship through the years have made my time here at the University of Florida not only knowledgeable but also enjoyable.

I am also thankful for my committee members Dr. Steven Bruner, Dr. Nicole Horenstein, Dr. Ronald Castellano and Dr. Yousong Ding for their time, advice and suggestions.

And lastly, I would like to thank my family and friends for their love and support throughout my entire degree. Especially my husband Steven for his love and pronounced encouragement to pursue my dreams.

TABLE OF CONTENTS

page

LIST OF TABLES

Table page

LIST OF FIGURES

Figure page

LIST OF ABBREVIATIONS

^{1}H NMR	Proton nuclear magnetic resonance
A^{500}	Absorbance at 500 nm
acac	Acetylacetonate
AcOH	Acetic acid
Ala	Alanine
Arg	Arginine
Asp	Aspartate
Asn	Asparagine
BINAP	2,2'-Bis(diphenylphosphino)-1,1'-binaphthyl
bipy	Bipyridine
BuOH	Butanol
CoA	Coenzyme A
Cys	Cysteine
d.e.	Diastereomeric excess
D_2O	Deuterium Oxide
DCC	*N*,*N*′-Dicyclohexylcarbodiimide
DHAP	Dihydroxyacetone phosphate
DKR	Dynamic kinetic resolution
DMSO	Dimethyl sulfoxide
DNA	Deoxyribonucleic acid
DOE	Design of experiments
DOPS	Dihydroxyphenylserine
e.e.	Enantiomeric excess
Et_2O	Diethyl ether

Et_3N	Triethylamine
*e*TA	L-Threonine aldolase from *E. coli*
FAA	Trifluoroacetylacetone
GC/MS	Gas chromatographer/mass spectrometer
Glu	Glutamate
Gln	Glutamine
Gly	Glycine
H_2O	Water
Hg	Mercury
Hht	3-Hydroxyhomotyrosine
His	Histidine
Hmp	3-Hydroxy-4-methylproline
HPLC	High pressure liquid chromatography
HRP	Horseradish peroxidase
Ile	Isoleucine
iPr_2EtN	Hunig's base or *N*,*N*-diisopropylethylamine
IPTG	Isopropyl-β-D-thiogalactopuranoside
KDA	Potassium diisopropylamide
L	Liter
LATA	L-*allo*-Threonine aldolase from *A. jandaei*
LB	Luria broth
Leu	Leucine
LpxC	UDP-3-*O*-(*R*-3-hydroxymyristoyl)-*N*-acetylglucosamine deacetylase
L-TA	L-Threonine aldolase
LTAPP	L-Threonine aldolase from P. *putida*

Lys	Lysine
MeBMT	3-Hydroxy-4-methyl-2-(methylamino)-6-octenoic acid
MeOH	Methanol
Met	Methionine
$Mg(ClO_4)_2$	Magnesium perchlorate
MPA	Methoxyphenylacetic acid
MS	Mass spectrometry
MSTFA	*N*-Methyl-*N*-(trimethylsilyl) trifluoroacetamide
NA	Noradrenaline
NMR	Nuclear magnetic resonance
nm	Nanometers
NOH	Neurogenic Orthostatic Hypotension
NTBB	Sodium tetraborate
$O.D._{600}$	Optical density at 600 nm
OPA/NAC	*ortho*-Phthalaldehyde-*N*-acetylcysteine
PCR	Polymerase chain reaction
Pd	Palladium
Phe	Phenylalanine
PLP	Pyridoxl 5'-phospate
ppm	Parts per million
Pro	Proline
Psi	Pounds per square inch
pybox	Pyridine bis(oxazoline)
Ru	Ruthenium
Ser	Serine

SPT	Serine palmitoyltransferase
TA	Threonine aldolase
*t*BuOMe	*tert*-Butyl methyl ether
THF	Tetrahydrofuran
Thr	Threonine
TLC	Thin layer chromatography
Trp	Tryptophan
*t*TA	L-*allo*-Threonine aldolase from *T. maritima*
Tyr	Tyrosine
UDP	Uridine diphosphate
UV-Vis	Ultaviolet-visible spectroscopy
Val	Valine
vvm	Volume of Air Under Standard Conditions per Volume of Liquid per Minute
wcw	Wet cell weight

Abstract of Dissertation Presented to the Graduate School
of the University of Florida in Partial Fulfillment of the
Requirements for the Degree of Doctor of Philosophy

APPLICATION OF NATIVE AND MUTANT THREONINE ALDOLASES TO CHEMICAL SYNTHESIS

By

Sarah Franz Beaudoin

December 2017

Chair: Jon D. Stewart
Major: Chemistry

β-Hydroxy-α-amino acids are an important class of natural products that have found many uses in pharmaceuticals. Although several “chemical” strategies have been described for these products, we chose a biocatalytic approach since it could allow for a one step synthesis of these amino acids. Threonine aldolases (TAs) catalyze carbon-carbon bond formation between glycine and an aldehyde, producing β-hydroxy-α-amino acids. Four L-TAs were cloned and overexpressed in *Escherichia coli* (*Aeromonas jandaei* L-*allo*-TA, *E. coli* L-TA, *Thermotoga maritima* L-*allo*-TA, and *Pseudomonas putida* L-TA). A Design of Experiments strategy was used to identify optimal reaction conditions for each enzyme. These conditions were used to characterize the substrate and stereoselectivity of each TA toward a panel of aldehyde acceptors. In general, the *A. jandaei* L-*allo*-TA performed best, and six representative examples were scaled up 10-fold in order to develop downstream steps for product isolation. The use of glycine oxidase to degrade the residual starting material simplified this process greatly.

We also solved the x-ray crystal structure of L-TA from *P. putida* using molecular replacement. Like the other TAs, *P. putida* L-TA was a homotetramer with the active

site composed of a ‘catalytic dimer’. This structure and others were used to design site directed mutagenesis studies.

Three *A. jandaei* L-*allo*-TA site saturation mutagenesis libraries (His 85, Tyr 89, and His 128) were screened against a variety of aldehyde acceptors to probe for enhanced enzyme activity and improved diastereoselectivity. Histidine 85 was found to be unequivocally essential for enzyme catalysis as any change at this position left the enzyme inactive. On the other hand, a few changes at positions 128 and 89 increased diastereoselectivity for a select group of aldehyde acceptors and in some cases, reversed diastereoselectivity completely. Finally, we showed that wild type *A. jandaei* L-*allo*-TA accepted fluorinated acetones, the first example of a non-aldehyde acceptor for TAs.

CHAPTER 1
β-HYDROXY-α-AMINO ACIDS

Introduction

β-Hydroxy-α-amino acids comprise an important class of natural products that include the natural amino acids threonine and serine as well as valuable precursors to a wide range of antibiotics such as vancomycin,[1] polyoxin A,[2] and myriocin.[3] They are also found in antifungal agents including sphingofungins,[4, 5] rhizobitoxine[6] and pharmaceuticals such as droxidopa[7, 8] and cyclosporine.[9] Droxidopa (L-*threo*-3,4-dihydroxyphenylserine or L-*threo*-DOPS) is the most notable member of this family since it is a prodrug for Parkinson's disease therapy that successfully crosses the blood-brain barrier and is metabolized to L-noradreline, which is responsible for increasing blood pressure and reducing lightheadedness in Parkinson's disease patients.[10] Additionally, Rhizobitoxine is an effective inhibitor of PLP-dependent enzymes that utilize the β-hydroxy-α-amino acid 4-hydroxy-L-threonine as a precursor.[6]

Other β-hydroxy-α-amino acids are useful in the food industry. D-Glucosaminic acid, or 2-amino-2-deoxy-D-gluconic acid, is a natural product from *Aeromonas oxydans* that acts as an artificial sweetener.[11] More recently, D-glucosaminic acid has been found useful as a building block for several glycosidase inhibitors, such as (2*S*,4*S*,5*R*)-4,5,6-trihydroxynorleucine.[12, 13] Figure 1-1 highlights a few examples of the β-hydroxy-α-amino acid motif (pink).

Since the 1980s, significant efforts have been devoted to producing these optically pure β-hydroxy-α-amino acids on large scales using chemical approaches. These include, but are not limited to, chiral glycine enolate,[14] Sharpless dihydroxylation, epoxidation, and aminohydroxylation,[15-17] *aza*-Claisen rearrangements of allylic

acetimidates,[18] addition of imides to aldehydes,[19, 20] organocatalytic asymmetric aldol reactions of α-amino aldehydes,[21] glycine Schiff's base,[22] dynamic kinetic resolution *via* ruthenium catalyzed dehydrogenation of *N*-substituted α-amino-β-keto esters,[23-30] aminohydroxylation of olefins,[31] aziridine ring-opening,[32] ammonium ylides,[33] chiral ammonium salts,[34, 35] and numerous others. This chapter describes a subset of the chemical synthesis approaches described above as well as a few of the pharmaceutical targets that are of key importance. Chapter two details the biocatalytic approach to β-hydroxy-α-amino acids by threonine aldolases.

Organic Synthesis Strategies for Synthesizing β-Hydroxy-α-amino Acids

By Addition of Imides to Aldehydes

In 2002, Willis and coworkers[19] devised a strategy to produce synthetically useful protected aryl variants of β-hydroxy-α-amino acids by a direct addition of an isothiocyanate-substituted ester to a variety of aryl aldehydes using an achiral catalyst. This approach was inspired by the popular chiral glycine enolate strategy, but allowed the use of a catalyst for both enolate formation and addition to the aldehyde. In order for coordination of the enolate's amino-alcohol group to coordinate to a metal catalyst, they used an isothiocyanate-substituted ester. A combination of Lewis acids (metal triflates) and weak amine bases (such as triethylamine) were investigated to find the optimal combination. The best mixture, 10 mol% magnesium perchlorate, 20 mol% triethylamine (Et_3N), and 10 mol% bipyridine (bipy), generated a 94% yield of ethyl isothiocyanatoacetate with benzaldehyde in 24 hours (Figure 1-2). Willis and coworkers investigated other aryl aldehydes using the same catalyst system and found it useful for a variety of aromatic aldehydes, although a 60 : 40 (*syn* : *anti*) mixture of diastereomers was obtained for most products.[19]

Subsequently, Willis *et al.* attempted to improve the catalyst system into a more highly enantioselective variant.[20] They exchanged the bipyridine ligand with an assortment of enantiomerically pure bidentate ligands; however, low enantioselectivities were obtained and they refocused their efforts on other aspects of the system. They used oxazolidinone as the glycine equivalent and reaction conditions for this system were optimized as before. The best conditions were 10 mol% magnesium perchlorate, 20 mol% Hünig's base (*N*,*N*-Diisopropyethylamine or *i*Pr$_2$EtN), and 11 mol% pyridine bis(oxazoline) (pybox). Reactions utilizing these conditions with benzaldehyde as the acceptor resulted in an 86% yield and an 85 : 15 (*syn* : *anti*) mixture of diastereomers (Figure 1-3). Willis and coworkers also tested the enantioselective catalyst system with other aryl aldehydes. Although most of the products retained the high diastereoselectivity (even up to 91 : 9), *ortho*-substituted phenyl rings were not tolerated well and resulted in a 50 : 50 ratio of diastereomers.[20]

One key advantage of this strategy is that all components are commercially available and reaction conditions are simple. Its relevance was demonstrated by Willis' successful synthesis of a protected amino acid with the same substitution pattern as the functionalized tyrosine residue found in vancomycin in a 78% yield and 94% d.e. (Figure 1-4a).

Seidel and coworkers[36] extended the Willis approach by substituting additional imide starting materials and catalysts. The dimethyl analog proved to be best along with 1-(4-nitrophenyl)-3-((1*R*,2*R*)-2-(pyrrolidin-1-yl)cyclohexyl)thiourea as the catalyst. This combination yielded the protected *syn*-amino acid in outstanding yields (>98%) and high selectivity (93 : 7) using benzaldehyde as the electrophile. Further optimization of

these conditions allowed the catalyst loading to be reduced from 20 to 5 mol% and the equivalents of aldehyde from 2 to 1.2. A variety of aldehydes were tested with the new enantioselective catalyst. Most aromatic aldehydes provided the same high yields and stereoselectivities as benzaldehyde; however, aliphatic aldehydes were less reactive and gave slightly lower stereoselectivities.[36] The only disadvantage of the improved catalyst was that it was not commercially available.

Recently, Feng and coworkers[37] sought a catalyst that could achieve these high yields and selectivities with better functional group tolerance. They employed *N*,*N*'-dioxide-metal complexes since they have proven to be useful chiral auxiliaries[38-41] and catalysts in enantioselective transformations.[42-45] In this study, seven different *N*,*N*'-dioxide ligands were coordinated to various metal salts for the aldol condensation between benzaldehyde and oxazolidinone. The optimum catalyst, an *N*,*N*'dioxide-nickel(II) catalyst complex, was subjected to optimization using temperature and solvent studies, followed by an extensive screening of thirty aldehydes under the optimal conditions (Figure 1-5). Most aldehydes gave >90% yield and diastereoselectivities >95%. The few exceptions were the troublesome aliphatic aldehydes identified previously by Li *et al.*[36] Nonetheless, the *N*,*N*'-dioxide-metal catalyst designed by Chen *et al*. provided better results even for these difficult cases. The system developed by Feng and coworkers is currently the best approach in this area, producing relatively high yields (up to 98%) and outstanding diastereoselectivity (up to >99 : 1) for a broad range of substrates.

Aziridine Ring-Opening

Aziridines, highly strained three-membered heterocycles, are extremely susceptible to ring opening reactions. For this reason, they are incredibly useful

intermediates for numerous products.[46-50] The earliest example was reported in 1895, when Gabriel and Stelzner documented the first acid catalyzed isomerization of an aziridine (Figure 1-6).[51] Over the years, chemists have extended the initial findings of Gabriel and Stelzner. Figure 1-7 represents a generalized summary of aziridine ring openings.

Since the discovery of asymmetric aziridine ring-openings, much emphasis has been placed on synthesizing these starting materials with different substituted patterns, including tri-substitutions.[49, 50, 52, 53] Ring-opening of aziridines to yield β-hydroxy-α-amino acids was first demonstrated in 2001 by Wulff and Loncaric in their synthesis of (–)-chloramphenicol, an antibacterial agent.[32] The optimized 4-step synthesis begins with commercially available *p*-nitrobenzaldehyde. The key aziridine ring-opening step is carried out using VAPOL as the catalyst and refluxing 1,2-dichloroethane to give the hydroxyl acetamide as a single diastereomer and an 80% yield. (–)-Chloramphenicol was obtained at >99% enantiomeric excess with a 74% yield by a simple reduction with sodium borohydride. This work is summarized in Figure 1-8.[32]

Recently, groups led by Somfai in Sweden[54] and Maruoka in Japan[53] devised similar strategies for synthesizing β-hydroxy-α-amino acid derivatives by aziridine ring rearrangements to oxazolidines and oxazolidinones, respectively. This idea is reminiscent of the Willis strategy described above, which used oxazolidinone as the glycine equivalent for the addition of imides to aldehydes.[20] Danielsson *et al.* combined a 1,3-dipolar cycloaddition with an aziridine and an aldehyde followed by simple hydrolysis to execute their plan (Figure 1-9). The only downside to this strategy was the

moderate diastereoselectivities, which depended on the starting aldehyde. Most reactions favored the *erythro* isomer with >50% diastereomeric excess.[54]

Hashimoto *et al.* devised an elegant strategy to synthesize α,α-disubstituted β-hydroxy-α-amino acids[55] by a ring rearrangement of trisubstituted aziridines to afford *trans*-oxazolidinones.[53] The rearrangement was mediated by trifilic acid at -40 ^{o}C in only 30 min. Since the reaction conditions for both the asymmetric aziridination and subsequent ring rearrangement were so similar, a one-pot method that yielded the oxazolidinone and provided straightforward starting materials for the β-hydroxy-α-amino acid derivatives.[53, 55] This work is summarized in Figure 1-10.

Chiral Glycine Enolate

The first account of a chiral glycine enolate used for the production of β-hydroxy-α-amino acids was published in 1981 by Mukaiyama.[56] Both the magnesium counter ion required in the second step as well as the strong base that allowed the nucleophilic addition to the aldehyde were optimized. Iodide and potassium diisopropylamide (KDA), respectively, proved best at these roles (Figure 1-11).[56] Mukaiyama and coworkers focused their efforts into using this strategy for the synthesis of other natural products.[57-59]

Shortly after, Evans and Weber designed their chiral glycine enolate using substituents originally developed for aldol condensations.[60, 61] An oxazolidinone was chosen as the chiral auxiliary for stereochemical control and an isothiocyanate as the activated group (Figure 1-12).[14, 62] Their focus, as with many others,[63-65] was to synthesize of the distinctive amino acid (MeBMT) in cyclosporine, an immunosuppressant (Figure 1-13). The previously reported synthesis of MeBMT by Wenger required 24 steps;[9] the Evans strategy reduced it to six steps. This publication

prompted later efforts to use chiral glycine enolates in the synthesis of β-hydroxy-α-amino acids and many other natural products such as α-amino acids[66-68] and chiral dienophiles.[69]

Evans and Weber continued their work and reported the total synthesis of echinocandin D, including two β-hydroxy-α-amino acid derivatives found within the natural product (3-hydroxyhomotyrosine, Hht, and 3-hydroxy-4-methylproline, Hmp) (Figure 1-13). They followed a similar plan as described in Figure 1-12 where each amino acid was synthesized in four steps from an (isothiocyanoacetyl)oxazolidinone. They completed the synthesis with an overall yield of 50%.[70]

Caddick, Parr, and Pritchard enhanced Evans and Weber's work by utilizing an imidizolidinone derivative as the chiral glycine enolate *versus* the standard oxazolidinone. The simple experimental conditions and high optical purity made their method attractive for preparing *syn*-β-hydroxy-α-amino acids.[68, 71] The chiral auxiliary, imidizolidinone, had been used previously by this group in the dynamic kinetic resolution method.[72, 73] Their synthetic approach with chiral glycine enolates is summarized in Figure 1-14. The diastereoselectivity for their synthesis ultimately depended on the R-group of the aldehyde. In the case shown in Figure 1-14, using benzaldehyde as the starting material gave an overall yield of 65% and a diastereomeric ratio of 97 : 3.[68]

All the methods established by Evans and Weber,[60] which were continued by Caddick, Parr, and Pritchard,[68] were very effective for obtaining *syn*-β-hydroxy-α-amino acids. An effective method for the *anti*-product remained elusive. Iwanowicz *et al.* addressed this issue by developing a novel oxazolidine-based chiral glycine equivalent. They varied steric bulk and found that large substituents were required not only at the 2-

and 4-positions of the oxazolidine but also on the carboxylic acid. Figure 1-15 summarizes their work for the synthesis of *anti*-β-hydroxy-α-amino acids.[74]

aza-Claisen Rearrangements of Allylic Acetimidates

The use of metal-catalyzed *aza*-Claisen rearrangements of allylic trichloroacetimidates to synthesize the corresponding trichloroacetamides was first reported by Overman in 1974 using Hg(II) salts.[75] He found that a wide variety of allylic trichloroacetimidates underwent a thermal [3,3]-sigmatropic rearrangement by refluxing *m*-xylene; however, when 0.10 equivalents of mercuric trifluoroacetate or mercuric nitrate were present, the reaction occurred almost instantaneously at room temperature. Stronger Lewis acids such as silver fluoroborate and aluminum chloride etherate failed to catalyze the rearrangement. The Overman group proposed a mechanism for the rearrangement, shown in Figure 1-16.[75-77] Although Overman's mission was to synthesize trichloroacetamide derivatives, it was also important to note that this rearrangement yielded chiral amines.

This new approach to asymmetric amines was extended by the discovery that Pd(II) salts were more effective at catalyzing the [3,3]-sigmatropic rearrangement of allylic esters.[78-80] Overman and Knoll reported that 4 mol% of $PdCl_2$(MeCN) could catalyze the rearrangement of a variety of allylic acetates at room temperature.[80] Both Hg(II) and Pd(II) salts were limited to allylic esters (unsubstituted at the C-2 position); however, Pd(II) was the preferred catalyst because the allylic rearrangements were faster and required lower catalyst loadings.[79]

It was not until the early 2000's that *aza*-Claisen rearrangements were used in the synthesis of β-hydroxy-α-amino acids by the Sutherland group.[81] *E*-allylic trichloroacetimidates were synthesized in six steps using commercially available α-

hydroxy acids. Pd(II) catalyzed the [3,3]-sigmatropic rearrangement with high yields and diastereoselectivities. Their method was applied to five different starting materials to define the scope of the reaction (Figure 1-17).[81] It is important to note that sterically-demanding substituents (*i.e.* R = isopropyl) can reduce some Pd(II) to Pd(0), which catalyzed the undesirable [1,3] rearrangement. This reduction was likely caused by β-elimination, which became competitive due to the slow rearrangement mediated by Pd(II). This effect could be eliminated by adding *p*-benzoquinone.[81, 82] This Pd(0)-catalyzed rearrangement was also observed by Overman, Ikariya and others.[78, 81, 83-85]

The Overman, Sutherland and Jirgensons groups continued their work on *aza*-Claisen rearrangements for several years, searching for better reaction conditions allowed by other catalysts such as Pt(II) and Au(I)[86-89] and solvents such as THF and toluene.[86] In most cases, the original conditions of $PdCl_2(MeCN)_2$ in THF proved superior, although Pt(II) and Au(I) were also effective at catalyzing the *aza*-Claisen rearrangement.

The Sutherland group attempted to maximize yields for their synthesis of the piperdine alkaloid (+)-α-conhydrine and its pyrolidine analogue, which both contain the 1,2-aminoalcohol functional group.[90] They likewise targeted the synthesis of (2*R*,3*S*)-2-amino-3,4-dihydroxybutyric acid using this strategy (Figure 1-18). The rearrangement proceeded with a 68% yield and a 4 : 1 ratio of diastereomers using the Pd(II) catalyst.[91] The *aza*-Claisen rearrangement has also been used in the synthesis of other important natural products including (+)-monanchorin,[92] clavaminol A, C and H,[93] 7-deoxypancratistatin analogues[94] and sphingosine.[95]

In 2003, the Overman group synthesized and tested five chiral palladacyclic catalysts for their ability to catalyze *aza*-Claisen rearrangements of trifluoroacetimidates. They found the asymmetric catalyst di-μ-chlorobis[(η^5-(*S*)-(p*R*)-2-(2′-(4′-isopropyl) oxazolinylcyclopentadienyl,1*C*,3'-*N*))-(η^4-tetraphenylcyclobutadiene)cobalt]dipalladium (COP-Cl) catalyzed the arrangement with high yields and enantioselectivities even for sterically hindered trifluoroacetimidates.[89, 96, 97] The Sutherland group used this catalyst in the synthesis of *syn*-1,2-aminoalcohols and found a diastereomeric ratio of 52 : 1, rather than the *anti*-isomer normally displayed by the Pd(II) catalyst.[98]

Dynamic Kinetic Resolution *via* Ruthenium Catalyzed Dehydrogenation of *N*-substituted α-Amino-β-keto Esters

The use of a dynamic kinetic resolution (DKR) for the synthesis of β-hydroxy-α-amino acids was first published in 1989 by both Noyori [28] and Genêt.[99] Their goal was to synthesize this product with high diastereoselectivities as most previously reported selectivities using kinetic resolution did not exceed 50%.[100] The idea was to racemize the starting material and employ an enantioselective hydrogenation catalyst that only accepted one of the starting material antipodes and also selectively formed only one diastereomer out of the four possible reduction products. Noyori *et al*. previously published a BINAP-Ru catalyst that gave high enantioselectivity at the β-carbon position, but the catalyst afforded a racemic mixture at the α-carbon.[101] By employing other BINAP-Ru catalysts along with sterically hindered functional groups allowed for selectivity between the *syn*- and *anti*-transition states. Genêt *et al.* used a different asymmetric catalyst, CHIRAPHOS-Ru, in the synthesis of L- and D-threonine (>99% d.e.).[29] Subsequently, the Genêt group synthesized a wide range of chiral Ru(II)-catalysts and investigated their utility in DKR of additional starting materials that

contained other functional groups such as α-chloro- or α-methyl-β-hydroxy moieties.[102-106] The general method is illustrated in Figure 1-19.

Since the initial publications by Noyori and Genêt, many other groups have devised different asymmetric Ru-catalysts for a variety of starting materials, including, but not limited to, *N*-substituted α-amino-β-keto esters (examples are summarized in reviews on DKR[105-110]). DKR has been used over the years in the synthesis of β-hydroxy-α-amino intermediates to many important compounds, including vancomycin,[111] statin and its analogues,[112] biphenomycin A,[113] (–)-balanol (a protein kinase C inhibitor),[114] carbapenems, [115] (2*S*,3*R*)-3-hydroxylysine,[116] the Parkinson's disease therapy drug, droxidopa,[117] gymnangiamide,[118] and many others. Two of these examples are summarized in Figure 1-20. The synthesis by DKR of one of the two β-hydroxy-α-amino acids in vancomycin was described by Genêt and coworkers in 1996.[111] Vancomycin contains both the (2*S*,3*R*) and (2*R*,3*R*) *p*-chloro-3-hydroxytyrosines linked with a central *p*-hydroxyphenylglycine (Figure 1-21). The DKR method was used for the key step in the synthesis of the *syn*-amino acid and involved an asymmetric Ru-catalyst, $RuBr_2$[(*R*)-MeOBIPHEP], which resulted in both high yields (>99%) and diastereoselectivities (>95%) (Figure 1-20a).[111] Genêt's group also devised a DKR strategy towards the amino acid precursor to (–)-balanol using the same catalyst (Figure 1-20b and Figure 1-22).

Over the course of a decade, much effort was devoted to synthesizing and screening a collection of asymmetric Ru-catalysts (most involving (*R*)-BINAP or (*R*)-MeOBIPHEP as the chiral ligand) for the DKR of numerous starting materials. In 2001, Mohar *et al.* sought to enhance the catalyst system by employing electron-withdrawing

fluorosulfonyl groups on the diamine ligand.[119] The more important challenge was to find a better catalyst for *anti*-product formation, as at the time, only a few had been reported.[105, 108] In 2004, the Genêt group disclosed a Ru-mediated hydrogenation with high *anti*-diastereoselectivity (>90%) for most starting materials using Ru(II)-catalysts with the SYNPHOS® ligand (Figure 1-23).[120, 121] This significantly improved the toolbox for DKR and allowed it to be used in the synthesis of precursors such as (+)-lactacystin[120] (Figure 1-23), symbioramide, sulfobacin A[122] and others.

In 2008, Makino *et al.* recognized that the *anti*-isomer of these products can also be formed by using [$RuCl_2$((*S*)–BINAP)] as the asymmetric catalyst.[123] They predicted that when the amine is unprotected, the reaction proceeds by a five-membered, cyclic transition state involving chelation between the amine and the keto-enol functional group formed by tautomerization. This yields the *anti*-product[123] (Figure 1-24a). The original hydrogenation reaction contains a protected amino group and involves a six-membered, cyclic transition state formed by chelation between the two carbonyl groups of the starting material. This rearrangement yields the *syn*-product[124] (Figure 1-24b).

Potential Targets

Droxidopa – A Parkinson's Disease Therapy

Dihydroxyphenylserine (DOPS) was first reported as a component of a coupling therapy with the tyrosine hydroxylase inhibitor, α-methyltyrosine. The decarboxylation of *threo*- or *erythro*-DOPS by DOPA decarboxylase in mammalian cells produces noradrenaline (NA). α-Methyltyrosine inhibits tyrosine hydroxylase in the brain and this blocks the synthesis of both NA and dopamine without affecting serotonin levels.[125] The coupling therapy allowed dopamine to be selectively targeted while NA was maintained at normal levels (Figure 1-25).[126, 127] By administering racemic *erythro*-DOPS to mice

that were previously depleted of NA, a buildup of the unnatural (*S*)-NA was found without the natural (*R*)-isomer.[128] Alternatively, L-*threo*-DOPS was decarboxylated to the natural form of NA in the brain and hearts of rats, while the D-*threo*-isomer was recalcitrant to decarboxylation. On the other hand, in the presence of D-*threo*-DOPS or *erythro*-DOPS, decarboxylase activity was inhibited by half.[129-131] NA is a molecule that produces analgesia by inhibiting the dorsal horn neurons that respond to noxious inputs.[132] NA alone cannot pass the blood-brain barrier; for this reason, L-*threo*-DOPS was clinically introduced as a precursor to noradrenaline by the direct conversion of L-*threo*-DOPS to L-NA *in vivo* by an aromatic L-amino acid decarboxylase because of its ability to cross the blood-brain barrier.[133]

L-*threo*-DOPS has been investigated for its ability to treat neurogenic orthostatic hypotension (NOH) in patients with disorders such as Parkinson's disease, familial amyloidotic polyneuropathy, pure autonomic failure and other pathologies.[134-141] Patients that suffer from NOH-related diseases are unable to maintain healthy blood pressure while in the standing position. In a study presented by Carvalho *et al.*, bedridden patients suffering from type I familial amyloidotic polyneuropathy who were administered L-*threo*-DOPS saw improvement after 3 – 5 days in their ability to walk freely and this effect continued throughout the six-month treatment.[135] In a double-blind, placebo-controlled crossover study administered by Kaufmann *et al.*, patients suffering from NOH experienced increased blood pressure and less lightheadedness while standing.[10]

Recently, droxidopa was examined for its ability to treat other diseases such as Alzheimer's disease.[142, 143] After one month of treatment, transgenic mice exhibited

improved learning in the Morris water maze test. Enhancement in learning was revealed to have a direct correlation between the NA levels in the brain and latency times in the water maze test.[142, 144] There has been additional interest in testing droxidopa's ability to treat a variety of other diseases or injuries including hemodynamic and renal alterations of liver cirrhosis in portal hypertensive rats,[145, 146] spinal cord injury,[147] down syndrome,[143] and more. In most studies, droxidopa had no significant side effects and was tolerated by most patients even after a 12-month study.[137, 140, 141, 148]

In 2007, Sudalai and coworkers developed a chemical synthesis of L-*threo*-DOPS by sodium periodate-mediated asymmetric bromohydroxylation with high regio- and diastereoselectivity.[149] This methodology was based on the chiral glycine enolate discussed previously and eliminated the need for heavy metals and molecular bromine/*N*-halo-succinimides as the halogen sources used by Herbert *et al.* and Hegedüs *et al.* in 2001 and 1975, respectively.[150, 151] The Sudalai preparation of droxidopa used carboxamide as the starting material and yielded L-*threo*-DOPS at an overall yield of 51% and >99% diastereomeric excess (Figure 1-26a).

Very recently, Guan *et al.* proposed a route towards the chemical synthesis of L-*threo*-DOPS by initially using a rhodium-catalyzed asymmetric hydrogenation of an enamide, which resulted in high yields and enantioselectivities (Figure 1-26b). They used this method on a variety of relating starting materials and achieved high *syn*-selectivity with all substituents (>95%).[152] In addition, Wang and coworkers used the DKR method first established by Noyori and Genêt in 1989[28, 99] and a Ru(II) catalyst to prepare droxidopa in gram quantities. Using different Ru(II) catalyst/base systems, they

developed an efficient way to make the *syn*-diastereomer (>99%) of droxidopa (Figure 1-26c).[117]

Baik *et al.* synthesized L-*threo*-DOPS by utilizing the low-specificity L-threonine aldolase from *S. coelicolor* A3(2) in one enzymatic step from simple starting materials (Figure 1-27).[8] To obtain a more thermostable biocatalyst, error-prone PCR was employed. One mutant (H177Y) retained 59% activity after heat treatment at 60 ºC, compared to wild type's 11%. Kinetic studies revealed that this mutation improved thermostability of the enzyme without affecting its catalytic ability to synthesize L-*threo*-DOPS.[8] Since the d.e. of the wild type enzyme was only 14%, Gwon *et al.* preformed additional rounds of error-prone PCR to improve diastereoselectivity, yielding six mutants. The best mutant (A48T) increased the d.e. by 3.3-fold. Unfortunately, even this improvement represented only a 43% d.e., still too low for a useful L-*threo*-DOPS synthetic process. They therefore combined several mutations using site directed mutagenesis to create three double variants. All double mutants retained L-*threo*-DOPS synthesis activity and also showed dramatically increased d.e. values compared to the wild type enzyme. The best double mutant (Y34C/A28T) was used to synthesize L-*threo*-DOPS in a batch process, yielding 3.7 mg/mL. Although mutagenesis was successful at improving the aldol condensation diastereoselectivity, more development would be required before this biocatalytic method could be employed on a large scale.

LPC-058 – A Potent Gram-Negative Bacteria Inhibitor

Zhou, Toone, and coworkers recently discovered a difluoromethyl-*allo*-threonyl hydroxamate, LPC-058, that displayed broad-spectrum antibiotic activity toward Gram-negative bacteria. Steady state kinetic studies revealed that LPC-058 exhibited up to a 44-fold greater potency over other inhibitors of the same class for a wide variety of

Gram-negative pathogens.[153, 154] LPC-058 inhibits UDP-3-O-(*R*-3-hydroxymyristoyl)-N-acetylglucosamine deacetylase (LpxC), which catalyzes the first irreversible step in lipid A biosynthesis. Lipid A is the outermost monolayer of the outer membrane of Gram-negative bacteria and is comprised of lipopolysaccharides. These are essential to protect against antibiotics and detergents.[155, 156] Inhibitors that target LpxC bind competitively with the natural substrate (Figure 1-28). The long acyl chain of the substrate (and the extended aryl network of the inhibitor) is encapsulated by hydrophobic interactions made from a unique 'β-α-α-β sandwich' of the enzyme.[156]

The initial, 10-step synthesis of LPC-058 was reported by Zhou, Toone and coworkers. This route began from a difluoro-threonine methyl ester and a diacetylene carboxylic acid. These were later coupled to yield the final product (Figure 1-29).[153] The same authors continued their work by optimizing reaction conditions. On a large scale, their initial approach was expensive due to the chiral sulfoxide employed to synthesize the difluoro-threonine methyl ester starting material. It also required tedious chromatographic separation of the diastereomers. They improved the synthesis of both starting materials and also shortened the route by two steps (Figure 1-30).[153, 157]

Rhizobitoxine – A PLP-Dependent Enzyme Inhibitor

Rhizobitoxine was first discovered in the 1960s by Owens *et al.* as a phytotoxin that inhibited greening of new leaf tissue and was produced by certain strains of soy beans such as *Rhizvobium japonticum*.[158, 159] Shortly after its discovery, it was also found to inhibit many other pathways such as a PLP-dependent enzyme in the methionine biosynthesis by *Salmonella typhimurium*, β-cystathionase,[160, 161] and ethylene biosynthesis in sorghum seedlings by hindering the conversion of methionine

to ethylene.[159] Interest in the absolute configuration[162] and total synthesis[163] of this amino acid peaked when its potential as a herbicide was investigated.[164]

During the course of two decades, the effects of rhizobitoxine was investigated in many different plants, such as pears and avocado.[165, 166] Although a total synthesis was established, Mitchell *et al.* discovered that rhizobitoxine along with L-*threo*-hydroxythreonine (a biosynthetic intermediate for this phytotoxin) could be isolated from *Pseudomonas andropogonis.*[167, 168] Shortly after, they established a proposed biosynthetic pathway by using ^{14}C- and ^{13}C-labeled materials. In this pathway, ^{14}C-aspartate and ^{14}C-homoserine were tested by feeding experiments and both of these precursors led to incorporation of the ^{14}C-label into rhizobitoxine. It was suggested that hydroxythreonine was the common product of both (Figure 1-31). Although the route from hydroxythreonine to rhizobitoxine is not known, it has been hypothesized that serinol, which is found to accumulate in soy bean nodules, could directly couple to hydroxythreonine to yield 3-hydroxydihydrorhizobitoxine and upon dehydration, would result in rhizobitoxine. Although 3-hydroxydihydrorhizobitoxine has not been found in cell extracts, it may be present in low quantities or it may dehydrate immediately to its final form without being released from the cell.[6, 169, 170]

Over the past two decades, research on rhizobitoxine has slowed, mainly focusing on its biosynthesis. Some efforts were made to find a positive role for rhizobitoxine. Duodu *et al.* found that some plant species, like *Vigna radiata* (mungbean), are susceptible to high levels of ethylene. The use of *B. elkanii* rhizobitoxine mutant strains was found to jump start aborted nodules at all stages of development.[171]

Sphingofungins – Antifungal Agents

The search for new and safe antifungal medications increased greatly in the early 1980s when there was a rise in patients suffering from AIDS-related fungal infections.[172] A new family of antifungal agents, fumifungin, were first discovered in 1987 from *A. Fumigatus* Fresenius 1863. This led to the discovery of a similar class of antifungal agents, sphingofungins,[173] which were isolated from a different strain of *A. Fumigatus* (ATCC 20857) (sphingofungins A – D) and *P. Variotii* (ATCC 74079) (sphingofungins E and F) by a Merck group in 1992.[174-176] These natural products were identified for their antibiotic effects and by their ability to inhibit serine palmitoyltransferase (SPT).[177] Sphingofungins A, B, C, and D were the first to be investigated (Figure 1-32). Sphingofungins A – C and E – F were found to be potent antifungal agents against *C. neoformans* and showed selective activity towards *Candida* species and others. Sphingofungin D was notably less potent than its counterparts.[176, 177]

Since their discovery in 1992, there has been much effort in the total synthesis of sphingofungins.[5] The first 10-step synthesis was published in 1994 by Mori, who used *N*-acetyl D-mannosamine, 1-heptyne, and (*R*)-epoxyoctane as the starting materials.[178, 179] Shortly thereafter, Kobayashi *et al.* developed a 7-step synthetic route utilizing simple, achiral compounds produced by catalytic asymmetric aldol reactions and chiral heterocycles as key intermediates.[180, 181] The most prominent and widely used total synthesis was established by Trost *et al.* in 2001 by asymmetric allylic alkylation of a *gem*-diacetate palladium catalyst as the key step and methyl-substituted azlactone as starting materials.[182, 183] These total syntheses are summarized in Figure 1-33.

Sphingofungins act as antifungal agents against a variety of fungal species by inhibiting SPT, an enzyme essential in the biosynthesis of sphingolipids.[176, 177] This

PLP-dependent enzyme catalyzes the condensation a fatty acyl-CoA (in this case palmitoyl-CoA) with serine to biosynthesize 3-ketodihydrosphingosine (Figure 1-34). Sphingofungins are known to inhibit this enzyme alone, but not others in the pathway. Zweerink *et al.* discovered that when *S. cerevisiae* was grown in the presence of both the inhibitor and the other downstream intermediates in the pathway, sphingolipids were still successfully biosynthesized.[177]

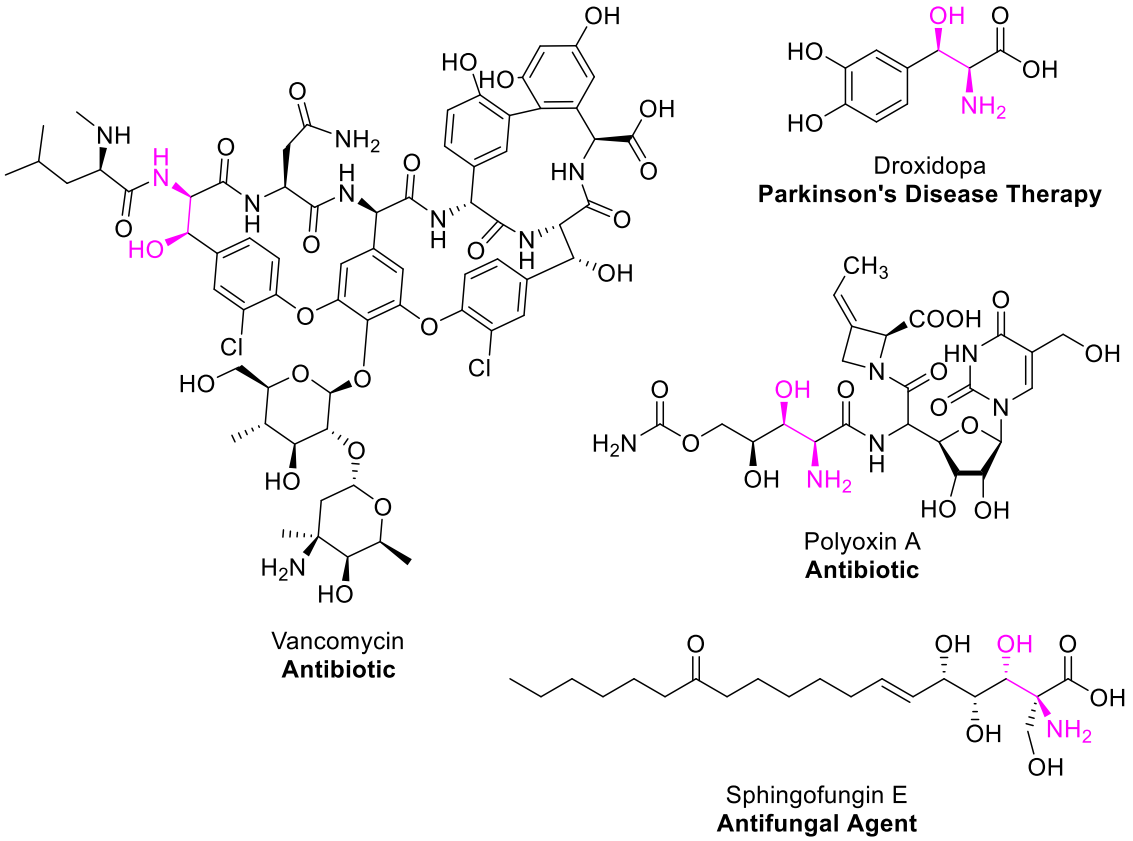

Figure 1-1. Examples of β-hydroxy-α-amino acids as precursors to or stand-alone pharmaceuticals

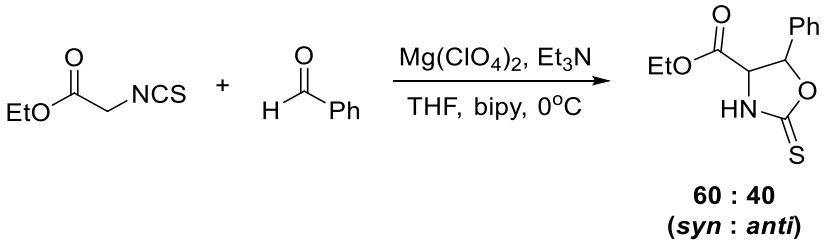

Figure 1-2. Addition of ethyl isothiocyanatoacetate to benzaldehyde

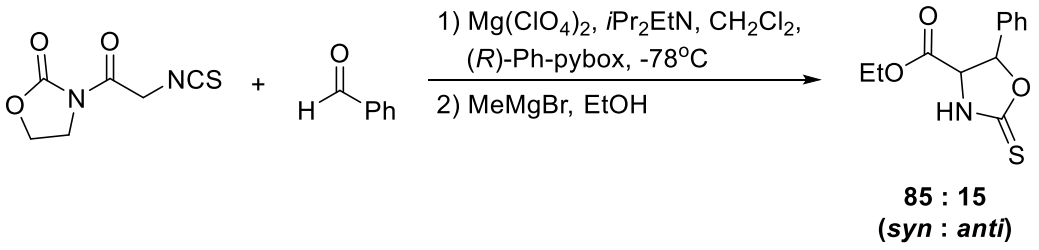

Figure 1-3. Addition of oxazolidinone to benzaldehyde

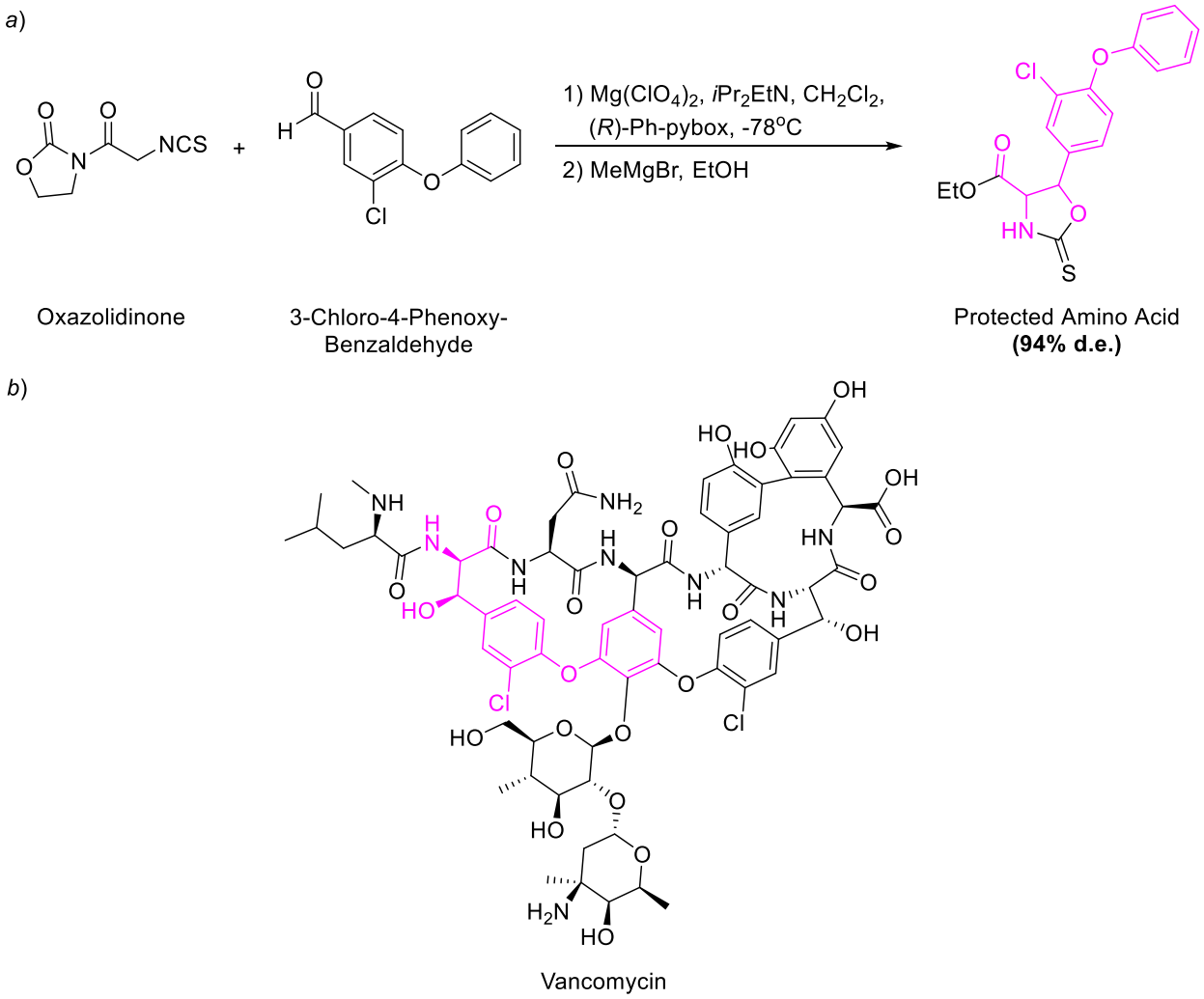

Figure 1-4. Addition of oxazolidinone to 3-chloro-4-phenoxybenzaldehyde to yield (*a*) the protected amino acid, a precursor to (*b*) vancomycin

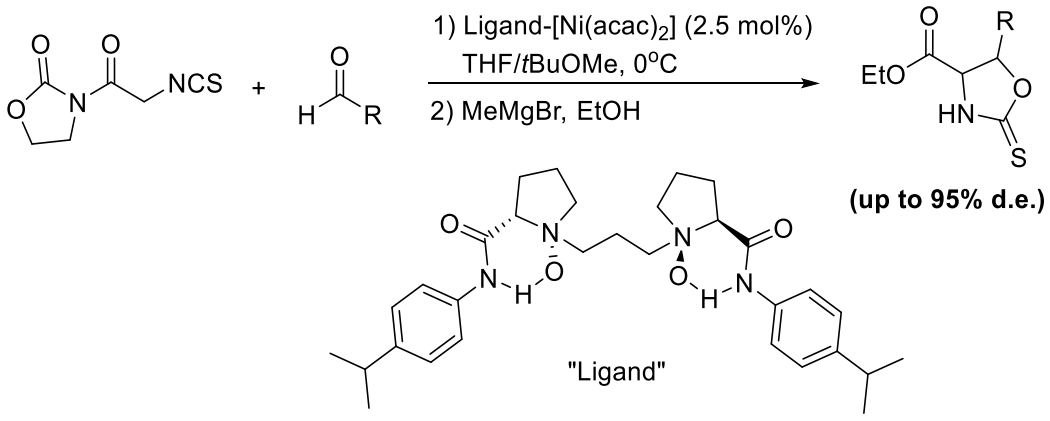

Figure 1-5. Addition of oxazolidinone to an aldehyde by *N*,*N*'-dioxide-nickel(II) catalyst complex

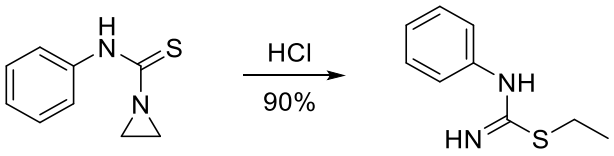

Figure 1-6. First documented example of an acid catalyzed aziridine ring opening

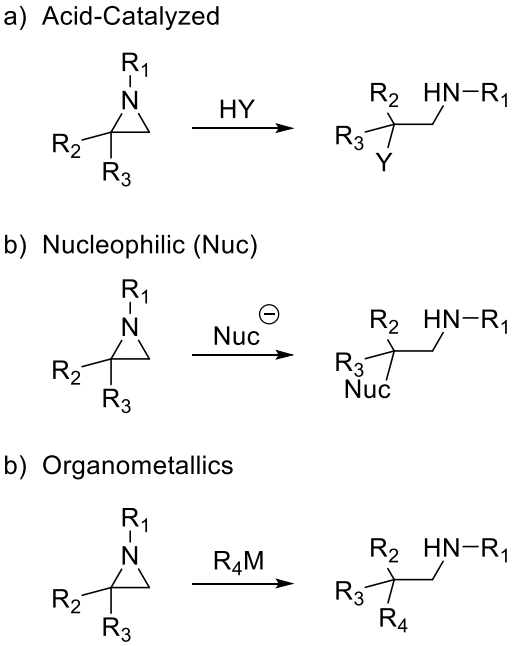

Figure 1-7. Generalized summary of aziridine ring openings

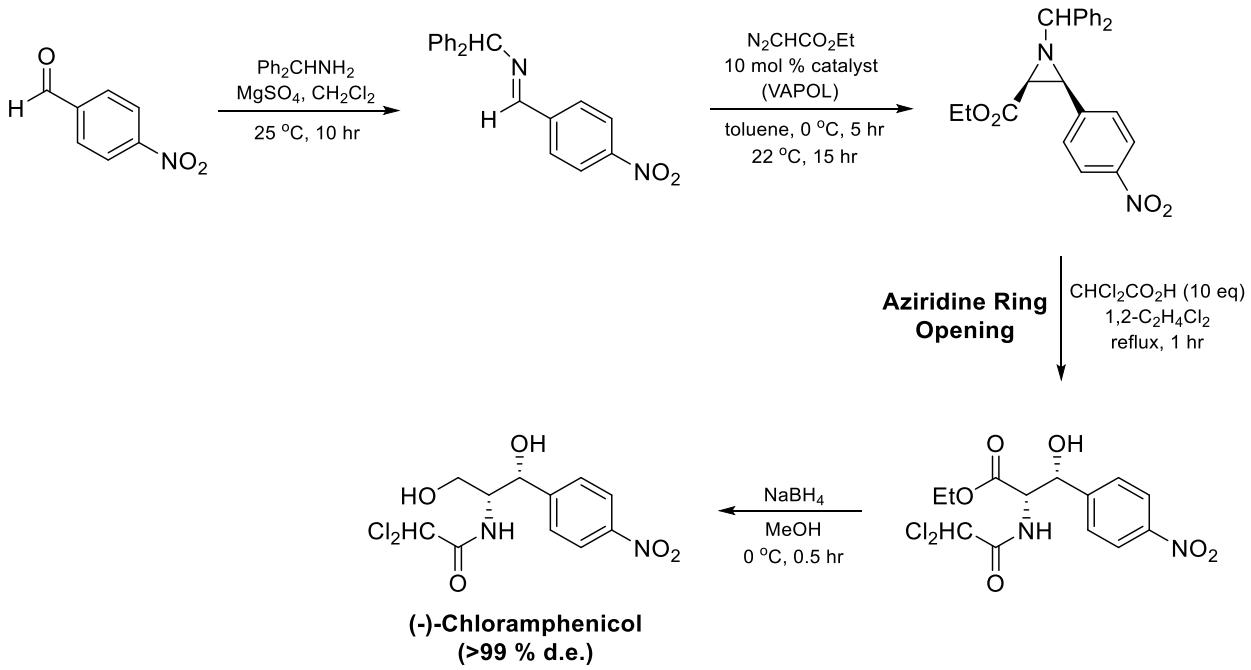

Figure 1-8. Optimized synthesis of (–)-chloramphenicol by aziridine ring-opening strategies

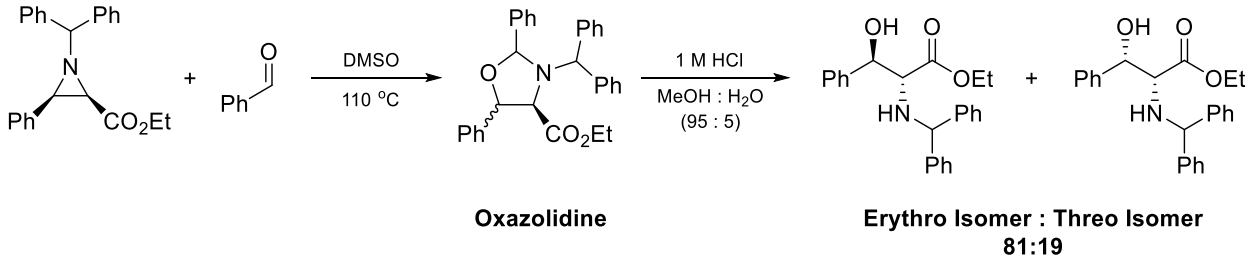

Figure 1-9. Synthesis of β-hydroxy-α-amino acid ethyl esters by a 1,3-dipolar cycloaddition with an aziridine and benzaldehyde

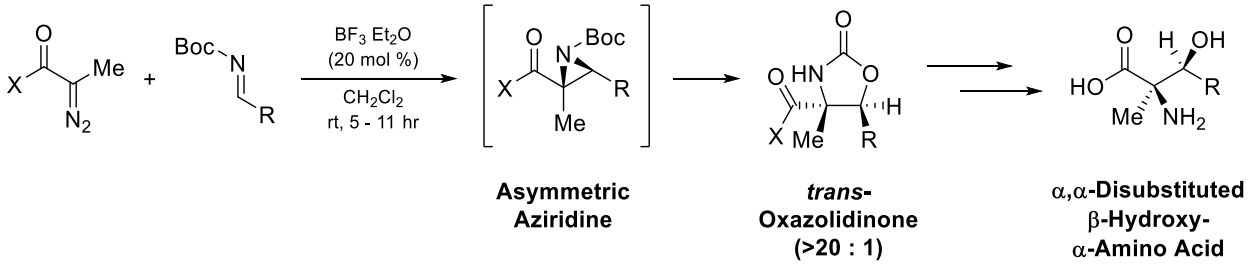

Figure 1-10. One-pot synthesis of *trans*-oxazolidinones by an asymmetric aziridine intermediate

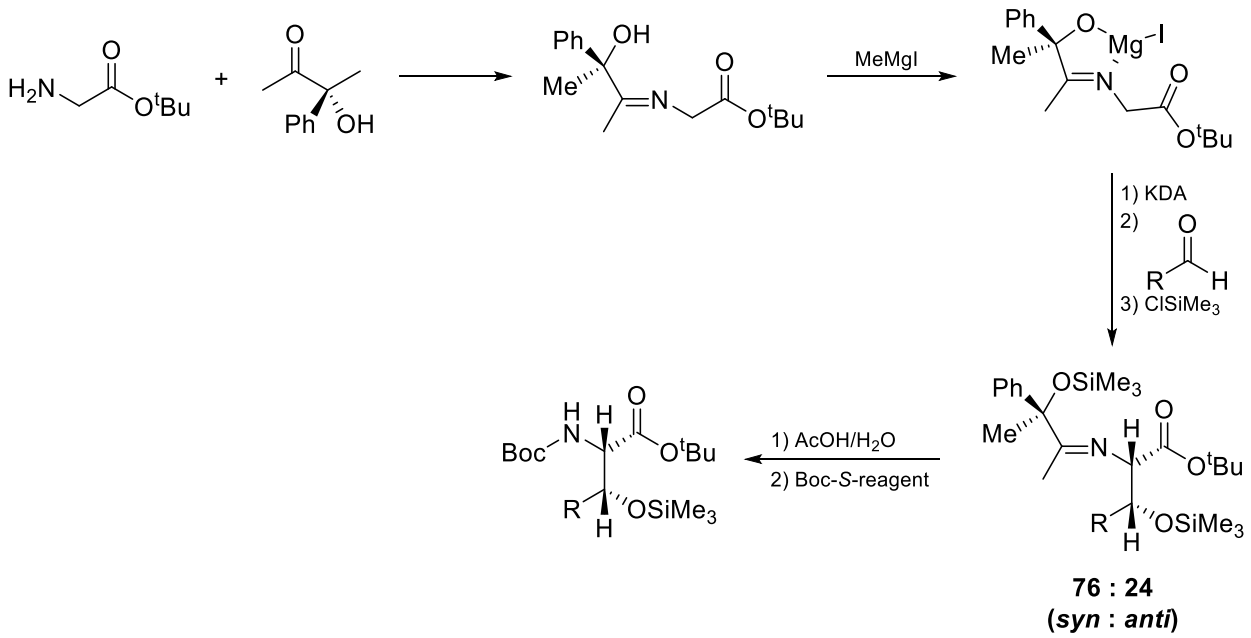

Figure 1-11. First approach of a chiral glycine enolate for β-hydroxy-α-amino acid synthesis

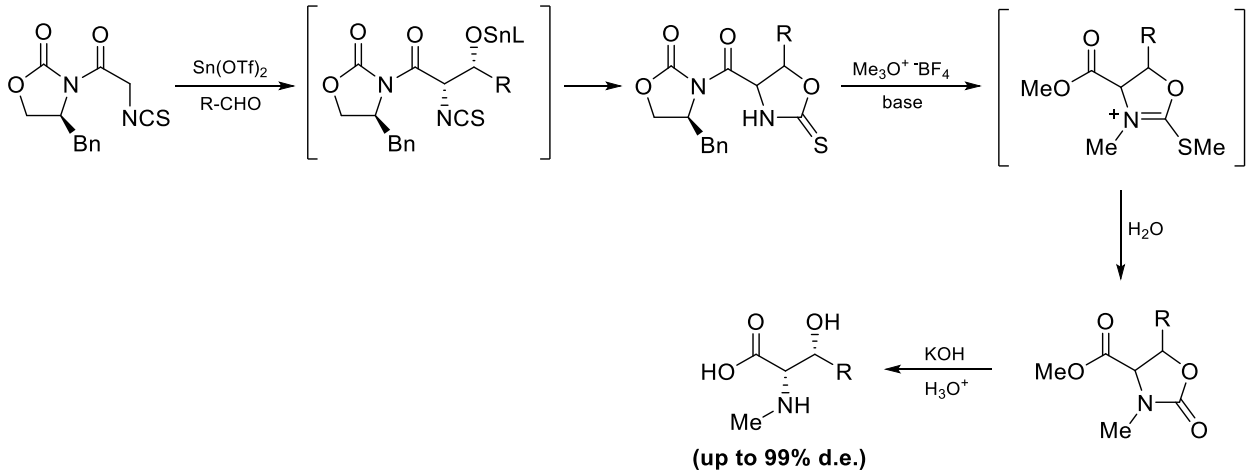

Figure 1-12. Evans and Weber's initial route to *syn*-β-hydroxy-α-amino acids by oxazolidinone chiral glycine enolates

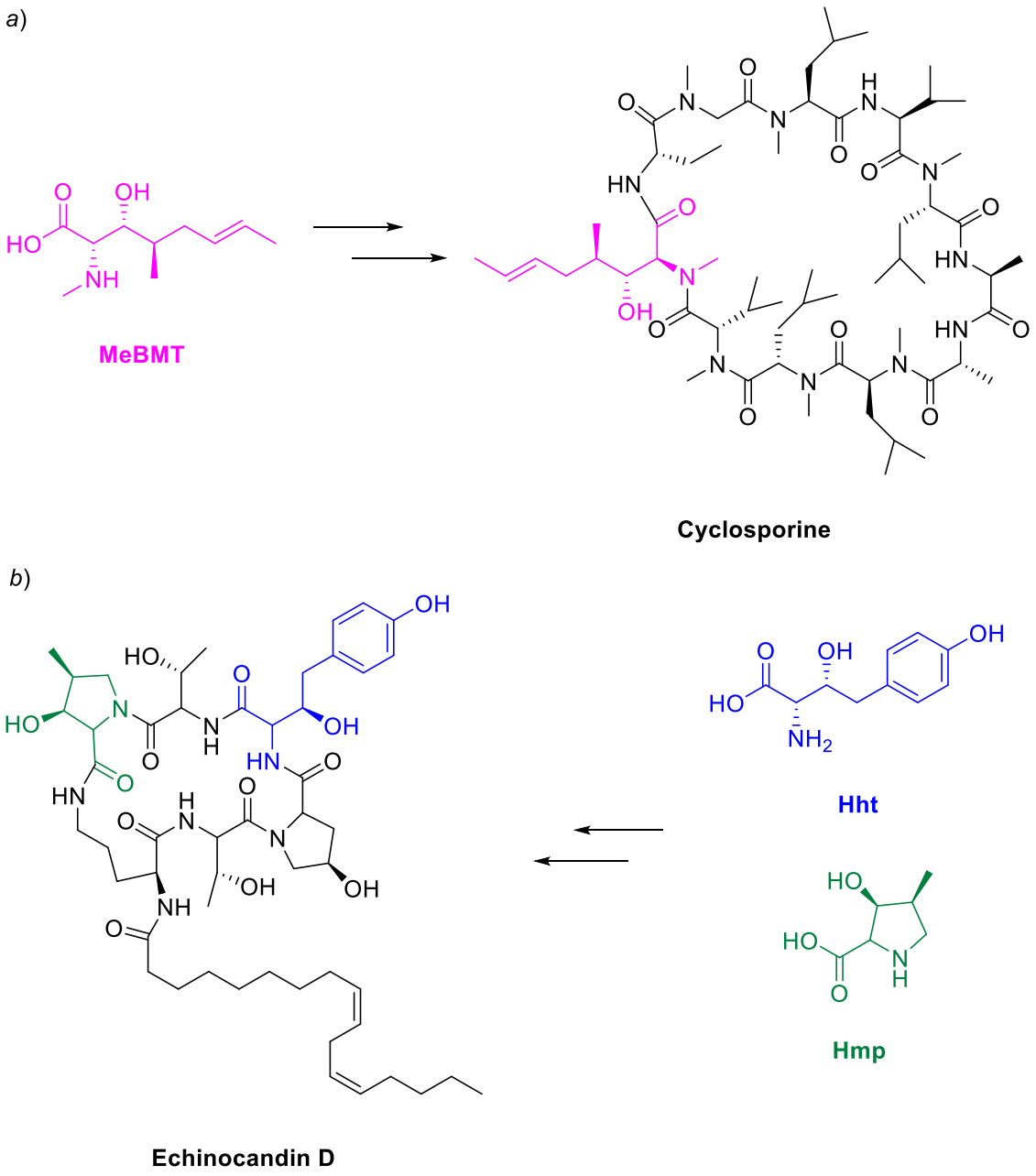

Figure 1-13. The natural products (*a*) cyclosporine and (*b*) echinocandin D

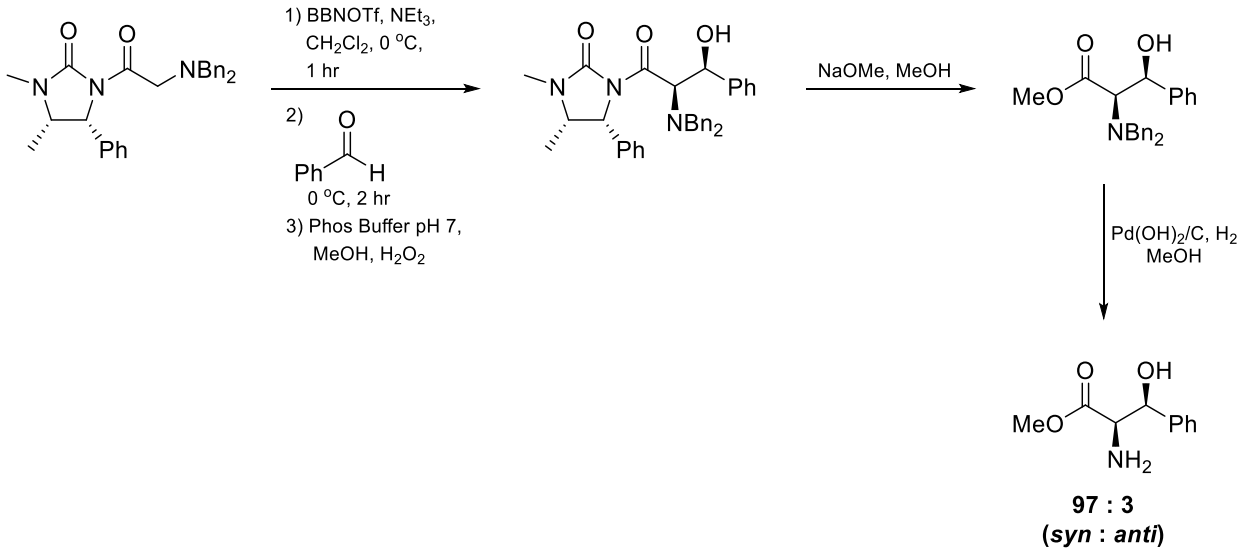

Figure 1-14. Caddick *et al.* route to *syn*-β-hydroxy-α-amino acids by imidizolidinone chiral glycine enolates

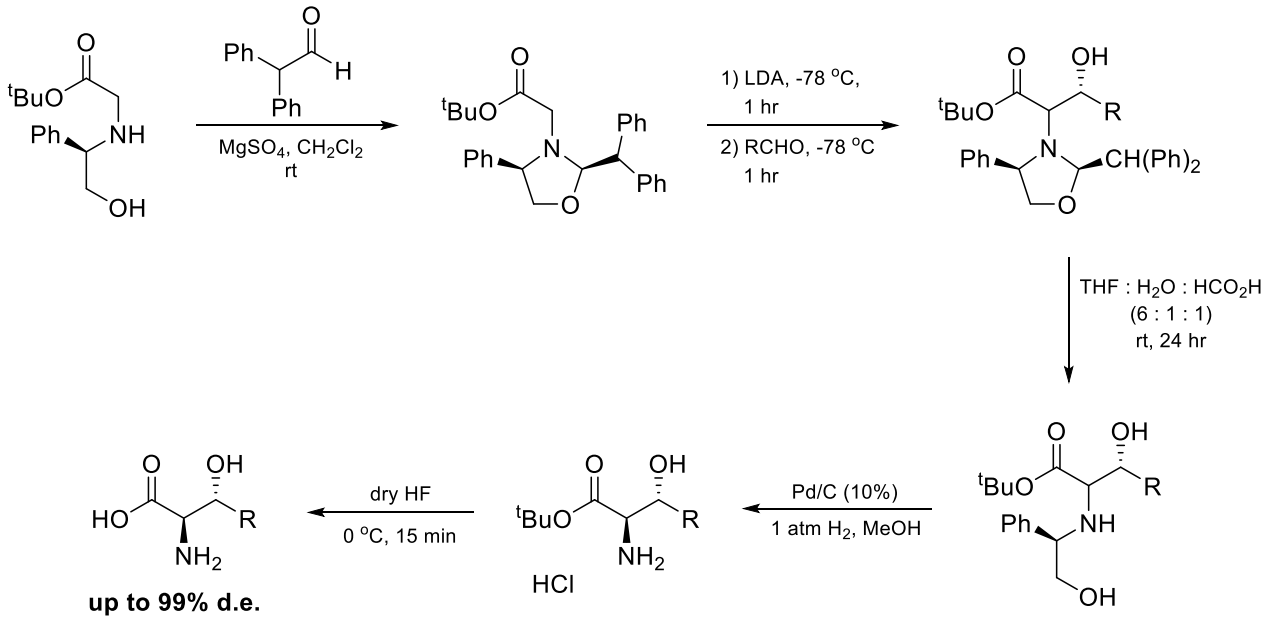

Figure 1-15. Iwanowicz's route to *anti*-β-hydroxy-α-amino acids by chiral glycine enolates

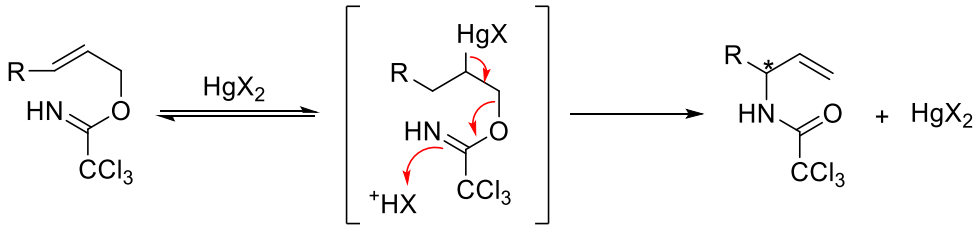

Figure 1-16. First proposed mechanism for metal-catalyzed *aza*-Claisen rearrangements

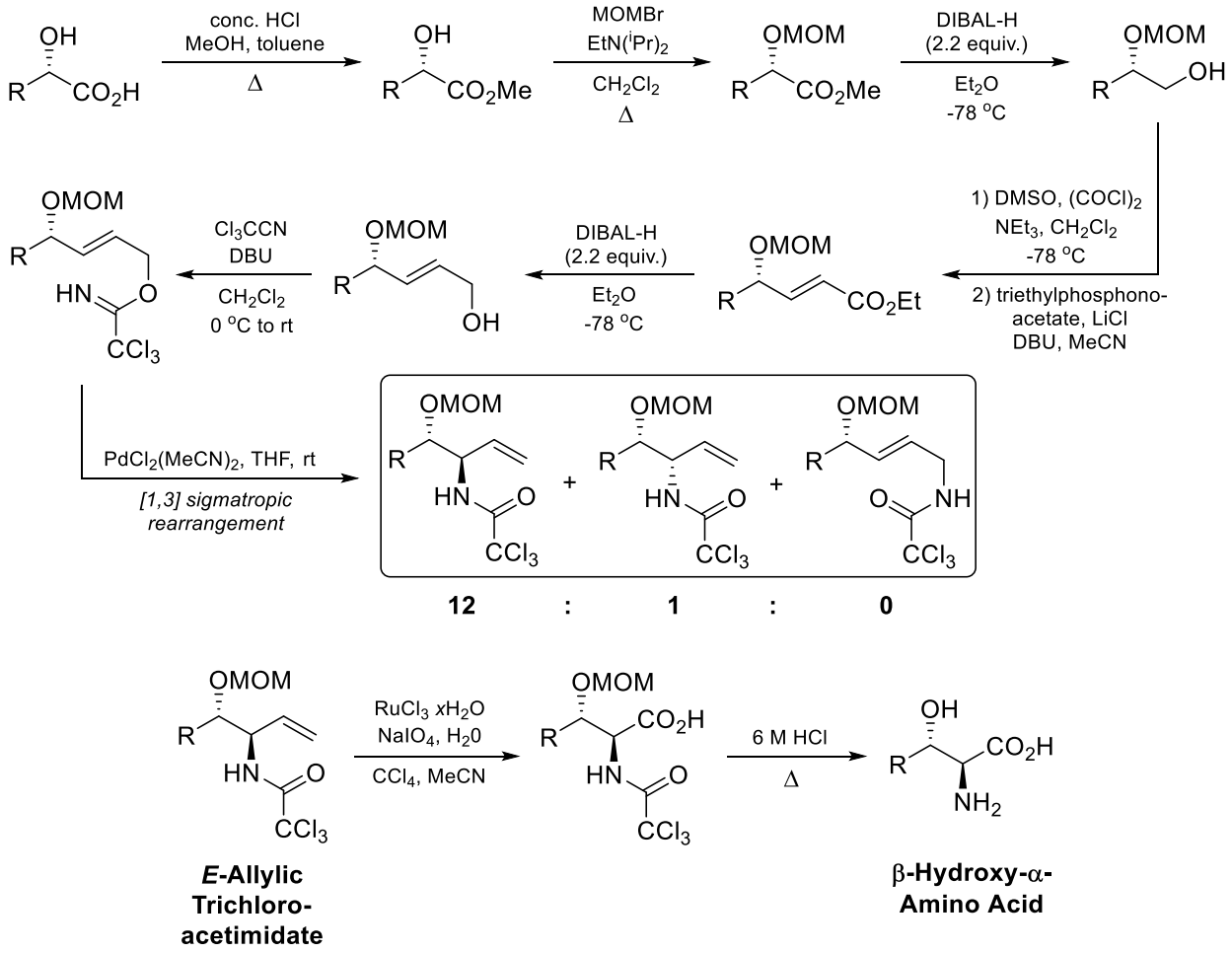

Figure 1-17. Synthesis of β-hydroxy-α-amino acids by means of *aza*-Claisen rearrangement

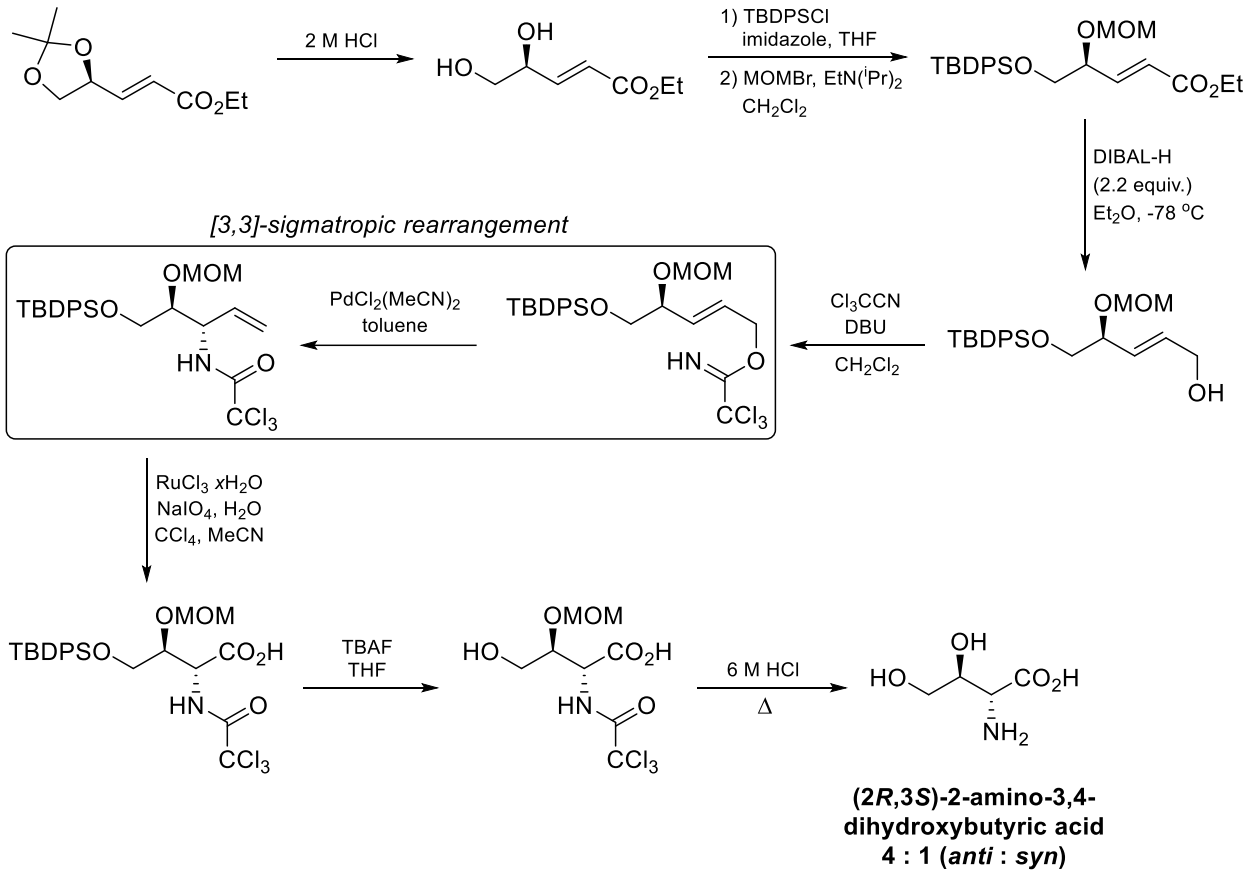

Figure 1-18. The synthesis of (2*R*,3*S*)-2-amino-3,4-dihydroxybutyric acid by *aza*-Claisen rearrangement

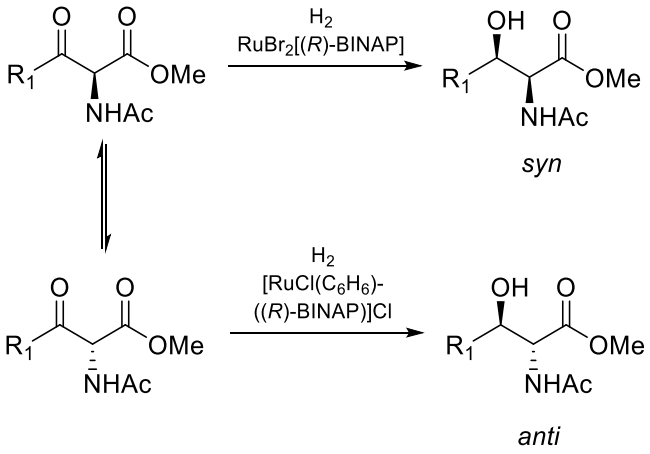

Figure 1-19. Dynamic kinetic resolution

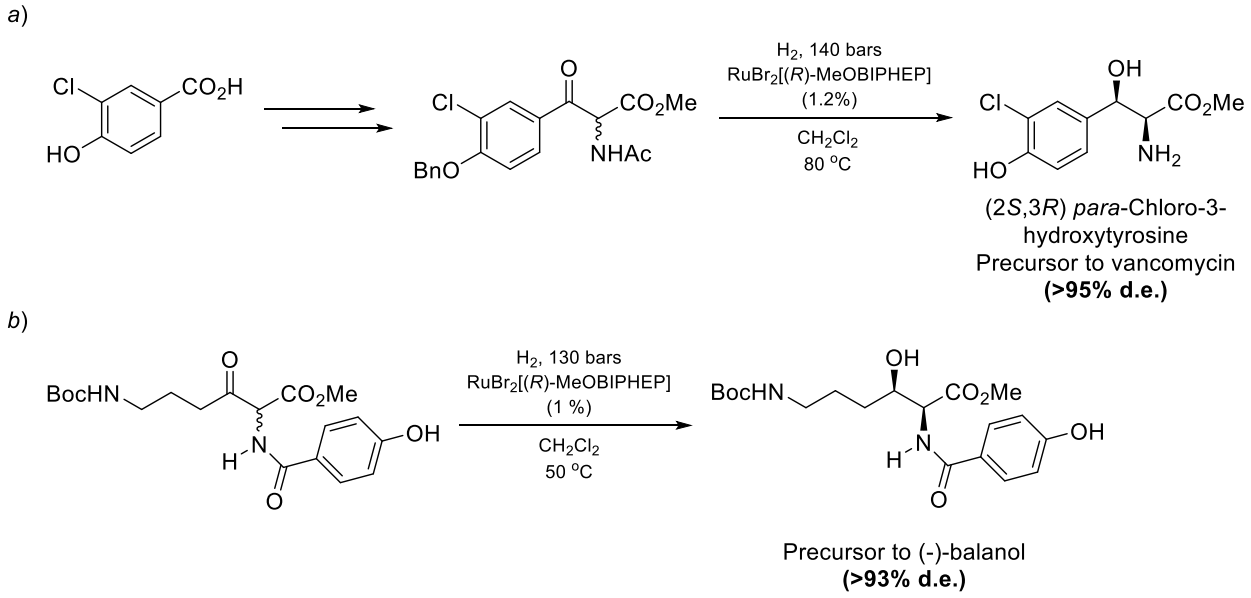

Figure 1-20. Dynamic kinetic resolution towards the synthesis of important intermediates

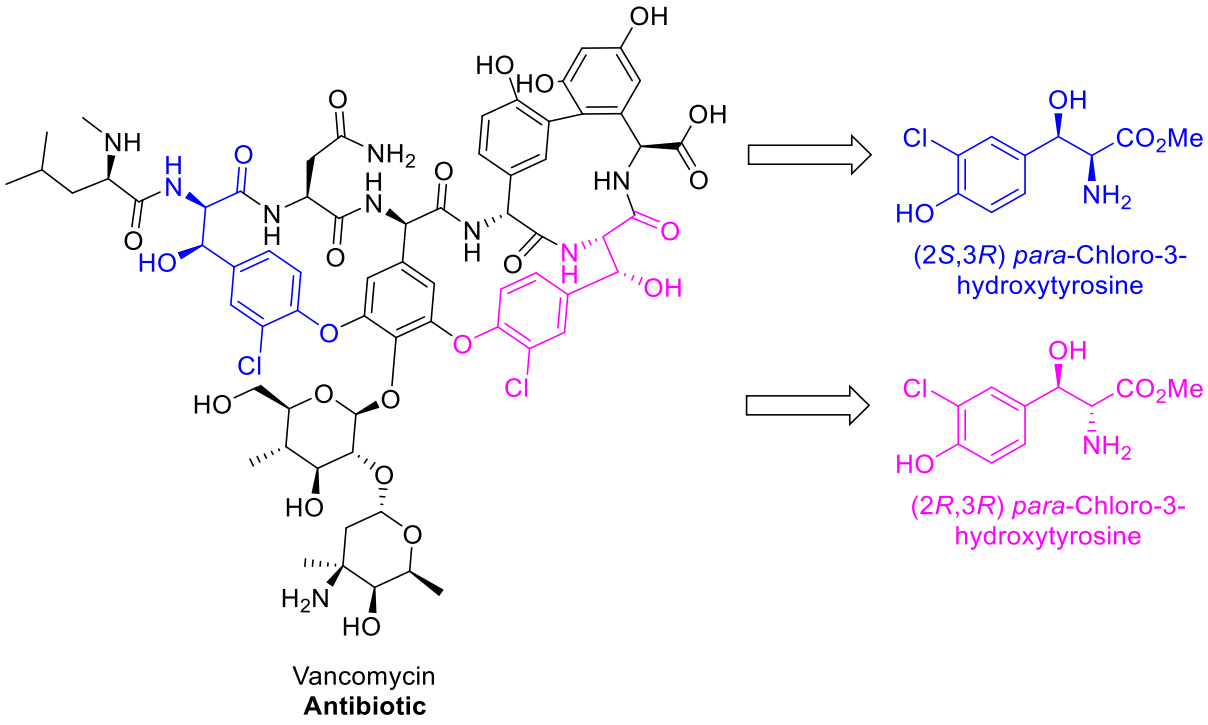

Figure 1-21. (2*S*,3*R*) and (2*R*,3*R*) *para*-chloro-3-hydroxytyrosines in vancomycin

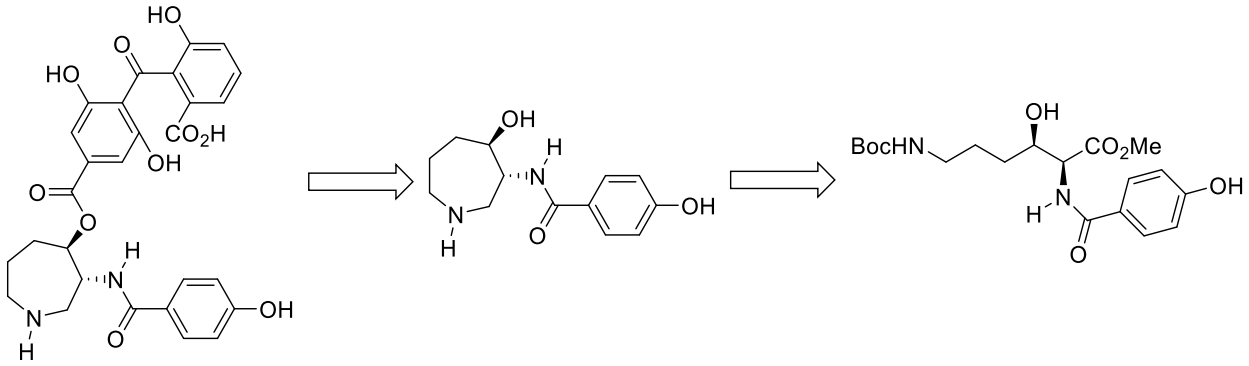

Figure 1-22. A β-hydroxy-α-amino intermediate in (–)-balanol

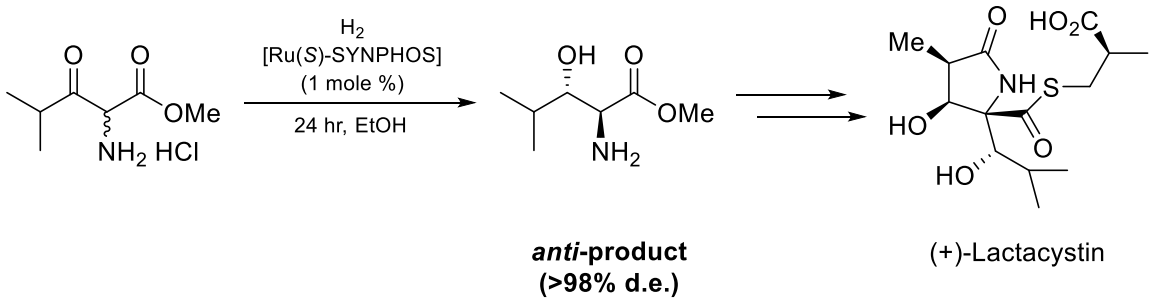

Figure 1-23. Dynamic kinetic resolution towards *anti*-β-hydroxy-α-amino acids

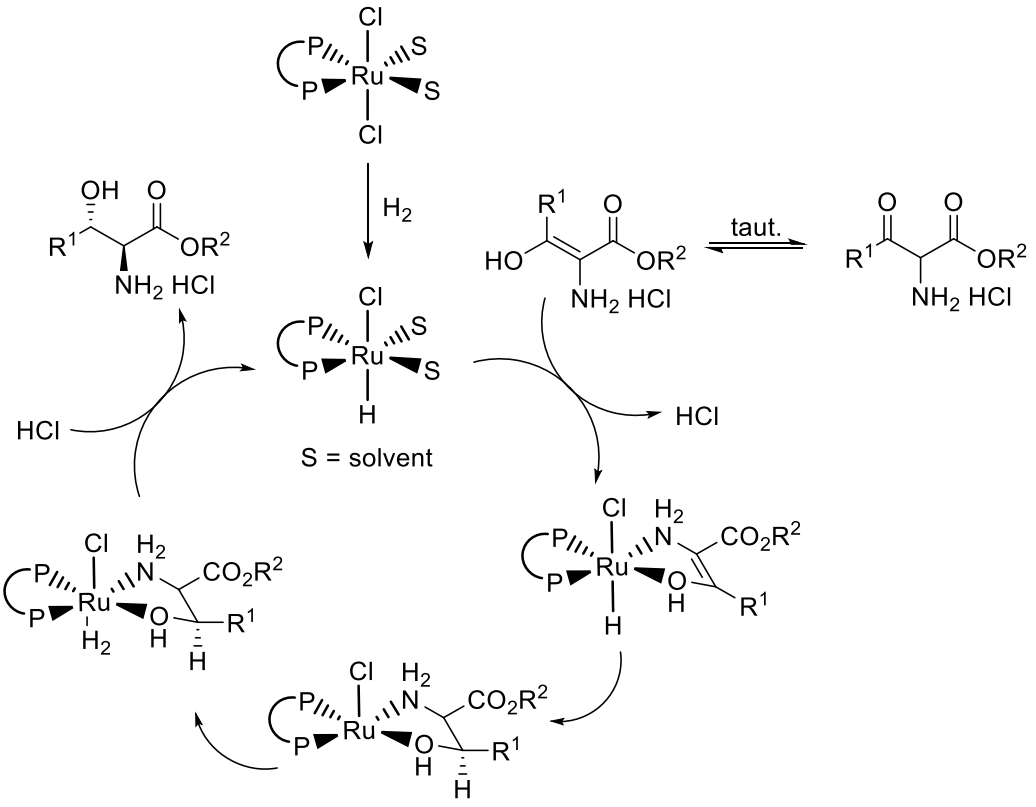

(*a*)

Figure 1-24. Proposed mechanism for dynamic kinetic resolution for (*a*) *anti*- and (*b*) *syn*-β-hydroxy-α-amino acids

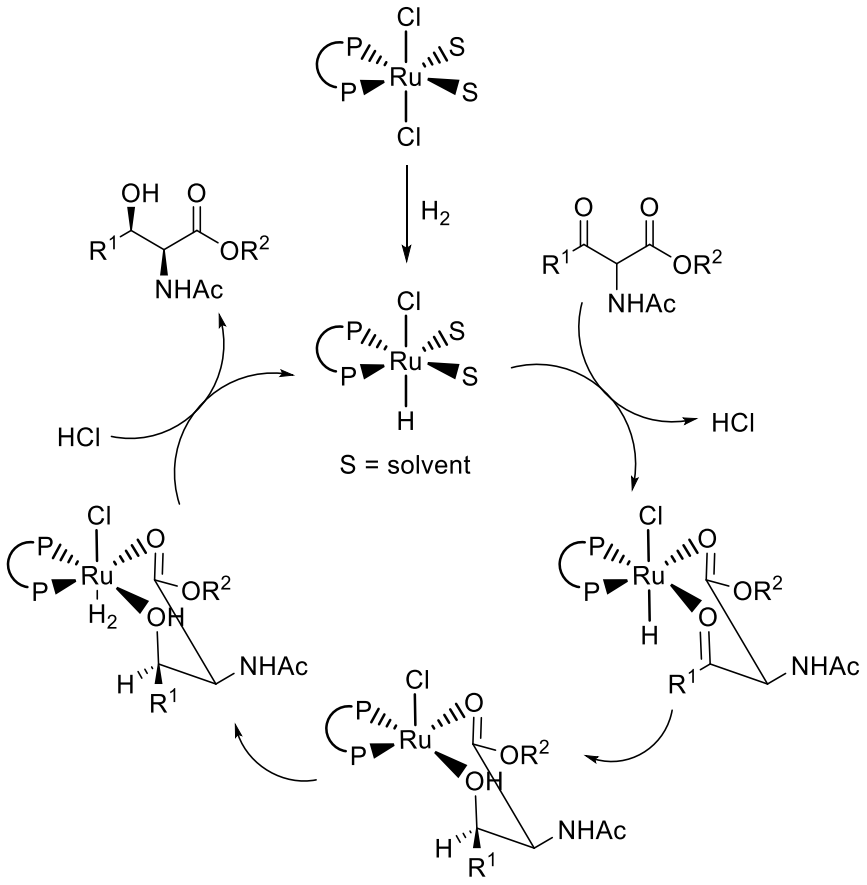

(*b*)

Figure 1-24. Continued

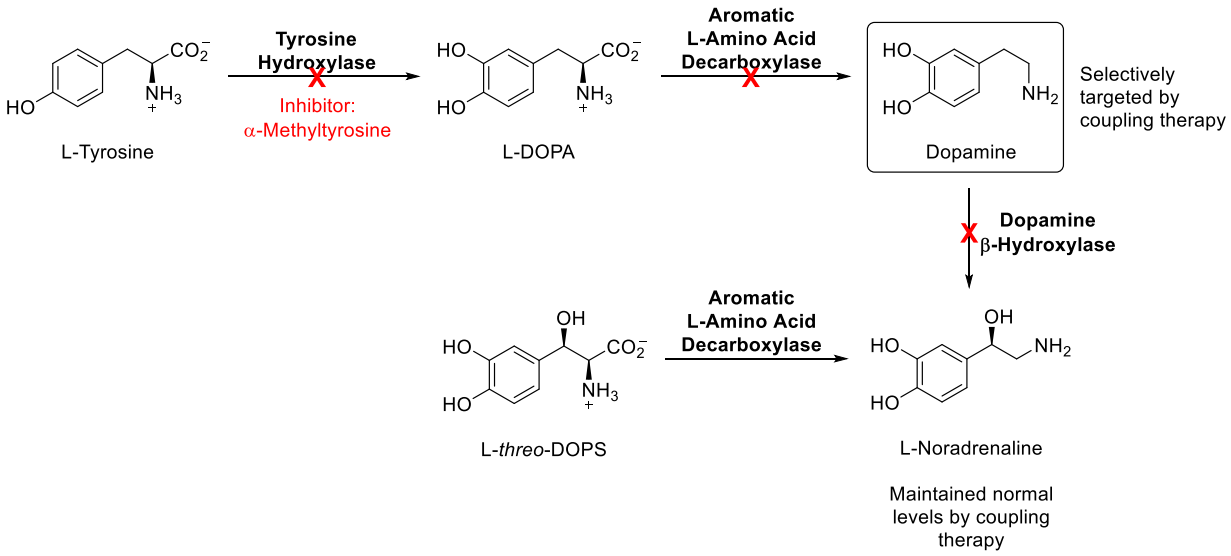

Figure 1-25. Coupling therapy: selectively targeting dopamine synthesis by α-methyltyrosine inhibitor

a) Sudalai Method

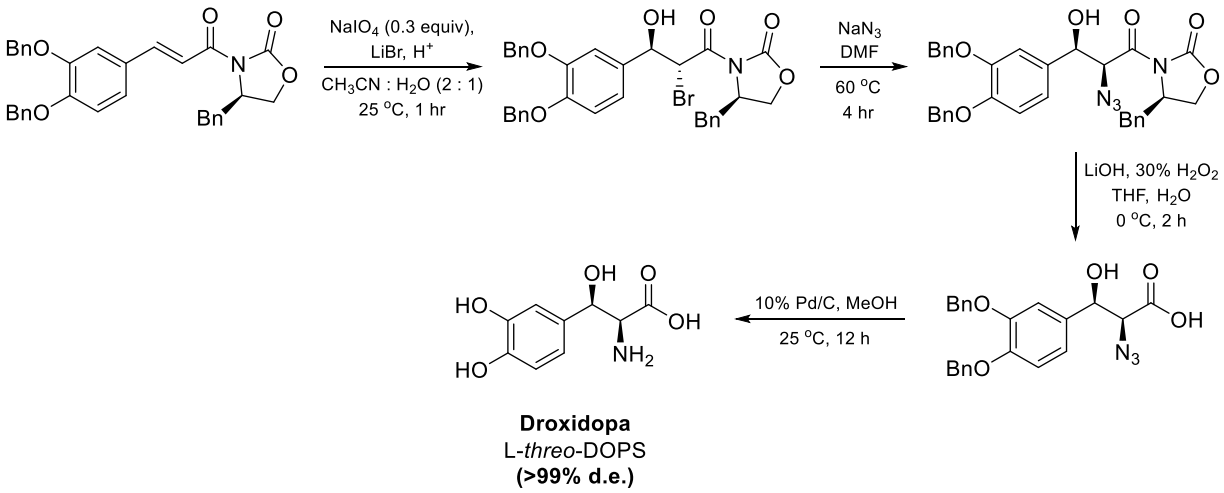

b) Guan *et. al.* Method

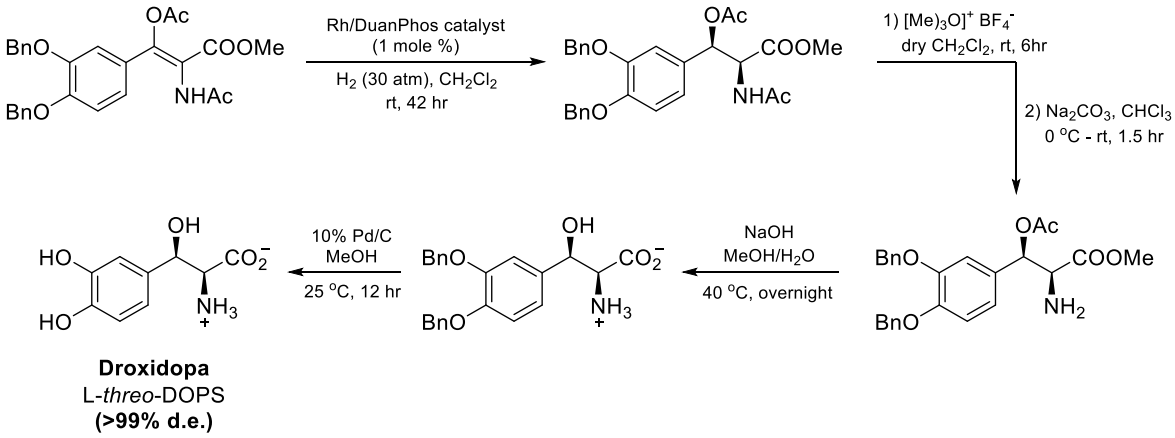

c) Wang Method

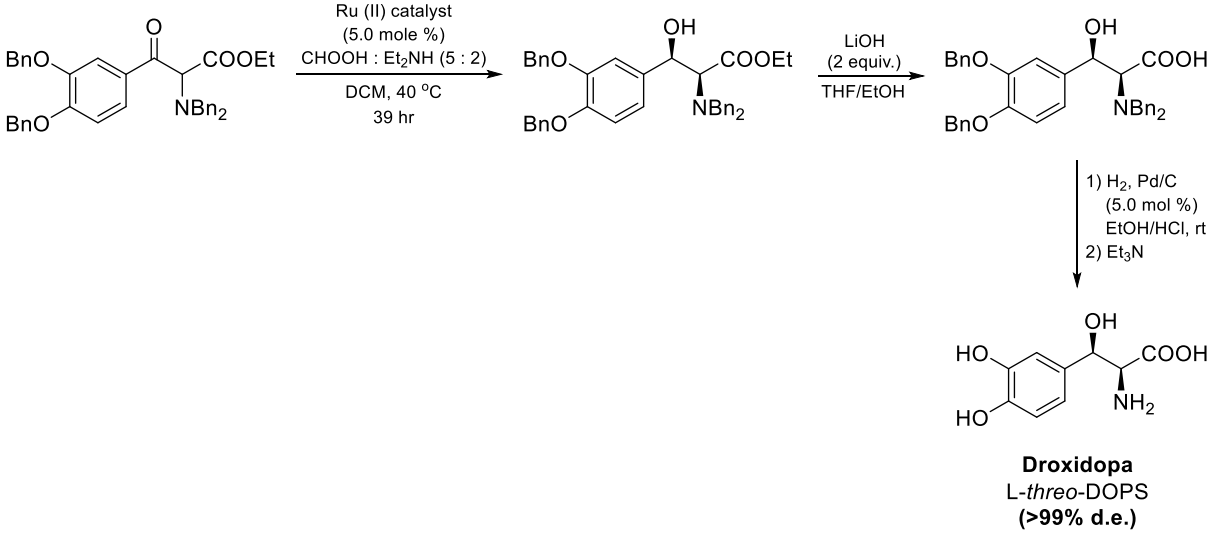

Figure 1-26. Organic synthesis strategies to L-*threo*-dihydroxyphenylserine

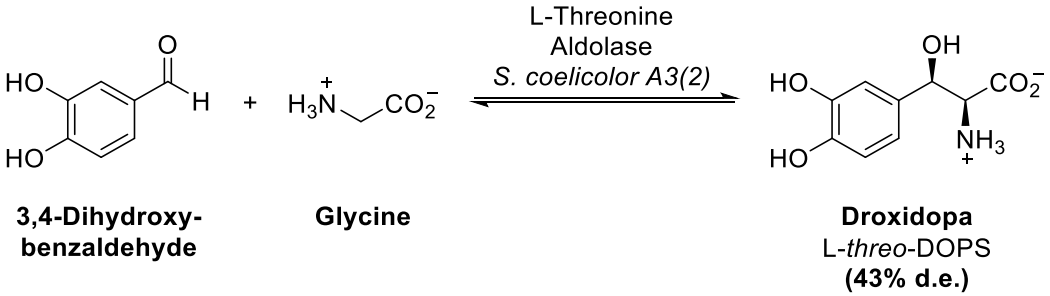

Figure 1-27. Biocatalytic synthesis of L-*threo*-dihydroxyphenylserine by L-threonine aldolase

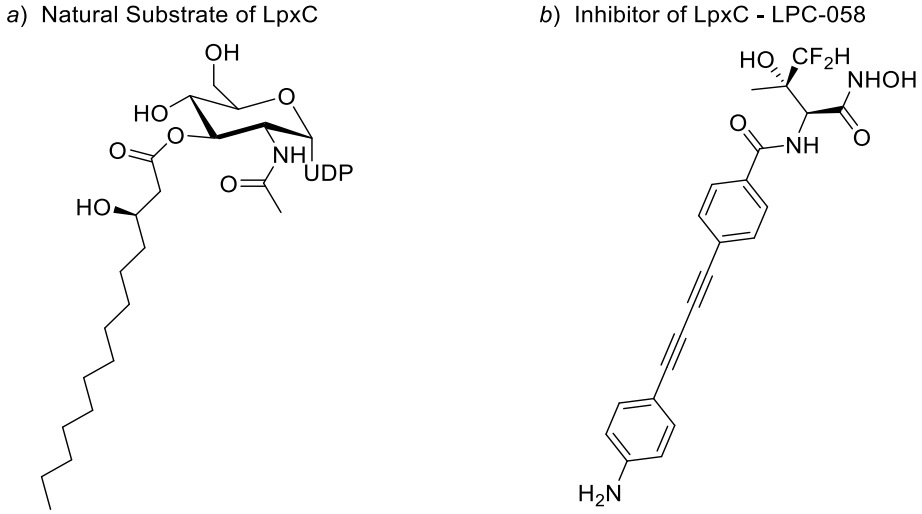

Figure 1-28. Structure comparison of the natural substrate of LpxC *versus* the inhibitor

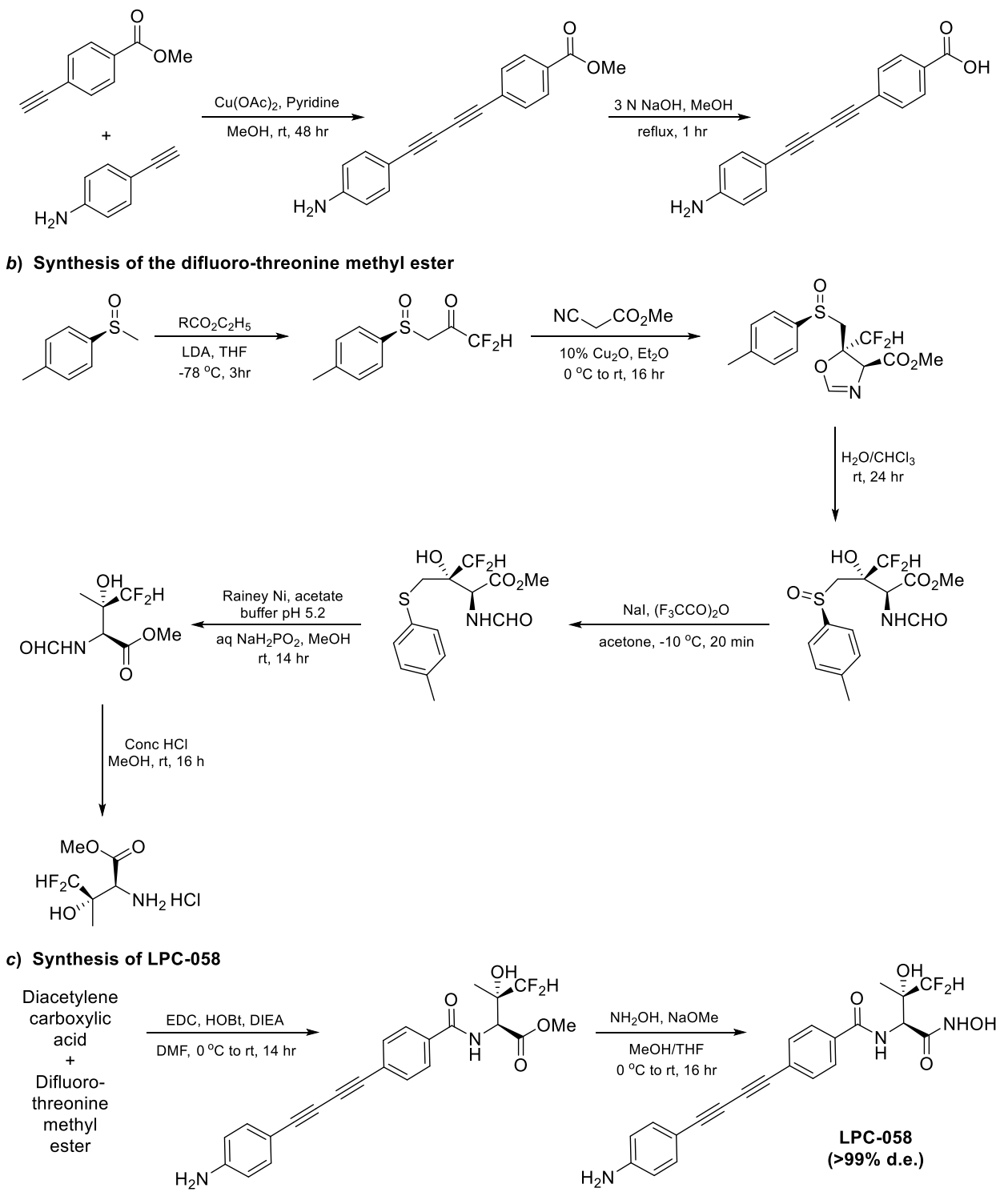

Figure 1-29. Initial Route to LPC-058

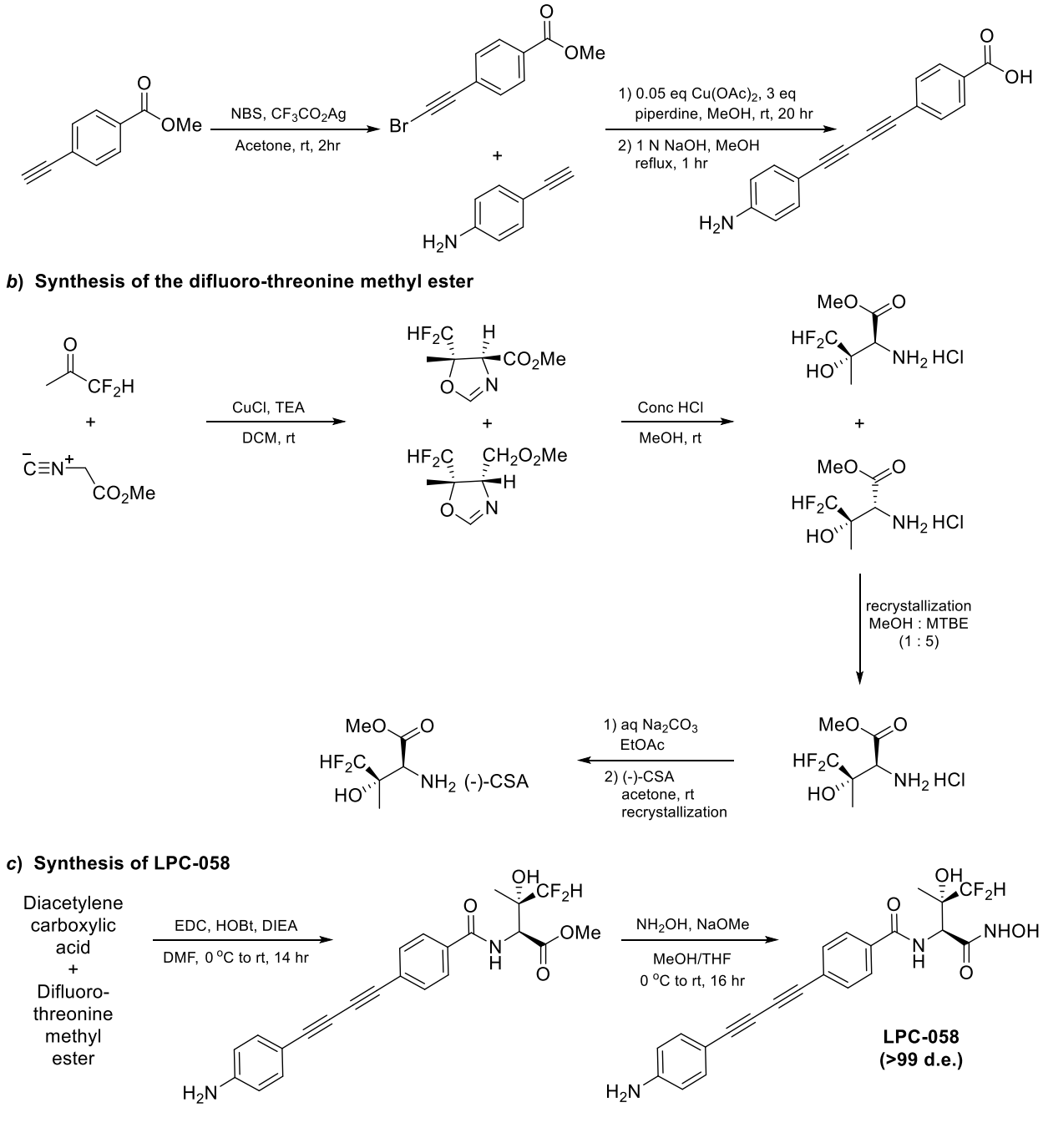

Figure 1-30. Final route in the synthesis of LPC-058

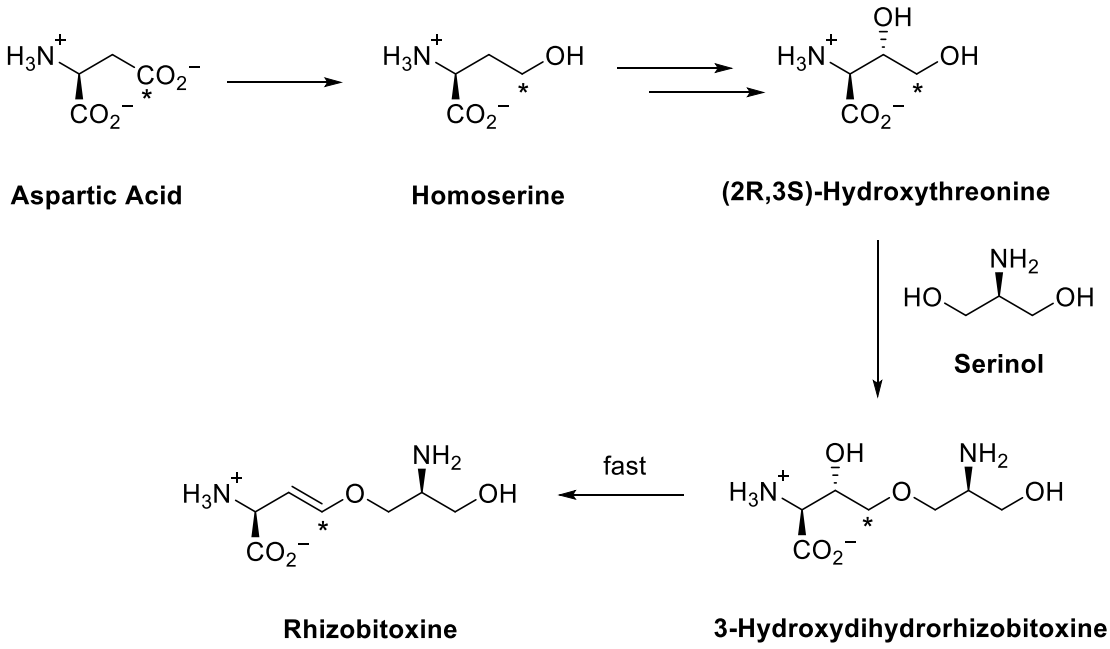

Figure 1-31. Proposed rhizobitoxine biosynthesis pathway

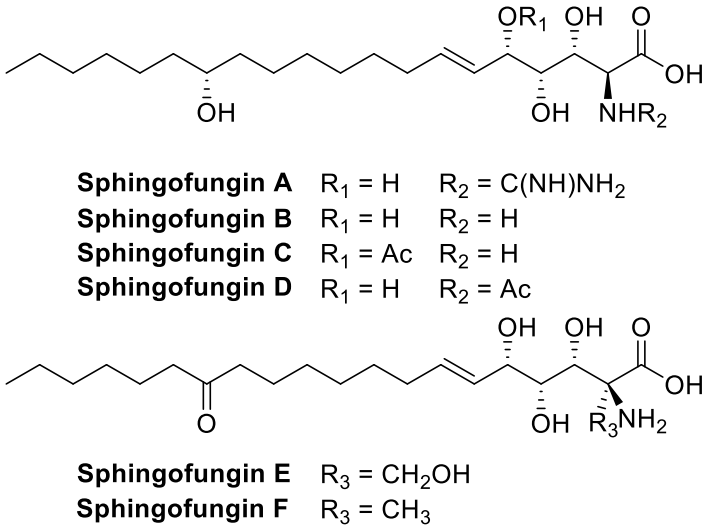

Figure 1-32. Sphingofungins A – F

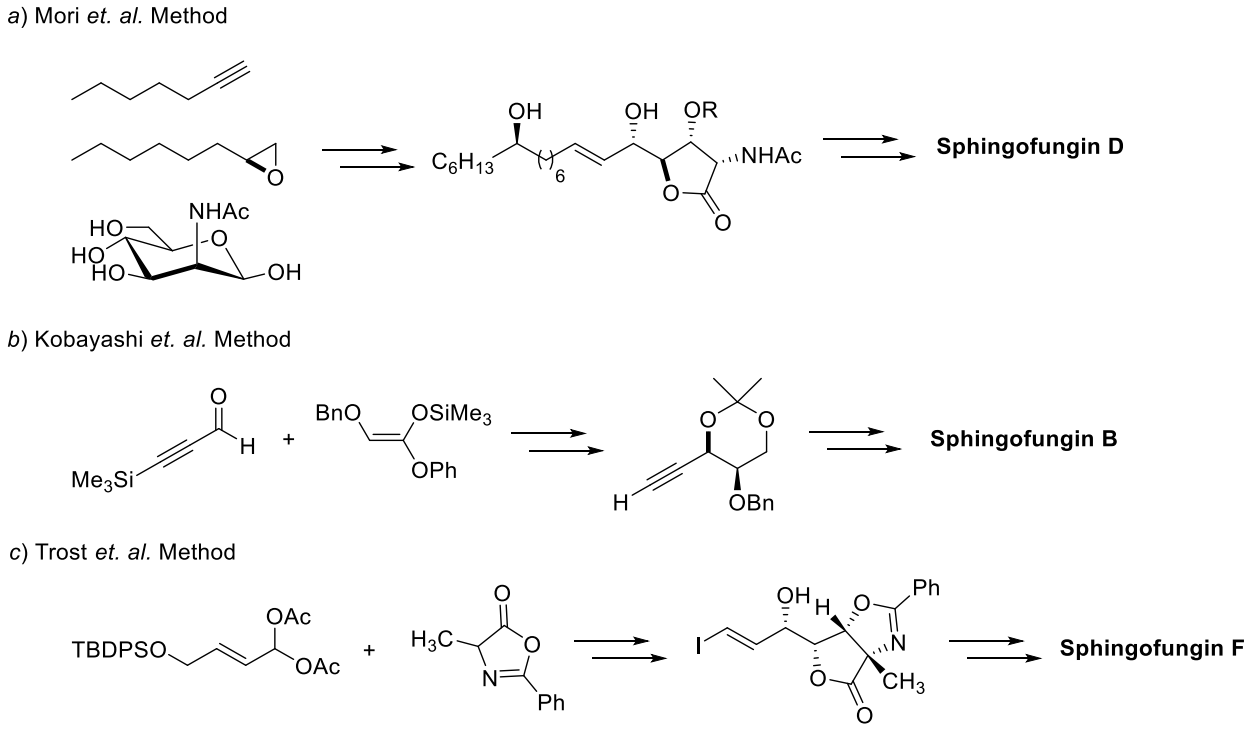

Figure 1-33. Sphingofungin synthesis strategies

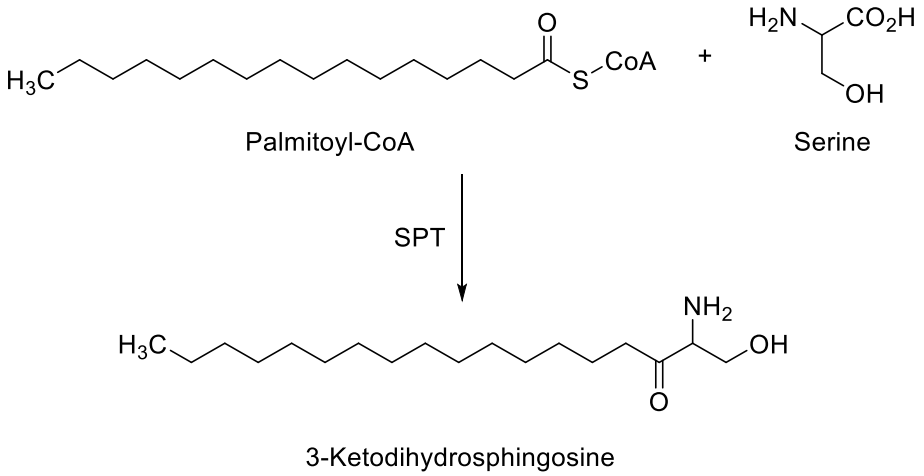

Figure 1-34. The first step in the biosynthesis of sphingolipids, serine palmitoyltransferase

CHAPTER 2[i]
THREONINE ALDOLASE AS BIOCATALYSTS

Introduction

Aldol condensations are one of the most common ways that nature accomplishes carbon–carbon bond formation and/or cleavage. The reaction is widely applicable since many common metabolites—especially carbohydrates—contain aldehyde or ketone moieties and this allows them to function as either enol(ate) nucleophiles or electrophiles. Because the same molecule can serve as both donor and acceptor, the scope of accessible products is very large. The aldol addition product is usually favored, although the exact equilibrium position is dictated by the relative thermodynamic stabilities of the reactants and products as well as their concentrations. A variety of aldolases have evolved to facilitate these conversions in both primary and secondary metabolic pathways. Native aldolases generally tolerate little or no variation in the enol(ate) partner and this is often used to classify these enzymes. By contrast, aldolases usually accept a wide variety of aldehyde electrophiles, which forms the foundation of their synthetic versatility.

Interest in using aldolases for non-native substrates grew rapidly in the 1980s after a seminal publication by Wong *et al*.[185] Carbohydrates and their derivatives were logical targets for the first-generation syntheses involving aldolases because the reactions closely mimicked their normal metabolic roles and substrate acceptance was simplified. In this regard, dihydroxyacetone phosphate (DHAP)-dependent aldolases

[i] A review of threonine aldolases was published in 2014 by Sarah E. Franz and Jon D. Stewart with the title “Chapter Three: Threonine Aldolases” in *Advances in Applied Microbiology*. Reference: 184. Franz, S. E.; Stewart, J. D., Chapter Three - Threonine Aldolases. In *Advances in Applied Microbiology*, Sima Sariaslani and Geoffrey Michael, G., Ed. Academic Press: 2014; Vol. Volume 88, pp 57-101.

found particular utility and many ingenious applications were developed using a diverse range of aldehyde acceptors. The subsequent identification of four stereocomplementary DHAP aldolases that provided each of the four possible diastereomeric aldol addition products allowed this technology to mature into a well-accepted synthetic methodology.[186, 187]

The major drawback of DHAP-dependent aldolases is their near complete specificity for DHAP. This narrows the scope of accessible products to those containing this substructure (or those derivable by subsequent transformations of the DHAP moiety) and motivated a search for aldolases that accept other enol(ate) donors. These efforts yielded pyruvate-dependent aldolases and 2-keto-3-deoxygluconate aldolase, *N*-acetylneuraminic acid (NeuAc) lyase, and 2-keto-3-deoxy-6-phosphogluconate aldolase, all of which have been applied to organic synthesis (examples are summarized in Brovetto *et al*. 2011 and Clapes *et al*. 2010).[186, 187]

To date, all known PLP-dependent aldolases utilize α-amino acids as their native substrates (typically glycine, serine, or threonine). In particular, threonine aldolases (TAs) have emerged as useful enzymes for organic synthesis since the aldol reaction creates two new, adjacent stereocenters (Figure 2-1). These enzymes have been divided into four classes based on their stereochemical preferences: high-specificity L- and D-threonine aldolases and low-specificity L- and D-threonine aldolases. The high-specificity enzymes can be further subdivided into the threonine and *allo*-threonine subtypes. It should be noted that even those enzymes designated as “low-specificity” are in fact highly selective for a particular α-carbon configuration; the “low-specificity” term arises because they yield a mixed population of β-carbon configurations.

The possibility of forming only one enantiomer (out of the four potential products) starting from simple, inexpensive building blocks has motivated most of the efforts in this research area. This chapter briefly summarizes the range of substrates and products that have been employed with TAs and then describes our structural knowledge of these enzymes and the efforts to use this information to increase their substrate range and stereoselectivities.

The Mechanism of Threonine Aldolase

All of the aforementioned aldolases follow chemical mechanisms that involve either a metal ion-stabilized enol(ate) or a synthetically equivalent enamine intermediate (utilizing an active-site Lys side chain that initially forms a Schiff's base with the donor carbonyl). Pyridoxal 5'-phosphate (PLP)-dependent aldolases follow a fundamentally different pathway (Figure 2-2). These enzymes first establish a Schiff's base between the substrate's amino group and PLP (referred to as an external aldimine). The cationic pyridinium ring facilitates deprotonation on the α-carbon to the amine by an enzyme general base, yielding a highly resonance-stabilized anion. This nucleophile adds to the aldehyde acceptor, thereby forming the *C-C* bond and yielding a Schiff's base complex between the aldol product and the PLP cofactor. The catalytic cycle is completed by an analogous Schiff's base exchange (transaldimination) that transfers the cofactor from the product back to the active-site lysine's side chain (referred to as an internal aldimine).

Threonine Aldolases Utilized for Chemical Synthesis

A handful of TAs have dominated the published synthetic applications, particularly the L-TAs from *Aeromonas jandaei*,[188, 189] *Candida humicola*,[190] *Pseudomonas putida*,[191, 192] *Streptomyces coelicolor*,[193] *Escherichia coli*,[194-197]

Aeromonas veronii,[198] *Shewanella loihica*,[198] and *Raoultella ornithinolytica*,[198] along with D-TAs produced by *Alcaligenes xylosoxidans*,[7, 191, 192, 199, 200] *Pseudomonas* sp.,[188] *Xanthomonas oryzae*,[196] *Arthrobacter* sp.[200, 201] *Pseudomonas aeruginosa*,[198] and *Pseudomonas protegens*[198]. In addition to these *bona fide* TAs, the Hilvert group has developed a mutant alanine racemase from *Geobacillus stearothermophilus* that endows the variant with D-TA activity.[202, 203] This alanine racemase is evolutionarily related to D-TAs, and the mutation removed one of the two acid–base groups required for alanine epimerization. All of these workhorse enzymes have been cloned and overexpressed in *E. coli* at high levels, which simplifies their use in chemical synthesis. The Griengl group recently created and surveyed a larger collection of these enzymes in hopes of uncovering examples with higher diastereoselectivities.[204] Whether the "C_β diastereoselectivity problem" can best be overcome by testing additional wild-type isolates or by applying protein engineering technologies to existing TAs awaits experimental testing.

Substrate Selectivity of Threonine Aldolase

In 2014, we published a book chapter that contained a complete list of synthetic applications of TAs that were published by early 2014 (Tables 2-1 – 2-4).[184] The examples have been grouped first by the amino acid donor nucleophile (glycine, alanine, serine, or cysteine; Tables 2-1 – 2-4, respectively). Within each table, examples are ordered by increasing size and structural complexity of the aldehyde acceptor (alkyl aldehydes followed by aryl aldehydes). In most cases, aldol products were not isolated from the reaction mixtures and only fractional conversions based on chromatographic analysis (typically HPLC) are available. Stereochemical purities were

almost universally assessed by chromatographic separations. Finally, it should be noted that large excesses of the amino acid were typically employed to drive reactions toward the desired aldol product. For these reasons, the fractional conversion achieved in a given example should only be taken as a rough guide with regard to estimating the synthetic feasibility of a preparative-scale reaction.

Glycine/Alkyl Aldehydes

Simple alkyl aldehydes can be converted to L-*anti*-products with high diastereoselectivities by the *E. coli* L-TA (Table 2-1, entries 4, 11, and 16).[196] The active site of this enzyme can accommodate relatively large *n*-alkyl aldehydes, although the *anti*-diastereoselectivity and fractional conversion decline as aldehyde size increases (Table 2-1, entries 24 and 30). To date, a D-TA with comparable levels of diastereoselectivity has not been identified, although the *A. xylosoxidans* enzyme can show good *syn*-selectivity in favorable cases (*e.g.*, Table 2-1, entry 19).

TAs generally tolerate relatively bulky and highly substituted aldehyde acceptors. α-Halo-, α-alkoxy-, and α-amino moieties are acceptable, even when the latter are derivatized by large protecting groups such as benzyl and Cbz (Table 2-1, entries 40 – 59). The main drawback is that diastereomeric mixtures are usually obtained and the preferences for C_β-stereochemistry are relatively modest. Aldehyde acceptors with β-substituents—even relatively large ones—are also tolerated by TAs (Table 2-1, entries 60 – 78). The general conclusion is that nearly all alkyl aldehydes can serve as acceptors for glycine; however, it is likely that a mixture of diastereomers will be obtained at the β-carbon. Preexisting chiral centers in the aldehyde have modest impacts on diastereoselectivity (Table 2-1, entries 57 – 59 and 75 – 79).

Table 2-1. Synthetic applications of threonine aldolases using glycine as the donor

Aldehyde Acceptor	Product	Enzyme	Yield or Conversion	d.e.	Entry	References
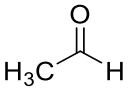	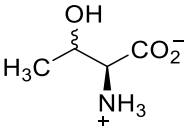	*C. humicola* L-TA	30–40%	N/A	1	190
		P. putida L-TA	n.d.	4% (*anti*)	2	192
		E. coli L-TA	40% (24 h)	82% (*anti*)	3	196
		E. coli L-TA	35% (3 h)	99% (*anti*)	4	196
	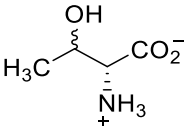	*A. xylosoxidans* D-TA	n.d.	2% (*anti*)	5	192
		X. oryzae D-TA	60% (3 h)	6% (*syn*)	6	196
		X. oryzae D-TA	50% (24 h)	6% (*syn*)	7	196
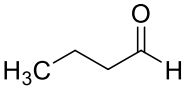	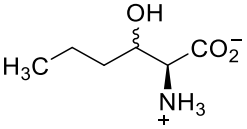	*C. humicola* L-TA	30%	n.d.	8	190
		P. putida L-TA	71%	28% (*syn*)	9	192
		E. coli L-TA	18% (24 h)	97% (*anti*)	10	196
		E. coli L-TA	15% (3 h)	99% (*anti*)	11	196
	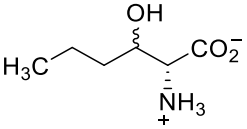	*A. xylosoxidans* D-TA	52%	9% (*syn*)	12	192
		X. oryzae D-TA	37%	3.3% (*syn*)	13	196
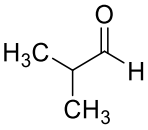	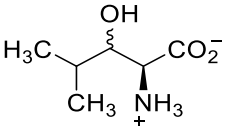	*P. putida* L-TA	55%	42% (*syn*)	14	192
		E. coli L-TA	10% (3 h)	76% (*anti*)	15	196
		E. coli L-TA	1% (24 h)	99% (*anti*)	16	196
	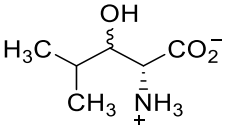	Y265A Ala racemase	0%	n.d.	17	202
		X. oryzae D-TA	49%	86% (*syn*)	18	196
		A. xylosoxidans D-TA	24%	>95% (*syn*)	19	192

Table 2-1. Continued

Aldehyde Acceptor	Product	Enzyme	Yield or Conversion	d.e.	Entry	References
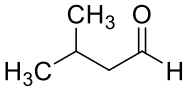	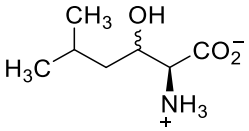	*P. putida* L-TA	94%	10% (*syn*)	20	192
	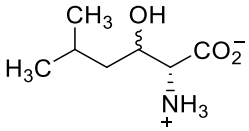	*A. xylos-oxidans* D-TA	65%	54% (*syn*)	21	192
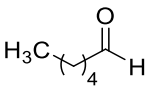	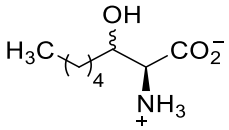	*P. putida* L-TA	92%	31% (*syn*)	22	192
		E. coli L-TA	16% (24 h)	26% (*anti*)	23	196
		E. coli L-TA	7% (3 h)	84% (*anti*)	24	196
	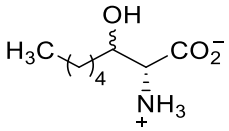	*X. oryzae* D-TA	31% (3 h)	22% (*syn*)	25	196
		X. oryzae D-TA	23% (24 h)	28% (*syn*)	26	196
		A. xylos-oxidans D-TA	42% (30% DMSO)	68% (*syn*)	27	192
		A. xylos-oxidans D-TA	33% (no cosolvent)	73% (*syn*)	28	192
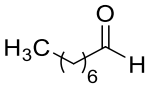	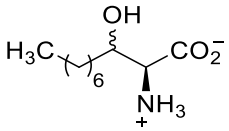	*P. putida* L-TA	25%	9% (*syn*)	29	192
		E. coli L-TA	2%	44% (*anti*)	30	196
	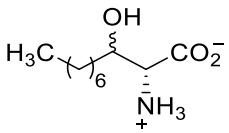	*X. oryzae* D-TA	3%	38% (*syn*)	31	196
		A. xylos-oxidans D-TA	12%	55% (*syn*)	32	192
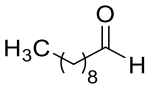	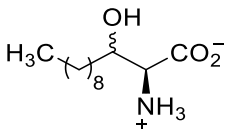	*P. putida* L-TA	29%	23% (*anti*)	33	192
	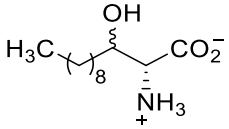	*A. xylos-oxidans* D-TA	<1%	n.d.	34	192

Table 2-1. Continued

Aldehyde Acceptor	Product	Enzyme	Yield or Conversion	d.e.	Entry	References
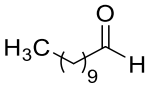	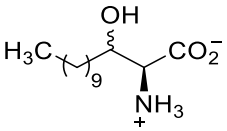	*P. putida* L-TA	33%	15% (*anti*)	35	192
	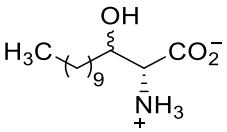	*A. xylos-oxidans* D-TA	<1%	n.d.	36	192
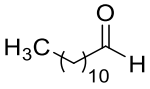	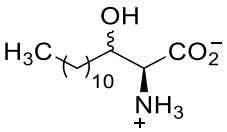	*P. putida* L-TA	11%	15% (*anti*)	37	192
	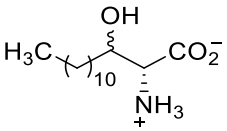	*A. xylos-oxidans* D-TA	<1%	n.d.	38	192
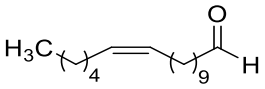	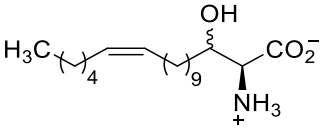	*C. humi-cola* L-TA	30%	n.d.	39	190
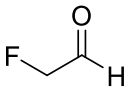	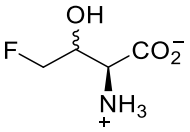	*P. putida* L-TA	50%	93% (*syn*)	40	192
	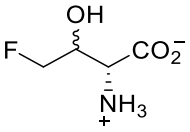	*A. xylos-oxidans* D-TA	30%	97% (*syn*)	41	192
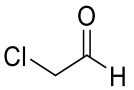	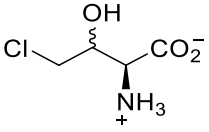	*C. humi-cola* L-TA	<5%	n.d.	42	190
		P. putida L-TA	65%	40% (*syn*)	43	192
	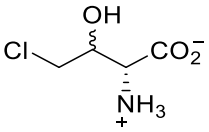	*A. xylos-oxidans* D-TA	26%	73% (*syn*)	44	192

Table 2-1. Continued

Aldehyde Acceptor	Product	Enzyme	Yield or Conversion	d.e.	Entry	References
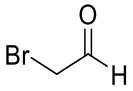	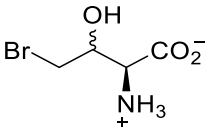	*P. putida* L-TA	20%	73% (*syn*)	45	192
	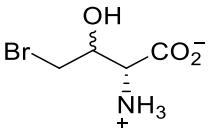	*A. xylos-oxidans* D-TA	6%	82% (*syn*)	46	192
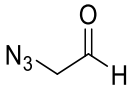	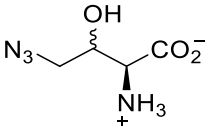	*C. humicola* L-TA	>75%	n.d.	47	190
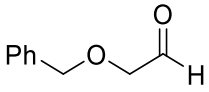	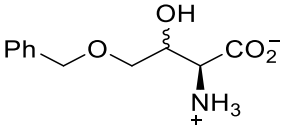	*E. coli* L-TA	13%	0%	48	197
		E. coli L-TA	30%	20% (*syn*)	49	194
		C. humicola L-TA	>75%	84% (*anti*)	50	190
		E. coli L-TA	36%	88% (*anti*)	51	196
	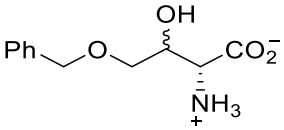	*X. oryzae* D-TA	80%	40% (*syn*)	52	196
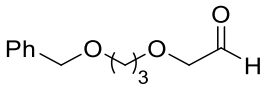	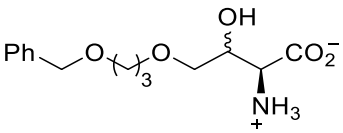	*C. humicola* L-TA	45-75%	84% (*anti*)	53	190
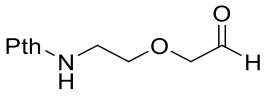	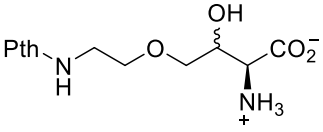	*C. humicola* L-TA	45-75%	84% (*anti*)	54	190
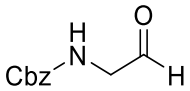	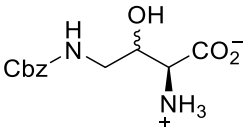	*E. coli* L-TA	18%	40% (*syn*)	55	194
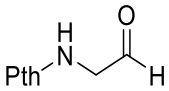	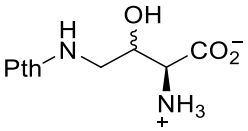	*C. humicola* L-TA	30%	n.d.	56	190

Table 2-1. Continued

Aldehyde Acceptor	Product	Enzyme	Yield or Conversion	d.e.	Entry	References
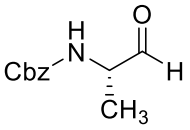	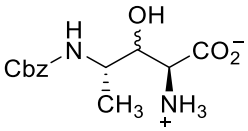	*E. coli* L-TA	129%	41% (*syn*)	57	194
		E. coli L-TA	54%	64% (*syn*)	58	194
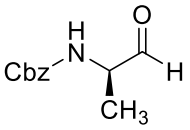	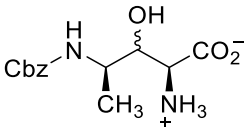	*E. coli* L-TA	40%	68% (*syn*)	59	194
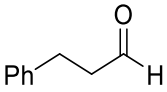	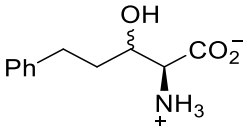	*C. humicola* L-TA	10-30%	n.d.	60	190
		E. coli L-TA	10% (30% DMSO)	44% (*anti*)	61	196
		E. coli L-TA	5% (no co-solvent)	66% (*anti*)	62	196
	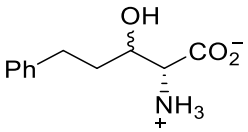	*X. oryzae* D-TA	16%	74% (*syn*)	63	196
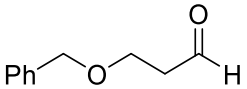	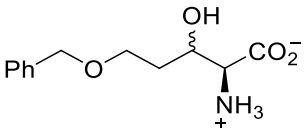	*C. humicola* L-TA	53%	6% (*anti*)	64	190
		E. coli L-TA	10%	88% (*anti*)	65	196
	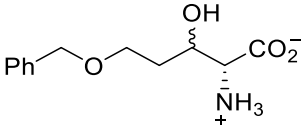	*X. oryzae* D-TA	45% (3 h)	29% (*syn*)	66	196
		X. oryzae D-TA	35% (25 min)	64% (*syn*)	67	196
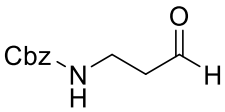	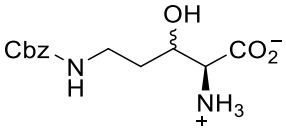	*E. coli* L-TA	11%	0%	68	194
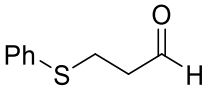	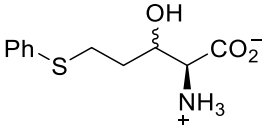	*C. humicola* L-TA	>75%	n.d.	69	190

Table 2-1. Continued

Aldehyde Acceptor	Product	Enzyme	Yield or Conversion	d.e.	Entry	References
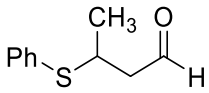	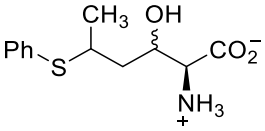	*C. humicola* L-TA	10%	n.d.	70	190
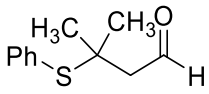	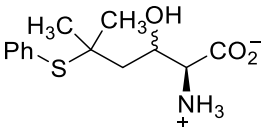	*C. humicola* L-TA	10-30%	n.d.	71	190
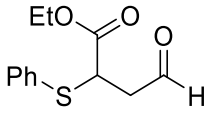	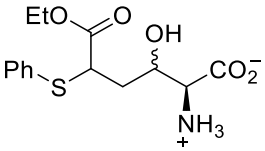	*C. humicola* L-TA	10%	n.d.	72	190
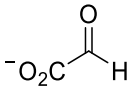	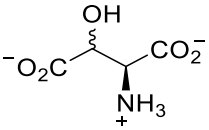	*E. coli* L-TA	67%	0%	73	197
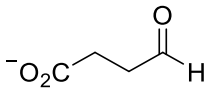	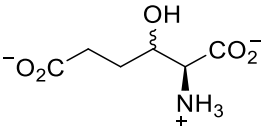	*E. coli* L-TA	34%	n.d.	74	197
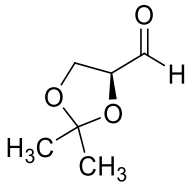	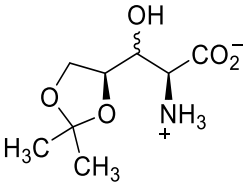	*E. coli* L-TA	35%	92% (*anti*)	75	196
	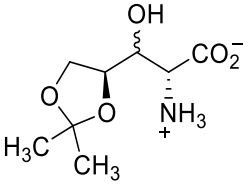	*X. oryzae* D-TA	73%	40% (*syn*)	76	196
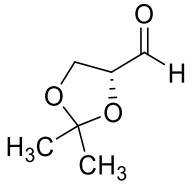	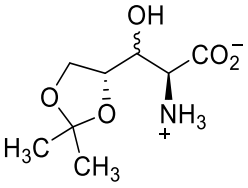	*E. coli* L-TA	70%	0%	77	196
	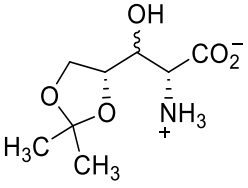	*X. oryzae* D-TA	84%	76% (*syn*)	78	196

Table 2-1. Continued

Aldehyde Acceptor	Product	Enzyme	Yield or Conversion	d.e.	Entry	References
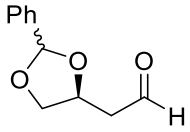	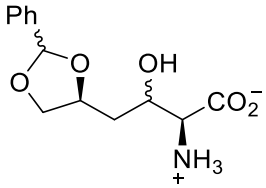	*C. humicola* L-TA	30%	n.d.	79	190
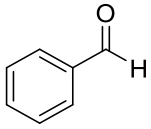	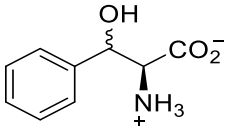	*T. maritima* L-*allo*-TA	25% (5 min)	76% (*syn*)	80	204
		P. putida L-TA	80% (30 min)	21% (*syn*)	81	192
		P. aeruginosa L-TA	80% (30 min)	21% (*syn*)	82	204
		A. jandaei L-*allo*-TA	30% (5 min)	27% (*syn*)	83	204
		P. putida L-TA	40% (1 min)	>30% (*syn*)	84	192
		P. aeruginosa L-TA	10% (1 min)	>30% (*syn*)	85	204
		E. coli L-TA	9% (24 h)	60% (*syn*)	86	196
		E. coli L-TA	3% (3 h)	71% (*syn*)	87	196
		A. jandaei L-*allo*-TA	<20% (<1 min)	*anti*	88	204
		S. cerevisiae L-low-TA	60% (5 h)	22% (*anti*)	89	204
		S. cerevisiae L-low-TA	4% (1 min)	40% (*anti*)	90	204
		C. humicola L-TA	45%	40% (*anti*)	91	190
		B. bronchiseptica L-low-TA	10% (5 min)	70% (*anti*)	92	204
	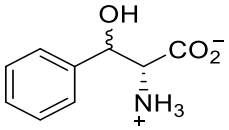	*S. pomperoyl* D-low-TA	80% (5 days)	21% (*syn*)	93	204
		X. oryzae D-TA	10% (24 h)	73% (*syn*)	94	196

Table 2-1. Continued

Aldehyde Acceptor	Product	Enzyme	Yield or Conversion	d.e.	Entry	References
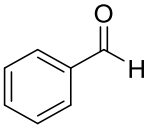	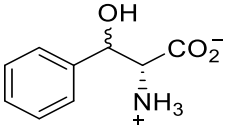	*X. oryzae* D-TA	11% (3 h)	74% (*syn*)	95	196
		Y265A Ala racemase	17% (24 h)	76% (*syn*)	96	202
		Y265A Ala racemase	10% (3 h)	97% (*syn*)	97	202
		A. xylosoxidans D-TA	79%	98% (*syn*)	98	192
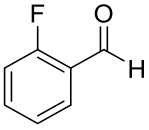	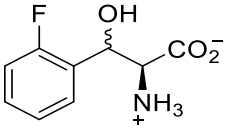	*P. putida* L-TA	68%	35% (*syn*)	99	192
	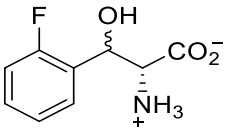	*A. xylosoxidans* D-TA	68%	95% (*syn*)	100	192
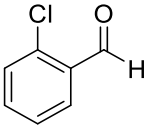	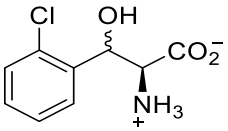	*P. putida* L-TA	90%	52% (*syn*)	101	192
	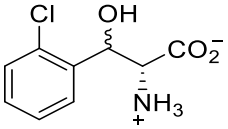	*A. xylosoxidans* D-TA	27%	67% (*syn*)	102	192
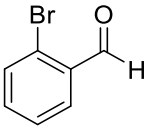	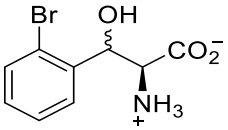	*P. putida* L-TA	79%	34% (*syn*)	103	192
	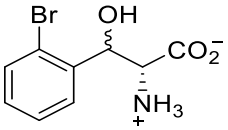	*A. xylosoxidans* D-TA	6%	35% (*syn*)	104	192
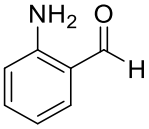	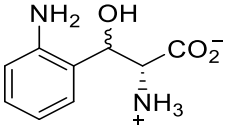	Y265A Ala racemase	<1%	n.d.	105	202
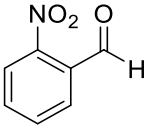	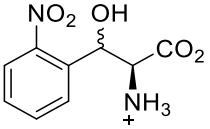	*P. putida* L-TA	99%	32% (*syn*)	106	192
		E. coli L-TA	93% (24 h)	42% (*anti*)	107	196

Table 2-1. Continued

Aldehyde Acceptor	Product	Enzyme	Yield or Conver-sion	d.e.	Entry	References
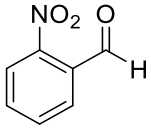	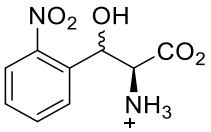	*E. coli* L-TA	46% (3 h)	68% (*anti*)	108	196
	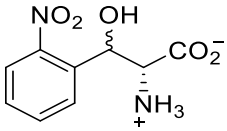	*X. oryzae* D-TA	89% (3 h)	44% (*syn*)	109	196
		A. xylosoxidans D-TA	18%	65% (*syn*)	110	192
		Y265A Ala racemase	1%	>97% (*syn*)	111	202
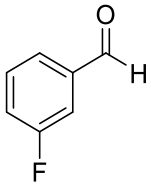	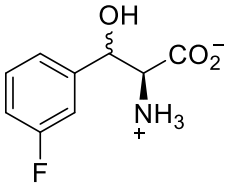	*P. putida* L-TA	64%	27% (*syn*)	112	192
	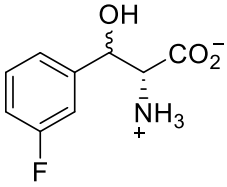	*A. xylosoxidans* D-TA	54%	81% (*syn*)	113	192
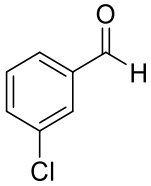	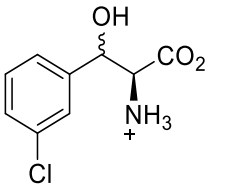	*P. putida* L-TA	69%	30% (*syn*)	114	192
	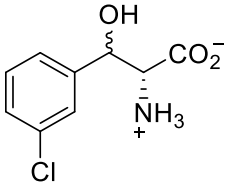	*A. xylosoxidans* D-TA	60%	85% (*syn*)	115	192
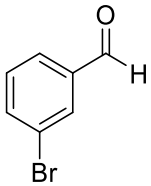	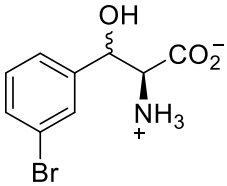	*P. putida* L-TA	63%	55% (*syn*)	116	192

Table 2-1. Continued

Aldehyde Acceptor	Product	Enzyme	Yield or Conversion	d.e.	Entry	References
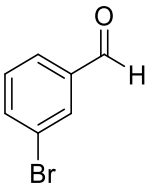	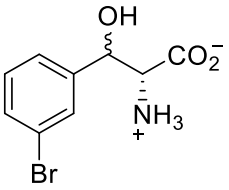	*A. xylosoxidans* D-TA	43%	71% (*syn*)	117	192
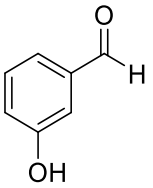	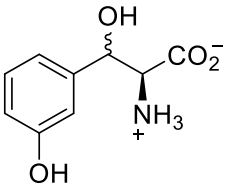	*E. coli* L-TA	43%	46% (*syn*)	118	196
		P. putida L-TA	56%	51% (*syn*)	119	192
	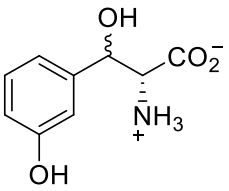	*X. oryzae* D-TA	53% (24 h)	46% (*syn*)	120	196
		X. oryzae D-TA	54% (3 h)	48% (*syn*)	121	196
		Y265A Ala racemase	3%	70% (*syn*)	122	202
		A. xylosoxidans D-TA	76%	86% (*syn*)	123	192
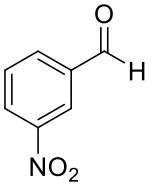	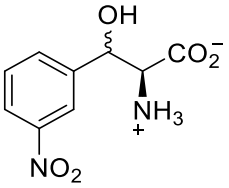	*P. putida* L-TA	74%	21% (*syn*)	124	192
	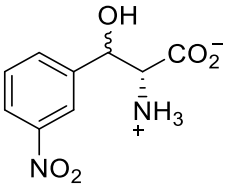	*A. xylosoxidans* D-TA	90%	80% (*syn*)	125	192
		Y265A Ala racemase	55% (24 h)	85% (*syn*)	126	202
		Y265A Ala racemase	20% (3 h)	93% (*syn*)	127	202
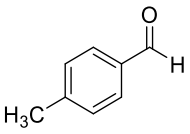	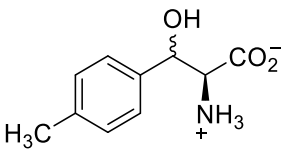	*E. coli* L-TA	17%	20% (*anti*)	128	196
	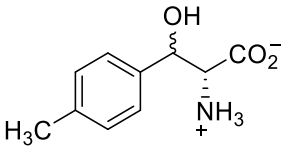	*X. oryzae* D-TA	25%	14% (*anti*)	129	196

Table 2-1. Continued

Aldehyde Acceptor	Product	Enzyme	Yield or Conversion	d.e.	Entry	References
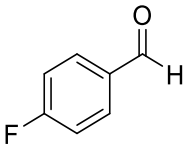	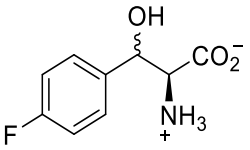	*P. putida* L-TA	51%	29% (*syn*)	130	192
	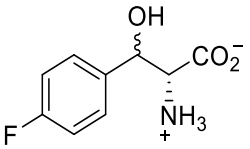	*A. xylosoxidans* D-TA	42%	91% (*syn*)	131	192
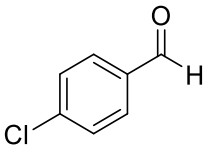	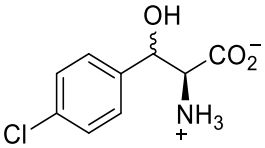	*P. putida* L-TA	57%	17% (*syn*)	132	192
	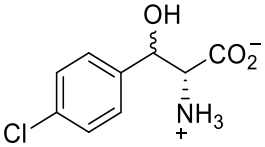	*A. xylosoxidans* D-TA	26%	86% (*syn*)	133	192
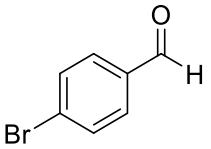	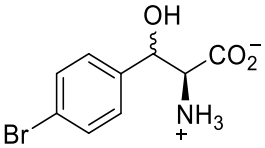	*P. putida* L-TA	47%	14% (*syn*)	134	192
	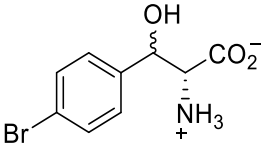	*A. xylosoxidans* D-TA	12%	74% (*syn*)	135	192
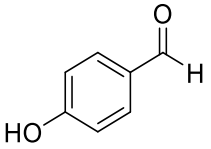	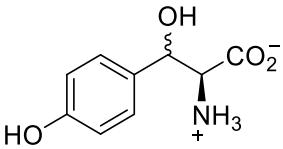	*P. putida* L-TA	11%	36% (*syn*)	136	192
		C. humicola L-TA	30%	40% (*anti*)	137	190
	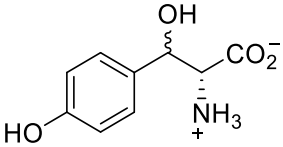	*A. xylosoxidans* D-TA	15%	70% (*syn*)	138	192

Table 2-1. Continued

Aldehyde Acceptor	Product	Enzyme	Yield or Con-version	d.e.	Entry	Referen-ces
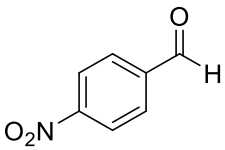	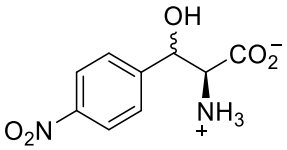	*P. putida* L-TA	79%	24% (*syn*)	139	192
		E. coli L-TA	53% (24 h)	6% (*anti*)	140	196
		E. coli L-TA	35% (3 h)	28% (*anti*)	141	196
	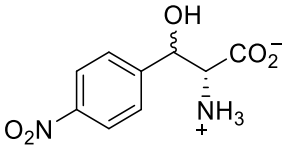	*X. oryzae* D-TA	88% (24 h)	10% (*syn*)	142	196
		X. oryzae D-TA	72% (3 h)	16% (*syn*)	143	196
		Y265A Ala racemase	36% (24 h)	40% (*syn*)	144	202
		A. xylos-oxidans D-TA	31%	75% (*syn*)	145	192
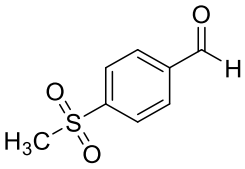	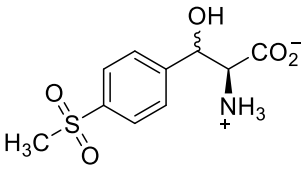	*P. putida* L-TA	68%	53% (*syn*)	146	192
	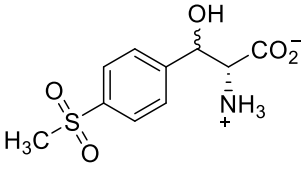	*A. xylos-oxidans* D-TA	63%	99% (*syn*)	147	192
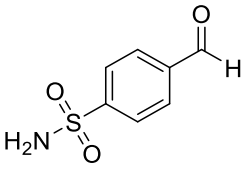	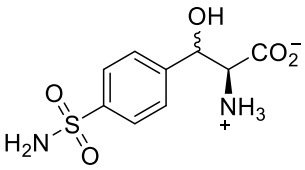	*P. putida* L-TA	92%	24% (*syn*)	148	192
	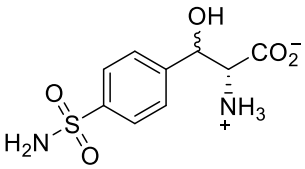	*A. xylos-oxidans* D-TA	53%	>90% (*syn*)	149	192

Table 2-1. Continued

Aldehyde Acceptor	Product	Enzyme	Yield or Conversion	d.e.	Entry	References
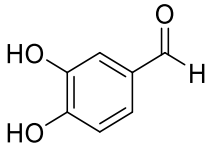	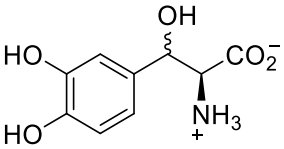	*P. putida* L-TA	<1%	n.d.	150	192
		S. coelicolor L-TA	n.d.	14% (*syn*)	151	193
		V81I/R241C/ Y306C *S. coelicolor* L-TA	n.d.	21% (*syn*)	152	193
		R241C/A287V *S. coelicolor* L-TA	n.d.	21% (*syn*)	153	193
		Y306C *S. coelicolor* L-TA	n.d.	26% (*syn*)	154	193
		Y36C/Y306C/ R316C *S. coelicolor* L-TA	n.d.	28% (*syn*)	155	193
		Y39C/Y306C *S. coelicolor* L-TA	n.d.	38% (*syn*)	156	193
		Y39C/T306C/ A48T *S. coelicolor* L-TA	n.d. (fourfold of wt)	43% (*syn*)	157	193
		E. coli L-TA	71%	60% (*syn*)	158	195
	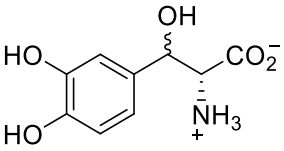	*A. xylosoxidans* D-TA	<1%	n.d.	159	192
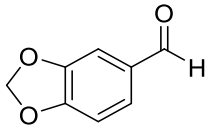	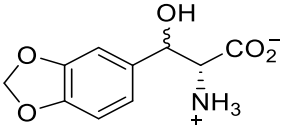	Y265A Ala racemase	5%	70% (*syn*)	160	202
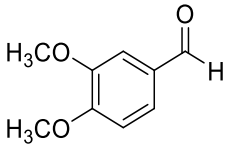	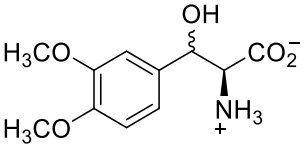	*P. putida* L-TA	15%	16% (*syn*)	161	192

Table 2-1. Continued

Aldehyde Acceptor	Product	Enzyme	Yield or Conversion	d.e.	Entry	References
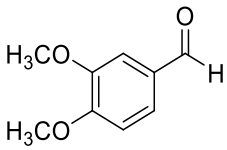	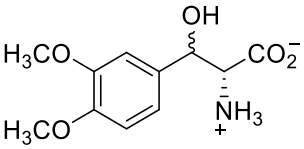	*A. xylosoxidans* D-TA	16%	46% (*syn*)	162	192
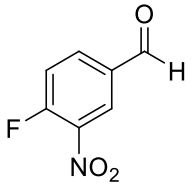	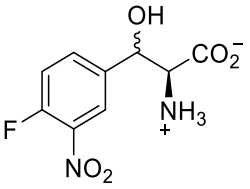	*E. coli* L-TA	21% (24 h)	40% (*anti*)	163	196
		E. coli L-TA	19% (3 h)	50% (*anti*)	164	196
	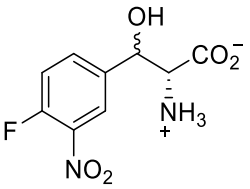	*X. oryzae* D-TA	49% (24 h)	30% (*syn*)	165	196
		X. oryzae D-TA	42% (3 h)	52% (*syn*)	166	196
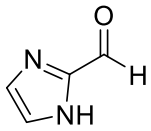	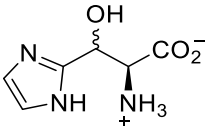	*E. coli* L-TA	40%	32% (*syn*)	167	196
	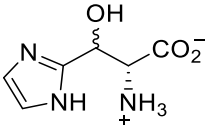	*X. oryzae* D-TA	60%	22% (*syn*)	168	196
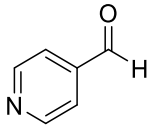	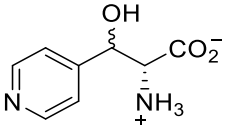	*A. xylosoxidans* D-TA	70%	99% (*syn*)	169	200
		Arthrobacter sp. D-TA	70%	99% (*syn*)	170	200

Note: Alkyl aldehydes are shown first, in the approximate order of increasing size and structural complexity. Aryl aldehydes follow, also in the order of increasing size and structural complexity. When a given reaction has been carried out by more than one threonine aldolase, entries are arranged in the order of increasing *anti*-selectivity, followed by increasing *syn*-selectivity for both L- and D-selective aldolases. n.d., not determined or not reported. d.e., diastereomeric excess = % major diastereomer - % minor diastereomer.

Glycine/Aryl Aldehydes

Because it is a critical component of some semisynthetic β-lactam antibiotics, phenylserine has been a key target for TAs (Table 2-1, entries 80 – 98). A number of L-

TAs yield the desired target from benzaldehyde and glycine, although the diastereoselectivity is incomplete. By contrast, *A. xylosoxidans* D-TA produces the D-*syn*-product with both high conversion and excellent diastereoselectivity (Table 2-1, entry 98). This is one of the more successful uses of TAs in preparative synthesis. Interestingly, the engineered alanine racemase also gives very good D-*syn*-diastereoselectivity in this reaction, although this is tempered by poor fractional conversion (Table 2-1, entries 96 and 97).

A variety of monosubstituted benzaldehydes have been tested as glycine acceptors by a variety of TAs (Table 2-1, entries 99 – 149). In many cases, the *A. xylosoxidans* D-TA affords good diastereoselectivity as does the alanine racemase point mutant. The *P. putida* L-TA also accepts a wide variety of monosubstituted benzaldehydes; however, the diastereoselectivities are generally poor to moderate. The Yamada group published an early study focused on 4-methylthiophenylserine involving the same substrate pair as entries 146 and 147, but employing a low-specificity D-TA from *Arthrobacter* sp. DK-38.[201] Unfortunately, the diastereomeric purity of the product was not reported.

Next to phenylserine itself, 3,4-dihydroxyphenylserine has been the most popular application of TAs in preparative synthesis since this compound has been used to treat Parkinson's disease (Table 2-1, entries 151 – 158). Earlier synthetic routes involved difficult separations of diastereomeric mixtures; the possibility that an enzyme could directly yield only the desired material was a major impetus in exploring TAs as an alternative. Interestingly, some further derivatization of the hydroxyl groups of 3,4-dihydroxybenzaldehyde can be tolerated, for example, 3,4-methylenedioxy or 3,4-

dimethoxy (Table 2-1, entries 160 – 162), but monomethoxy analogs were not accepted by the enzyme.[191, 192]

In 2015, the Goldberg group from Bristol-Myers Squibb used the D-TAs from *A. xylosoxidans* and *Arthrobacter* sp. DK-38 to synthesize (2*R*,3*S*)-2-amino-3-hydroxy-3-(pyridin-4-yl)propanoic acid, a precursor to a developmental drug candidate. The reactions were carried out at 4 ºC with a 10 : 1 molar ratio of glycine : aldehyde. The desired β-hydroxy-α-amino acid precipitated from the solution and was isolated by simple filtration with 99% d.e. and 70% overall conversion (Table 2-1, entry 169 and 170).[200] The use of precipitation to drive the aldol product formation was a simple and elegant solution to the otherwise unfavorable equilibrium problem that also avoids the erosion of diastereoselectivity after extended reaction times.

Other Amino Acid Donors (D-Ala, D-Ser, and D-Cys)

After screening a variety of native TAs, the Griengl group identified two enzymes that accepted more complex amino acids in addition to glycine.[188] Despite forming only L-threonine and analogs when glycine was the donor, the *A. jandaei* enzyme could also accept D-Ala as a substrate. More surprisingly, L-Ala was not accepted. A panel of representative aldehydes was tested as partners for D-Ala, and the results paralleled those observed for Gly with the same aldehydes (Table 2-2). Despite the relatively poor diastereoselectivities (caused by mixtures at the C_β chiral center), these results are significant since a quaternary, non-racemizable center is created at the α-carbon with very high enantioselectivities. This remains a difficult challenge in organic synthesis. In addition to the *A. jandaei* enzyme, a D-TA from *Pseudomonas* sp. also utilized D-Ala and a variety of aldehyde acceptors, albeit with modest diastereoselectivities.

The same pair of aldolases described in the preceding text also accepted D-Ser and D-Cys as nucleophiles in aldol reactions (Tables 2-3 and 2-4, respectively).[188, 198] While neither fractional conversion nor diastereoselectivities were high, the ability to exercise high control over a quaternary α-carbon center is an equally impressive achievement.

Very recently,[ii] Fesko *et al.* searched for more TAs that might have broader amino donor specificity by using the sequences of *A. jandaei* L-*allo*-TA and *Pseudomonas sp*. D-TA to search sequence databases for related proteins. Ten TAs were found with sequence similarities of 55 – 85 % compared to the "bait" genes. Among these, only five showed aldol condensation with D-Ala and D-Ser (Tables 2-2 and 2-3, respectively).[198] These included *A. veronii* L-TA, *S. loihica* L-TA, *R. ornithinolytica* L-TA, *P. aeruginosa* D-TA and *P. protegens* D-TA. Among the most impressive examples were provided by the D-TAs with the *m*-nitrobenzaldehyde and D-Ala (Table 2-2, entries 33 and 34). This gave moderate conversions (>45%) but high diastereoselectivities (>80% for the *syn*-isomer).

Table 2-2. Synthetic applications of threonine aldolases using alanine as the donor

Aldehyde Acceptor	Product	Enzyme	Yield or Conversion	d.e.	Entry	References
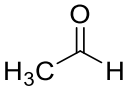	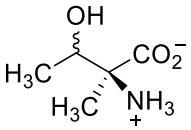	*A. jandaei* L-*allo*-TA	20%	46% (*anti*)	1	188
	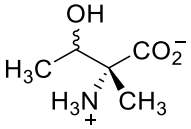	*Pseudomonas* sp. D-TA	54%	42% (*syn*)	2	188

[ii] Not included in the published paper "Chapter 3: Threonine Aldolases" by Sarah E. Franz and Jon D. Stewart, but included here to complete the story of amino donor selectivity of threonine aldolase.

Table 2-2. Continued

Aldehyde Acceptor	Product	Enzyme	Yield or Conversion	d.e.	Entry	References
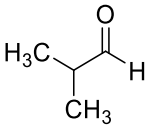	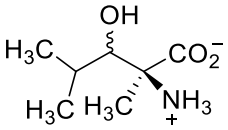	*A. jandaei* L-*allo*-TA	6%	26% (*anti*)	3	188
		A. veronii L-TA	45%	21% (*syn*)	4	198
		S. loihica L-TA	6%	11% (*anti*)	5	198
		R. ornithinolytica L-TA	8%	5% (*anti*)	6	198
	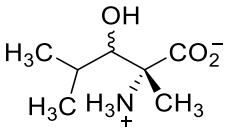	*Pseudomonas* sp. D-TA	32%	66% (*syn*)	7	188
		P. aeruginosa D-TA	29%	60% (*syn*)	8	198
		P. protegens D-TA	21%	17% (*syn*)	9	198
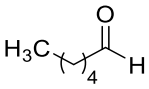	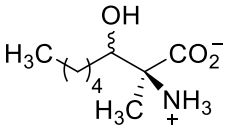	*A. jandaei* L-*allo*-TA	58%	8% (*anti*)	10	188
		A. veronii L-TA	48%	32% (*anti*)	11	198
		S. loihica L-TA	4%	18% (*anti*)	12	198
		R. ornithinolytica L-TA	18%	21% (*anti*)	13	198
	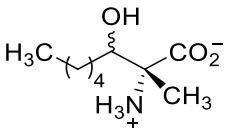	*Pseudomonas* sp. D-TA	84%	33% (*syn*)	14	188
		P. aeruginosa D-TA	55%	13% (*syn*)	15	198
		P. protegens D-TA	30%	16% (*syn*)	16	198
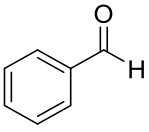	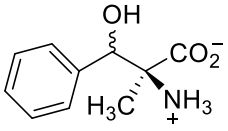	*A. jandaei* L-*allo*-TA	35%	6% (*anti*)	17	188
		A. veronii L-TA	30%	0	18	198
		S. loihica L-TA	10%	74% (*syn*)	19	198
		R. ornithinolytica L-TA	21%	0	20	198
	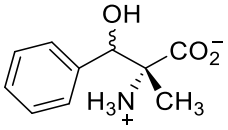	*Pseudomonas* sp. D-TA	11%	65% (*syn*)	21	188

Table 2-2. Continued

Aldehyde Acceptor	Product	Enzyme	Yield or Conversion	d.e.	Entry	References
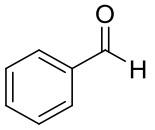	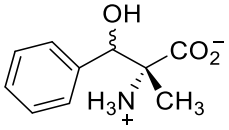	*P. aeruginosa* D-TA	11%	65% (*syn*)	22	198
		P. protegens D-TA	9%	55% (*syn*)	23	198
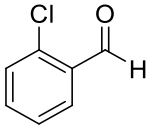	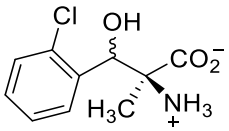	*A. jandaei* L-*allo*-TA	24%	35% (*syn*)	24	188
	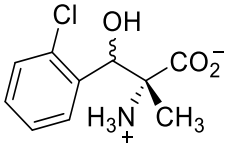	*Pseudomonas* sp. D-TA	21%	95% (*syn*)	25	188
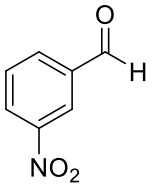	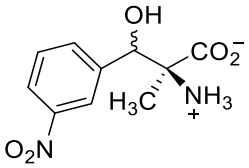	*A. jandaei* L-*allo*-TA	60%	7% (*anti*)	26	188
		A. veronii L-TA	92%	4% (*syn*)	27	198
		S. loihica L-TA	23%	16% (*anti*)	28	198
		R. ornith-inolytica L-TA	64%	40% (*syn*)	29	198
	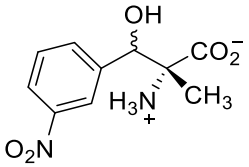	Y265A Ala racemase	12% (24 h)	65% (*syn*)	30	202
		Pseudomonas sp. D-TA	36%	76% (*syn*)	31	188
		Y265A Ala racemase	6% (24 h)	80% (*syn*)	32	202
		P. aeruginosa D-TA	69%	80% (*syn*)	33	198
		P. protegens D-TA	45%	92% (*syn*)	34	198
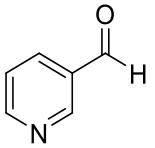	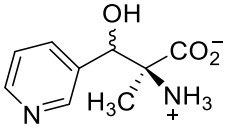	*A. veronii* L-TA	97%	20% (*syn*)	35	198
		S. loihica L-TA	18%	73% (*syn*)	36	198
		R. ornith-inolytica L-TA	52%	12% (*syn*)	37	198

Table 2-2. Continued

Aldehyde Acceptor	Product	Enzyme	Yield or Conversion	d.e.	Entry	References
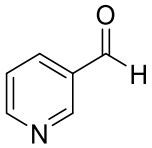	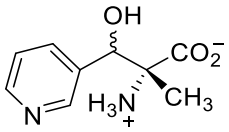	*P. aeruginosa* D-TA	56%	88% (*syn*)	38	198
		P. protegens D-TA	38%	80% (*syn*)	39	198
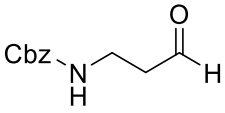	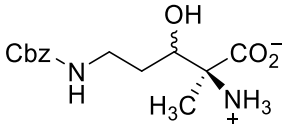	*A. veronii* L-TA	29%	28% (*anti*)	40	198
		S. Ioihica L-TA	10%	36% (*anti*)	41	198
		R. ornith-inolytica L-TA	27%	31% (*anti*)	42	198
	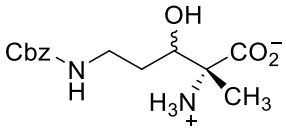	*P. aeruginosa* D-TA	27%	17% (*syn*)	43	198
		P. protegens D-TA	16%	49% (*syn*)	44	198

Note: Alkyl aldehydes are shown first, in the approximate order of increasing size and structural complexity. Aryl aldehydes follow, also in the order of increasing size and structural complexity. When a given reaction has been carried out by more than one threonine aldolase, entries are arranged in the order of increasing *anti*-selectivity, followed by increasing *syn*-selectivity for both L- and D-selective aldolases. n.d., not determined or not reported. d.e., diastereomeric excess = % major diastereomer - % minor diastereomer.

Table 2-3. Synthetic applications of threonine aldolases using serine as the donor

Aldehyde Acceptor	Product	Enzyme	Yield or Conversion	d.e.	Entry	References
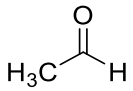	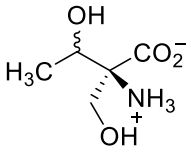	*A. jandaei* L-*allo*-TA	6%	65% (*anti*)	1	188
	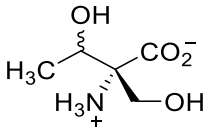	*Pseudomonas* sp. D-TA	23%	11% (*anti*)	2	188
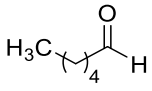	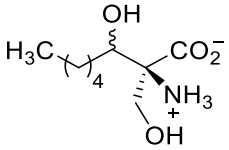	*A. jandaei* L-*allo*-TA	30%	45% (*anti*)	3	188
		A. veronii L-TA	23%	41% (*anti*)	4	198

Table 2-3. Continued

Aldehyde Acceptor	Product	Enzyme	Yield or Conver-sion	d.e.	Entry	References
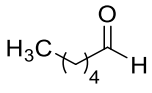	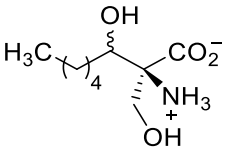	*S. loihica* L-TA	<1%	95% (*anti*)	5	198
		R. ornithinolytica L-TA	6%	53% (*anti*)	6	198
	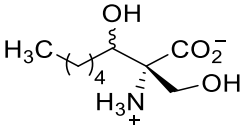	*Pseudomonas* sp. D-TA	43%	24% (*anti*)	7	188
		P. aeruginosa D-TA	11%	2% (*anti*)	8	198
		P. protegens D-TA	8%	9% (*anti*)	9	198
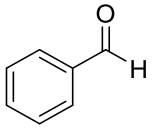	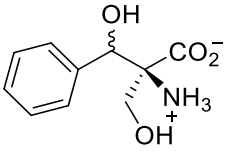	*A. jandaei* L-*allo*-TA	10%	40% (*anti*)	10	188
		A. veronii L-TA	15%	55% (*syn*)	11	198
		S. loihica L-TA	4%	62% (*syn*)	12	198
		R. ornithinolytica L-TA	6%	54% (*syn*)	13	198
	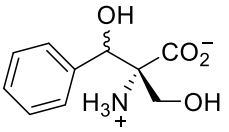	*Pseudomonas* sp. D-TA	<1%	n.d.	14	188
		P. aeruginosa D-TA	n.d.	n.d.	15	198
		P. protegens D-TA	n.d.	n.d.	16	198
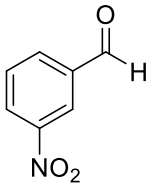	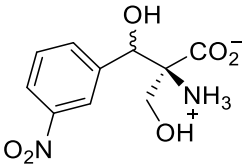	*A. jandaei* L-*allo*-TA	15%	65% (*anti*)	17	188
		A. veronii L-TA	39%	22% (*anti*)	18	198
		S. loihica L-TA	2%	0	19	198
		R. ornithinolytica L-TA	8%	0	20	198
	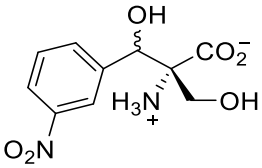	*Pseudomonas* sp. D-TA	<5%	23% (*anti*)	21	188
		P. aeruginosa D-TA	4%	23% (*anti*)	22	198
		P. protegens D-TA	1%	4% (*syn*)	23	198

Table 2-3. Continued

Aldehyde Acceptor	Product	Enzyme	Yield or Conversion	d.e.	Entry	References
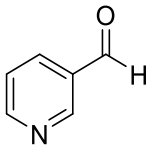	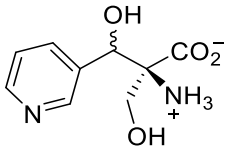	*A. veronii* L-TA	25%	44% (*anti*)	24	198
		S. Ioihica L-TA	5%	80% (*anti*)	25	198
		R. ornith-inolytica L-TA	4%	95% (*anti*)	26	198
	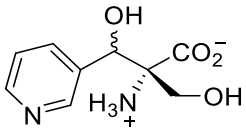	*P. aerug-inosa* D-TA	5%	79% (*anti*)	27	198
		P. protegens D-TA	n.d.	n.d.	28	198
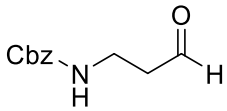	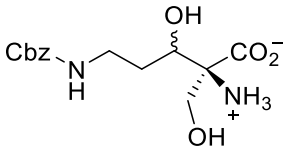	*A. veronii* L-TA	17%	60% (*anti*)	29	198
		S. Ioihica L-TA	n.d.	n.d.	30	198
		R. ornith-inolytica L-TA	4%	95% (*anti*)	31	198
	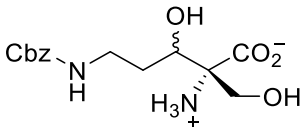	*P. aerug-inosa* D-TA	6%	35% (*anti*)	32	198
		P. protegens D-TA	n.d.	n.d.	33	198

Note: Alkyl aldehydes are shown first, in the approximate order of increasing size and structural complexity. Aryl aldehydes follow, also in the order of increasing size and structural complexity. When a given reaction has been carried out by more than one threonine aldolase, entries are arranged in the order of increasing *anti*-selectivity, followed by increasing *syn*-selectivity for both L- and D-selective aldolases. n.d., not determined or not reported. d.e., diastereomeric excess = % major diastereomer - % minor diastereomer.

Table 2-4. Synthetic applications of threonine aldolases using cysteine as the donor

Aldehyde Acceptor	Product	Enzyme	Yield or Conversion	d.e.	Entry	References
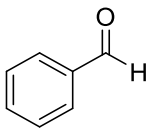	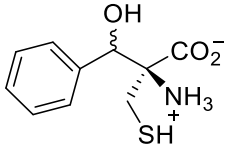	*A. jandaei* L-*allo*-TA	27%	18% (*anti*)	1	188

Table 2-4. Continued

Aldehyde Acceptor	Product	Enzyme	Yield or Conversion	d.e.	Entry	References
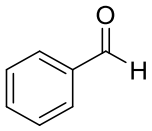	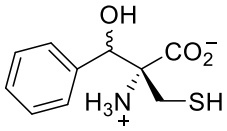	*Pseudomonas* sp. D-TA	33%	20% (*anti*)	2	188
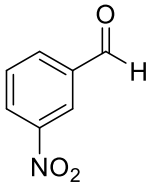	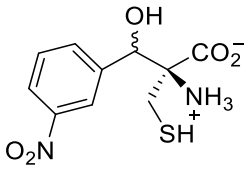	*A. jandaei* L-*allo*-TA	30%	12% (*anti*)	3	188
	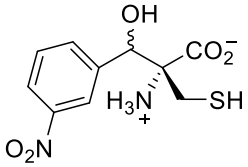	*Pseudomonas* sp. D-TA	39%	6% (*anti*)	4	188

Note: Alkyl aldehydes are shown first, in the approximate order of increasing size and structural complexity. Aryl aldehydes follow, also in the order of increasing size and structural complexity. When a given reaction has been carried out by more than one threonine aldolase, entries are arranged in the order of increasing *anti*-selectivity, followed by increasing *syn*-selectivity for both L- and D-selective aldolases. n.d., not determined or not reported. d.e., diastereomeric excess = % major diastereomer - % minor diastereomer.

Structures of Threonine Aldolases

In addition to the extensive catalytic characterization studies carried out with TAs, our understanding of their structures has also increased in recent years. Several representative crystal structures are known, although some key enzymes used widely for synthesis remain unsolved. Interestingly, L- and D-TAs are structurally and evolutionarily distinct, the former belonging to the aspartate aminotransferase family and the latter to the alanine racemase family. Currently, much more is known about the structures of L-TAs than their D counterparts.

T. maritima L-*allo*-Threonine Aldolase

The first crystal structure of a TA was reported by Kielkopf and Burley in 2001 and 2002 (PDB codes 1JG8 and 1M6S).[205] This is a low-specificity enzyme produced

by a thermophilic organism. Its amino acid sequence is similar to those of several L-TAs that have been applied to chemical synthesis (including those from *A. jandaei*, *E. coli*, *P. aeruginosa*, and *S. cerevisiae*). In addition to the native enzyme, cocrystallized forms with either Gly (PDB code 1LW5) or L-*allo*-Thr (PDB code 1LW4) were also solved. External aldimine formation with either amino acid did not change the overall protein structure apart from a small rotation of the PLP ring. Of the four active sites in the homotetrameric enzyme, two were fully occupied with substrate/product, a third was partially occupied and the fourth showed only the resting form (the internal aldimine, in which the PLP cofactor forms a Schiff's base with a Lys side chain). Whether the diversity of active site occupancies reflects kinetic cooperativity or was an artifact of the crystallization process remains unknown. The β-hydroxyl group of bound L-*allo*-Thr interacted with both an active-site histidine side chain (residue 83) and an ordered water molecule that was in turn hydrogen bonded to the phosphate of PLP. This suggests that the side chain of His 83 might act as a general acid–base group in the catalytic mechanism.

E. coli L-Threonine Aldolase

Safo, Contestabile, and coworkers solved several X-ray crystal structures of the low-specificity L-TA from *E. coli.*[206] The overall structure of the unliganded enzyme (PDB code 4LNJ) was similar to that of the *T. maritima* L-*allo*-TA described above.[205] One key difference is that the active sites of the homotetrameric *E. coli* enzyme are composed of residues that converge from three subunits.[iii] In common with other

[iii] Active sites in most homologues are formed at the dimer interface between two subunits.

enzymes in this family, each monomer consists of two domains with the PLP cofactor located at their interface and bound via a Schiff's base with Lys 197.

Cocrystallizing *E. coli* L-TA with L-Ser yielded a mixture of glycine bound to PLP by a Schiff's base in the active site along with a fraction in which the cofactor was covalently bound to Lys 197 (PDB code 4LNM).[206] External aldimine formation did not change the overall protein structure, although the PLP ring rotated slightly within the active site, a phenomenon observed previously in other PLP-dependent enzymes. When *E. coli* L-TA was cocrystallized with L-Thr (PDB code 4LNL), one active site contained the glycine/PLP covalent complex and the other contained a mixed population of this species along with a mixture of PLP covalently bound to L-Thr and L-*allo*-Thr. Importantly, the side-chain hydroxyl groups of both amino acids were located in the same position; their respective methyl groups occupied different locations. This has important ramifications for the catalytic mechanism since the aldol/retro-aldol reaction involves direct acid–base interactions with this functional group. It also suggests ways to modify the active site to enhance β-carbon stereoselectivity.

The β-hydroxyl group makes hydrogen bonds with both His 83 and His 126, suggesting that these might play a role as general acid/base catalysts. Surprisingly, the mutation of either His 83 or His 126 alone was tolerated by the enzyme, although some variants at these positions were unstable and precipitated after extended storage. Moreover, replacing His 126 with Asn or Phe actually increased k_{cat} values by up to three-fold, although compensating changes in K_M blunted the impact somewhat. These results argue against a direct acid–base role by either His side chain, which was further supported by the retention of some catalytic activity in a double His 83/His 126 variant.

At this time, the identity of the group responsible for β-hydroxyl protonation/ deprotonation remains a mystery.

Two replacements were also made for Phe 87, which had been proposed to be a key determinant of substrate specificity. The properties of both the Ala and Asp mutants were not in accord with predictions, leaving this as another open issue. The authors also pointed out that the active site is much larger than needed to accommodate the relatively small substrate acetaldehyde. Furthermore, L-*allo*-Thr is not a recognized metabolite in *E. coli*. It is therefore possible that the true physiological role of this enzyme—despite its being named "L-threonine aldolase"—may actually involve different (and possibly multiple) substrates in the native host rather than Thr and/or *allo*-Thr.

A. jandaei L-*allo*-Threonine Aldolase[iv]

In 2014, Tanokura, Shimizu, Kawabata, and coworkers solved the crystal structure of both the wild type enzyme and the H128Y/S292R variant of the L-*allo*-TA from *A. jandaei* DK-39 (PDB codes 3WGB and 3WGC, respectively).[207] The overall structure of this aldolase and its mutant variant are similar to the other two structures that were highlighted earlier.[205, 206] The TA family has been reported as homotetramers and function as catalytic dimers by forming interfaces between the two large domains. The most important and conserved active site residues in the TA family are Ser 8, His 85, Arg 171, Lys 199, and Arg 313. The amino acid residues Arg 171, Arg 313, and Ser 8 anchor the substrate/product to the active site by interactions between the aldimine and the amino acid side chains. The side chain of Lys 199 forms the Schiff's base with

[iv] Not included in the published paper "Chapter 3: Threonine Aldolases" by Sarah E. Franz and Jon D. Stewart, but included here to complete the story of the structure of threonine aldolase.

PLP and any mutations at this site render the enzyme inactive.[189] Finally, His 85 is responsible for the regulation of the degree of stereospecificity between the L- and L-*allo*-stereomers and pi-stacks with the pyridinium ring of PLP to help stabilize the active site.[205-207]

The noteworthy differences between the wild type enzyme and the H128Y/S292R double mutant occurred between Ala 123 and Pro 131. When His 128 was mutated to Tyr, the residue's side chain moved 4.2 Å out of the active site.[207] The electron-density map for the residue at position 292 in both the wild type and mutant structures was poor and therefore could not confirm how this position differed.

The L-*allo*-TA from *A. jandaei* prefers the substrate L-*allo*-Thr to that of L-Thr with k_{cat}/K_M values of 26.9 $mM^{-1}s^{-1}$ and 0.00203 $mM^{-1}s^{-1}$, respectively (Table 2-5). The double mutation H128Y/S292R presented a three-fold and 322-fold increase in k_{cat}/K_M towards L-*allo*-Thr and L-Thr, respectively (compared to the wild type enzyme). Additionally, the single mutations at these two positions showed similar k_{cat}/K_M towards L-*allo*-Thr, however the H128Y mutant exhibited a higher increase in k_{cat}/K_M toward L-Thr than the S292R mutant, supporting the notion that the mutation of His 128 to Tyr was likely the site of improved activity. The enhanced activity for the S292R mutant could not be explained due lack of structural information at the distorted loop where the position resides.

Table 2-5. Kinetic parameters for L-*allo*-threonine aldolase from *A. jandaei* and its mutants

	L-*allo*-Thr			**L-Thr**		
Enzyme	**k_{cat} (s^{-1})**	**K_M (mM)**	**k_{cat}/K_M (mM^{-1} s^{-1})**	**k_{cat} (s^{-1})**	**K_M (mM)**	**k_{cat}/K_M (mM^{-1} s^{-1})**
Wild Type	13.8	0.513	26.9	0.641	31.6	0.00203
H128Y/S292R	22.0	0.386	83.3	2.140	3.27	0.65400
H128Y	16.5	0.402	41.0	1.810	4.48	0.40400
S292R	18.3	0.444	41.2	0.913	32.7	0.02790

Note Reference: Qin *et al.* 2014

The side chain of His 128 (along with that of His 85) was found to be in hydrogen bonding distance to recognize the hydroxyl group on L-*allo*-Thr and explains why this enzyme prefers L-*allo*-Thr as the native substrate. Surprisingly, Qin *et al.* discovered that when this residue was mutated to a Tyr, the residue moved 4.2 Å outwards from the active site to form a new hydrogen bond with Val 31, expanding the active site and explaining why this mutation has broad substrate stereoselectivity. To confirm this, they carried out site saturation mutagenesis of His 128 and discovered that only a few amino acid substitutions (*i.e.* Tyr, Phe, and Met) resulted in an improved activity towards L-*allo*-Thr.[207] On the other hand, replacement by Tyr, Phe, Leu, Ser, Met, Trp, Ile, Lys, and Val resulted in an increased activity towards L-Thr as compared to the wild type enzyme. Most hydrophobic substitutions showed an increased activity towards L-Thr due to the hydrophobic interactions between the residue's side chains and methyl group of L-Thr. Overall, the mutant that showed highest activity towards both L-*allo*-Thr and L-Thr was H128Y.

A. xylosoxidans D-Threonine Aldolase[v]

Very recently, Gruber, Schürmann, and coworkers crystallized the very first D-TA from *A. xylosoxidans* (PDB code 4V15).[208] In order to improve crystal quality, they methylated the D-TA by the selective lysine methylation method established by Rayment in 1997[209] that successfully enhanced the quality of the crystals from 3.5 Å to well under 2 Å resolution. Interestingly, there was no indication of methylated lysines in the electron density, showing the improvement was a "stabilizing side effect" due to some process during the methylation. Based on homology models, D-TAs belong to the

[v] Not included in the published paper "Chapter 3: Threonine Aldolases" by Sarah E. Franz and Jon D. Stewart, but included here to complete the story of the structure of threonine aldolase.

alanine racemase family (type III fold)[210] which differs from that of L-TAs, indicating a different evolutionary origin.

Unlike L-TAs, the presence of divalent ions (particularly manganese) for aldolase activity in D-TAs is crucial.[7, 211] In the structure of *A. xylosoxidans* D-TA, a Mn^{2+} ion was modeled into the ion binding site located relatively close to PLP. The octahedral coordination sphere of the Mn^{2+} ion was coordinated by two amino acid residues, His 347 and Asp 349, and four water molecules. The Mn^{2+} ion binding site was located 5 Å from the aldehyde group of PLP and nearly coplanar with the pyridinium ring of the cofactor. The role of the Mn^{2+} ion was determined by modeling (2*R*,3*S*)-phenylserine as an external aldimine and the ion was found to coordinate with the β-hydroxyl group of the substrate with a Mn-O distance of 2.3 Å, replacing a water molecule that is typically coordinated to the metal in the active site.

The overall structure of *A. xylosoxidans* D-TA is completely different from that of L-TAs;[205-207] however, the proposed mechanism for D-TAs derived from this crystal structure is similar to that of L-TAs. The only noteworthy difference between the mechanisms is the use of the Mn^{2+} ion by D-TA's as a replacement for the second His residue in L-TAs. Both of these components interact with the β-hydroxyl group of the substrate. Although the overall structures are unalike, D-TAs and L-TAs are classified as enantio-complementarity enzymes, which by definition are enzymes that fold differently, but whose active sites are mirror images.[212] In this case, they both include the active site His that deprotonates the hydroxyl group of the substrate, but the His residue in D-TA is positioned at the *re*-face of PLP and His residue in L-TA is positioned at the *si*-face.

Other Threonine Aldolase Structures

In addition to the more complete studies described in the preceding text, several other TA crystal structures have been solved as part of structural genomics projects with little or no additional data available. One example from *Leishmania major* was reported in 2011 (PDB code 1SVV). A second example was described in 2010, a TA from *Listeria monocytogenes* EGD-E (PDB code 3PJ0). No published synthetic applications of these enzymes have appeared in the literature as of late 2017. Very recently, Hirato *et al.* successfully crystallized the D-TA from *Chlamydomonas reinhardtii* at a 1.85 Å resolution and they are currently solving the structure.[213] The final structural entry, which lacks a formal literature citation, is the phenylserine aldolase from *P. putida* (PDB code 1V72).

Protein Engineering Studies of Threonine Aldolases

Recent years have witnessed significant improvements in protein engineering methodologies, high-throughput screening, and selections along with structure determination using X-ray crystallography. These developments have made it possible for even smaller academic laboratories to undertake protein mutagenesis projects aimed at improving the performance of biocatalysts in synthetic applications. Surprisingly, only a relatively few examples where these techniques have been applied to TAs have been published as of late 2017, and these are summarized in the succeeding text.

The selection and/or screening methodology dictates the number of variants that can be screened, and this is nearly always the limiting factor in protein engineering studies. In cases where L-Thr is the desired product, enabling growth of a Thr auxotroph in minimal medium can be used to select the desired variants. Even when

substrates beyond L-Thr itself are targeted, this can be a useful "prescreen" since it can easily be applied to libraries containing up to 10^{10} variants.[vi] The danger is that the best mutant for a novel conversion may have lost the ability to accept glycine and/or acetaldehyde and would therefore be missed in such a native activity "prescreen." It is also more challenging to devise growth-based high throughput assays that directly interrogate stereoselectivity (both enantioselectivity and diastereoselectivity) without resorting to GC or HPLC analyses. In such cases, library sizes are practically limited to <1000 members unless pooling/deconvolution strategies are employed.[214]

Improving Catalytic Activity

Lee and coworkers devised a growth-based selection for TAs with greater catalytic efficiencies based on the observation that aldehydes such as acetaldehydes depress the growth rate of *E. coli*.[215] In the synthetic direction, TAs consume aldehydes; by depleting the local medium of the toxic substrate, transformed *E. coli* cells grow at correspondingly faster rates (positive selection). In principle, this is a generally applicable strategy that should allow the most active TA variants to predominate. The authors also considered a negative selection based on an analogous strategy (using the acetaldehyde from Thr degradation to inhibit cell growth). Unfortunately, this proved impossible to implement in practice since the levels of acetaldehyde never rose to toxic levels.

The positive selection strategy was applied to *P. aeruginosa* L-TA with the goal of increasing its catalytic efficiency.[215] Error-prone PCR yielded a library of *ca.* 20,000 colonies that were grown in the presence of 20 mM acetaldehyde under conditions

[vi] In these cases, the library size is limited primarily by transformation efficiency.

where the cloned TA variants were overexpressed. The initial selection provided ten hits, and plasmid DNA was isolated from each. After retransformation, five of the ten plasmids retained the ability to confer high level acetaldehyde resistance and these were further characterized. The best variant exhibited a two-fold improvement in catalytic activity as compared to the wild type.

Despite the relatively modest impact on catalytic activity, the selection method devised in this study may be useful in other protein engineering studies. In cases where expanded substrate range is desired, supplementing the growth medium with both acetaldehyde and the amino donor might allow one to identify the desired variants.[vii] This selection scheme should also be applicable to other aldehyde acceptors, although the precise concentrations needed for cell toxicity will need to be established empirically for each substrate.

Improving Thermostability

As described previously, the stereoselective synthesis of 3,4-dihydroxy-phenylserine has been an important synthetic application for TAs. Baik and coworkers cloned and expressed an L-TA from *S. coelicolor* A3(2) as the basis for their strategy.[8] While the wild type enzyme provided an acceptable reaction rate and stereoselectivity, its longevity under process conditions was too low for practical use. Error-prone PCR was therefore used to introduce random changes throughout the entire length of the protein. Approximately, 15,000 clones were individually screened for the ability to degrade L-Thr after a 65 ºC heat treatment step (using a colorimetric assay for the

[vii] In practice, it may also be necessary to reduce glycine levels to favor reaction with the amino donor of interest. This can be accomplished by employing a stringent glycine auxotroph and supplementing the growth medium with limiting concentrations of glycine. Hilvert and coworkers have developed one example of a glycine auxotrophic host strain that might be useful in this strategy. 216.Giger, L.; Toscano, M. D.; Bouzon, M.; Marliere, P.; Hilvert, D., *Tetrahedron* **2012,** *68* (37), 7549-7557.

acetaldehyde by-product). This search yielded eight variants that appeared to be more thermostable than the wild type enzyme; four were chosen for additional studies. All four had only single amino acid changes and all four changes were unique. The best mutant (H177Y) retained 86% of the original activity after 20 min at 60 ºC; under similar conditions, the wild type retained only 11%. Importantly, greater thermostability was not achieved at the expense of catalytic activity, and the H177Y variant had essentially the same steady-state kinetic values as the parent protein. In whole-cell format, the improved variant performed at the same level for 20 successive batch reactions and provided a final product concentration of 4 g/L.

Because the targeted level of enzyme improvement was reached after one generation of mutagenesis and selection, the beneficial mutations were not examined combinatorically nor were additional random mutations added to the best first-generation variants. In the absence of data, one must speculate as to whether the observed thermostabilities are the best that can be reached. The major drawback to the final process is that the molar yield of the final product was only 0.7%, based on the aldehyde added (glycine was present in vast excess).

Wieteska and coworkers used site-directed mutagenesis at the interchain interface of *T. maritima* L-*allo*-TA[viii] to improve its thermostability. These efforts were based on the crystal structure reported by Kielkopf *et al*.[205, 217] They targeted sites that allowed for additional salt bridges or new intrachain disulfide bonds. Among the ten predicted thermostable mutants, only two actually showed increased thermotolerance

[viii] Not included in the published paper “Chapter 3: Threonine Aldolases” by Sarah E. Franz and Jon D. Stewart, but included here to complete the story of the improving thermostability of threonine aldolase.

(P56C and A21C). The P56C mutation increased stability by 10 – 15% on average with no loss in activity.[217]

Improving Stereoselectivity

Enzymes are by nature homochiral catalysts, and the ability to direct reactions into single product enantiomers is one of their most important attributes. As noted previously, TAs create two adjacent stereocenters, and as a general rule, these enzymes are highly selective at the α-carbon. By contrast, they often have relatively lower diastereoselectivity, which is manifest by a mixture of configurations at the β-carbon. Reversibility also plays a role in governing stereoselectivity. For any chiral center, a racemic mixture is always the thermodynamic minimum. When more than one stereocenter is present (as is the case for TAs), a diastereomeric mixture of enantiomers nearly always occurs at equilibrium. While the precise composition depends on the actual product structure, it is rare that a single diastereomer predominates at equilibrium for most synthetically interesting targets. For these reasons, it is almost always essential that preparative reactions be carried out under kinetically controlled conditions and the reverse (retro-aldol) reaction should be avoided as much as possible. The main drawback is that the yield of the desired product is almost always low when reactions are limited to far-from equilibrium conditions.

Several years ago, the Griengl group carefully analyzed the properties of representative TAs.[204] This study included members of all four available classes: high-specificity L-Thr, L-*allo*-Thr, and D-Thr types and a low-specificity L-Thr type. The formation of phenylserine from glycine and benzaldehyde was chosen as the model system. As expected, all four TA types yielded the same thermodynamic mixture of products (60 : 40, *syn* : *anti*) after extended reaction times. Of the four classes, only the

high-specificity D-TA provided high diastereoselectivity under kinetic conditions in the early phase of the reaction; the rest gave mixtures of products from the start. Interestingly, the high-specificity D-TA reached the equilibrium product mixture only after five days (compared to ≤5 h for the other three aldolase types). This observation is critical since it demonstrates conclusively that high diastereoselectivity combined with good product yield is possible using TAs. Put another way, Griengl's study showed conclusively that rapid β-carbon epimerization is not an intrinsic flaw of TAs. This implies that the problem can be removed from other TAs using the appropriate protein engineering.

Griengl and coworkers subsequently carried out an NMR study to understand why some TAs catalyzed rapid product epimerization at the β-carbon while others did not.[204] ^{13}C-Labeled *syn*-product was mixed in a 60 : 40 ratio with unlabeled *anti*-product in the presence of glycine, benzaldehyde, and enzyme that matched their equilibrium values. Based on the known chemical mechanism for TAs, the relevant species can be deduced (Figure 2-3). Both β-carbon epimerization and the back-reaction to free glycine proceed *via* the cofactor-stabilized anion that results from retro-aldol cleavage of the *syn*-product external aldimine. The NMR study yielded the relative rates of ^{13}C label transfer from the *syn*-product to the *anti*-product and to free glycine, which can also be described as the partition ratio for the cofactor-stabilized anion. In comparing data from the four TAs, three yielded partition ratios ranging from 0.5 to 20 (epimerization/back-reaction). As expected, these values correlated with the initial diastereoselectivities of the reactions. Because it was not possible to measure microscopic rate constants under the experimental conditions, the relative net rate constants could not be further

decomposed into the individual contributions from the multiple steps that occur in each branch. It might be possible to measure the relative contributions of proton transfer steps and aldehyde binding/release by incorporating additional isotopic labels. This would provide extremely valuable guidance for future protein engineering studies by focusing the improvements on the most relevant step(s) in the reaction pathway.

Introducing and Optimizing Threonine Aldolase Activity into a Novel Scaffold

In 2003, the Hilvert group reported that a single amino acid substitution was sufficient to convert a PLP-dependent alanine racemase from *G. stearothermophilus* into a TA.[218] The specific mutation (Y265A) was designed to allow a histidine side chain (His 83) to act as an acid–base group for oxyanion protonation/deprotonation in the aldol reaction. In addition, the smaller Ala side chain created additional active site volume to allow larger substrates to bind. While the catalytic activity was relatively modest when assessed against the standard glycine/benzaldehyde benchmark reaction, the mutant was more than five orders of magnitude more efficient than the starting racemase. The mutant enzyme was also highly selective for the D-configuration at the α-carbon. The preference, if any, for β-carbon stereochemistry, was not reported.

In a follow-up study, the ability of the Y265A mutant to accept α-methyl substrates was assessed.[219] This is an important application since aldol condensations that yield quaternary centers remain particularly challenging. Steady-state kinetic constants were measured for three substrates (Figure 2-4). Interestingly, the steady-state kinetic values for α-hydrogen and α-methyl (2*R*,3*S*)-diastereomers were very similar, implying that steric bulk at the α-carbon was well tolerated. This may be a consequence of the evolutionary heritage of the enzyme, which originally bound Ala.

The D-*anti* analog had a *ca.* ten-fold lower k_{cat} value, but K_M was also decreased by a similar extent so that the k_{cat}/K_M ratio was nearly the same. Given the large number of microscopic rate constants in the catalytic cycle of TAs, it is very difficult to determine which individual step(s) was impacted and a deeper understanding will require future pre-steady-state kinetic investigations.

To support future protein engineering studies, the Hilvert group recently developed a new growth-based selection system for TAs.[216] Rather than target Thr, their strategy uses an engineered *E. coli* strain with four simultaneously inactivated genes essential for glycine biosynthesis. This "clean" glycine auxotroph can only grow in minimal medium when supplemented with the amino acid or when retro-aldol activity by a cloned TA yields glycine. The advantage of this selection is that the substrate of interest can be directly interrogated. This includes selection for stereoselectivity if a diastereomerically pure Thr analog added to the growth medium. The systems' only limitation is that glycine must be the amino acid partner in the aldol/retro-aldol reaction. The utility of this screen was demonstrated by creating a library of simultaneous random amino acid replacements at four positions in a previously uncharacterized L-TA from *Caulobacter crescentus* CB15. The data revealed that only one of the four amino acids (His 91) was absolutely essential for catalytic activity.

Conclusions and Future Work

TAs have been clearly established as useful catalysts for asymmetric organic synthesis. Their ability to control the stereochemistry at the α-carbon is excellent and they accept a diverse array of acceptor aldehydes. On the other hand, these enzymes have several drawbacks that must be overcome before they can be employed routinely. The lack of stereochemical control at the β-carbon is a significant problem that detracts

from synthetic utility. As Griengl's work has shown, it is possible to decouple C_β epimerization from retro-aldol cleavage. Enhancing these properties is an obvious target for protein engineering efforts. The establishment of several selection/screening methodologies for TAs should simplify these studies.

The other major drawback of TAs is that high substrate concentrations are usually needed to drive the conversion to products (and avoid equilibrating conditions that erode diastereomeric purities). While glycine is inexpensive, many aldehydes of synthetic interest do not share this trait and this practically limits the range of usable substrates. One possibility is to employ coupled enzyme systems that further convert the aldol product in an effectively irreversible reaction, for example, by lipase-mediated acylation or redox conversions. Similar strategies have proven quite useful in transaminations and may provide inspiration to this field as well.[220]

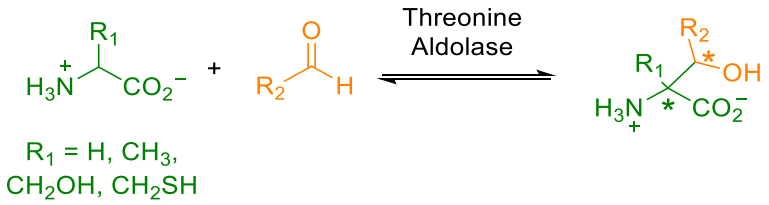

Figure 2-1. Aldol condensation with threonine aldolase

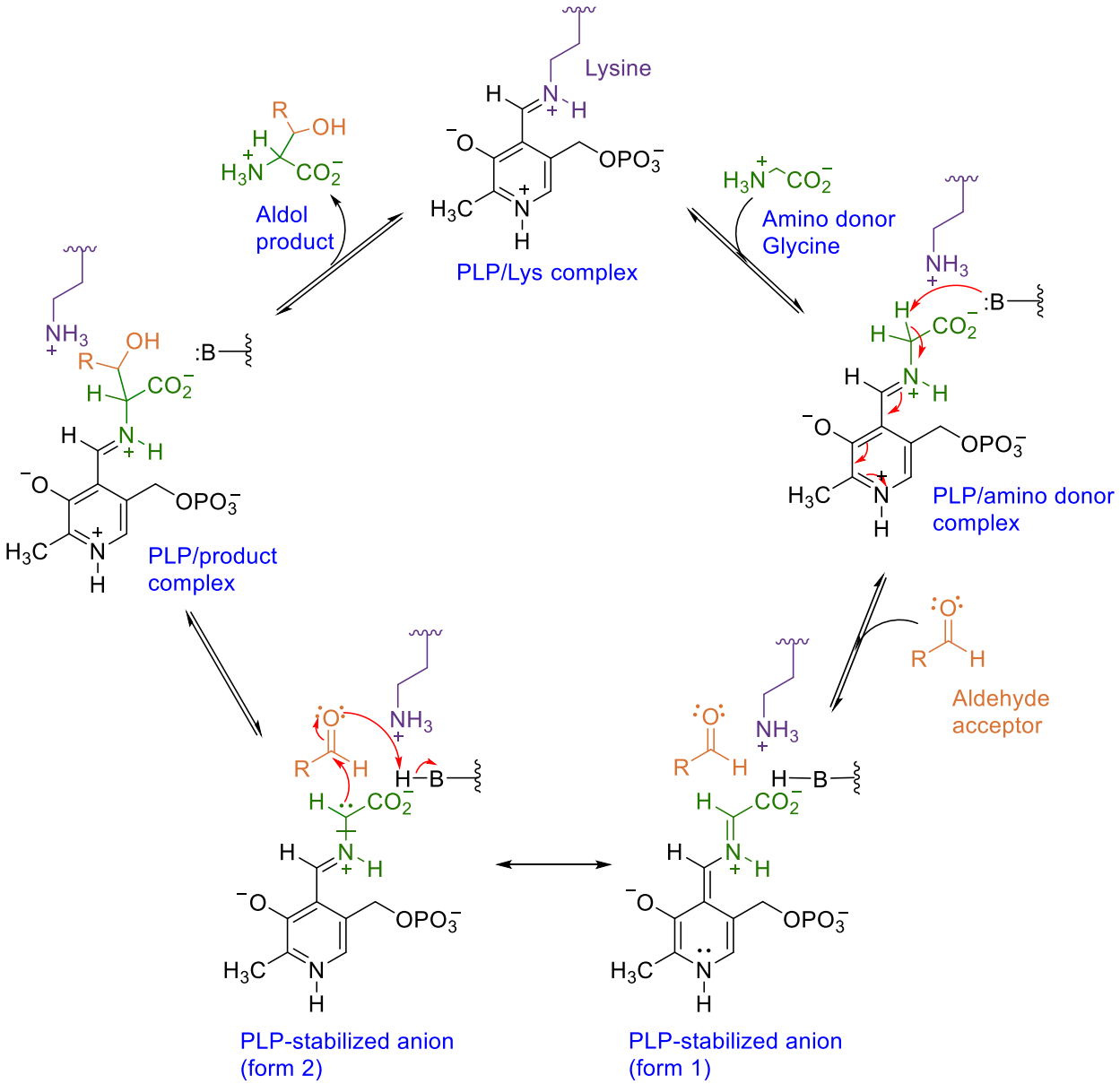

Figure 2-2. Mechanism of threonine aldolase

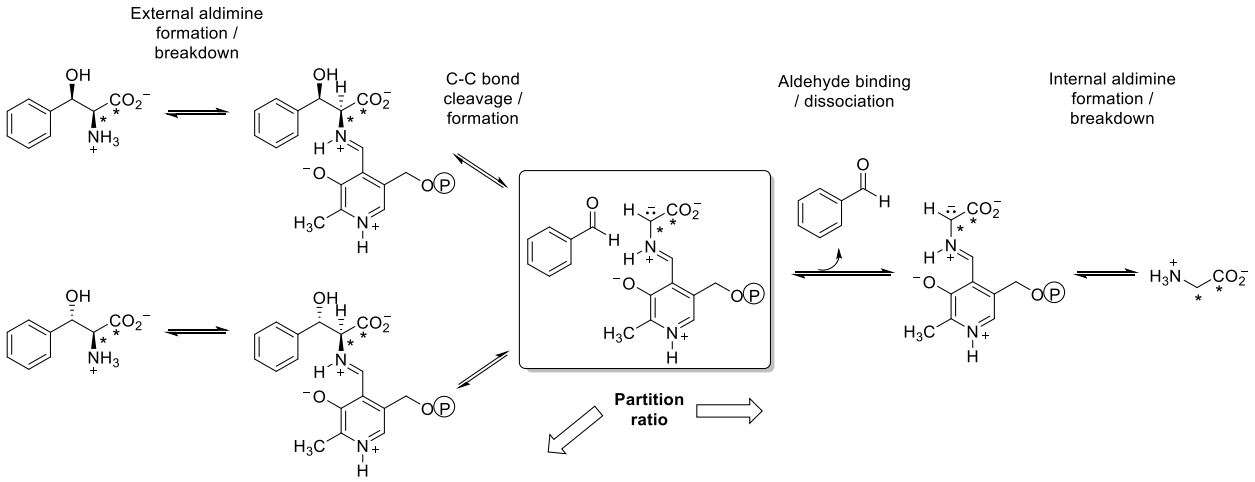

Figure 2-3. Threonine aldolase kinetic pathway

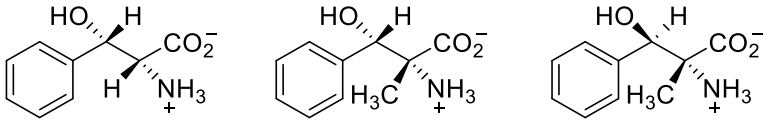

	(2R,3S)	(2R,3S)	(2R,3R)
	D-*syn*	D-*syn*	D-*anti*
k_{cat}	5.7/min	2.8/min	0.16/min
K_M	8.5 mM	2.8 mM	0.14 mM

Figure 2-4. Aldol products from a mutant Ala racemase

CHAPTER 3
SUBSTRATE PROFILING OF THREE THEONINE ALDOLASES

Introduction

β-Hydroxy-α-amino acids comprise an important class of natural products that often serve as building blocks for antibiotics such as vancomycin[1], polyoxin A[2], and rhizobitoxine[6]. Several pharmaceuticals also incorporate these building blocks, most notably droxidopa (L-*threo*-3,4-dihydroxyphenylserine, L-DOPS), an important therapy for Parkinson's disease whose ability to cross the blood-brain barrier is the key to its effectiveness.[7, 8] D-Glucosaminic acid (2-amino-2-deoxy-D-gluconic acid), produced by *Aeromonas oxydans*, can act as an artificial sweetener.[221] More recently, D-glucosaminic acid has been found useful as a building block for several glycosidase inhibitors, such as (2*S*,4*S*,5*R*)-4,5,6-trihydroxynorleucine.[12, 13]

Many strategies for synthesizing β-hydroxy-α-amino acids in optically pure form have been devised. Chemical approaches include a chiral glycine enolate[14], Sharpless dihydroxylation, epoxidation, aminohydroxylation[15-17] and *aza*-Claisen rearrangements of allylic acetimidates[18] among others. The target compounds can also be prepared by enzymatic aldol additions of glycine to aldehydes using threonine aldolases (TAs) (Figure 3-1).[184, 222, 223] These PLP-dependent enzymes feature an active site lysine[7] that forms a Schiff's base with the cofactor in the resting state of the enzyme that subsequently acts as a general base during the catalytic cycle. In general, TAs are nearly specific for glycine as the nucleophile, although some exceptions have been noted, *e.g.* L-Ala, L- Ser and L-Cys.[184, 188, 189, 198, 222, 223] By contrast, TAs tolerate a wide variety of aldehyde acceptors, ranging from long chain aliphatic aldehydes to

substituted benzaldehydes and heteroaromatic aldehydes.[184, 222, 223] It is this latter property that has generated interest in using TAs for preparative synthesis.

While a large number of aldehydes have been tested as substrates for TAs, much substrate spectrum remains to be explored. One goal of this study was to better define the substrate range and stereoselectivity of three key family members, *Aeromonas jandaei* L-*allo*-threonine aldolase (L-*allo*-TA), *Escherichia coli* L-threonine aldolase (L-TA) and *Thermotoga maritima* L-*allo*-threonine aldolase (L-*allo*-TA). A second important goal was to develop general methods for isolating the aldol products from these reactions, which would make TAs much more useful for preparative synthesis. In a few favorable cases, the β-hydroxy-α-amino acid precipitates in nearly pure form from the reaction mixture;[224] however, this is not generally the case and instead, a highly polar product must be isolated from an aqueous mileu that also contains buffers, salts, proteins and (usually) a large excess of glycine.

Reactions catalyzed by TAs are readily reversible and a large excess of glycine is often used to favor the desired aldol conversion. Unfortunately, this seriously complicates product isolation since two α-amino acids with similar ionic properties are simultaneously present in the reaction mixture (glycine and the desired β-hydroxy-α-amino acid product). We sought to overcome this problem by selective degradation of glycine after the completion of the aldol reaction. To the best of our knowledge, this strategy has not been explored previously. Glycine oxidase is an FAD-dependent enzyme that oxidatively deaminates glycine to yield glyoxalate (Figure 3-2). Enzymes of this family are involved in thiamin pyrophosphate biosynthesis and are also important in degrading the herbicide glyphosate.[225, 226] For this study, we chose glycine oxidase

from *Bacillus subtilis* since it has been cloned, overexpressed in *E. coli* and screened against a wide range of amino acids.[227, 228] *B. subtilis* glycine oxidase accepts only Gly and small D-amino acids. Its substrate selectivity is therefore orthogonal to the product spectrum of threonine aldolases, which would allow it to be added directly to a TA reaction mixture with no possibility of degrading the desired aldol product.

The reversibility of TA-catalyzed reactions has serious, negative consequences on stereoselectivity. While control of the α-carbon configuration is essentially complete, prolonged reaction times often lead to erosion of stereopurity at the β-carbon. This loss of stereochemical integrity is a complex interplay of enzyme, substrate and reaction conditions. For this reason, we chose several representative TAs and two time points in order to identify combinations that afforded both high product concentrations and high diastereoselectivities.

Results and Discussion

Gene Cloning and Protein Overexpression

Genes encoding the three required TAs were obtained by colony PCR[229] (*E. coli* L-TA and *T. maritima* L-*allo*-TA) or by chemical gene synthesis (*A. jandaei* L-*allo*-TA). Each was individually ligated into pET-15b and the resulting plasmids were used to transform the *E. coli* overexpression strain BL21-Gold(DE3). All TAs were efficiently overproduced by the recombinant strains, which allowed crude lysates to be employed for screening reactions. Control reactions were carried out for each aldehyde substrate with a crude extract from an un-transformed *E. coli* strain; none gave significant aldol product.

Derivatization of Amino Acids for Analysis

In order to analyze the overall conversion and diastereomeric excess of the natural products as they are being synthesized, we worked through a series of analytical techniques for derivatizing amino acids for GC/MS or HPLC detection. The challenge was that we not only needed to detect the presence of the products, but also separate the diastereomers. We first employed a technique used by Khuhawar *et al.* using trifluoroacetylacetone (Figure 3-3a); however, there was no detection of L-Thr and its diastereomer L-*allo*-Thr using this strategy.[230] Our next approach was to deploy the standard OPA/NAC method (Figure 3-3b) established by Nimura and Kinoshita in 1986 and used in most TA papers.[231-233] Although derivatization was a success, Thr and Gly derivatives were close in retention time to each other. Since Gly is used in a five times molar excess in the reactions, separation would have been an issue. The bigger reason for finding another derivatization method was that the derivatized amino acids were analyzed by HPLC and since we planned to screen over a dozen substrates, the lack of an auto-sampler would have made analysis tedious. Therefore, we sought for a derivatization method that allowed for GC/MS analysis since an autosampler was readily available in our lab.

N-Methyl-*N*-(trimethylsilyl) trifluoroacetamide (MSTFA) derivatization was first established in the late 1960's by Donike,[234] but not used on amino acids until the 1990's by Yoon (Figure 3-3c). Since the late 1960's, MSTFA has been used in the silylation of numerous compounds such as phenolics, sterols, and sugars.[234-236] The original protocol allowed for three evaporation events to ensure samples were completely free from water, including the removal of the original solvent system, addition and removal of 80% MeOH, and lastly addition and removal of methylene chloride. This monotonous

evaporation protocol was explored and optimization revealed that evaporation under speed vacuum was only required one time to remove the original solvent system. The derivatization conditions required 70 µL of MSTFA and 40 µL of dried pyridine for every 5 – 20 nmol of amino acid at 37 ºC and vigorous shaking (250 rpm) for 30 minutes. However, since MSTFA is somewhat expensive and pyridine is toxic, we fine-tuned the quantities of both derivatization reagents. Optimization revealed that only 50 µL of MSTFA and 1 µL of dried pyridine were required for derivatization. The derivatization techniques explored are summarized in Figure 3-3.

Additionally, it was possible to detect un-derivatized Gly and amino acids products by thin layer chromatography (TLC) with a ninhydrin stain.[197] Ninhydrin reacts with primary amines, so this was an obvious method for the detection of amino acids. This method was only used as an initial detection of product formation and subsequent MSTFA derivatization was required for conversion and selectivity values.

Optimization of Reaction Conditions

Prior to carrying out extensive aldehyde screening studies, we used the DOE methodology to identify optimal conditions for each of the three overexpressed TAs. Based on previous literature, the starting point was 25 ºC, pH 8 and a 5-fold molar excess of glycine *versus* the aldehyde. Variations of each of these three parameters were investigated: reaction pH (5, 7, 8, 9.7 and 12), reaction temperature (4 ºC, 18 ºC, 25 ºC, 37 ºC and 42 ºC) and the glycine : aldehyde ratio (2, 4, 8, and 10). A total of 92 individual reactions were carried out for each enzyme – substrate pair and both relative conversion and product diastereomeric excess values were determined for each. Aldehydes chosen to optimize each enzyme gave measurable, but incomplete

conversions under standard conditions; this allowed both improved and detrimental changes to the reaction conditions to be identified.

For *A. jandaei* L-*allo*-TA, reactions involved glycine and aldehyde **10** (Table 3-1). The starting conditions gave a relative conversion[i] of 0.11 using a 10 : 1 ratio of glycine : aldehyde. Conversion increased significantly as pH, temperature and substrate molar ratio were increased. Solving for the optimal conditions (pH 9.7, 37 ºC and a glycine : aldehyde ratio of 10) gave a relative conversion of 0.68, more than a 6-fold improvement. In addition, an 87% d.e. was obtained, underscoring the power of this process improvement strategy.

The outcomes of reactions catalyzed by *E. coli* L-TA and *T. maritima* L-*allo*-TA were also improved by the DOE strategy, albeit more modestly. These studies involved aldehydes **6** and **10**, respectively (Table 3-1). The *E. coli* enzyme performed best under the same conditions as its *A. jandaei* counterpart while the *T. maritima* enzyme required slightly higher pH value of 12.

Table 3-1. Substrate specificity of L-TA-catalyzed aldol reactions

Entry	Aldehyde	Product	Enzyme[a]	Reaction Time (hr)	Conversion[b] (%)	d.e.[a] (%)
1	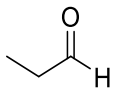 **1**	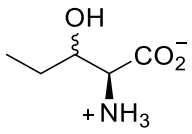	A	4	22	99
				20	28	99
			B	4	<5[c]	--[c]
				20	6	99
			C	4	<5[c]	--[c]
				20	13	99

[i] Relative conversions for these studies were defined as the peak area ratio of MSTFA-derivatized product/internal standard using GC/MS.

Table 3-1. Continued

Entry	Aldehyde	Product	Enzyme[a]	Reaction Time (hr)	Conversion[b] (%)	d.e. (%)
2	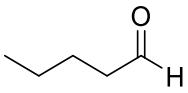 **2**	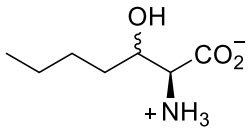	A	4	10	99 (*anti*)
				20	23	96 (*anti*)
			B	4	<5[c]	--[c]
				20	<5[c]	--[c]
			C	4	<5[c]	--[c]
				20	16	33 (*anti*)
3	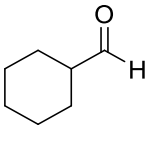 **3**	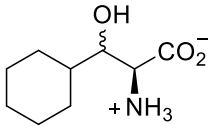	A	4	29	19 (*syn*)
				20	32	23 (*syn*)
			B	4	10	61 (*anti*)
				20	17	51 (*anti*)
			C	4	20	12 (*syn*)
				20	35	37 (*syn*)
4	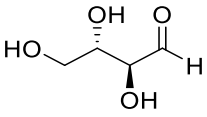 **4**	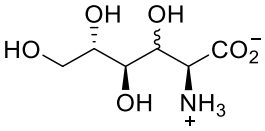	A	4	52	n.d.[d]
				20	71	n.d.[d]
			B	4	--	--
				20	<5[c]	--
			C	4	--	--
				20	--	--
5	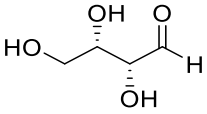 **5**	--	A	4	--	--
				20	--	--
			B	4	--	--
				20	--	--
			C	4	--	--
				20	--	--
6	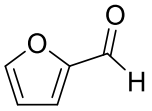 **6**	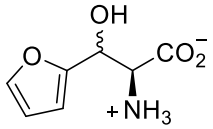	A	4	13	28
				20	18	17
			B	4	<5[c]	--[c]
				20	<5[c]	--[c]
			C	4	<5[c]	--[c]
				20	7	17
7	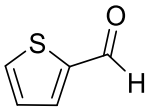 **7**	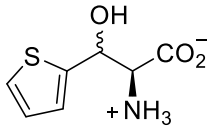	A	4	6	47
				20	12	21
			B	4	<5[c]	--[c]
				20	<5[c]	--[c]
			C	4	<5[c]	--[c]
				20	6	9

Table 3-1. Continued

Entry	Aldehyde	Product	Enzyme[a]	Reaction Time (hr)	Conversion[b] (%)	d.e. (%)
8	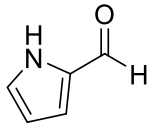 **8**	--	A	4	--	--
				20	--	--
			B	4	--	--
				20	--	--
			C	4	--	--
				20	--	--
9	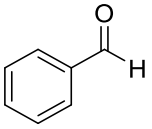 **9**	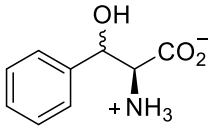	A	4	11	31 (*anti*)
				20	19	26 (*anti*)
			B	4	<5[c]	--[c]
				20	<5[c]	--[c]
			C	4	<5[c]	--[c]
				20	14	12 (*anti*)
10	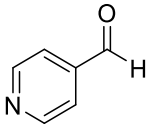 **10**	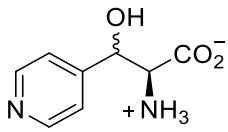	A	4	30	73 (*syn*)
				20	63	30 (*anti*)
			B	4	--	--
				20	<5[c]	--[c]
			C	4	31	20 (*syn*)
				20	47	18 (*syn*)
11	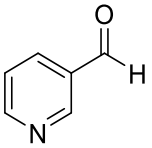 **11**	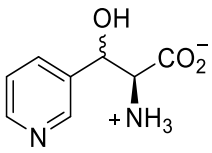	A	4	43	11
				20	70	18
			B	4	<5[c]	--[c]
				20	<5[c]	--[c]
			C	4	<5[c]	--[c]
				20	21	4
12	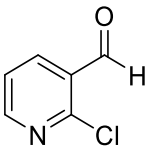 **12**	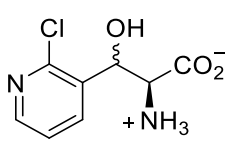	A	4	37	49 (*syn*)
				20	66	41 (*syn*)
			B	4	<5[c]	--[c]
				20	25	34 (*anti*)
			C	4	<5[c]	--[c]
				20	14	6 (*syn*)
13	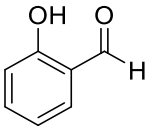 **13**	--	A	4	--	--
				20	--	--
			B	4	--	--
				20	--	--
			C	4	--	--
				20	--	--

Table 3-1. Continued

Entry	Aldehyde	Product	Enzyme[a]	Reaction Time (hr)	Conversion[b] (%)	d.e. (%)
14	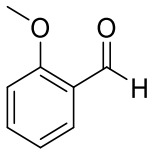 **14**	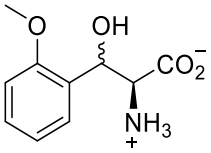	A	4	29	99 (*syn*)
				20	58	24 (*syn*)
			B	4	--	--
				20	<5[c]	--[c]
			C	4	10	56 (*syn*)
				20	35	12 (*syn*)
15	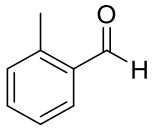 **15**	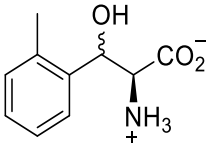	A	4	5	27 (*syn*)
				20	8	20 (*syn*)
			B	4	--	--
				20	<5[c]	--[c]
			C	4	<5[c]	--[c]
				20	<5[c]	--[c]
16	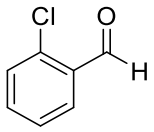 **16**	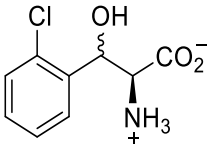	A	4	73	n.d.[d]
				20	80	n.d.[d]
			B	4	<5[c]	--[c]
				20	8	n.d.[d]
			C	4	<5[c]	--[c,d]
				20	7	n.d.[d]
17	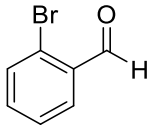 **17**	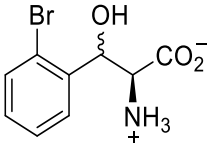	A	4	47	n.d.[d]
				20	68	n.d.[d]
			B	4	<5[c]	--[c]
				20	8	n.d.[d]
			C	4	<5[c]	--[c]
				20	11	n.d.[d]
18	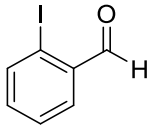 **18**	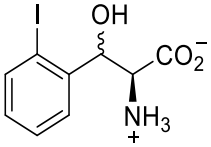	A	4	8	n.d.[d]
				20	13	n.d.[d]
			B	4	<5[c]	--[c]
				20	7	n.d.[d]
			C	4	<5[c]	--[c]
				20	6	n.d.[d]

Note: Reaction mixtures contained 500 mM glycine, 100 mM aldehyde, 0.05 mM PLP, 20% ethanol, and 10 µL of enzyme lysate in 1 mL of 50 mM Tris-Cl, pH 9.7 (Enzymes A, B) or 50 mM CAPS, pH 12 (Enzyme C). Reactions were incubated at 37 ºC.

[a] Enzyme A: *A. jandaei* L-*allo*-TA; Enzyme B: *E. coli* L-TA; Enzyme C: *T. maritima* L-*allo*-TA.

[b] Conversion and diastereomeric excess values were determined by GC-MS after MSTFA derivatization. Reactions with 1 – 5% conversions are listed as "<5%" and no values for diastereomeric purity are provided since the small peak sizes preclude accurate integration.

[c] Accurate values for conversion and diastereomeric excess could not be determined due to the very low peak areas.

[d] It was not possible to determine the diastereoselectivity of this reaction by chiral-phase GC since temperatures required for elution were greater than the maximum column temperature.

Screening of Aldehyde Acceptors

Once optimized reaction conditions had been identified, the substrate ranges of the three selected L-TAs were investigated using various aldehyde acceptors (Table 3-1). Aldehydes **1** and **9** are well-known substrates for TA-catalyzed reactions; they were included here to allow comparisons to previous studies. Aldehydes **2** and **4** – **6** have not previously been tested as TA substrates.[184] Cyclohexanecarboxaldehyde **3** is a very sterically demanding acceptor, and previous studies had failed to identify a suitable TA for this substrate.[237] Hetereocyclic aldehyde **10** was used very successfully with a D-TA by Goldberg *et al*.;[224] here, our goal was to identify a stereocomplementary L-TA. Aldehydes, **11** – **15**, have not been previously studied as TA substrates to the best of our knowledge. The *ortho*-halogenated analogs **16** – **18** previously explored for other TAs by Steinreiber *et al*. were included for comparison.[191] All screening reactions used a 5 : 1 molar ratio of glycine : aldehyde. Under these conditions, conversions were expected to be modest; the goal was to identify useful enzyme/substrate combinations, rather than to form high product titers in this phase of the study.

All three L-TAs were found to accept a wide range of new aldehydes, although the overall performance of the *A. jandaei* L-*allo*-TA was nearly always superior. As expected, diastereoselectivities at 4 hr were greater than those at 20 hr; however, very low conversions at 4 hr often thwarted accurate stereochemical measurements. The smallest substrate (propionaldehyde **1**) gave only a single diastereomer regardless of reaction time (Table 3-1, entry 1). This is particularly interesting since the active site binding pocket can accommodate much larger aldehydes in multiple orientations. That a small aldehyde seemingly occupies only one orientation with very high preference testifies to the complexity of TA substrate binding interactions. Valeraldehyde **2** also

gave high diastereoselectivity with *A. jandaei* L-*allo*-TA as well as with the *T. maritima* enzyme (Table 3-1, entry 2). Bulky aldehyde **3** was accepted by all three enzymes examined. While the diastereoselectivities were modest, it was possible to find enzymes that favored both the *syn*- and *anti*-diastereomers (Table 3-1, entry 3).

Neither D-threose nor D-erythrose were accepted significantly by any of the three enzymes (Table 3-1, entries 4 and 5).[ii] Furan-, thiophene- and pyrrole-2-carboxaldehydes presented an interesting contrast (Table 3-1, entries 6 – 8). While the first two aldehydes gave some conversion, the last was not a substrate for any of the three TAs. The conversions are correlated with the carbonyl IR stretching frequencies, which give an approximate measure of electrophilicity.[iii]

We also tested a variety of aromatic aldehydes as possible acceptors for TAs (Table 3-1, entries 9 – 18). Our data for benzaldehyde itself confirmed the modest *anti*-selectivity that had been observed previously. Pyridines **10** and **11** can be considered formal benzaldehyde analogs. While both were also accepted by two of the TAs, the *syn*-diastereomers were favored in each case (Table 3-1, entries 10 and 11). The presence of an *o*-chloro substituent allowed the aldehyde to be accepted by all three TAs, with one favoring the *syn*-product, one the *anti*-product and the third with essentially no diastereoselectivity (Table 3-1, entry 12).

The intriguing stereochemical results from aldehyde **12** prompted us to investigate a series of *ortho*-substituted benzaldehydes (Table 3-1, entries 13 – 18). All but *o*-salicylaldehyde **13** afforded aldol products with varying degrees of

[ii] The aldol product of D-erythrose was confirmed by MS (Figure A-1).

[iii] Furfural, 1700 cm-1, thiophene-2-carboxaldehyde, 1680 cm-1, pyrrole-2-carboxaldehyde, 1650 cm-1

diastereoselectivity. A. *jandaei* L-*allo*-TA was particularly useful for these substrates, although *o*-iodobenzaldehyde **18** was a poor substrate, even for this enzyme.

Given the ability of the TAs to accept relatively bulky *ortho*-substituents (Table 3-1, entries 14 – 18), the inability to form aldol products from **13** was puzzling. We tested the ability to **13** to bind to the active site of *A. jandaei* L-allo-TA by adding equal concentrations of **9** and **13**. As expected, only the aldol product from **9** was formed. In addition, the product concentration was approximately half that from an analogous reaction lacking **13**. That **13** can act as a competitive inhibitor supports the notion that can bind to the active site, but once bound, cannot undergo nucleophilic addition.

Screening of Amino Donors

Although these enzymes were found to accept a wide variety of aldehyde acceptors, their high selectivity for glycine is a disadvantage (Figure 3-4). The amino donors **21** – **23** (Figure 3-4a) showed no conversion to the aldol product, even though as previously stated, some L-TAs show conversion with these amino donors.[188, 189, 198, 222, 223] Additionally, other unconventional amino donors were also investigated, such as amino donors **24** and **25**, but unfortunately these substrates showed no conversion to the aldol product (Figure 3-4b).

Optimizing Isolation and Purification Procedure

The screening results suggested that TAs were powerful tools in the synthesis of β-hydroxy-α-amino acids, however, an effective method for isolation and separation from starting materials, particularly Gly, has not been described. Since the reaction required five equivalents of Gly to afford suitable yields, the purification process of separating large amounts of Gly from the aldol product was very difficult. Only a few methods were found in the literature for isolating β-hydroxy-α-amino acids from its Gly

starting material, including MeOH precipitations,[192, 196] ion-exchange chromatography,[196, 197, 238] activated carbon,[238] and silica gel chromatography.[192, 197] The first attempt at solving this problem began with the large scale reaction with Gly and aldehyde **10**. The unreacted aldehyde was extracted with ether and the aqueous phase lyophilized to afford a white residue. MeOH precipitated most of the Gly, enzyme, and phosphate buffer salts. The mixture was filtered and MeOH evaporated under reduced pressure for ^{1}H NMR analysis. It was found that deuterated MeOH cannot be used in this approach, as MeOH overlaps with the chemical shift of Gly, however deuterated water (D_2O) was the obvious choice as it dissolves all amino acids. In the first isolation attempt, a large amount of Gly was present in our crude product, showing that further purification was required.

Additional MeOH precipitation steps were employed in an attempt to allow for easy isolation of the products without using column chromatography; however traces of Gly were always found in the ^{1}H NMR spectrum. We therefore explored chromatographic strategies to separate Gly from the aldol products. After an initial MeOH precipitation step, the crude product was applied to an ion exchange resin to allow for separation. Despite testing different elution solvents, glycine could not be separated from the product with this strategy.

Silica gel chromatography was the second strategy investigated for purifying the amino acid products. The appropriate solvent system was established as 50% EtOH and 5% AcOH in water through TLC with a ninhydrin stain. Although this method was slightly better at separating Gly from the desired aldol products, only around 20% of the aldol products were isolated. With the failure of these two purification strategies, we

explored a biocatalytic alternative to remove the excess Gly prior to downstream purification steps.

One obvious approach to removing excess glycine was to exploit glycine oxidase, an FAD dependent enzyme that oxidatively deaminated Gly to glyoxylate (Figure 3-2). The glycine oxidase gene from *B. subtilis* was chemically synthesized by Genscript, cloned into a pET-15b vector, and overexpressed in *E. coli*. The advantage of this enzyme was that it was extremely selective for Gly and small D-amino acids. Administration of any larger amino acid, including threonine and the TA-catalyzed aldol products, resulted in no conversion to the corresponding glyoxylate analogue.

The crude extract containing *B. subtilis* glycine oxidase was purified by binding its hexahistidine tag to a HiTrap Chelating HP column. After elution, the purified enzyme was concentrated to 5 mg/mL and activity was measured by monitoring the formation of H_2O_2 by UV-Vis spectroscopy at 500 nm by a coupled HRP assay.[228] Purified glycine oxidase (2 mg) was added to the TA reaction mixture after a single MeOH precipitation step to remove most of the glycine, followed by ion exchange chromatography to separate glyoxylate from the aldol product (Figure 3-5). By utilizing this biocatalyst, problems of isolating and purifying β-hydroxy-α-amino acids were solved.

Preparative Conversions

Taken together, our screening results support the current view that TA-catalyzed reactions have broad substrate tolerance, but suffer from a loss of diastereoselectivity as the reaction progresses. Employing a large molar excess of glycine is a common approach to maximizing conversion over short reaction times. When only small-scale screening reactions are considered, this is not a problem; however, if preparative

reactions are contemplated, the residual glycine must be removed and the desired β-hydroxy-α-amino acid purified. Because these downstream operations have generally received less attention, we chose six examples from our screening efforts for preparative reactions (Table 3-2). Glycine oxidase was used to simplify downstream processing by removing excess glycine from the reaction mixture (Figure 3-5).

Table 3-2. Preparative-scale reaction results

Entry	Aldehyde	Major Product	Isolated Yield (%)	Mole Fraction *anti* : *syn*[a]
1	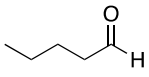 **2**	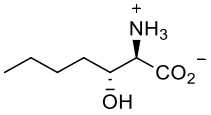	16	0.60 : 0.40
2	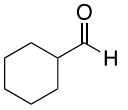 **3**	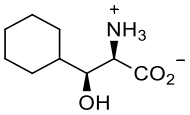	50	0.14 : 0.86
3	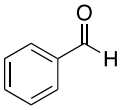 **9**	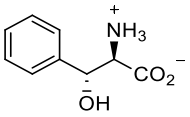	32	0.33 : 0.66
4	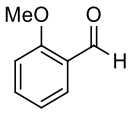 **14**	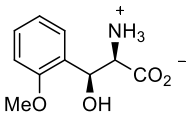	22	0.10 : 0.90
5	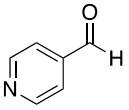 **10**	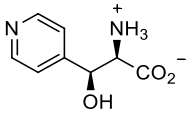	28	0.33 : 0.66
6	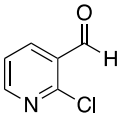 **12**	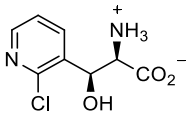	50	0.33 : 0.66

Note: Reactions were catalyzed by *A. jandaei* L-*allo*-threonine aldolase at pH 9.7. Excess glycine was removed by glycine oxidase prior to aldol product isolation (Figure 2-3). See Figures A-2 – 7 for NMR spectra.

[a] The diastereomeric composition was determined by NMR analysis (*anti* ≡ *erythro*; *syn* = *threo*).

Because *A. jandaei* L-*allo*-TA provided the best conversions and diastereoselectivities, all preparative-scale reactions employed this enzyme. Screening reaction conditions were scaled-up ten-fold. After the 4 hr, any unreacted aldehyde was

removed by extracting with diethyl ether, then the water was removed by lyophilization. The solid was extracted with two portions of methanol, which left most unreacted glycine and buffer salts undissolved. After evaporating the methanol, the residue was dissolved in buffer at pH 8.0 and glycine oxidase was added to decompose any remaining glycine. An anion-exchange resin eluted with 0.5% aqueous acetic acid was used for final purification prior to final lyophilization the afforded the aldol products. While some yields were disappointing, *e.g.* entries 1 and 4, others were more synthetically relevant. The low yields were mainly due to poor conversions by the enzymes, rather than to losses during isolation.

Assignment of Relative Configurations[iv]

The diastereomeric compositions of aldol products isolated from all six preparative-scale reactions were elucidated by the *J*-analysis method of Matsumori[239] and the results are shown in Table 3-2. Elucidation of the relative stereochemistry of two chiral carbons separated by a single bond implies simultaneous elucidation of the rotamer equilibrium. The expected coupling constants in the three staggered rotamers of the two diastereomers are given in Table 3-3. As is often the case, two of the rotamers – here **Ia** and **IIa** – display the same pattern of coupling constants. The values for large and small coupling constants were taken from the values reported by Matsumori[239] for the case where the two carbons carry oxygen atoms: $^{3}J_{H\text{-}H}$: large 7-10 Hz, small 0-4 Hz; $^{3}J_{C\text{-}H}$: large 5-7 Hz, small 1-3 Hz; $^{2}J_{C\text{-}H}$ large -4 to -6 Hz, small 0-2 Hz.

[iv] All relative configurations were assigned by Ion Ghiviriga at the University of Florida by NMR analysis.

Table 3-3. Expected values for diagnostic coupling constants in pure staggered conformers of the two diastereomers

	Ia	Ib	Ic
(2*S*,3*S*) + (2*R*,3*R*) *anti (erythro)*	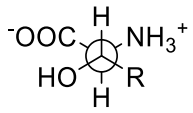	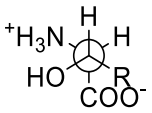	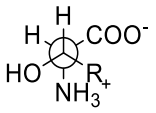
$^{3}J_{H2-H3}$, Hz	lg	sm	sm
$^{3}J_{H2-C4}$, Hz	sm	sm	lg
$^{3}J_{H3-C1}$, Hz	sm	lg	sm
$^{2}J_{H2-C3}$, Hz	lg	sm	lg
$^{2}J_{H3-C2}$, Hz	lg	lg	sm
	IIa	IIb	IIc
(2*S*,3*R*) + (2*R*,3*S*) *syn (threo)*	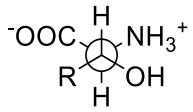	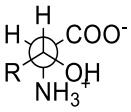	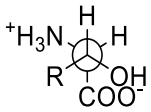
$^{3}J_{H2-H3}$, Hz	lg	sm	sm
$^{3}J_{H2-C4}$, Hz	sm	sm	lg
$^{3}J_{H3-C1}$, Hz	sm	sm	lg
$^{2}J_{H2-C3}$, Hz	lg	sm	lg
$^{2}J_{H3-C2}$, Hz	lg	sm	lg

The H-H coupling constants were measured in the proton spectrum. The H-C coupling constants were measured in the *f1* dimension of EXSIDE spectra.[240] The values are given in Table 3-4. The ^{1}H and ^{13}C chemical shifts assignments, on which the elucidation of the relative stereochemistry relies, were based on the cross-peaks seen in the gHMBC spectra.[v]

[v] For Tables and 2D NMR, see supporting information section, Table A-1 and Figures A-2 – 7.

Table 3-4. Diagnostic coupling constants measured in the two diastereomers of M and m

	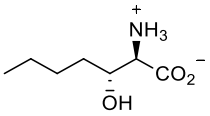		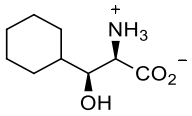		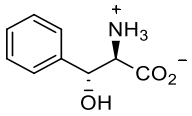	
Rotamer, x	Ic + Ib, 0.60	IIb + IIa, 0.40	IIb, 0.86	0.14	IIb + IIa, 0.66	Ic + Ia, 0.33
$^3J_{H2\text{-}H3}$, Hz	3.7 sm	4.5 sm-m	3.3 sm	3.8 sm	4.3 sm-m	4.2 sm
$^3J_{H2\text{-}C4}$, Hz	3.6 m	1.1 sm	0.6 sm	*nm*	0.7 sm	4.8 m-lg
$^3J_{H3\text{-}C1}$, Hz	2.7 m-sm	1.4 sm	*1.2 sm*	*nm*	1.3 sm	1.5 sm
$^2J_{H2\text{-}C3}$, Hz	*4.5 lg*	*<0.4 sm*	*sm*	*nm*	2.6 m	5.7 lg
$^2J_{H3\text{-}C2}$, Hz	3.1 m-lg	2.5 m-sm	*sm*	*nm*	0.9 sm	*<0.2 sm*
	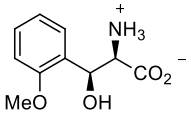		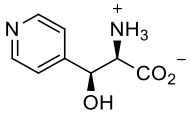		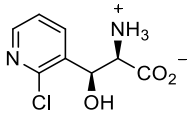	
Rotamer, x	IIb, 0.90	0.10	IIb +IIa, 0.66	Ic + Ib 0.33	IIb, 0.66	Ib, 0.33
$^3J_{H2\text{-}H3}$, Hz	*2.6 sm*	*2.9 sm*	*4.1 sm-m*	*3.4 sm*	*4.0-sm*	*2.9-sm*
$^3J_{H2\text{-}C4}$, Hz	*0.5 sm*	*nm*	*0.3 sm*	*2.8 m-sm*	*sm*	*sm*
$^3J_{H3\text{-}C1}$, Hz	*0.9 sm*	*nm*	*0.6 sm*	*2.6 m-sm*	*sm*	*5.7-lg*
$^2J_{H2\text{-}C3}$, Hz	*2.4 sm-m*	*nm*	*2.2 m*	*3.4 m-lg*	*1.2*	*1.2*
$^2J_{H3\text{-}C2}$, Hz	*1.0 sm*	*nm*	*1.2 sm*	*2.4 m*	*sm*	*4.3-lg*

Note: Some values are missing for the minor diastereomers where they were in low concentration; in these cases (products derived from aldehydes **3** and **14**), the minor was assigned as 'not the major' diastereomer.

The elucidation of the stereochemistry of the products derived from aldehyde **2** illustrates the methodology. For the minor product, the coupling constants are all small, as in **IIb**. Larger values, *i.e*. *m-sm,* for $^3J_{H2\text{-}H3}$ and $^2J_{H3\text{-}C2}$ indicate that **IIa** is also present. In the major diastereomer, a large $^2J_{H2\text{-}C3}$ would point towards **Ia**, **Ic**, **IIa** and / or **IIc**. A small $^3J_{H2\text{-}H3}$ is consistent with **Ic** and/or **IIc**, but not with **Ia** and **IIa**. Finally, a small $^3J_{H3\text{-}C1}$ is consistent with **Ic**. Medium values for $^3J_{H2\text{-}C4}$, $^3J_{H3\text{-}C1}$ and $^2J_{H3\text{-}C2}$ demonstrate that the rotamer of **I** in which these coupling constants are of opposite magnitude, *i.e.* some **1b** is also present. Both the *anti*- (major) and *syn*-diastereomers prefer the conformations in which the OH and the NH_3^+ groups are *gauche*, which can be explained by hydrogen bonding or electrostatic interactions.

For the aldol product derived from aldehyde **3**, the coupling constants indicate that the major species corresponds to rotamer **IIb**. The same *gauche* conformational preference is observed for the hydroxyl and ammonium moieties, but conformers in which the bulkier cyclohexyl group is *gauche* to the carboxyl are absent. The high diastereomeric ratio precludes measuring all of the coupling constants for the minor product, but the H2-H3 coupling points towards **Ib** or **Ic**. The steric requirements of an aromatic moiety are less than of a cyclohexyl, and although the preferred conformations are still **IIb** for the *anti*- and **Ic** for the *syn*-diastereomers, some other rotamers are also present.

The absolute stereochemistry of these 3-hydroxy-2-amino acids was determined by derivatization with methoxyphenylacetic acid (MPA).[241] D_2O or methanol-*d4*, which dissolve the 2-hydroxy-1-amino acid, are not appropriate solvents for the esterification, which uses DCC as a hydrization reagent. The methyl ester of the *n*-butyl amino acid was soluble in chloroform-d, while for the other 2-hydroxy-1-amino acids, pyridine-*d5* was used for derivatization. All the MPA esters were prepared in the NMR tube, and characterized in the reaction mixture.[242] The absolute stereochemistry of both chiral carbons C2 and C3 was determined for the *n*-butyl compound by double derivatization, and was found to be 2-*S,* 3-*S* in the major and 2-*S*, 3-*R* in the minor, in agreement with the relative stereochemistry found by *J*-analysis. For the methyl ester of the cyclohexyl compound, double derivatization proved the major to be 2-*S*, 3-*R*, and the minor 2-*R*, 3-*R*, again in agreement with the relative stereochemistry previously determined. The presence of the methoxy protons in position 1 of the ester allowed the elucidation of the stereochemistry of the phenyl compound by single derivatization to the amide. C2 was

found *S* in the major and *R* in the minor; using the knowledge of relative stereochemistry, the major was assigned as 2-*S*, 3-*R* and the minor as 2-*R*, 3-*R*.[vi]

Monitoring Transaldimination of Amino Donors

Since the initial screening of non-glycine amino donors was unsuccessful, the focus was directed to the first step in catalysis: transaldimination of the amino donors. An external aldimine has an absorbance of 422 nm, however an internal aldimine has an absorbance of 388 nm.[243] By utilizing UV-Vis spectroscopy, the formation of the external aldimine could be monitored by an increase in the absorbance at 422 nm. A simple kinetics experiment was run over ten minutes on the L-*allo*-TA from *A. jandaei* taking absorbance readings every 30 seconds at 422 nm. The results for these amino donors are shown in Figure 3-6. Gly was administered as the positive control as it is the native substrate for this enzyme. We found that the negative control (addition of PLP alone) gave virtually no increased absorbance at 422 nm over the ten min. Amino donors **21** and **22** (Figure 3-6, purple and red) showed optimistic results for the formation of the external aldimine. It is possible that the enzyme can form the external aldimine, but not undergo deprotonation of the α-carbon. Amino donors **24** and **25** (Figure 3-6, red and green) gave similar values to the PLP negative control, indicating no external aldimine formation.

Amino donors **24** and **25** were probed further to see if the enzyme, L-*allo*-TA from *A. jandaei*, allowed for any binding to the active site by adding equal amounts of Gly and **24** (or Gly and **25**) with aldehyde **9**. As expected, only the aldol product from Gly was formed, as seen in the initial screening results. However, the product

[vi] For Tables with chemical shifts, see supporting information section, Tables A-2 – 4.

concentration was reduced compared to the analogous reaction lacking **24** or **25**. This supports the perception that these amino donors **24** and **25** can bind to the active site, but once bound, cannot undergo transaldimination or aldol condensation with an aldehyde.

Probing α-Deprotonation of Amino Donors

The next step was to probe for deprotonation on the α-carbon of the amino donor, the next step in the catalytic cycle of TA. By applying deuterium oxide (D_2O) and mass spectrometry (MS), one can determine whether TAs can catalyze deprotonation on carbons adjacent to amines. The reaction was monitored by GC/MS to detect the possible increased molecular weight due to deuterium incorporation from the solvent. As the natural substrate, Gly was used as a positive control to test this method and to monitor the α-deprotonation of the enzyme. Gly was found to have complete deuterium exchange within 1.5 hours. However, analysis of non-glycine amino donors indicated no deuterium exchange of the α-proton after 24 or even 48 hours.

Although this experiment lead to the result that TAs do not deprotonate non-glycine amino donors, it did give some insight into the catalysis by these enzymes. The positive control was carried out in both the absence and presence of an aldehyde and in the presence of aldehyde **13**, a competitive inhibitor that binds to the active site but is unable to undergo aldol addition. The idea was to determine whether an aldehyde must be present for glycine deprotonation to occur. It was found that an aldehyde was *not* required for deprotonation of Gly. Secondly, these L-TAs are known to only make the L-isomer of these aldol products. Taken together, the assignment configuration of the preparative-scaled reactions confirmed this fact and that this experiment revealed that

only one proton was exchanged with deuterium over time, confirmed the fact that these enzymes only make the L-isomer. And lastly, we have developed an efficient method for monitoring the exchange of the α-proton with deuterium.

Investigation into the Thermodynamic Reversibility of Aldol Products

One of the major limitations of TAs is their reversibility that leads to loss of diastereoselectivity. This loss of d.e. has been seen in the literature[184, 192, 196, 204] and in our results (Table 3-1). The thermodynamic reversibility was monitored by proton nuclear magnetic resonance (^{1}H NMR) and MS experiments using deuterated acetaldehyde (Figure 3-7). The reaction was monitored by ^{1}H NMR at several time points, probing the reversibility by observing the transformation of the α-proton's signal from a doublet to a singlet. After 24 hrs, we saw approximately a 2 : 1 (singlet : doublet) ratio in the ^{1}H NMR spectrum, indicating some reversibility occurred overnight (Figure A-8g).

It was also possible to monitor the reversibility by MS and the addition of plus four in Thr's mass spectrum. The reaction was monitored at numerous time points and after 24 hrs the ratio between L-*allo*-Thr and L-*allo*-Thr-d4 was approximately 1 : 1 (Figure A-9f). Diastereomeric excess was also monitored in this experiment, however no loss in diastereoselectivity was found. This was expected as these are the natural substrates for this enzyme. By utilizing both of these techniques, it was confirmed that thermodynamic reversibility does occur, especially over a long period of time. For the natural substrates, no loss in d.e. was found, however the screening results indicate with larger aldehyde acceptors, reversibility was damaging to the d.e. of these products.

Conclusions

In summary, L-TAs from *A. jandaei*, *E. coli*, and *T. maritima* were tested on an assortment of aldehyde acceptors using glycine as the amino donor. *A. jandaei* L-*allo*-TA proved superior in all cases. The conversions using aldehyde acceptors could be scaled up moderately and the aldol products isolated from the reaction mixtures using glycine oxidase to degrade excess glycine. Establishing these downstream processing steps should increase the practical impact of TA-catalyzed reactions in asymmetric synthesis. Additionally, these L-TAs were screened against a handful of unnatural amino donors, nevertheless the results were inferior. To investigate this further, the transaldimination of amino donors was monitored by UV-Vis spectroscopy and revealed that both L-Ala and L-Ser undergo transaldimination with the active site PLP; however, aminomethylphosphonate and aminomethanesulfonate do not form the external aldimine. Sequentially, the α-deprotonation was monitored by MS and deuterium oxide; however, non-glycine amino donors exhibited no deuterium exchange.

Experimental Procedures

General. LB medium contained 10 g/L Bacto-Tryptone, 5 g/L Bacto-Yeast Extract and 10 g/L NaCl; 15 g/L agar was added for plates. PCR amplifications were performed with Phusion Hot Start II DNA polymerase using the manufacturer's protocols. Electroporation was carried out with a BioRad GenePulser apparatus using 0.2 cm cuvettes. Promega Wizard kits and CsCl buoyant density ultracentrifugation[244] were used for small- and large-scale plasmid purifications, respectively. Fluorescent Sanger DNA sequencing was performed by the University of Florida ICBR. GC/MS analysis employed a 30 m × 0.25 mm Beta Dex™ 225 column and ionization by EI at 70 eV. The temperature program involved an initial hold at 95 ºC for 5 min, an initial

increase of 5 ºC/min to 138 ºC followed by an increase of 10 ºC/min to 180 ºC, then a final increase of 2 ºC/min to 200 ºC and a hold at that temperature for 10 min.

Cloning of *A. jandaei* L-*allo*-TA. The gene encoding L-*allo*-TA from *A. jandaei* (accession number D87890) was synthesized by GenScript and ligated into a pUC-57 with flanking *Nde*I and *Xho*I restriction sites at the 5'- and 3'-ends, respectively. The TA gene was excised by digesting with these restriction enzymes and ligated with *Nde*I, *Xho*I-cut pET-15b (Novagen). After transformation into *E. coli* ElectroTen-Blue, plasmid DNA from a randomly-chosen colony was isolated, restriction mapped and then sequenced to verify the desired structure. The resulting plasmid (designated pSF3) was used to transform *E. coli* BL21-Gold(DE3) strain for protein overexpression.

Cloning of *E. coli* L-TA. The gene encoding L-TA (accession number NC000913) was amplified from *E. coli* ElectroTen-Blue by colony PCR[229] using 5'-ATAAGGACATCATATGATTGATTTAC-3' and 5'-ACGTC TGGATCCTTAACGCG-3' as forward and reverse primers, respectively. These primers also introduced flanking *Nde*I and *Bam*HI restriction sites (underlined). After purification, the PCR product was digested sequentially with *Nde*I and *Bam*HI, then ligated with *Nde*I, *Bam*HI-digested pET-15b. After transformation into *E. coli* ElectroTen-Blue, plasmid DNA from a randomly-chosen colony was isolated, restriction mapped and then sequenced to verify the desired structure. The resulting plasmid (designated pSF4) was used to transform *E. coli* BL21-Gold(DE3) strain for protein overexpression.

Cloning of *T. martima* L-*allo*-TA. The L-TA gene from *T. maritima* (accession number AE000512) was PCR-amplified from *T. maritima* genomic DNA using 5'-CGTGTGGGAGGTGACCATATGATCGATC TCAGGTCCGACACC-3' and 5'-

GAAATTTTTTGGA TCCTCAGGAGAATTTTCTGAAGAGTTTTTCGAAGA T-3' as forward and reverse primers, respectively. The gene was inserted into pET-15b in the same manner as *E. coli* L-TA, yielding pSF5, which was used to transform *E. coli* BL21-Gold(DE3) for protein overexpression.

Cloning of *B. subtilis* glycine oxidase. The complete coding sequence for *B. subtilis* glycine oxidase (accession number NC000964) was synthesized by GenScript and ligated into pUC57 with flanking *Nde*I and *Bam*HI restriction sites at the 5'- and 3'-ends, respectively. Silent mutations were introduced to the coding region to remove internal *Nde*I and *Bam*HI sites that occur in the native sequence. The gene was subcloned as an *Nde*I, *Bam*HI fragment between these sites into pET-15b. After transforming *E. coli* ElectroTen-Blue, plasmid DNA was isolated from a randomly-chosen colony, restriction mapped and sequenced to verify that the desired plasmid had been prepared (designated pSF9). This was used to transform *E. coli* BL21-Gold(DE3) for protein overexpression.

Protein overexpression. A single colony of the appropriate strain was used to inoculate 50 mL of LB medium supplemented with 100 µg/mL ampicillin. After shaking overnight at 37 ºC, a 40 mL portion of the preculture was added to 4 L of LB medium supplemented with 100 µg/mL ampicillin, 80 mL of 20% glucose, and 1.5 mL of Sigma Antifoam 204 in a New Brunswick M19 fermenter. The culture was grown at 37 ºC with stirring at 400 rpm and an air flow of 1 vvm until the $O.D._{600}$ reached 0.5 – 0.6. Protein overexpression was induced by adding 10 mL of 0.16 M IPTG (to yield a final concentration of 0.4 mM) and adjusting the temperature to 30 ºC and shaking. After 3 hr, the cells were harvested by centrifuging at 6,300 × *g* for 15 min at 4 ºC, resuspended

in 50 mM KP_i, pH 8.0 (1 mL buffer per gram wcw), then lysed by a French pressure cell at 17,000 psi. Insoluble debris was pelleted by centrifuging at 39,000 × *g* for 1 hr at 4 ºC and the yellow supernatant was used for TA-catalyzed reactions. Glycerol was added to a final concentration of 20% and the protein was stored in aliquots at -80 ºC.

Affinity purification of *B. subtilis* glycine oxidase. A crude extract containing glycine oxidase was prepared as described above, then the sample was applied to a 5 mL HiTrap Chelating HP column (GE Healthcare Life Sciences) that had been equilibrated with binding buffer (20 M NaP_i, 500 mM NaCl, 20 mM imidazole, pH 7.4). After washing with 50 mL of binding buffer, the desired protein was eluted by elution buffer (20 mM NaPi, 500 mM NaCl, 500 mM imidazole, pH 7.4). A flow rate of 2 mL/min was employed throughout. The eluate was concentrated by ultrafiltration (Amicon Ultra), then diluted with 50 mM KPi, pH 8.0 and re-concentrated. This was repeated two more times. The final glycine oxidase sample was diluted with the same buffer to 5 mg/mL, then glycerol was added to a final concentration of 10% and the protein was stored in aliquots at -80 ºC.

Enzyme assays for threonine aldolase. The activity of L-TAs was measured by mixing 0.1 mmol acetaldehyde, 1.0 mmol glycine, 10 nmol PLP and 20 µL of enzyme solution in 50 mM KPi, pH 8.0 (total volume of 1 mL). The mixture was gently rotated at room temperature and 5 µL aliquots were removed after 0.5 hr, 1.5 hr, 4 hr, and overnight. Samples were derivatized with MSTFA and analyzed by GC/MS. The temperature program involved an initial hold at 95 ºC for 5 min, an initial increase of 5 ºC/min to 120 ºC followed by an increase of 2 ºC/min to 138 ºC, then a final increase of 10 ºC/min to 200 ºC and a hold at that temperature for 5 min.

Enzyme assay for glycine oxidase. Glycine oxidase activity was measured by monitoring the formation of H_2O_2 by UV -Vis spectroscopy at 500 nm using a coupled HRP assay.[228] Reaction mixtures containing 10 mM glycine and 0.25 mg glycine oxidase (in 50 µL of 50 mM KPi, pH 8.0) were added to 1.5 mM 4-aminoantipyrine, 2 mM phenol, and 5 U HRP in 50 mM KPi, pH 8.0 (total volume of 1000 µL). After incubating at 37 ºC for 10 min, the A^{500} value was used to calculate units glycine oxidase activity.[228]

Enzyme kinetics. Kinetic experiments were executed at 422 nm for 10 minutes at room temperature, monitoring the absorbance every 30 seconds. The reaction contained 10 µmol of amino donor, 0.1 µmol of PLP, and 10 µL of enzyme lysate in buffer (total volume of 1 mL). After the addition of enzyme, the cuvette was inverted three times and the absorbance was immediately monitored for 10 minutes. The experiment was performed in triplicate and an average was taken for the final results.

Derivatization of amino acids by FAA derivatization. Amino acid standards were dissolved in 100 µL of buffer pH 8.0, following an addition of 0.1 M ammonium acetate pH 7.0 (200 µL) and 2% trifluoroacetylacetone (FAA) (200 µL). After heating for 95 ºC for 20 min, the solvent system acetonitrile : water : MeOH : pyridine (21 : 21 : 4 : 4) (200 µL) was added to the reaction mixture. The derivatized amino acid was extracted by chloroform (500 µL) and analyzed by GC/MS. The temperature program involved an initial hold at 95 ºC for 2 min, a temperature increase of 3 ºC/min to 200 ºC, and a hold at that temperature for 5 min.

Derivatization of amino acids by OPA/NAC derivatization. Amino acid standards (10 µL) were diluted with 0.2 M NTBB buffer pH 10.5 (500 µL). The

OPA/NAC derivatizing agent (200 µM OPA/600 µL NAC in MeOH) (10 µL) was added to the amino acid solution and inverted four times to mix. After incubating for 15 min at room temperature, the derivatized amino acids were analyzed by HPLC. A C_{18} column was used as the stationary phase. Potassium phosphate (50 mM) and acetonitrile were used as the mobile phase systems A and B, respectively. The solvents were filtered through a 0.22 µ membrane filter. The flow rate was 1 mL/min and the eluents were monitored at 250 nm. The injection volumes were 20 µL. The gradient was as follows: The initial mobile phase was solvent A (100%) for 1 mL/min for 10 min, the mobile phase was switched to solvent B (100%) for 3 min, and the final mobile phase was reverted back to solvent A (100%) for 15 min.

Derivatization of amino acids by MSTFA derivatization. The original procedure required reaction mixtures (or standards of 5 nmol of amino acid) to be dried completely under reduced pressure for 30 min by a Savant SpeedVac SVC100, then the residue was taken up by 80% MeOH (50 µL). The sample was then dried for a second time under reduced pressure for 30 min, following the addition of methylene chloride (40 µL). The sample was dried for a third and final time under reduced pressure for 10 min. The dried sample was taken up in the derivatization solvents: dried pyridine (40 µL) and MSTFA (70 µL). After shaking at 37 ºC for 30 min, the mixtures were analyzed by GC/MS.

Derivatization of amino acids by MSTFA derivatization (optimized). The optimized procedure aimed to limit the amount of drying steps and derivatization reagents. Reaction mixtures (or standards of 5 nmol of amino acid) were dried completely under reduced pressure for 30 min by a Savant SpeedVac SVC100. The

dried sample was taken up dry pyridine (1 µL) and MSTFA (50 µL). After shaking at 37 ºC for 30 min, the mixtures were analyzed by GC/MS. For L-Thr and L-*allo*-Thr standards and enzyme assay, the temperature program involved an initial hold at 95 ºC for 5 min, an initial increase of 5 ºC/min to 120 ºC followed by an increase of 2 ºC/min to 138 ºC, then a final increase of 10 ºC/min to 200 ºC and a hold at that temperature for 5 min. For screening reactions, the temperature program involved an initial hold at 95 ºC for 5 min, an initial increase of 5 ºC/min to 138 ºC followed by an increase of 10 ºC/min to 180 ºC, then a final increase of 2 ºC/min to 200 ºC and a hold at that temperature for 10 min.

Detection of amino acids by TLC with a ninhydrin stain. TLC silica gel plates (Merck 60 F254) were used to visualize Gly and amino acid products at 254 nm and by treatment with a 2% ninhydrin reagent (in methanol). The TLC solvent system contained BuOH : H_2O : AcOH (4 : 2 : 1). After separation by TLC, the silica plate was sprayed with 2% ninhydrin solution to visualize primary amines.

α-Deprotonation of amino donors without aldehyde 13. Reactions contained 7.5 µmol of amino donor, 750 nmol of PLP and 2.5 µL of enzyme lysate in buffer (total volume of 1 mL) made with D_2O. These were gently rotated overnight at room temperature and sampled after 0.5 hr, 1 hr, 1.5 hr, 3 hr, 5 hr and overnight for MSTFA derivatization and GC/MS analysis.

α-Deprotonation of amino donors with aldehyde 13. Reactions contained 3.75 µmol of *ortho*-hydroxybenzaldehyde (**13**), 7.5 µmol of amino donor, 750 nmol of PLP and 2.5 µL of enzyme lysate in buffer (total volume of 1 mL) made with D_2O.

These were gently rotated overnight at room temperature and sampled after 0.5 hr, 1 hr, 1.5 hr, 3 hr, 5 hr and overnight for MSTFA derivatization and GC/MS analysis.

Probing thermodynamic reversibility of aldol reactions by ^{1}H NMR. Six reactions were performed to complete this experiment. Positive control reactions contained (1) 0.1 mmol of Gly, 0.1 mmol of acetaldehyde, 10 µmol of PLP and 10 µL of enzyme lysate in buffer (total volume of 0.5 mL) made with D_2O, (2) 0.1 mmol of Gly, 0.1 mmol of acetaldehyde-d4, 10 µmol of PLP and 10 µL of enzyme lysate in buffer (total volume of 0.5 mL) made with D_2O, and (3) 50 µmol of L-*allo*-Thr, 0.5 µmol of PLP and 10 µL of enzyme lysate in buffer (total volume of 0.5 mL) made with D_2O. Negative control reactions contained (4) 50 µmol of L-*allo*-Thr and 0.1 mmol of acetaldehyde-d4 in buffer (total volume of 0.5 mL) made with D_2O and (5) 50 µmol of L-*allo*-Thr, 0.1 mmol of acetaldehyde, 0.5 µmol of PLP and 10 µL of enzyme lysate in buffer (total volume of 0.5 mL) made with D_2O. And lastly, the reversibility reaction contained (6) 50 µmol of L-*allo*-Thr, 0.1 mmol of acetaldehyde-d4, 0.5 µmol of PLP and 10 µL of enzyme lysate in buffer (total volume of 0.5 mL) made with D_2O. These were allowed to react overnight at room temperature and sampled after 0 hr, 1 hr, 3 hr, 6 hr, and overnight for ^{1}H NMR analysis.

Probing thermodynamic reversibility of aldol reactions by GC/MS. Six reactions were performed to complete this experiment. Positive control reactions contained (1) 0.2 mmol of Gly, 0.1 mmol of acetaldehyde, 20 µmol of PLP and 10 µL of enzyme lysate in buffer (total volume of 1 mL) made with D_2O, (2) 0.2 mmol of Gly, 0.1 mmol of acetaldehyde-d4, 20 µmol of PLP and 10 µL of enzyme lysate in buffer (total volume of 1 mL) made with D_2O, and (3) 0.1 mmol of L-*allo*-Thr, 10 µmol of PLP and 10

µL of enzyme lysate in buffer (total volume of 1 mL) made with D_2O. Negative control reactions contained (4) 0.1 mmol of L-*allo*-Thr and 0.1 mmol of acetaldehyde-d4 in buffer (total volume of 1 mL) made with D_2O and (5) 0.1 mmol of L-*allo*-Thr, 0.1 mmol of acetaldehyde, 10 µmol of PLP and 10 µL of enzyme lysate in buffer (total volume of 1 mL) made with D_2O. And lastly, the reversibility reaction contained (6) 0.1 mmol of L-*allo*-Thr, 0.1 mmol of acetaldehyde-d4, 10 µmol of PLP and 10 µL of enzyme lysate in buffer (total volume of 1 mL) made with D_2O. These were gently rotated overnight at room temperature and sampled after 0.5 hr, 1 hr, 1.5 hr, 3 hr, 5 hr and overnight for MSTFA derivatization and GC/MS analysis.

General procedure for screening aldehyde acceptors. Reactions contained 0.1 mmol of aldehyde, 0.5 mmol of glycine, 10 nmol of PLP and 10 µL of enzyme lysate in buffer (total volume of 1 mL). These were gently rotated overnight at room temperature and sampled after 4 hr and overnight for MSTFA derivatization and GC/MS analysis.

General procedure for screening amino donors. Reactions contained 0.1 mmol of aldehyde (acetaldehyde, hexanal, or benzaldehyde), 0.5 mmol of amino donor, 10 nmol of PLP and 10 µL of enzyme lysate in buffer (total volume of 1 mL). These were gently rotated overnight at room temperature and sampled after 4 hr and overnight for MSTFA derivatization and GC/MS analysis.

Design of Experiments. To optimize reaction conditions, all three TAs underwent a series of experiments varying temperature, pH, and glycine concentration. All reactions contained 0.1 mmol of aldehyde, 0.2 - 1.0 mmol of glycine, 10 nmol of PLP and 10 µL of enzyme lysate in buffer plus 2% (v/v) ethanol in a total volume of 1 mL.

The four different glycine concentrations were tested at five different temperatures (4 ºC, 18 ºC, 25 ºC, 37 ºC and 42 ºC) and four different pH values (6, 8, 9.7, and 12). The mixtures were gently rotated at the desired temperature, then 5 µL aliquots were taken after 4 hr and overnight. Samples were derivatized with MSTFA and analyzed by GC/MS.

Optimization of Purification Procedure. First purification attempt: After the TA-catalyzed reaction was completed, the unreacted aldehyde was removed by extraction with Et_2O (2 × 30 mL) and the aqueous layer was lyophilized. The solid residue was mixed thoroughly with 30 mL of MeOH and the solution was filtered and evaporated under reduced pressure. ^1H NMR analysis revealed the presence of a large amount of glycine.

Second attempt: After the TA-catalyzed reaction was completed, the unreacted aldehyde was removed by extraction with Et_2O (2 × 30 mL) and the aqueous layer was lyophilized. The solid residue was mixed thoroughly with 30 mL of MeOH and the solution was filtered and evaporated under reduced pressure. This procedure was repeated to remove additional unreacted glycine. ^1H NMR analysis revealed trace amounts of glycine.

Third attempt: After the TA-catalyzed reaction was completed, the unreacted aldehyde was removed by extraction with Et_2O (2 × 30 mL) and the aqueous layer was lyophilized. The solid residue was mixed thoroughly with 30 mL of MeOH and the solution was filtered and evaporated under reduced pressure. This procedure was repeated to remove additional unreacted glycine. The crude product was dissolved in water and applied to an 11 × 1.5 cm DOWEX, 1 × 2 (HO^- form) column. The column

was washed with 100 mL of deionized water, then the desired product was eluted by washing with 50 mL of 20% acetic acid. The solvent was removed using a SpeedVac to afford the final product. ^{1}H NMR analysis revealed no separation of glycine was achieved. Separately, different concentrations (10%, 5%, 2%, and 1%) of eluent solvent (acetic acid) were used in an attempt for a greater separation of glycine from the products, but only slight separation occurred with 1% AcOH.

Fourth attempt: After the TA-catalyzed reaction was completed, the unreacted aldehyde was removed by extraction with Et_2O (2 × 30 mL) and the aqueous layer was lyophilized. The solid residue was mixed thoroughly with 30 mL of MeOH and the solution was filtered and evaporated under reduced pressure. This procedure was repeated to remove additional unreacted glycine. The crude product was dissolved in 50% EtOH and 5% AcOH in water and applied to a 15 × 2 cm silica gel column. The column was washed with 50% EtOH and 5% AcOH in water. The solvent was found by attempting several solvent systems by TLC and ninhydrin stain, including such solvents systems as 100% EtOH, 80% EtOH, and 50% EtOH. The solvent that allowed for best separation was 50% EtOH and 5% AcOH in water (*rf* values of 0.3 and 0.7 for glycine and products, respectively). The fractions were monitored by TLC and ninhydrin stain. The solvent was removed using a SpeedVac to afford the final product. ^{1}H NMR analysis revealed a slight separation of products from glycine. Separately, a 20 x 2 cm silica gel column was used in the attempt to allow for great separation, but this was also unsuccessful.

The fifth and final attempt is summarized in the following section.

Preparative synthesis of β-hydroxy-α-amino acids using *A. jandaei* L-*allo*-TA. Reaction mixtures contained 2.0 mmol of aldehyde, 10 mmol glycine, 100 nmol PLP and 200 µL of enzyme lysate in 20 mL 50 mM Tris, pH 9.7 and 2% (v/v) ethanol. After gently rotating at 37 ºC for 4 hr, the unreacted aldehyde was removed by extraction with Et_2O (2 × 30 mL) and the aqueous layer was lyophilized. The solid residue was mixed thoroughly with 30 mL of MeOH and the solution was filtered and evaporated under reduced pressure. This procedure was repeated to remove additional unreacted glycine. The crude product was resuspended in 10 mL of 50 mM KP_i, pH 8.0, then 1 mg of purified glycine oxidase was added and the mixture was gently rotated at 37 ºC for 8 hr. An additional of 1 mg portion of purified glycine oxidase was then added and incubation at 37 ºC was continued for an additional 20 hr. The reaction mixture was lyophilized. The residue was stirred with MeOH, leaving most phosphate undissolved. After evaporating the solvent, the crude product was dissolved in water and applied to an 11 × 1.5 cm DOWEX, 1 × 2 (HO^- form) column. The column was washed with 100 mL of deionized water, then the desired product was eluted by washing with 50 mL of 0.5% acetic acid. The solvent was removed using a SpeedVac to afford the final product.

(2*S*,3*S*)-2-amino-3-hydroxyheptanoic acid. White solid 53 mg, 16% yield, 22% d.e., m.p. 226 ºC (lit. m.p. 223 – 224 ºC).[245] ^{1}H NMR (300 MHz, D_2O) δ 4.08 (1H, m), 3.65 – 3.84 (1H, dd), 1.3 – 1.45 (2H, m), 0.85 (3H, m) ppm. ^{13}C NMR (300 MHz, D_2O) δ 171.47, 69.39, 59.34, 32.76, 30.5, 27.39, 21.54, 13.07 ppm (Figure A-2).

(2*S*,3*R*)-2-amino-3-hydroxycyclohexanepropanoic acid. White solid 185 mg, 50% yield, 99% d.e., m.p. 210 ºC (lit. m.p. 216 – 217 ºC).[245] ^{1}H NMR (300 MHz, D_2O) δ

3.89 – 4.00 (1H, dd), 3.58 – 3.61 (1H, dd), 1.00 – 1.93 (11H, m) ppm. ^{13}C NMR (300 MHz, D_2O) δ 172.17, 74.90, 56.10, 39.41, 28.68, 28.29, 25.65, 25.22, 25.07 ppm (Figure A-3).

(2*S*,3*S*)-3-hydroxyphenylalanine. White solid 115 mg, 32% yield, 86% d.e., m.p. 188 – 190 ºC (lit. m.p. 189 – 191 ºC).[246] ^{1}H NMR (300 MHz, D_2O) δ 7.44 (5H, m), 5.29 – 5.27 (1H$_{anti}$, dd), 3.90 – 3.89 (1H, dd) ppm. ^{13}C NMR (300 MHz, D_2O) δ 171.79, 139.00, 128.89, 128.75, 128.52, 126.25, 125.82, 71.18, 60.70 ppm (Figure A-4).

2-amino-3-hydroxy-4-pyridinepropanoic acid. Orange solid 101 mg, 28% yield, 40% d.e., m.p. 180 ºC. ^{1}H NMR (300 MHz, D_2O) δ 8.57 (2H, m), 7.69 (2H, d), 5.70 – 5.69 (0.70H$_{syn}$, d), 5.58 – 5.57 (0.30H$_{anti}$, d), 3.97 – 4.17 (1H, dd) ppm. ^{13}C NMR (300 MHz, D_2O) δ 172.17, 153.10, 146.71, 145.44, 122.87, 122.51, 69.94, 59.92 ppm (Figure A-5).

3-hydroxy-2-methoxy-phenylalanine. White solid 91 mg, 22% yield, 89% d.e, m.p. 170 ºC. ^{1}H NMR (300 MHz, D_2O) δ 7.46 – 7.38 (2H, m), 7.04 – 7.01 (2H, m), 5.57 – 5.56 (1H$_{syn}$, dd), 4.41 – 4.40 (1H, dd), 3.81 (3H, s) ppm (Figure A-6).

2-amino-3-(2-chloro-3-pyridine)-3-hydroxypropanoic acid. Orange solid 215 mg, 50% yield, 56% d.e, m.p. 179 – 180 ºC. ^{1}H NMR (300 MHz, D_2O) δ 8.21 – 7.93 (2H, m), 7.44 – 7.36 (1H, m), 5.53 – 5.52 (0.65H$_{syn}$, d), 5.35 – 5.34 (0.30H$_{anti}$, d), 4.09 – 4.07 (1H, dd) ppm (Figure A-7).

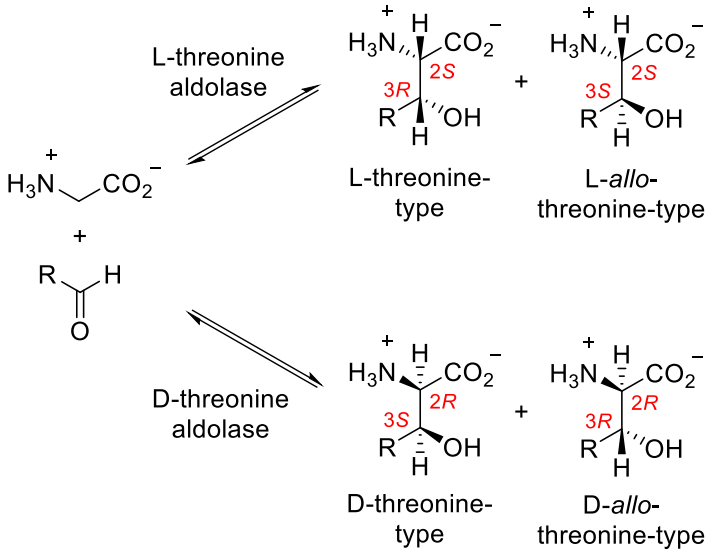

Figure 3-1. Threonine aldolase reactions

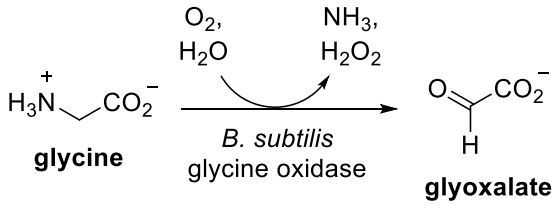

Figure 3-2. Glycine oxidase reaction

a) Khuhawar *et. al.* Method

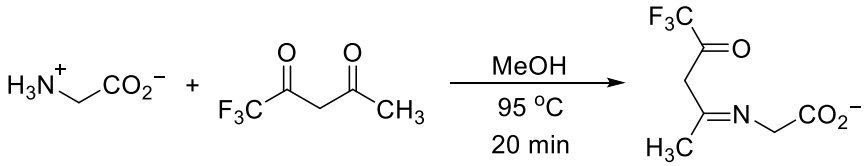

b) Nimura and Kinoshita Method

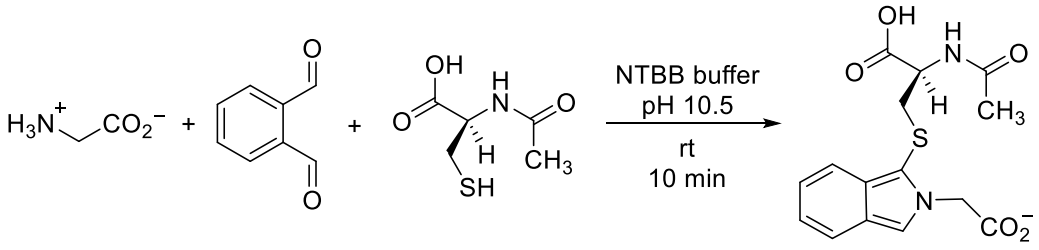

c) Donike/Yoon Method

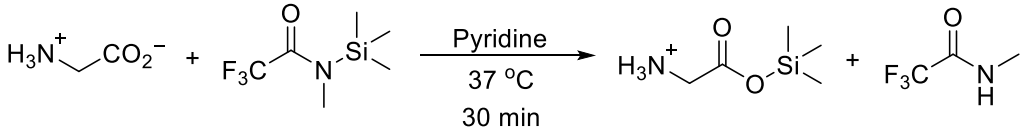

Figure 3-3. Derivatization of amino acids

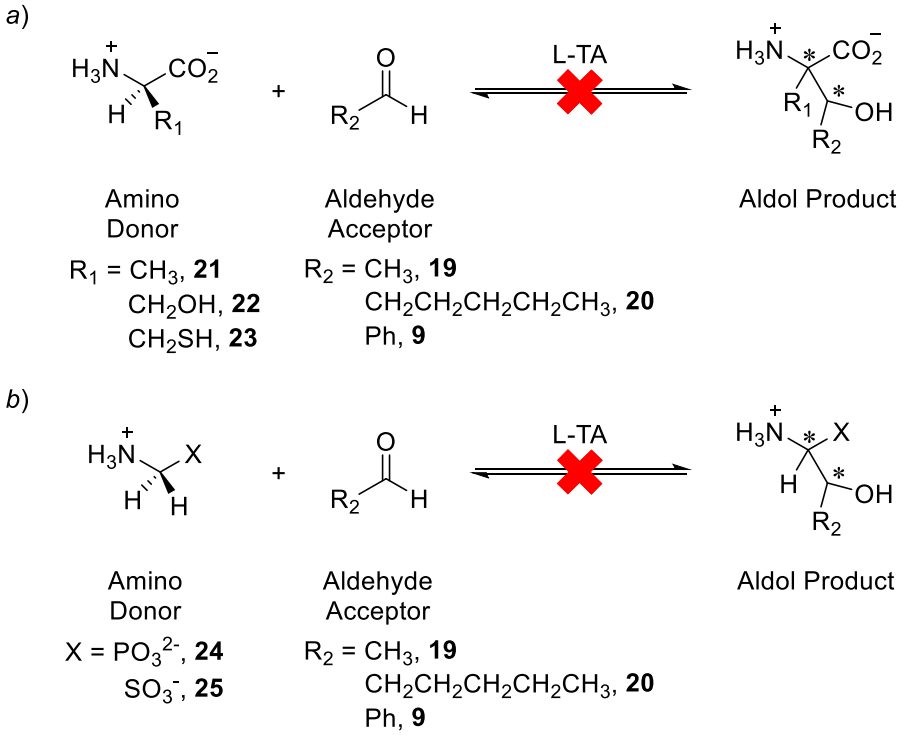

Figure 3-4. Screening of amino donors

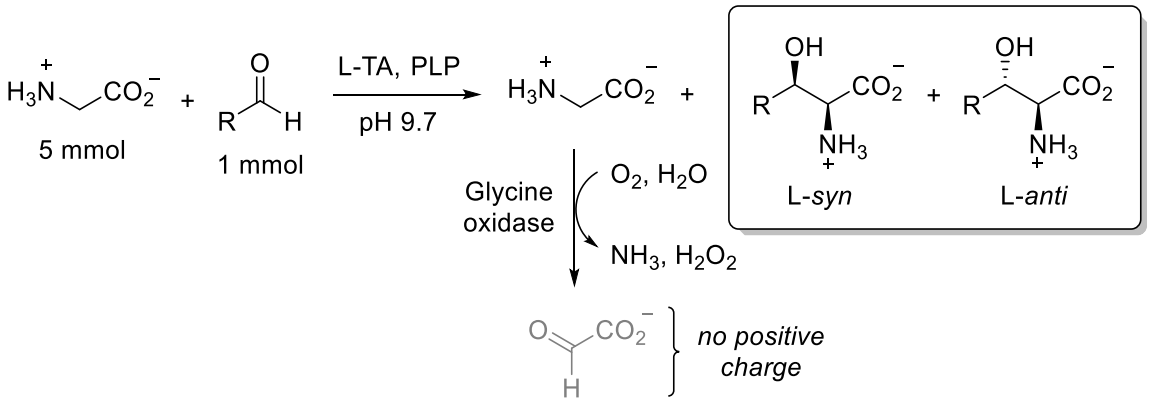

Figure 3-5. Preparative reactions

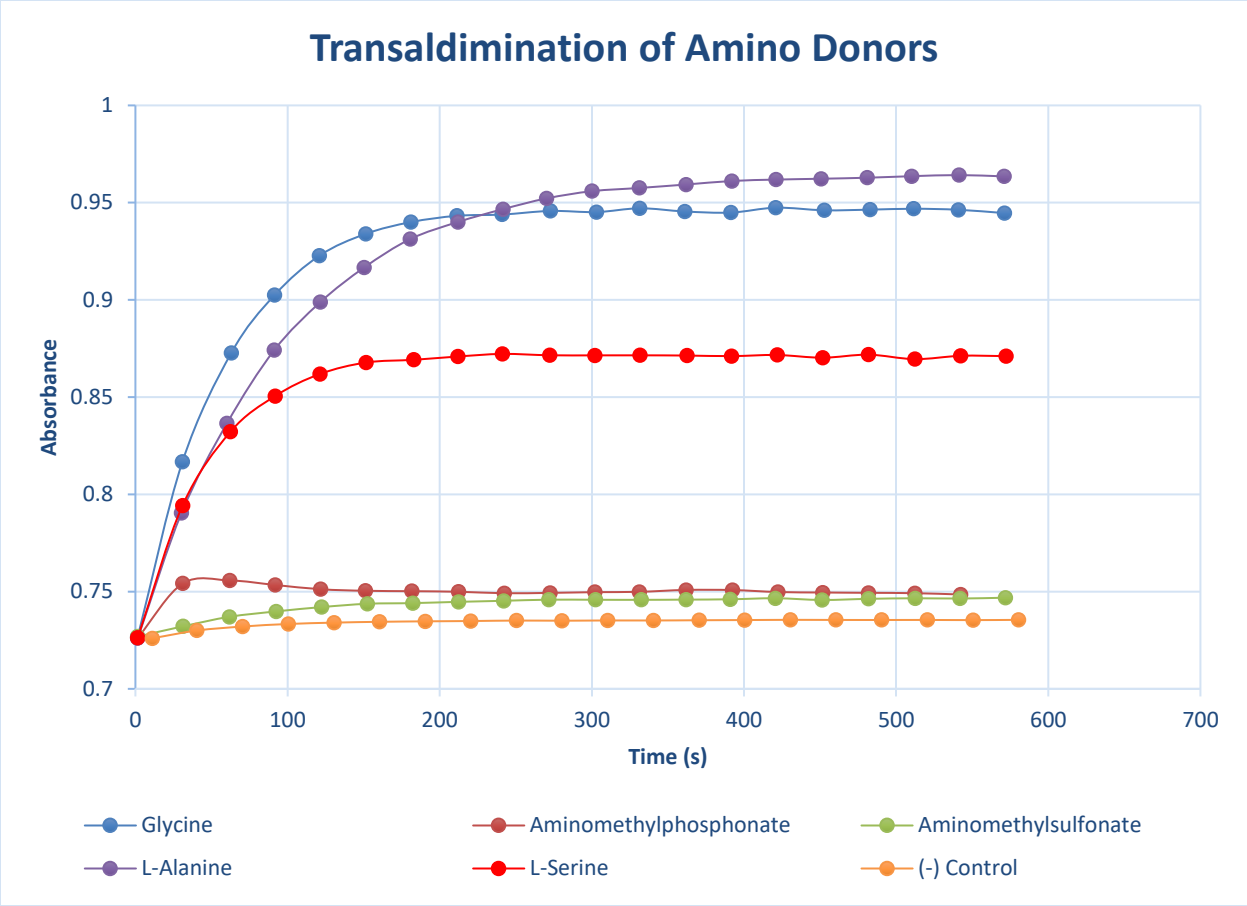

Figure 3-6. Transaldimination of amino donors

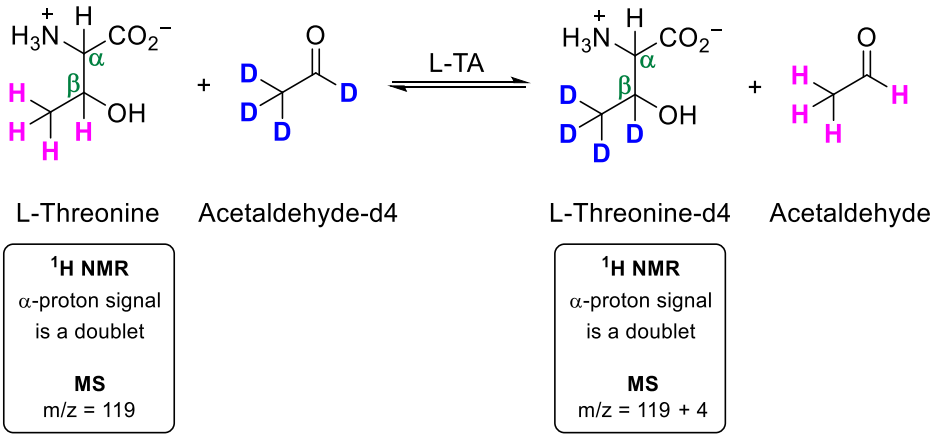

Figure 3-7. Thermodynamic reversibility of L-threonine

CHAPTER 4
STRUCTURE DETERMINATION AND SUBSTRATE PROFILING OF *P. putida* L-THREONINE ALDOLASE

Introduction

L-Threonine aldolases (L-TAs) catalyze the retro-aldol cleavage of threonine to glycine and acetaldehyde. Although named for the retro-aldol reaction, they also catalyze the formation of threonine by carbon-carbon bond formation at the α-position of the donor amino acid and the carbonyl carbon of the acceptor aldehyde. Many L-TAs have been characterized and screened against an assortment of aldehydes, ranging from long chain aliphatic aldehydes to an array of aromatic aldehydes with altered electronic effects.[184, 222, 223] TAs vary in their stereoselectivities at the α- or β-positions of the aldol products and have been named L-threonine aldolase, L-*allo*-threonine aldolase, low-specificity L-threonine aldolase/L-*allo*-threonine aldolase and D-threonine/D-*allo*-threonine aldolases. The ability of these enzymes to control two adjacent chiral centers along with *C-C* bond formation gives them potential for biotechnology. In recent years, these enzymes have been applied to the synthesis of important pharmaceuticals including L-*threo*-3,4-dihydroxyphenylserine, a Parkinson's disease therapy,[238] and (2*R*,3*S*)-2-amino-3-hydroxy-3-(pyridin-4-yl)-propanoic acid, a precursor to the drug development candidate (2*R*,3*S*)-2-amino-3-hydroxy-3-(pyridin-4-yl)-1-(pyrrolidin-1-yl)propan-1-one.[200]

Currently, three L-TAs, from *Thermogota maritima*,[205] *Aeromonas jandaei*,[207] and *E. coli*,[206] have known crystal structures. This collection of data has given us a detailed look at the enzyme's catalytic mechanism. The two most important and conserved amino acid residues within the active site are Lys 199 and His 85. The Lys forms the Schiff's base with PLP and any mutations at this site render the enzyme inactive.[189]

The His is responsible for regulating of the degree of stereoselectivity between the L- and L-*allo*- stereomers and may also be the catalytic base for the retro-aldol cleavage of threonine.[205-207]

Pseudomonas putida L-TA has been studied for its broad substrate range in producing β-hydroxy-α-amino acids.[184, 191, 192, 247] Although other L-TAs have shown a high tolerance in the synthesis of phenylserine derivatives and long chain amino acids,[184] the diastereoselectivity of *P. putida* L-TA was found to be rather poor with the remarkable exception of 4-fluorothreonine (93% d.e.).[191] On the other hand, in most cases, conversions were generally high for this family of enzymes. Additionally, temperature, pH, and co-solvent addition studies were executed by Steinreiber *et al.*, who found that the most favorable conditions were pH 8.0 and room temperature. Addition of co-solvents did not increase reactivity of the enzyme.[192]

Here, we report the crystal structure determination and substrate profiling results for L-TA from *P. putida* (LTAPP). The enzyme was screened against a variety of aldehyde acceptors. In comparison to other enzymes in the same class, diastereomeric purify was found to be quite low (Table 3-1). We hoped to use the crystal structure to understand the poor stereoselectivity found during screening studies.

Results and Discussion

Gene Cloning and Protein Overexpression

The gene encoding the L-TA was obtained by colony PCR[229] from a *P. putida* strain purchased from Carolina Biological Company. After amplification, the L-TA gene was ligated into pET-15b and the resulting plasmid was used to transform the *E. coli* overexpression strain BL21-Gold(DE3). The L-TA was efficiently overproduced by the recombinant strain, which allowed crude lysates to be employed for screening reactions.

Control reactions were carried out for each aldehyde substrate with a crude extract from an un-transformed *E. coli* strain; none gave significant aldol product.

Purification of *P. putida* L-Threonine Aldolase and Screening of Protein Crystals

After isolating the crude lysate, the L-TA was applied to a HiTrap Chelating HP column to separate the hexahistidine tagged L-TA by affinity chromatography. The eluate was concentrated by ultrafiltration and the purified protein was applied to a Superdex™ 200 column for further purification. The *N*-terminal hexahistidine tag was cleaved by using thrombin from bovine plasma. The histidine tag was separated from the desired protein by applying it to the same HiTrap Chelating HP column. The desired protein was concentrated by ultrafiltration and reconstituted in 50 mM KP_i, pH 8.0 for crystal screening.

Hampton Research 96-well screening kits were used for the initial screening of *P. putida* L-TA. All initial screenings used the sitting-drop vapour-diffusion method at room temperature with 10 and 15 mg/mL protein concentrations. After 72 hours, crystals were identified in the C-6 well of the Salt Rx HT kit. The precipitant solution contained 3.5 M sodium formate, 0.1 M sodium acetate trihydrate pH 4.6. Crystallization scale ups using both hanging-drop and sitting-drop vapour-diffusion methods and careful observation revealed that crystals formed in less than 24 hours.

Optimized crystal conditions were sought in order to slow crystallization. A 24-well large screening plate was set up with varied concentrations of both sodium formate (0.7 – 6.3 M) and sodium acetate (0.1 – 1 M) buffers. This screening revealed that crystals could not form in sodium formate and sodium acetate concentrations greater than 4.9 and 0.3 M, respectively. Some conditions grew crystals in 24 hours, however a

few wells presented crystal formation in 120 hours. Two of these crystals were determined at 2.80 and 2.82 Å resolutions, respectively.

The previous screening used 15 mg/mL of purified L-TA; the next attempt involved decreasing the protein concentration added to each drop (5 – 10 mg/mL) with varied concentrations of both sodium formate (2.1 – 4.9 M) and sodium acetate (0.1 – 0.2 M) buffers. As before, most of the conditions resulted in crystals after 24 hours; however, careful observation revealed that after 240 hours few rod-shaped crystals had formed. The final crystallization condition was a hanging-drop vapour-diffusion method with a precipitant solution of 2.1 M sodium formate, 0.1 M sodium acetate trihydrate pH 4.6 at room temperature with 5 mg/mL of L-TA (1 : 1, precipitant solution : protein). The crystals up to this point had been a tetragonal bipyramid shape, therefore the new rod-shaped crystal could have indicated a different packing of the crystal lattice that might have signified a better resolution. Two of these crystals were used to collect a full data set: one un-soaked and one soaked with the natural substrate L-Thr. These two L-TA structures were determined at 2.27 and 2.75 Å resolution, respectively.

Overall Structure of the L-Threonine Aldolase from *P. putida*

The crystal structure of L-TA from *P. putida* (LTAPP) was determined at 2.27 Å resolution and was a homotetramer. This is consistent with other crystallographic studies of L-TAs from *T. maritima*,[205] *E. coli*,[206] and *A. jandaei*.[207] The structure was first determined by molecular replacement with the *E. coli* L-TA (PDB code 4LNJ). The data collection and refinement statistics are summarized in Table 4-1.

Table 4-1. Data collection and refinement statistics

	LTAPP[a]		LTAPP[a]
Resolution range	26.71 - 2.275 (2.356 - 2.275)	CC(work)	0.957 (0.855)
Space group	C 1 2 1	CC(free)	0.960 (0.663)
Unit cell	198.167 186.96 53.269 90 98.924 90	Number of non-hydrogen atoms	11258
Total reflections	585838 (53082)	Macromolecules	10667
Unique reflections	87029 (8273)	Ligands	84
Multiplicity	6.7 (6.4)	Solvent	507
Completeness (%)	99.42 (95.01)	Protein residues	1375
Mean I/sigma(I)	14.50 (2.65)	RMS(bonds)	0.014
Wilson B-factor	41.45	RMS(angles)	1.30
R-merge	0.08797 (0.6277)	Ramachandran favored (%)	94.13
R-meas	0.09536 (0.682)	Ramachandran allowed (%)	5.06
R-pim	0.03654 (0.2635)	Ramachandran outliers (%)	0.81
CC1/2	0.998 (0.879)	Rotamer outliers (%)	1.91
CC*	0.999 (0.967)	Clashscore	10.79
Reflections used in refinement	87014 (8270)	Average B-factor	54.48
Reflections used for R-free	1999 (190)	macromolecules	54.67
R-work	0.1814 (0.2745)	ligands	53.89
R-free	0.2215 (0.3123)	solvent	50.52

[a] Statistics for the highest-resolution shell are shown in parentheses.

In the structure of LTAPP (Figure 4-1a), two of the four chains (A and D or B and C) come together to form a 'catalytic dimer'. Each monomer contains 12 α-helices and 8 β-sheets, shown in Figure 4-1b. The overall structure of a single monomer equates well to the structure of *E. coli* L-TA (Figure 4-1c), which contains 13 α-helices and 9 β-sheets. The two differences are highlighted in the zoomed view in Figure 4-1d,e. The purple loop (Figure 4-1d) in LTAPP is shown as the 9th β-sheet in *E. coli* L-TA.[206] Additionally, it is shown as a β-sheet in *T. maritima* L-*allo*-TA[205] and a loop in *A. jandaei* L-*allo*-TA[207] (Figure 4-1f,g). The green loop succeeding one of the α-helices on the surface of the protein is approximately 13 amino acid residues long. By comparing its position and length with other L-TAs shown in green in Figure 4-1e-g, we can determine that it is very flexible as it is located on the surface of the protein and contains several more amino acid residues (4 – 7) than other L-TAs. Since LTAPP has a slightly longer loop and is perceived as flexible, it could have distorted the folding of the preceding α-helix, displaying the multiple conformations shown by the electron density at this position (not shown).

The Active Site of Threonine Aldolase

The binding pocket of the TA family is composed of positively charged residues in order to stabilize the negatively charged PLP and substrate/product. The electrostatic surface potential is displayed in Figure 4-2a to show the binding pocket of one monomer. The active site of this family is comprised of five conserved residues: Ser 10, His 89, Arg 177, Lys 207, and Arg 321 (Figure 4-2b). The two most important and conserved amino acid residues within the active site are Lys 207 and His 89. Lys207 is essential for catalytic activity since it forms a Schiff's base with the PLP cofactor. Mutations at this position leave the enzyme inactive.[189] His 89 is responsible

for regulating of the degree of diastereospecificity between the L- and L-*allo*-stereoisomers.[205-207]

A more detailed illustration of the active site pocket is represented in Figure 4-3a. The unbound PLP has hydrogen bonding interactions with Gly 64, Thr 65, and Arg 177 to stabilize the negatively charged phosphate and hydroxide groups along with Asp 174 to help stabilize the pyridinium ring of PLP. In addition to the hydrogen bonding interactions, His 89 donates pi-stacking interactions with the pyridine ring to help position the cofactor in the active site.

Although we were unsuccessful at soaking our crystals with the native substrate, there is a clear binding pocket for the substrate shown as a gray circle in Figure 4-3a. As described in previous crystallographic studies,[205-207] the carboxylic group of the PLP-Gly interacts with the side chains of Ser 10, Arg 177, and Arg 321. When the aldol condensation occurs, His 89 and His 133 hydrogen bond to the hydroxyl group of threonine. These interactions are summarized in Figure 4-3b-d.

Structural Comparison of L-Threonine Aldolases

As mentioned previously, crystal structures of L-TAs from *T. maritima*,[205] *E. coli*[206] and *A. jandaei*[207] have been solved. Sequence alignment (Figure 4-4) of the three enzymes with LTAPP resulted in 43 completely conserved residues (shown in red). Among these conserved residues 16 are located within the active site, 9 of which are highlighted in Figure 4-3a (gray).

The remaining 7 conserved residues include Asp 11, Tyr 35, Asn 68, Glu 94, Gly 175, Ala 176, and Asn 290 (Figure 4-5). Only Tyr 35 is sufficiently close to interact directly with the substrate/product (Figure 4-5a). All other amino acid residues hydrogen bond to one of the conserved active site residues. The Asp 11 hydrogen

bonds to εN-Arg 177, Asn 290 with γO-Asp 11, Asn 68 with γO-Asp 174, and Glu 94 with γN-His 89 (Figure 4-5b-c).

The overall secondary structures of the four L-TAs were very comparable at all angles (Figure 4-6a). The only major differences was in surface loops and the loops in Figure 4-1d-e. In order to see key differences in the active site residues, all four structures were aligned and active site residues highlighted. As shown in Figure 4-6b, the cofactor and conserved residues occupy the same space and interact with the same amino acid residues. The only residue within the active site that differs in LTAPP from the other L-TAs crystallized thus far was the 93 position. In LTAPP this position was occupied by Asp; however, Tyr was found at the analogous position in *T. maritima* L-*allo*-TA and *E. coli* L-TA and Phe occurred at this location in *A. jandaei* L-*allo*-TA.[205-207] This particular position is helpful to define the hydrophobic pocket where the methyl group of L-Thr binds for the native reaction. Site saturation mutagenesis at this position might determine whether this site plays an important role in the poor diastereoselectivity of this enzyme and this will be in the subject of the following chapter.

Optimization of Reaction Conditions

Prior to carrying out extensive aldehyde screening studies, we used the same DOE methodology employed in the previous chapter to identify optimal conditions for the overexpressed L-TA from *P. putida*. A total of 92 individual reactions with varied temperature (4 ºC, 18 ºC, 25 ºC, 37 ºC and 42 ºC), glycine : aldehyde ratio (2, 4, 8, and 10) and pH (5, 7, 8, 9.7 and 12) were carried out for the enzyme – substrate pair and both relative conversion and product diastereomeric excess values were determined for each. Based on previous literature, the starting point was 25 ºC, pH 8 and a 5-fold

molar excess of glycine *versus* the aldehyde. The starting conditions gave a relative conversion[i] of 0.51 using a 4 : 1 ratio of glycine : aldehyde.

Aldehyde **10** (Table 4-2) was chosen to optimize the enzyme as it gave measurable, but incomplete conversions under standard conditions; this allowed both improved and detrimental changes to the reaction conditions to be identified. The only condition that affected the relative conversion with aldehyde **10** was the glycine to aldehyde ratio. Conversion increased slightly as the substrate molar ratio was increased; solving for the optimal conditions (pH 8, 25 ºC and a glycine : aldehyde ratio of 10) and presenting a relative conversion of 0.89, less than a 2-fold improvement. Although the outcome of this DOE strategy was more modest than others, it did provide that the increased ratio of glycine *versus* aldehyde increased the overall conversion.

Table 4-2. Substrate specificity of L-TA-catalyzed aldol reactions

Entry	Aldehyde	Product	Reaction Time (hr)	Conversion[a] (%)	d.e.[a] (%)
1	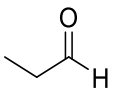 **1**	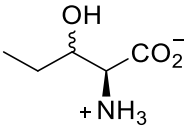	4 20	59 78	99 99
2	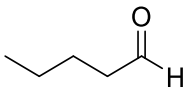 **2**	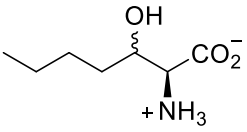	4 20	69 72	26 13
3	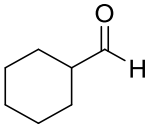 **3**	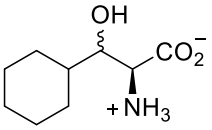	4 20	35 48	37 25
4	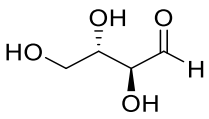 **4**	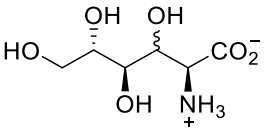	4 20	35 50	n.d.[c] n.d.[c]

[i] Relative conversions for these studies were defined as the peak area ratio of MSTFA-derivatized product/internal standard using GC/MS.

Table 4-2. Continued

Entry	Aldehyde	Product	Reaction Time (hr)	Conversion[a] (%)	d.e.[a] (%)
5	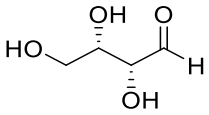 **5**	--	4 20	-- --	-- --
6	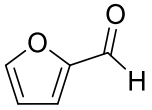 **6**	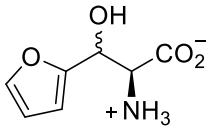	4 20	24 36	33 28
7	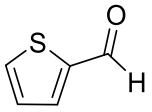 **7**	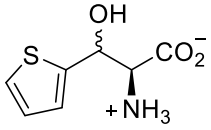	4 20	8 9	20 12
8	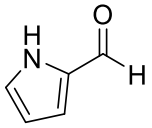 **8**	--	4 20	-- --	-- --
9	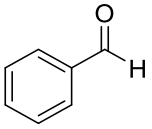 **9**	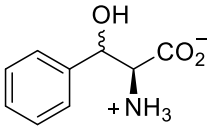	4 20	22 24	16 14
10	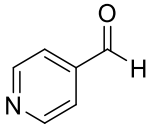 **10**	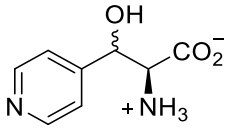	4 20	5 47	42 13
11	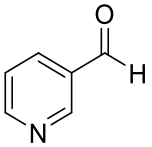 **11**	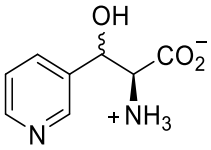	4 20	60 58	10 13
12	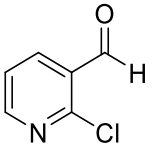 **12**	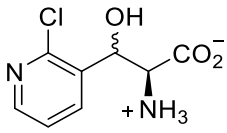	4 20	6 32	48 45
13	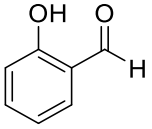 **13**	--	4 20	-- --	-- --

Table 4-2. Continued

Entry	Aldehyde	Product	Reaction Time (hr)	Conversion[a] (%)	d.e.[a] (%)
14	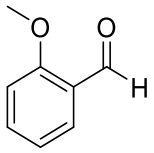 **14**	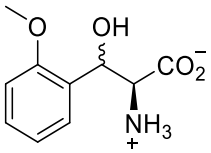	4 20	24 64	n.d.[c] n.d.[c]
15	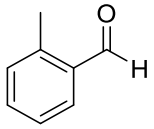 **15**	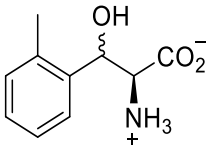	4 20	<5[b] 11	--[b] n.d.[c]
16	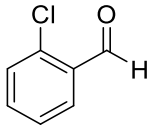 **16**	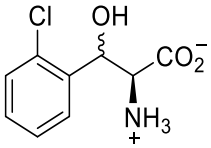	4 20	54 75	n.d.[c] n.d.[c]
17	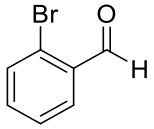 **17**	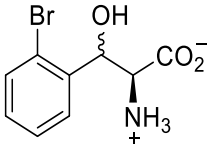	4 20	14 30	n.d.[c] n.d.[c]
18	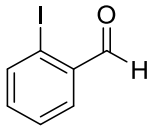 **18**	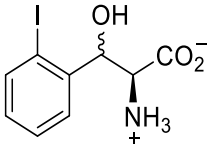	4 20	<5[b] <5[b]	--[b] --[b]

Note: Reaction mixtures contained 500 mM glycine, 100 mM aldehyde, 0.05 mM PLP, 20% ethanol, and 10 µL of enzyme lysate in 1 mL of 50 mM KP_i, pH 8. Reactions were incubated at 25 ºC.

[a] Conversion and diastereomeric excess values were determined by GC/MS after MSTFA derivatization. Reactions with 1 – 5% conversions are listed as "<5%" and no values for diastereomeric purity are provided since the small peak sizes preclude accurate integration.

[b] Accurate values for conversion and diastereomeric excess could not be determined due to the very low peak areas.

[c] It was not possible to determine the diastereoselectivity of this reaction by chiral-phase GC since temperatures required for elution were greater than the maximum column temperature.

Screening of Aldehyde Acceptors

Once optimized reaction conditions had been identified, the substrate range of the *P. putida* L-TA was investigated using numerous aldehyde acceptors (Table 4-2). The aldehydes were selected so that relative conversions and diastereoselectivities could be compared with the other L-TAs from the previous chapter (Table 3-1). Overall, the diastereoselectivity of this enzyme was poor, which agrees with literature reports.[191]

The only aldehyde that displayed diastereoselectivities greater than 50% was **1**. The aldol condensation of this aldehyde with glycine gave a two-fold increase in relative conversion compared to the L-TAs from *A. jandaei*, *E. coli*, and *T. maritima* while retaining the 99% d.e. Although conversions of other aldehyde acceptors with this L-TA were improved from the other L-TAs, the diastereoselectivity was always inadequate.

Conclusion

The structure of *P. putida* L-TA was successfully crystallized and data collected at a resolution of 2.27 Å. Molecular replacement and refinement strategies were used to build the final model of the structure and it was determined to be a homotetramer, comparable to other L-TAs in its class. The active site lysine was determined to be Lys 207 and other highly conserved amino acid residues included: Ser 10, His 89, His 133, Arg 177, and Arg 321. Comparison with the other structures revealed two main differences. First, the loop located near the active site was slightly longer than the others (4 – 7 amino acid residues), which distorts the folding of the preceding α-helix. Second, the amino acid residue at position 93 differed. In LTAPP, it was an Asp residue; however, in other L-TAs, the residue at the analogous position was a large aromatic residue (Tyr or Phe). We also extensively screened the enzyme with a variety of aldehyde acceptors. This study revealed that the enzyme has a broad substrate tolerance, although diastereoselecivity was poor in most cases. This deficiency could be due to the extended loop or to the acidic residue at position 93, or to other, more subtle factors. Mutagenesis studies of this position are described in the following chapter.

Experimental Procedures

General. LB medium contained 10 g/L Bacto-Tryptone, 5 g/L Bacto-Yeast Extract and 10 g/L NaCl; 15 g/L agar was added for plates. PCR amplifications were performed with Phusion Hot Start II DNA polymerase using the manufacturer's protocols. Electroporation was carried out with a BioRad GenePulser apparatus using 0.2 cm cuvettes. Promega Wizard kits and CsCl buoyant density ultracentrifugation were used for small- and large-scale plasmid purifications, respectively. Fluorescent Sanger DNA sequencing was performed by the University of Florida ICBR. Crystallography kits for 96-well screening were purchased from Hampton Research. GC/MS analysis employed a 30 m x 0.25 mm Beta Dex™ 225 column and ionization by EI at 70 eV. The temperature program involved an initial hold at 95 ºC for 5 min, an initial rate of 5 ºC/min to 138 ºC, followed by a rate of 10 ºC/min to 180 ºC, and a final rate of 2 ºC/min to 200 ºC, held at that temperature for 10 min.

Plasmid construction. The L-TA gene from *P. putida* (accession number AP013070) was isolated and amplified from a *P. putida* strain purchased from Carolina Biological Company by colony PCR[229] using 5' – CGTTCACAGGACCGTCATATGACA GATAAGAGCCAACAATTCGCC – 3' and 5' – CTGGCTTGCCGGCGATTGGGGATCC TCAGGCGGTGATGATGCTGCGGATA – 3' as forward and reverse primers, respectively. These primers also introduced flanking *Nde*I and *Bam*HI restriction sites (underlined). After purification, the PCR product was digested sequentially with *Nde*I and *Bam*HI, then ligated with *Nde*I, *Bam*HI-digested pET-15b. After transformation into *E. coli* ElectroTen-Blue, plasmid DNA from a randomly-chosen colony was isolated, restriction mapped and then sequenced to verify the desired structure. The resulting

plasmid (designated pSF6) was used to transform *E. coli* BL21-Gold(DE3) strain for protein overexpression.

Protein purification. A single colony of *E. coli* BL21-Gold(DE3) containing pSF6 was used to inoculate 50 mL of LB medium supplemented with 100 µg/mL ampicillin. After shaking at 37 ºC until becoming turbid, a 40 mL portion of the preculture was added to 4 L of LB medium supplemented with 100 µg/mL ampicillin, 80 mL of 20% glucose, and 1.5 mL of antifoam 204 in a New Brunswick M19 fermenter. The culture was grown at 37 ºC with stirring at 400 rpm and an air flow of 4 vvm until the $O.D._{600}$ reached 0.5 – 0.6. Protein overexpression was induced by adding of 10 mL of 0.16 M IPTG (to yield a final concentration of 0.4 mM) and adjusting the temperature to 30 ºC and shaking. After 3 hours, the cells were harvested by centrifugation at 6,300 × g for 15 min at 4 ºC, resuspended in 50 mM KP_i, pH 8.0 (1 mL/g), then lysed by a French pressure cell at 17,000 psi. Insoluble debris was pelleted by centrifugation at 39,000 × g for 1 hr at 4 ºC and a portion of the yellow supernatant was used for TA-catalyzed reactions. The remaining crude lysate was applied to a 5 mL HiTrap Chelating HP column (GE Healthcare Life Sciences) that had been equilibrated with binding buffer (0.02 M NaH_2PO_4, 0.5 M NaCl, 20 mM imidazole, pH 7.4). After washing with 50 mL of binding buffer, the desired protein was eluted by elution buffer (0.02 M NaH_2PO_4, 0.5 M NaCl, 0.5 M imidazole, pH 7.4). A flow rate of 2 mL/min was employed throughout. The eluate was concentrated by ultrafiltration (Amicon Ultra) to yield a final concentration of 25 mg/mL. The purified protein was applied to a Superdex™ 200 column (Pharmacia Biotech) that had been equilibrated with 50 mM Tris-HCl, 50 mM NaCl, pH 7.4. The desired protein was eluted with the same buffer. A flow rate of

0.3 mL/min was employed throughout. The eluate was concentrated by ultrafiltration (Amicon Ultra) to yield a final concentration of 25 mg/mL. The *N*-terminal histidine tag was cleaved using thrombin from bovine plasma. The histidine tag was separated from the desired protein by applying it to the same treatment described above using the 5 mL HiTrap Chelating HP column. The desired protein was eluted with binding buffer and eluate was concentrated by ultrafiltration (Amicon Ultra), then diluted with 50 mM KP_i, pH 8.0 and re-concentrated. This was repeated 2 more times. The final L-TA sample was concentrated to 15 mg/mL and used for immediately for crystal screening.

Crystal screening. The first round of crystallization screening of the L-TA from *P. putida* used two commercial screening kits from Hampton Research (PEG Rx HT (HR2 – 086) and Crystal Screen Cryo HT (HR2 – 133)). These kits were used with the sitting-drop vapor-diffusion method at room temperature with 10 – 15 mg/mL protein concentrations (added at a ratio of 1 : 1, precipitant solution : protein solution). This screening resulted in one only condition that formed quasi crystals.

The second round used three commercial screening kits from Hampton Research (Salt Rx HT (HR2 – 136), Index HT (HR2 – 134) and Additive Screen HT (HR2 – 138)). The additive screen kit used the precipitant solution that formed quasi crystals from the first round of screening (0.075 M HEPES pH 7.5, 0.6 M NaH_2PO_4 $1H_2O$, 0.6 M KH_2PO_4, 25% glycerol). The screening was accomplished with the sitting-drop vapor-diffusion method at room temperature with 10 and 15 mg/mL protein concentrations (added at a ratio of 1 : 1, precipitant solution : protein solution). Within 72 hours, this screening revealed four conditions that formed quasi crystals and one that formed ordered crystals in well C-6 of the Salt Rx HT screening kit. The precipitant

solution consisted of 3.5 M sodium formate, 0.1 M sodium acetate trihydrate pH 4.6. A large scale screening with careful observation using these same conditions revealed the protein had actually crystallized within 24 hours.

Attempts to optimize crystal growth involved varying concentrations of both salts (0.7 M – 6.3 M sodium formate and 0.1 – 1 M sodium acetate trihydrate pH 4.6) and monitoring crystal formation daily. The protein concentration used was 15 mg/mL and it was added at different ratios with the precipitant solution (1 : 4, 2 : 4, and 3 : 4) *via* both the hanging-drop and sitting-drop vapor-diffusion method at room temperature. Within 24 hours, some conditions resulted in crystallized protein with a tetragonal bipyramidal shape; however, a few wells showed crystal formation in 120 hours with a precipitant solution consisting of 2.1 M (or 2.8 M) sodium formate, 0.1 M sodium acetate trihydrate pH 4.6.

In the final optimization screening study, the concentrations of both salts (2.1 M – 4.9 M sodium formate and 0.1 – 0.2 M sodium acetate trihydrate pH 4.6) were varied and the protein concentration decreased. Crystal formation was monitored daily. The protein concentration used in this screening was 5 - 10 mg/mL and it was added at different ratios with the precipitant solution (1 : 4, 2 : 4, and 3 : 4) *via* the hanging-drop vapour-diffusion method at room temperature. As before, most of the conditions resulted in crystals after 24 hours, but careful observation revealed that after 240 hours, a few rod-shaped crystals had formed with a precipitant solution consisting of 2.1 M sodium formate, 0.1 M sodium acetate trihydrate pH 4.6. Two of these crystals were used to collect a complete data set for X-ray diffraction analysis: one un-soaked and one soaked with the natural substrate L-Thr (5 mM) for 1 hour at room temperature.

Data collection. The crystals were flash-cooled in liquid nitrogen using 20% (v/v) glycerol as a cryoprotectant. X-ray diffraction data were collected at the Advanced Photon Source (Argonne National Laboratory) on beamline 21-ID-G. Reflection data were processed using XDS.[248] The structure of LTAPP was solved by the molecular-replacement method using AUTOMR in the PHENIX suite[249] using the structure of L-TA from *E. coli* (Accession number NC000913; PDB entry 4LNJ).[206] Manual model building and refinement were performed with *Coot*[250] and *phenix.refine*,[251] respectively. The structure was refined at 2.27 Å resolution with an R factor and an R_{free} of 0.1799 and 0.2171, respectively.

Amino acid derivatization. Reaction mixtures were dried completely under reduced pressure for 30 min by a Savant SpeedVac SVC100, then the residue was taken up in pyridine (1 µL) and MSTFA (50 µL). After shaking at 37 ºC for 30 min, the mixtures were analyzed by GC/MS.

General procedure for screening aldehyde acceptors. Reactions contained 0.1 mmol of aldehyde, 0.5 mmol of glycine, 10 nmol of PLP and 10 µL of enzyme lysate in 50 mM KP_i pH 8 buffer (total volume of 1 mL). These were gently rotated overnight at room temperature and sampled after 4 hr and overnight for MSTFA derivatization and GC/MS analysis.

General procedure for screening amino donors. Reactions contained 0.1 mmol of aldehyde (acetaldehyde, hexanal, or benzaldehyde), 0.5 mmol of amino donor, 10 nmol of PLP and 10 µL of enzyme lysate in 50 mM KP_i pH 8 buffer (total volume of 1 mL). These were gently rotated overnight at room temperature and sampled after 4 hr and overnight for MSTFA derivatization and GC/MS analysis.

Design of experiments. To optimize reaction conditions, the L-TA was used in a series of experiments with varied temperature, pH, and glycine ratio. All reactions contained 0.1 mmol of aldehyde, 0.2 - 1.0 mmol of glycine, 10 nmol of PLP and 10 µL of enzyme lysate in buffer plus 2% (v/v) ethanol in a total volume of 1 mL. The four different glycine concentrations were tested at five different temperatures (4 ºC, 18 ºC, 25 ºC, 37 ºC and 42 ºC) and four different pH values (6, 8, 9.7, and 12). The mixtures were gently rotated at the desired temperature, then 5 µL aliquots were taken after 4 hr and overnight. Samples were derivatized with MSTFA and analyzed by GC/MS.

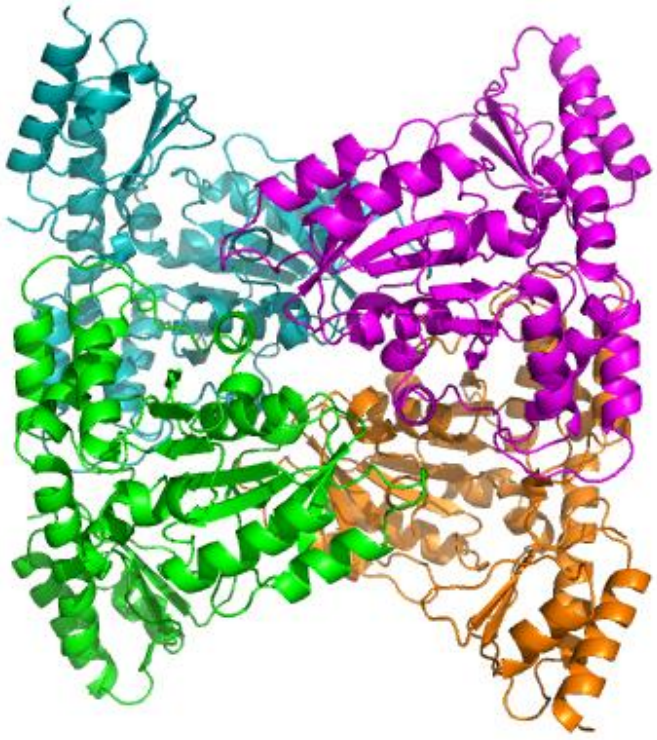

(*a*)

Figure 4-1. Ribbon representation of *P. putida* L-threonine aldolase. (*a*) The homotetramer of LTAPP. The four monomers are colored teal (chain A), green (chain B), orange (chain C), and magenta (chain D). (*b*) Chain C of LTAPP showing PLP binding in yellow. (*c*) Monomer of *E. coli* L-TA (salmon) showing PLP binding in yellow for a comparison of structure with LTAPP. (*d* - *g*) Zoomed view of *N*- and *C*-terminus highlighting main differences in structure. The purple loop indicates the extra β-sheet in *E. coli* L-TA (salmon) and small α-helix in *T. maritima* L-*allo*-TA (yellow) and the longer loop is shown in green. Part of the green loop was deleted in the *A. jandaei* L-*allo*-TA (brown) structure.

(*b*)

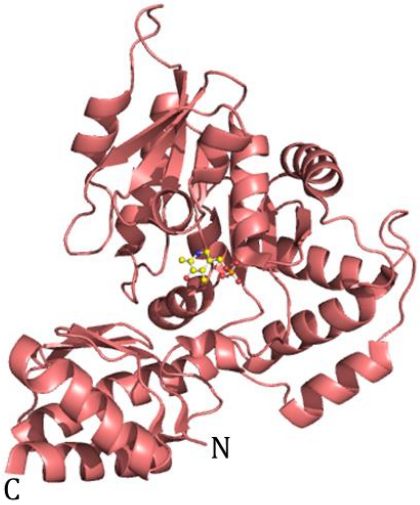

(*c*)

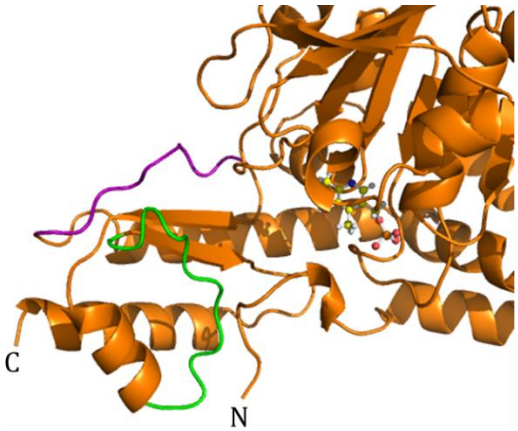

(*d*)

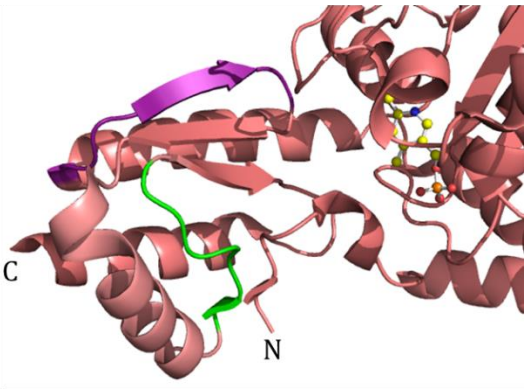

(*e*)

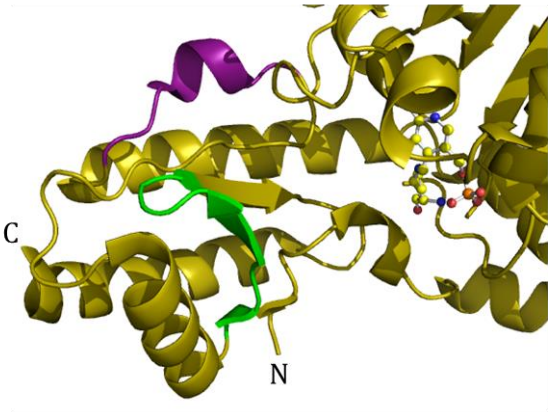

(*f*)

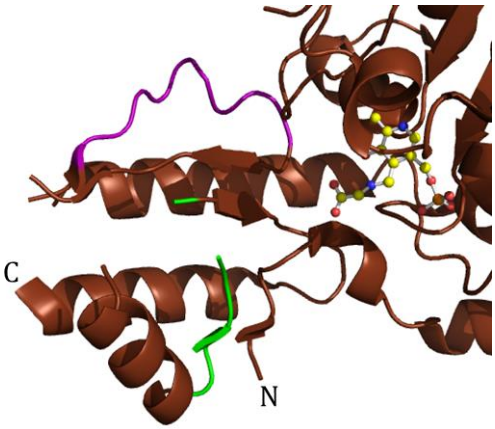

(*g*)

Figure 4-1. Continued

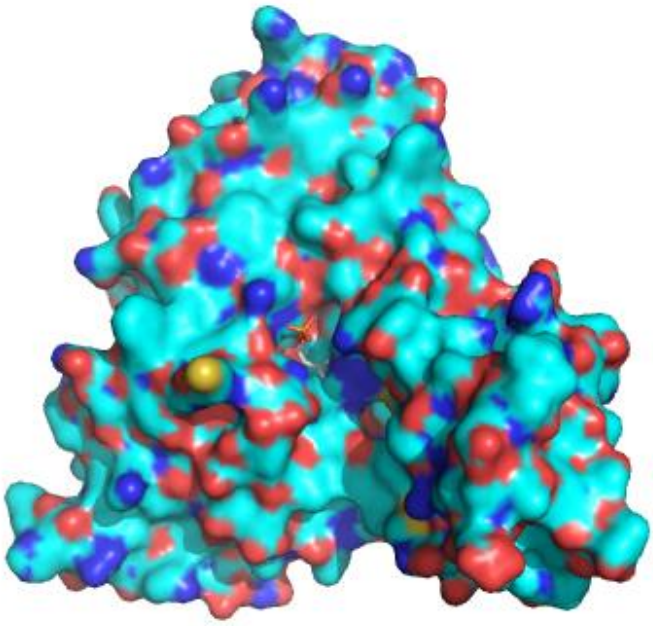

(*a*)

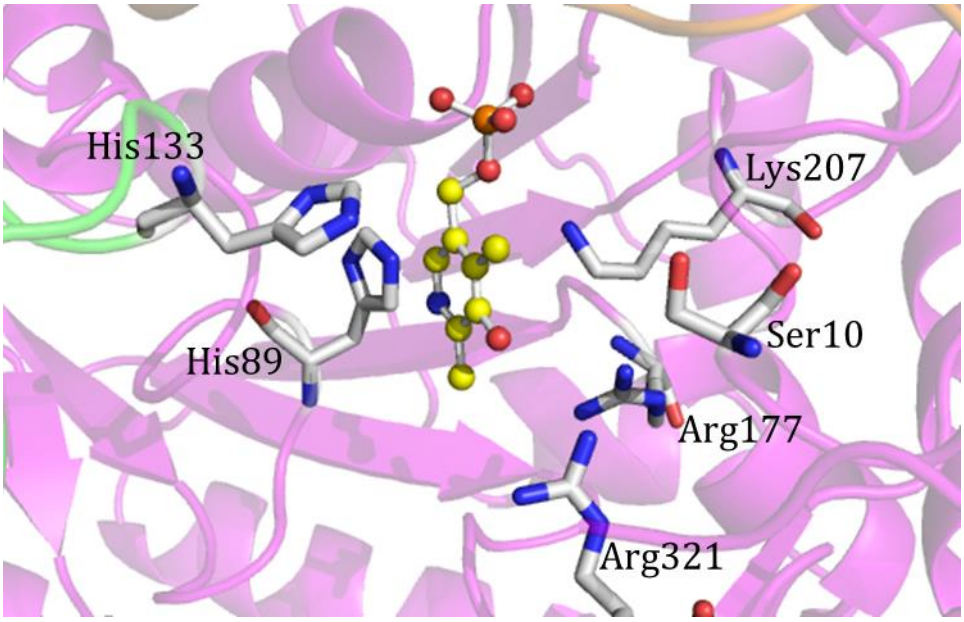

(*b*)

Figure 4-2. Overview of the active site of *P. putida* L-threonine aldolase. (*a*) Electrostatic surface potential displayed in blue for positive residues, red for negative, yellow for sulfur containing residues, and cyan for neutral residues. PLP is shown as sticks in active site hole. (*b*) Active site with conserved residues highlighted. PLP (yellow) is shown in predicted position.

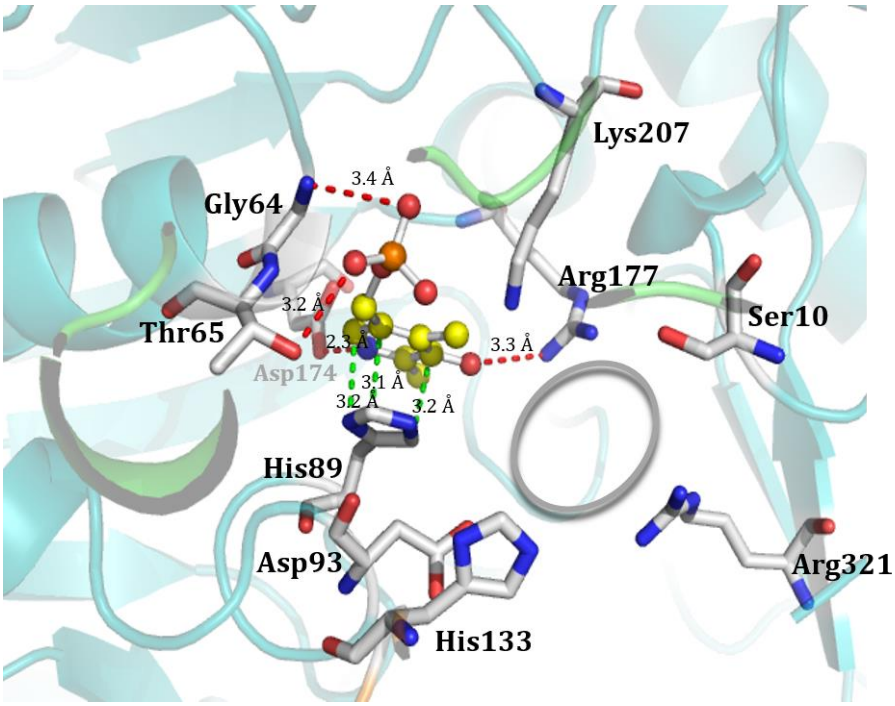

(*a*)

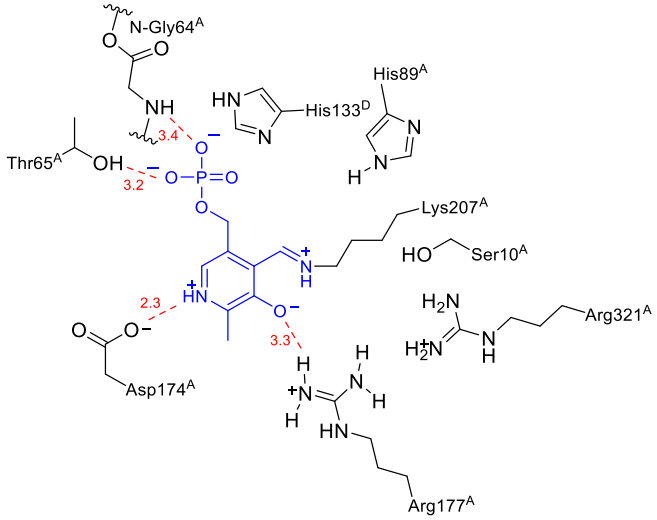

(*b*)

Figure 4-3. Overview of the active site pocket of chain A from *P. putida* L-threonine aldolase showing key interactions between residues in the active site and the pyridoxal phosphate cofactor. Red dashed lines show hydrogen bonding and green dashed lines show pi bonding interactions between His 89 and PLP. (*a*) PyMOL representation. Gray circle denotes the space in the active site that the substrate/product binds. (*b*) Chemical structure representation of internal aldimine. (*c*) Chemical structure representation of Gly-PLP. (*d*) Chemical structure representation of Thr-PLP.

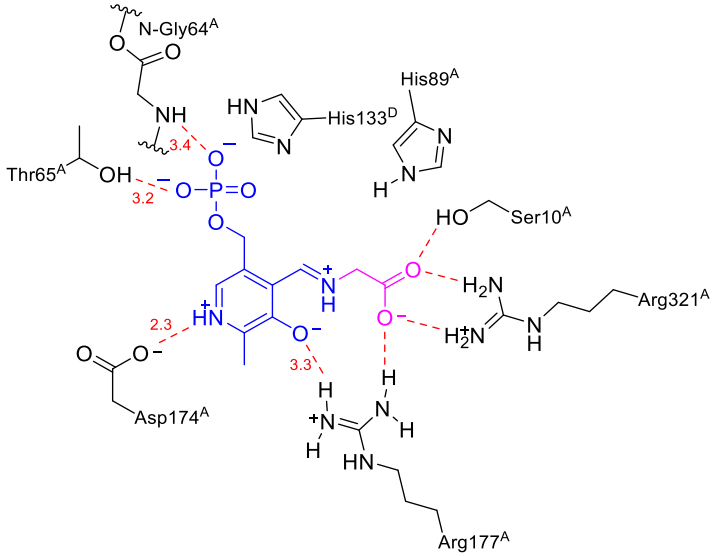

(*c*)

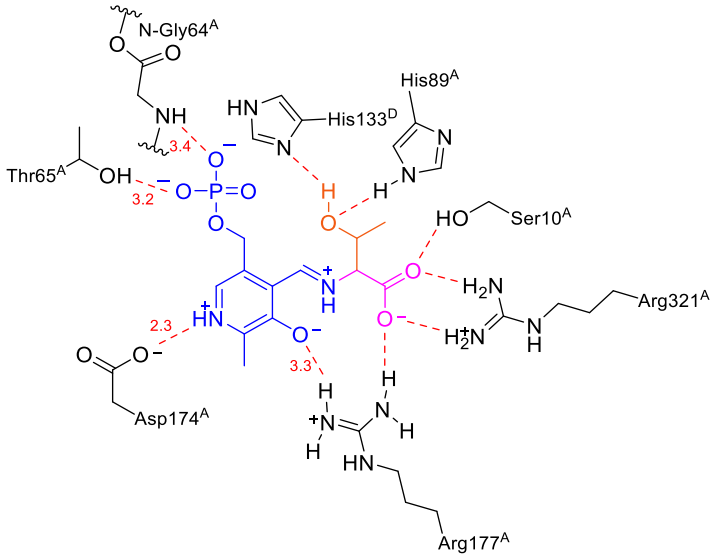

(*d*)

Figure 4-3. Continued

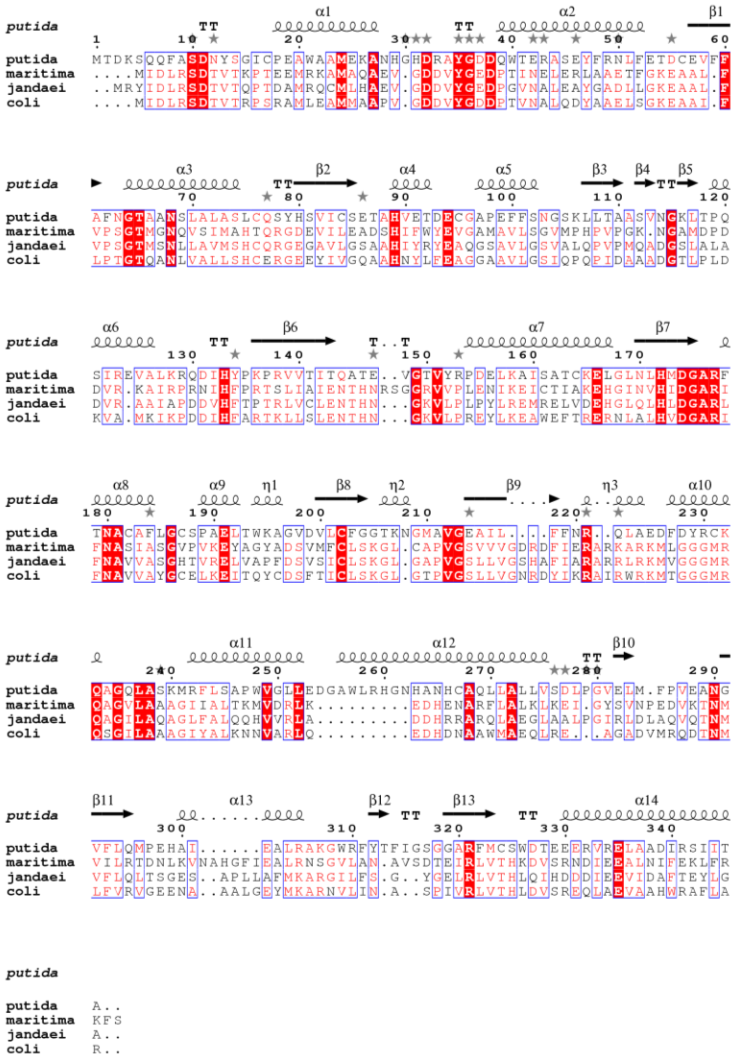

Figure 4-4. ESPript sequence alignment of four threonine aldolases[ii]

[ii] Reference: 252. Robert, X.; Gouet, P., *Nucleic Acids Research* **2014,** *42* (W1), W320-W324.

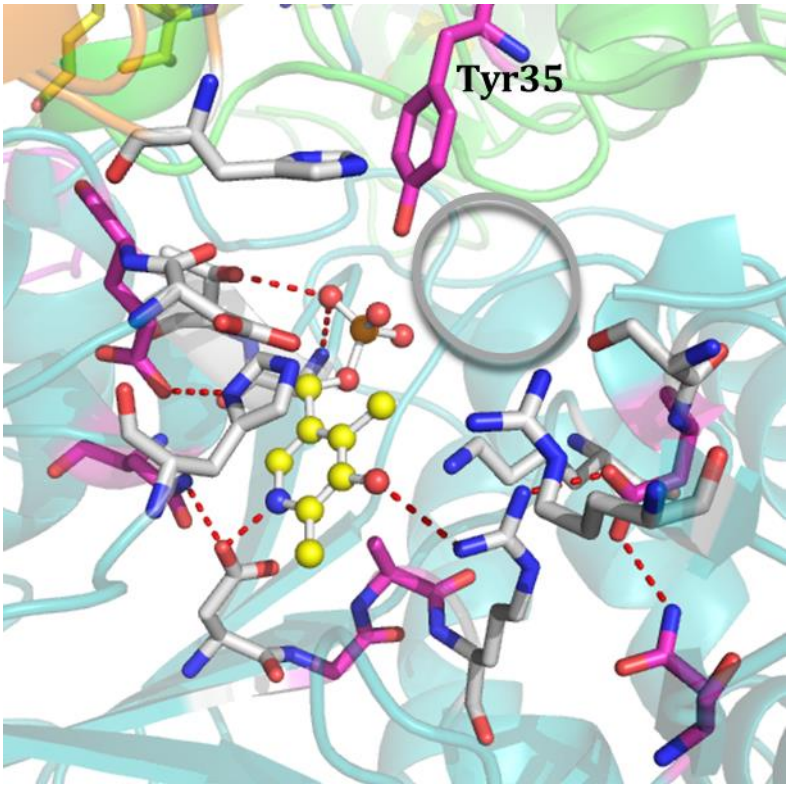

(*a*)

Figure 4-5. Detailed view of the active site pocket of chain A from *P. putida* L-threonine aldolase showing key interactions between conserved residues in the active site. Red dashed lines show hydrogen bonding between residues. Magenta residues highlight the conserved active site residues found after sequence alignment. (*a*) Tyr 35 lies in close range to the binding pocket. The gray circle represents the space in the active site in which the substrate/product likely binds. (*b*) Hydrogen bonding between Asn 68 – Asp 174 and Glu 94 – His 89. (*c*) Hydrogen bonding between Asn 290 – Asp 11 – Arg 177.

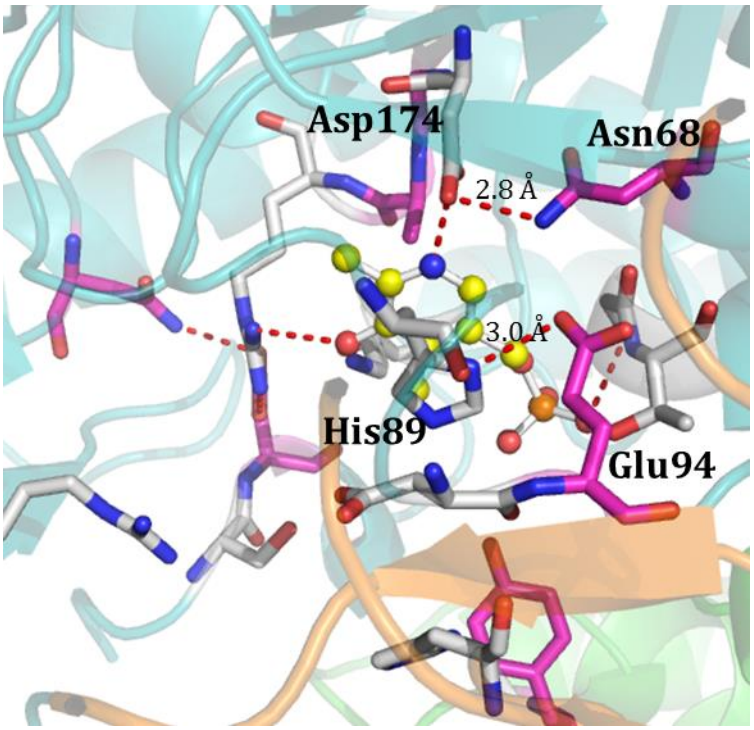

(*b*)

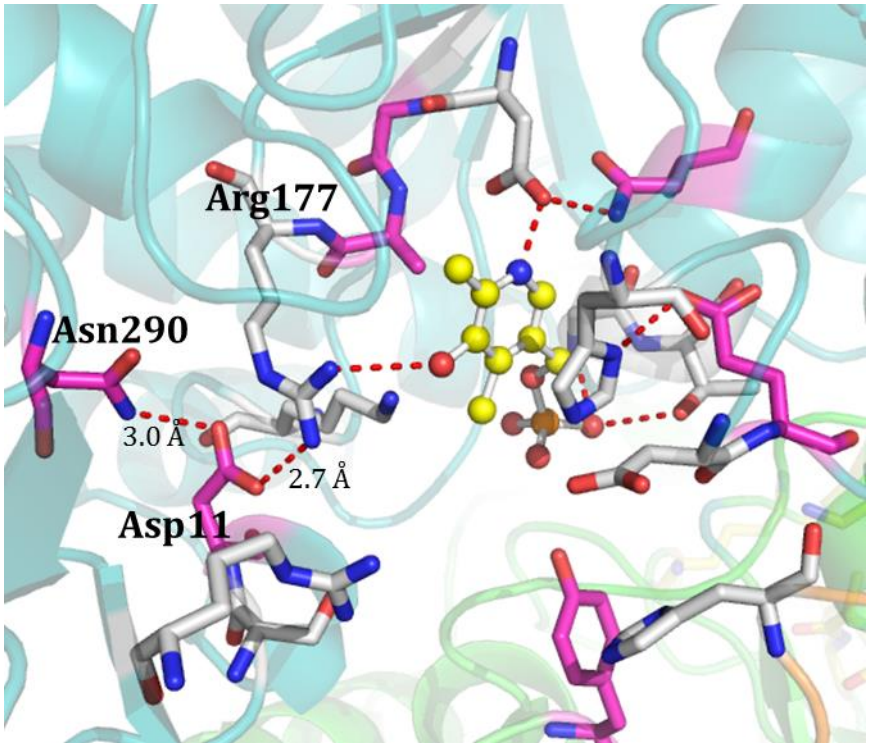

(*c*)

Figure 4-5. Continued

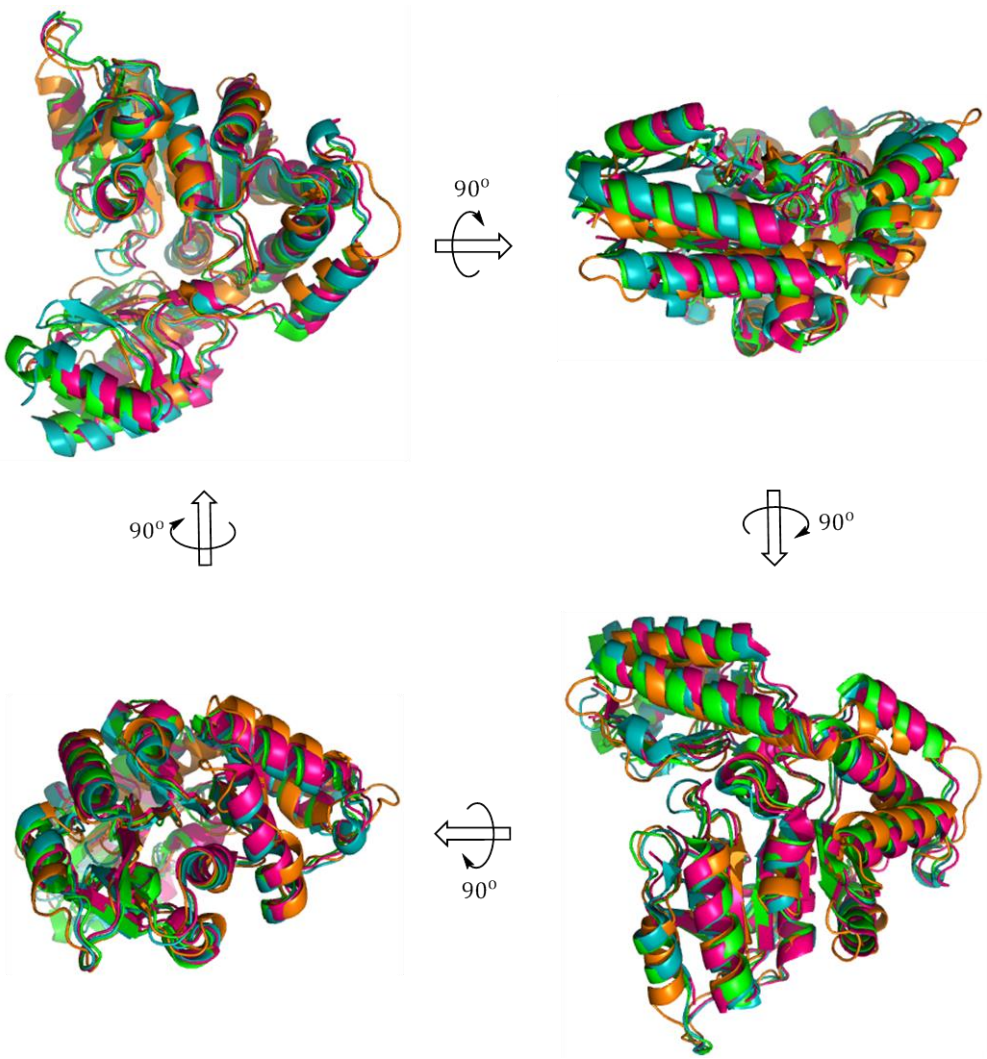

(*a*)

Figure 4-6. Structural comparison of four L-threonine aldolases. *T. maritima* L-*allo*-TA (teal), *Aeromonas jandaei* L-*allo*-TA (pink), and *Escherichia coli* L-TA (green) and the studied enzyme, *P. putida* L-TA (orange). (*a*) Secondary structure alignments rotated at 90º to show structual similarities. (*b*) Active site alignment with key residues highlighted. PLP shown in yellow.

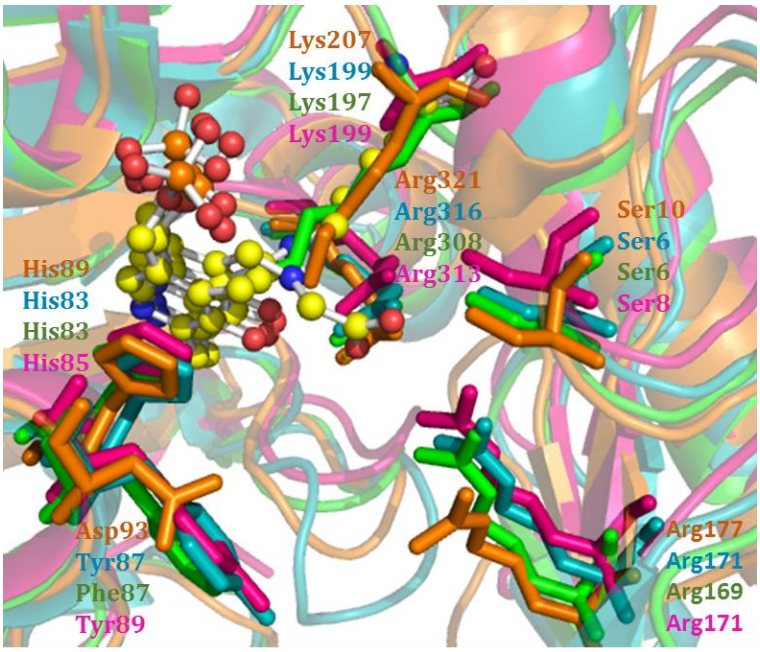

(*b*)

Figure 4-6. Continued

CHAPTER 5
SITE SATURATION MUTAGENESIS OF *A. jandaei* L-*allo*-THREONINE ALDOLASE

Introduction

Threonine aldolases (TAs) are PLP-dependent enzymes that have proven useful in the synthesis of β-hydroxy-α-amino acids.[184, 223] They catalyze the *C*-*C* bond formation between glycine and an aldehyde acceptor, resulting in two adjacent stereocenters. These enzymes are very good at controlling the α-stereochemistry, but typically show much lower diastereoselectivity at the β-carbon, particularly with longer reaction times or when larger aldehyde acceptors are used. This loss of diastereoselectivity must be addressed before TAs can be considered synthetically useful.

Site saturation mutagenesis (SSM) has been widely employed to improve a variety of enzyme characteristics such as substrate range, stereoselectivity, and thermostability.[253-258] Mutations in and around the active site have usually proven to be the most influential for substrate specificity and enantioselectivity.[259-262] Applying SSM to the active site residues of a TA was an obvious strategy to tackle the diastereoselectivity problem.

TAs have been studied extensively for their substrate tolerance on a broad range of aldehyde acceptors,[184] but few mutagenesis studies have been performed with these enzymes to this date. These include the work done by Baik and coworkers on the enzymatic synthesis of droxidopa.[8, 193, 238] They used error-prone PCR on the L-TA from *S. coelicolor* A3(2) and found that the triple mutation Y39C/T309C/A48T offered a four-fold increase in overall conversion and three-fold increase in diastereoselectivity (14% to 43% d.e. for the *syn*-isomer) compared to the wild type enzyme.[193]

The crystal structure of *A. jandaei* L-*allo*-TA was solved by Qin *et al.* in 2014.[207] These authors also carried out random mutagenesis and SSM of His 128. Random mutagenesis and screening of approximately 3,000 colonies revealed only one variant that showed significant activity towards L-*allo*- and L-Thr (H128Y/S292R). The double mutant showed a three-fold and 322-fold increased k_{cat}/K_M towards the two substrates, respectively. Enzyme kinetic studies of the two single mutants revealed that H128Y was likely the position of increased selectivity towards L-Thr. Therefore, Qin *et al.* preformed SSM on His 128 and found increased relative activity towards L-Thr with the Phe, Trp, Tyr, Ile, Leu, Met, and Ser variants. Interestingly, H128Y proved superior.[207] Although these mutants were useful in the retro-aldol cleavage of L-Thr, Qin *et al.* did not further screen for aldol condensation to L-Thr.

Here, we report three SSM libraries of *A. jandaei* L-*allo*-TA at active site residues His 85, His 128, and Tyr 89. Each library was initially screened against three representative aldehyde acceptors and interesting variants were further screened for altered substrate tolerance. We also hoped to solve the diastereoselectivity problem by this approach.

Results and Discussion

Site Saturation Mutagenesis Library Construction and Overexpression

The gene encoding wild type L-*allo*-TA from *A. jandaei* was originally obtained by chemical gene synthesis from GenScript. The native gene was ligated into pET-15b and the resulting plasmid was used to transform the *E. coli* overexpression strain BL21-Gold(DE3). Individual primer sets were deployed in 19 individual PCR amplifications to obtain a collection of plasmids with each of the 19 possible variants. After confirming

each mutation by Sangar sequencing, the plasmids were used to transform *E. coli* BL21-Gold(DE3) to isolate each mutant.

Histidine 85 Library

Three positions within the active site were chosen to undergo SSM on the L-*allo*-TA from *A. jandaei*: His 85, His 128, and Tyr 89. The crystal structure of this TA was solved by Qin *et al.*[207] in 2014. These data–along with the structures from *T. maritima*,[206] *E. coli*,[206] and *P. putida* (Chapter 4)–were used to choose these three positions. Histidine 85 was selected since it is responsible for regulating of the degree of stereoselectivity between the L- and L-*allo*-configurations by hydrogen bonding to the hydroxyl group of the product. Along with histidine 85, histidine 128 also hydrogen bonds to the hydroxyl group of the products. Qin *et al.* preformed SSM at this position and found enhanced activity for the retro-aldol cleavage of L-Thr; however, these variants were never tested for their aldol condensation activity. Histidine 128 was selected for this reason. And lastly, tyrosine 89 was chosen for its location in the hydrophobic pocket where the methyl group of L-*allo*-Thr resides. This residue is not conserved in the L-TA family and therefore believed to be an interesting site for SSM.[205-207]

All three SSM libraries were screened against three aldehyde acceptors (**3**, **9**, and **11**). These aldehydes (one aliphatic aldehyde and two aromatic aldehydes) were chosen to minimize screening efforts while still obtaining a broad picture of the substrate selectivity of the mutants. Unfortunately, all mutations at the 85 position rendered the enzyme completely inactive. This could be due to His 85 acting as the catalytic base. Originally, water was predicted to be the catalytic base[205-207] for the retro-aldol cleavage of L-*allo*-Thr; that is why we considered this site safe for mutagenesis. His 85 could

also be important for its pi-stacking interactions with the pyridinium ring of the PLP cofactor. It is possible that this His residue is required to stabilize and position the cofactor within the active site. See Table 5-1 for full screening results.

Table 5-1. Screening of histidine 85 mutants against aldehyde acceptors

Entry	Aldehyde	Product	Variant	Conversion[a] (%)	d.e.[a] (%)
1	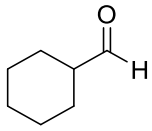 **3**	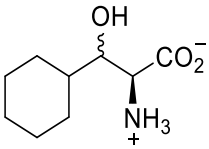	H85G	--	--
			H85A	<1[b]	--[b]
			H85V	<1[b]	--[b]
			H85I	<1[b]	--[b]
			H85L	<1[b]	--[b]
			H85P	<1[b]	--[b]
			H85M	<1[b]	--[b]
			H85F	<1[b]	--[b]
			H85Y	<1[b]	--[b]
			H85W	--	--
			H85S	<1[b]	--[b]
			H85C	<1[b]	--[b]
			H85T	<1[b]	--[b]
			H85N	<1[b]	--[b]
			H85Q	<1[b]	--[b]
			H85R	<1[b]	--[b]
			H85K	<1[b]	--[b]
			H85D	--	--
			H85E	--	--
			W.T.	25	26
2	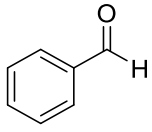 **9**	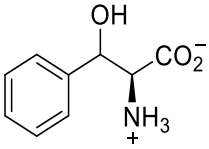	H85G	2	--[b]
			H85A	3	--[b]
			H85V	5	18
			H85I	5	25
			H85L	1	--[b]
			H85P	2	--[b]
			H85M	2	--[b]
			H85F	6	9
			H85Y	1	--[b]
			H85W	1	--[b]
			H85S	2	--[b]
			H85C	1	--[b]
			H85T	6	18
			H85N	3	--[b]
			H85Q	2	--[b]
			H85R	4	--[b]
			H85K	4	--[b]
			H85D	2	--[b]
			H85E	1	--[b]
			W.T.	19	26

Table 5-1. Continued

Entry	Aldehyde	Product	Variant	Conversion[a] (%)	d.e.[a] (%)
			H85G	--	--
			H85A	<1[b]	--[b]
			H85V	<1[b]	--[b]
			H85I	1	--[b]
			H85L	--	--
			H85P	--	--
			H85M	--	--
			H85F	3	--[b]
			H85Y	<1[b]	--[b]
3	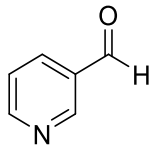 **11**	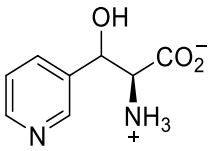	H85W	--	--
			H85S	<1[b]	--[b]
			H85C	--	--
			H85T	1	--[b]
			H85N	<1[b]	--[b]
			H85Q	<1[b]	--[b]
			H85R	6	99
			H85K	3	--[b]
			H85D	3	--[b]
			H85E	--	--
			W.T.	70	18

Note: Reaction mixtures contained 500 mM glycine, 100 mM aldehyde, 0.05 mM PLP, 20% ethanol, and 10 µL of enzyme lysate in 1 mL of 50 mM Tris Base, pH 9.7. Reactions were incubated at 37 ºC.
[a] Conversion and diastereomeric excess values were determined by GC/MS after MSTFA derivatization. Reactions with less and 1% conversions are listed as "<1%" and no values for diastereomeric purity are provided since the small peak sizes preclude accurate integration.
[b] Accurate values for conversion and diastereomeric excess could not be determined due to the very low peak areas.

Histidine 128 Library

The second His that occupies the active site of these TAs is located at position 128 in the L-*allo*-TA from *A. jandaei*. Along with His 85, this His residue also hydrogen bonds to the hydroxyl group of the products. di Salvo *et al.* observed that this His was quite flexible, presenting two different conformations in the electron density map of the crystal structure.[206] Qin *et al.* took this observation and mutated His 128 to Tyr and found that the Tyr side chain moved 4.2 Å out of the active site. This group carried out SSM on this position, but only monitored the retro-aldol cleavage of L-*allo*-Thr. They found that the enzyme tolerated substitutions by many amino acids, but the Tyr mutant gave the best results – an 8.4-fold increase in selectivity towards L-Thr. They did not

test aldol condensation activity.[207] We therefore hypothesized that mutagenesis might create sufficient room within the active site to accommodate larger, more functionalized acceptor aldehydes and/or potentially different amino donors.

The initial screening results of the His 128 mutants revealed increased diastereoselectivity with aldehyde **3**. On the other hand, mutations at this position neither increased conversion nor diastereoselectivities for the aromatic aldehydes **9** and **11**. These results are displayed in Table 5-2. Amino acid residues with increased diastereoselectivity were primarily hydrophobic amino acids like Ala, Ile, and Phe.

Table 5-2. Initial screening of histidine 128 mutants against aldehyde acceptors

Entry	Aldehyde	Product	Variant	Conversion[a] (%)	d.e.[a] (%)
1	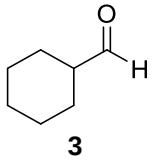 **3**	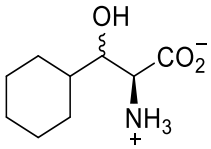	H128G	<5[b]	--[b]
			H128A	12	60
			H128V	37	11
			H128I	18	99
			H128L	<5[b]	--[b]
			H128P	<5[b]	--[b]
			H128M	<5[b]	--[b]
			H128F	5	99
			H128Y	19	99
			H128W	--	--
			H128S	--	--
			H128C	--	--
			H128T	<5[b]	--[b]
			H128N	31	99
			H128Q	<5[b]	--[b]
			H128R	--	--
			H128K	--	--
			H128D	<5[b]	--[b]
			H128E	<5[b]	--[b]
			W.T.	25	26
2	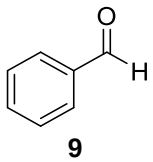 **9**	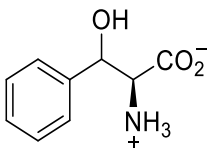	H128G	<5[b]	--[b]
			H128A	26	16
			H128V	12	12
			H128I	<5[b]	--[b]
			H128L	<5[b]	--[b]
			H128P	17	14
			H128M	<5[b]	--[b]
			H128F	5	16
			H128Y	16	4
			H128W	<5[b]	--[b]

Table 5-2. Continued

Entry	Aldehyde	Product	Variant	Conversion[a] (%)	d.e.[a] (%)
2	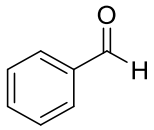 **9**	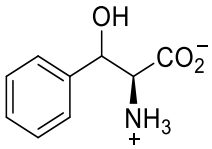	H128S	<5[b]	--[b]
			H128C	<5[b]	--[b]
			H128T	<5[b]	--[b]
			H128N	16	13
			H128Q	<5[b]	--[b]
			H128R	<5[b]	--[b]
			H128K	<5[b]	--[b]
			H128D	<5[b]	--[b]
			H128E	<5[b]	--[b]
			W.T.	19	26
3	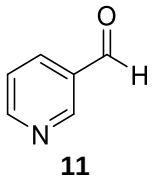 **11**	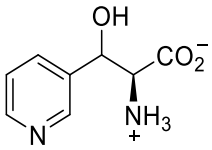	H128G	<5[b]	--[b]
			H128A	43	10
			H128V	34	9
			H128I	<5[b]	--[b]
			H128L	--	--
			H128P	34	8
			H128M	<5[b]	--[b]
			H128F	<5[b]	--[b]
			H128Y	24	17
			H128W	--	--
			H128S	--	--
			H128C	--	--
			H128T	<5[b]	--[b]
			H128N	7	39
			H128Q	<5[b]	--[b]
			H128R	<5[b]	--[b]
			H128K	--	--
			H128D	<5[b]	--[b]
			H128E	<5[b]	--[b]
			W.T.	70	18

Note: Reaction mixtures contained 500 mM glycine, 100 mM aldehyde, 0.05 mM PLP, 20% ethanol, and 10 µL of enzyme lysate in 1 mL of 50 mM Tris Base, pH 9.7. Reactions were incubated at 37 ºC.
[a] Conversion and diastereomeric excess values were determined by GC/MS after MSTFA derivatization. Reactions with 1 – 5% conversions are listed as "<5%" and no values for diastereomeric purity are provided since the small peak sizes preclude accurate integration.
[b] Accurate values for conversion and diastereomeric excess could not be determined due to the very low peak areas.

More extensive screening of the Ile, Phe, Tyr, Asn, and other variants was carried out on a variety of aliphatic aldehydes, *i.e*. straight chain, cyclic, branched, and unsaturated aldehydes and a few aromatic aldehydes (Tables 5-3 and 5-4). The Ile mutant showed >90% d.e. across all aliphatic aldehydes screened; however, conversions were uniformly low (<20%). Neither increasing the enzyme concentration nor adjusting temperature or pH improved these conversions. Substituting purified

enyzme was also unsuccessful. The Asn mutant gave comparable diastereoselectivities (>85%, with the exception of aldehyde **38**) along with reasonable conversions. Applying DOE strategies to this mutant increased conversion only slightly, at 25 ºC and pH 8.

Table 5-3. Extended screening of histidine 128 mutants against aliphatic aldehydes

Entry	Aldehyde	Product	Variant	Conversion[a] (%)	d.e.[a] (%)
1	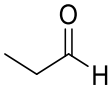 **1**	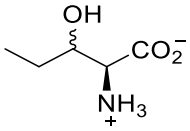	H128V	5	99
			H128I	2	--[b]
			H128T	3	--[b]
			H128P	5	99
			H128F	3	--[b]
			H128Y	5	99
			H128N	6	99
			W.T.	9	99
2	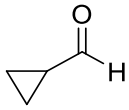 **26**	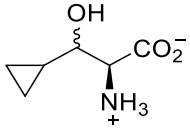	H128I	3	--[b]
			H128F	3	--[b]
			H128Y	11	99
			H128N	10	99
			W.T.	27	99
3	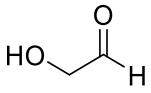 **27**	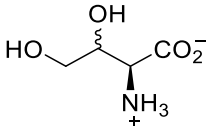	H128I	<1[b]	--[b]
			H128F	--	--
			H128Y	<1[b]	--[b]
			H128N	<1[b]	--[b]
			W.T.	6	99
4	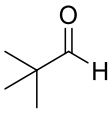 **28**	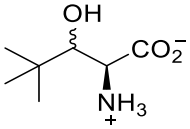	H128I	--	--
			H128F	3	--[b]
			H128Y	4	--[b]
			H128N	<1[b]	--[b]
			W.T.	3	--[b]
5	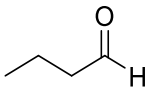 **29**	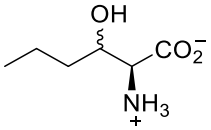	H128I	4	--[b]
			H128F	4	--[b]
			H128Y	24	99
			H128N	16	96
			W.T.	42	99
6	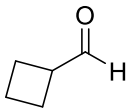 **30**	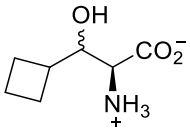	H128I	3	--[b]
			H128F	3	--[b]
			H128Y	14	99
			H128N	17	96
			W.T.	79	97
7	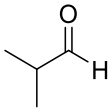 **31**	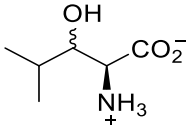	H128I	7	99
			H128F	11	99
			H128Y	12	99
			H128N	31	99
			W.T.	27	58

Table 5-3. Continued

Entry	Aldehyde	Product	Variant	Conversion[a] (%)	d.e.[a] (%)
8	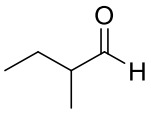 **32**	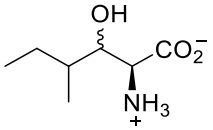	H128I	3	--[b]
			H128F	4	--[b]
			H128Y	3	--[b]
			H128N	3	--[b]
			W.T.	3	--[b]
9	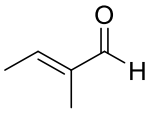 **33**	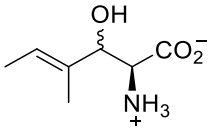	H128I	--	--
			H128F	--	--
			H128Y	--	--
			H128N	--	--
			W.T.	--	--
10	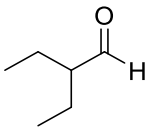 **34**	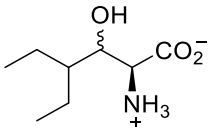	H128I	1	--[b]
			H128F	3	22
			H128Y	25	58
			H128N	16	31
			W.T.	64	58
11	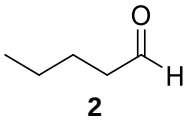 **2**	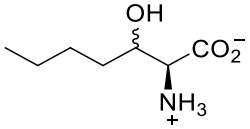	H128A	14	99
			H128V	43	99
			H128I	9	99
			H128T	30	99
			H128P	28	99
			H128F	5	99
			H128Y	24	99
			H128N	28	99
			W.T.	80	99
12	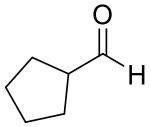 **35**	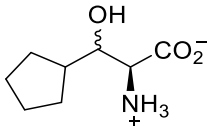	H128I	19	93
			H128F	16	57
			H128Y	91	70
			H128N	50	82
			W.T.	92	83
13	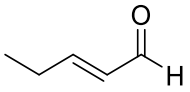 **36**	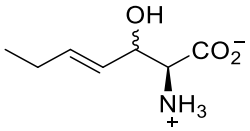	H128I	--	--
			H128F	--	--
			H128Y	<1[b]	--[b]
			H128N	<1[b]	--[b]
			W.T.	4	12
14	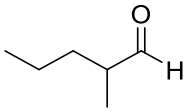 **37**	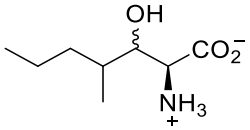	H128I	5	--[c]
			H128F	10	--[c]
			H128Y	--	--
			H128N	15	--[c]
			W.T.	--	--
15	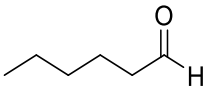 **20**	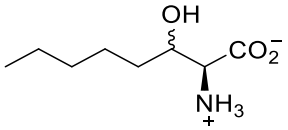	H128I	5	99
			H128F	5	99
			H128Y	31	63
			H128N	20	94
			W.T.	34	41
16	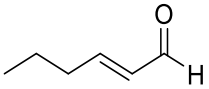 **38**	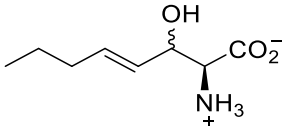	H128I	<1[b]	--[b]
			H128F	--	--
			H128Y	<1[b]	--[b]
			H128N	5	16
			W.T.	3	--[b]

Table 5-3. Continued

Entry	Aldehyde	Product	Variant	Conversion[a] (%)	d.e.[a] (%)
17	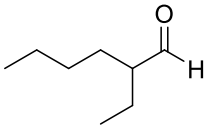 **39**	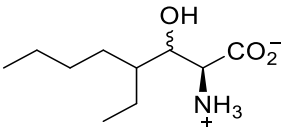	H128I	--	--
			H128F	3	--[b]
			H128Y	--	--
			H128N	<1[b]	--[b]
			W.T.	2	--[b]

Note: Reaction mixtures contained 500 mM glycine, 100 mM aldehyde, 0.05 mM PLP, 20% ethanol, and 10 µL of enzyme lysate in 1 mL of 50 mM Tris Base, pH 9.7. Reactions were incubated at 37 ºC.
[a] Conversion and diastereomeric excess values were determined by GC/MS after MSTFA derivatization. Reactions with less than 1% conversions are listed as "<1%" and no values for diastereomeric purity are provided since the small peak sizes preclude accurate integration.
[b] Accurate values for conversion and diastereomeric excess could not be determined due to the very low peak areas.
[c] Accurate values for diastereomeric excess could not be determined due to the original aldehyde acceptor being a racemic mixture and four possible products were made.

Table 5-4. Extended screening of histidine 128 mutants against aromatic aldehydes

Entry	Aldehyde	Product	Variant	Conversion[a] (%)	d.e.[a] (%)
1	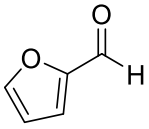 **6**	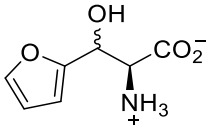	H128A	17	13
			H128V	15	11
			H128T	4	--[b]
			H128P	11	8
			H128Y	16	5
			W.T.	11	20
2	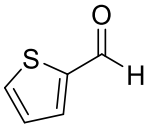 **7**	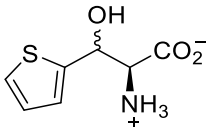	H128A	7	2
			H128V	7	22
			H128T	4	--[b]
			H128P	11	16
			H128Y	7	38
			W.T.	12	21
3	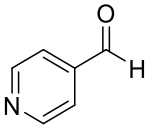 **10**	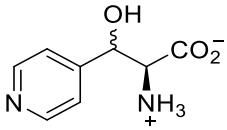	H128A	43	36
			H128V	44	17
			H128T	<1[b]	--[b]
			H128P	22	87
			H128Y	36	18
			W.T.	63	30
4	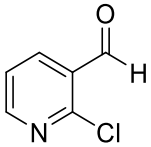 **12**	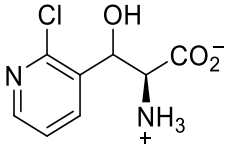	H128A	35	40
			H128V	41	33
			H128T	5	62
			H128P	29	30
			H128Y	23	20
			W.T.	66	41

Note: Reaction mixtures contained 500 mM glycine, 100 mM aldehyde, 0.05 mM PLP, 20% ethanol, and 10 µL of enzyme lysate in 1 mL of 50 mM Tris Base, pH 9.7. Reactions were incubated at 37 ºC.
[a] Conversion and diastereomeric excess values were determined by GC/MS after MSTFA derivatization. Reactions with 1 – 5% conversions are listed as "<5%" and no values for diastereomeric purity are provided since the small peak sizes preclude accurate integration.
[b] Accurate values for conversion and diastereomeric excess could not be determined due to the very low peak areas.

Tyrosine 89 Library

We also carried out SSM on the non-conserved amino acid at position 89, which is most commonly a Tyr in L-TAs,[206, 207] but can be Phe[205] or Asp (Chapter 4). This residue is located in the hydrophobic pocket occupied by the methyl group of L-*allo*-Thr when it is bound as an external aldimine with PLP. This residue is thought to control the preference for this isomer.[205-207] Since the residue at position 89 is not conserved, we hypothesized that a mutation at this position may allow for larger aldehyde acceptors to bind.

The initial screening of these mutations offered some unexpected results. Figure 5-2 represents the amino acid mutations that offer conversions >5%. The Gly, Glu and Trp substitutions offered increased diastereoselectivities with aldehyde **3** as the substrate. Interestingly, the steric bulk of the amino acid side chain did correlate with increased diastereoselectivity since both Gly and Trp showed the same effect. When all 19 variants were tested with benzaldehyde **9**, we found increased diastereoselectivity with the Pro and Glu mutants. With respect to the 3-pyridinecarboxaldehyde **11**, diastereoselectivity was increased only slightly by Asn and Gln substitutions. By contrast, the Pro mutant showed completely reversed diastereoselectivity. The Ala, Gln and Lys variants also showed reversed diastereoselectivity. The Y89P mutants increased the wild type diastereoselectivity (to 81% d.e.) with benzaldehyde **9**, but gave almost completely reversed selectivity for 3-pyridinecarboxaldehyde **11** (to 91% d.e.) despite the very similar sizes of the aldehydes. Table 5-5 summarizes these results for the initial screening.

Table 5-5. Initial screening of tyrosine 89 mutants against aldehyde acceptors

Entry	Aldehyde	Product	Variant	Conversion[a] (%)	d.e.[a] (%)
1	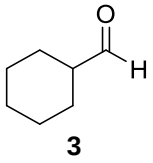 **3**	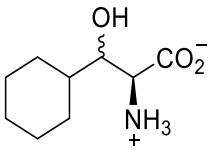	Y89G	12	99
			Y89A	6	6
			Y89V	<5[b]	--[b]
			Y89I	<5[b]	--[b]
			Y89L	7	65
			Y89P	<5[b]	--[b]
			Y89M	<5[b]	--[b]
			Y89H	5	34
			Y89F	5	99
			Y89W	6	99
			Y89S	<5[b]	--[b]
			Y89C	6	13
			Y89T	<5[b]	--[b]
			Y89N	<5[b]	--[b]
			Y89Q	<5[b]	--[b]
			Y89R	<5[b]	--[b]
			Y89K	<5[b]	--[b]
			Y89D	15	26
			Y89E	23	88
			W.T.	25	26
2	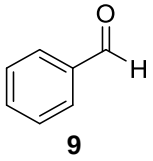 **9**	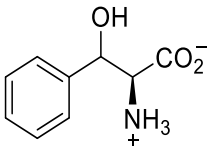	Y89G	10	15
			Y89A	12	50
			Y89V	<5[b]	--[b]
			Y89I	<5[b]	--[b]
			Y89L	10	21
			Y89P	5	81
			Y89M	9	17
			Y89H	8	32
			Y89F	10	22
			Y89W	9	33
			Y89S	6	26
			Y89C	12	40
			Y89T	8	18
			Y89N	12	49
			Y89Q	11	58
			Y89R	<5[b]	--[b]
			Y89K	12	36
			Y89D	16	48
			Y89E	7	85
			W.T.	19	26
3	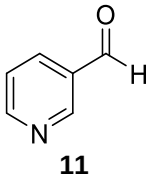 **11**	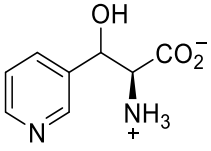	Y89G	18	14[c]
			Y89A	28	52[c]
			Y89V	--	--
			Y89I	<5[b]	--[b]
			Y89L	35	13[c]
			Y89P	7	91[c]
			Y89M	19	12[c]
			Y89H	12	18[c]
			Y89F	17	16[c]
			Y89W	27	11[c]

Table 5-5. Continued

Entry	Aldehyde	Product	Variant	Conversion[a] (%)	d.e.[a] (%)
3	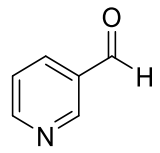 **11**	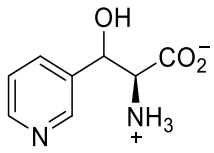	Y89S	16	15[c]
			Y89C	26	36[c]
			Y89T	25	7[c]
			Y89N	31	70
			Y89Q	24	54[c]
			Y89R	<5[b]	--[b]
			Y89K	25	44[c]
			Y89D	47	31
			Y89E	38	41
			W.T.	70	18

Note: Reaction mixtures contained 500 mM glycine, 100 mM aldehyde, 0.05 mM PLP, 20% ethanol, and 10 µL of enzyme lysate in 1 mL of 50 mM Tris Base, pH 9.7. Reactions were incubated at 37 ºC.
[a] Conversion and diastereomeric excess values were determined by GC/MS after MSTFA derivatization. Reactions with 1 – 5% conversions are listed as "<5%" and no values for diastereomeric purity are provided since the small peak sizes preclude accurate integration.
[b] Accurate values for conversion and diastereomeric excess could not be determined due to the very low peak areas.
[c] Reverse diastereoselectivity was observed.

More extensive screening was performed on interesting variants identified by the initial characterization. The Gly, Trp, Asp and Glu variants were tested against a variety of aliphatic aldehyde acceptors (Table 5-6). In most cases, diastereoselectivity was increased compared to the wild type enzyme by at least one of the four mutations. Non-cyclic, branched aldehyde acceptors (**28**, **31** and **34**) revealed reversed diastereoselectivity with all four mutations. Pivaldehyde **28** was particularly interesting as the overall conversion was increased seven-fold by the Y89D mutation, which also completely reversed the diastereoselectivity (99% d.e.). Isobutryaldehyde **31** presented similar results: a 2.7-fold increase in conversion (73%) as well as 99% d.e. for the opposite diastereomer. Surprisingly, cyclic aliphatic aldehydes did not show reversed diastereoselectivity.

Table 5-6. Extended screening of tyrosine 89 mutants against aliphatic aldehydes

Entry	Aldehyde	Product	Variant	Conversion[a] (%)	d.e.[a] (%)
1	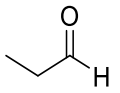 **1**	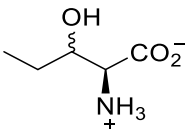	Y89G	3	--[b]
			Y89W	4	--[b]
			Y89D	8	78
			Y89E	4	--[b]
			W.T.	9	99
2	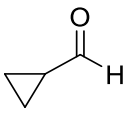 **26**	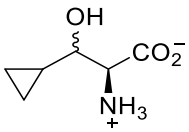	Y89G	8	99
			Y89W	11	99
			Y89D	33	99
			Y89E	15	99
			W.T.	27	99
3	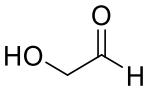 **27**	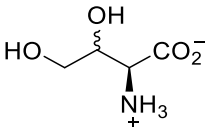	Y89G	1	--[b]
			Y89W	2	--[b]
			Y89D	<1	--[b]
			Y89E	<1	--[b]
			W.T.	6	99
4	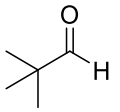 **28**	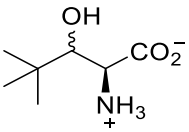	Y89G	9	99[d]
			Y89W	11	99[d]
			Y89D	22	99[d]
			Y89E	13	99[d]
			W.T.	3	--[b]
5	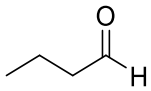 **29**	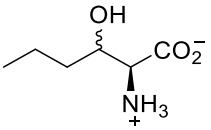	Y89G	8	99
			Y89W	11	99
			Y89D	26	99
			Y89E	10	99
			W.T.	42	99
6	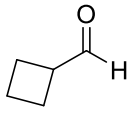 **30**	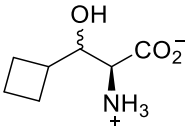	Y89G	14	99
			Y89W	17	72
			Y89D	70	58
			Y89E	75	66
			W.T.	79	97
7	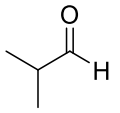 **31**	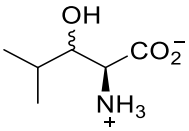	Y89G	9	92[d]
			Y89W	11	94[d]
			Y89D	73	99[d]
			Y89E	22	97[d]
			W.T.	27	58
8	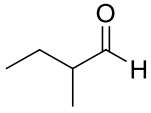 **32**	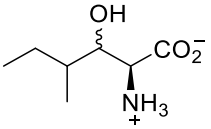	Y89G	2	--[b]
			Y89W	4	--[b]
			Y89D	16	--[c]
			Y89E	3	--[b]
			W.T.	3	--[b]
9	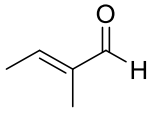 **33**	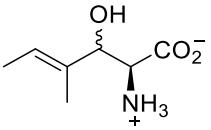	Y89G	--	--
			Y89W	--	--
			Y89D	--	--
			Y89E	--	--
			W.T.	--	--
10	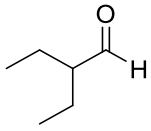 **34**	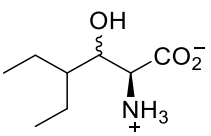	Y89G	<1	--[b]
			Y89W	1	--[b]
			Y89D	8	74[d]
			Y89E	<1	--[b]
			W.T.	64	58

Table 5-6. Continued

Entry	Aldehyde	Product	Variant	Conversion[a] (%)	d.e.[a] (%)
11	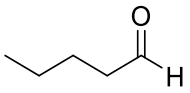 **2**	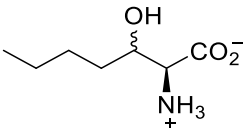	Y89G	6	93
			Y89W	12	99
			Y89D	40	99
			Y89E	9	99
			W.T.	80	99
12	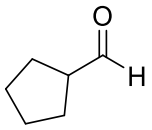 **35**	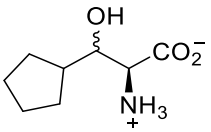	Y89G	12	89
			Y89W	14	16
			Y89D	23	57
			Y89E	20	80
			W.T.	92	83
13	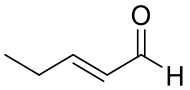 **36**	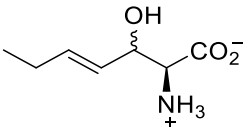	Y89G	--	--
			Y89W	<1	--[b]
			Y89D	<1	--[b]
			Y89E	<1	--[b]
			W.T.	4	--[b]
14	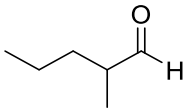 **37**	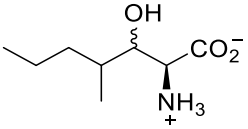	Y89G	<1	--[b]
			Y89W	2	--[b]
			Y89D	2	--[b]
			Y89E	1	--[b]
			W.T.	--	--
15	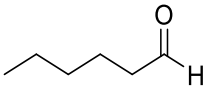 **20**	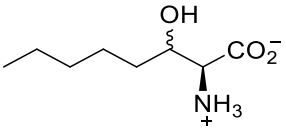	Y89G	<1	--[b]
			Y89W	<1	--[b]
			Y89D	<1	--[b]
			Y89E	--	--
			W.T.	34	41
16	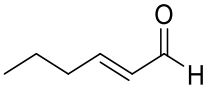 **38**	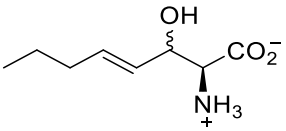	Y89G	--	--
			Y89W	--	--
			Y89D	--	--
			Y89E	--	--
			W.T.	3	--[b]
17	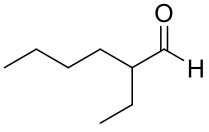 **39**	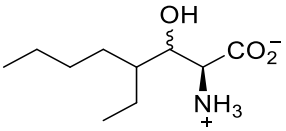	Y89G	--	--
			Y89W	3	--[b]
			Y89D	6	--[c]
			Y89E	2	--[b]
			W.T.	2	--[b]

Note: Reaction mixtures contained 500 mM glycine, 100 mM aldehyde, 0.05 mM PLP, 20% ethanol, and 10 µL of enzyme lysate in 1 mL of 50 mM Tris Base, pH 9.7. Reactions were incubated at 37 ºC.

[a] Conversion and diastereomeric excess values were determined by GC/MS after MSTFA derivatization. Reactions with 1 – 5% conversions are listed as "<5%" and no values for diastereomeric purity are provided since the small peak sizes preclude accurate integration.

[b] Accurate values for conversion and diastereomeric excess could not be determined due to the very low peak areas.

[c] Accurate values for diastereomeric excess could not be determined due to the original aldehyde acceptor being a racemic mixture and four possible products were made.

[d] Reverse diastereoselectivity was observed.

The final screening efforts for this library were carried out to investigate the reversed diastereoselectivity observed for aldehyde **11**. The Ala, Leu, Pro and Glu

mutants were tested with a few aromatic aldehyde acceptors (Table 5-7). The Pro substitution (Y89P) was by far the most interesting mutation as it single handedly triggered elevated and reversed diastereoselectivity (91% d.e.) for aldehyde **10** (Table 5-7, entry 3) and **11** (Table 5-5, entry 3). On the other hand, it increased diastereoselectivity (81% d.e.) for the original diastereomer with benzaldehyde **9** as the substrate (Table 5-5, entry 2).

Table 5-7. Extended screening of tyrosine 89 mutants against aromatic aldehydes

Entry	Aldehyde	Product	Enzyme	Conversion[a] (%)	d.e.[a] (%)
1	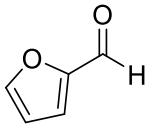 **6**	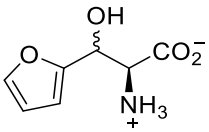	Y89A	11	92
			Y89L	5	4
			Y89P	9	30
			Y89E	--	--
			W.T.	11	20
2	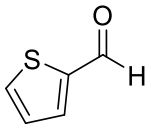 **7**	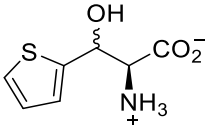	Y89A	3	--[b]
			Y89L	3	--[b]
			Y89P	<1	--[b]
			Y89E	--	--
			W.T.	12	21
3	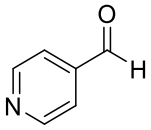 **10**	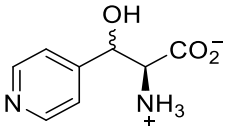	Y89A	46	31[c]
			Y89L	--	--
			Y89P	29	57[c]
			Y89E	1	--[b]
			W.T.	63	30
4	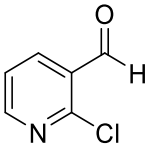 **12**	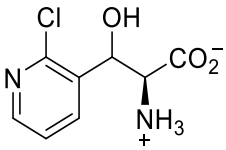	Y89A	7	3
			Y89L	9	24
			Y89P	6	12
			Y89E	12	26
			W.T.	66	41

Note: Reaction mixtures contained 500 mM glycine, 100 mM aldehyde, 0.05 mM PLP, 20% ethanol, and 10 µL of enzyme lysate in 1 mL of 50 mM Tris Base, pH 9.7. Reactions were incubated at 37 ºC.
[a] Conversion and diastereomeric excess values were determined by GC/MS after MSTFA derivatization. Reactions with 1 – 5% conversions are listed as "<5%" and no values for diastereomeric purity are provided since the small peak sizes preclude accurate integration.
[b] Accurate values for conversion and diastereomeric excess could not be determined due to the very low peak areas.
[c] Reverse diastereoselectivity was observed.

In the previous chapter, it was observed that the L-TA from *P. putida* contained an Asp residue at position 93, analogous to the Tyr 89 in *A. jandaei*. We predicted that this position may have been the culprit for the observed poor diatereoselectivites of this

enzyme. In the case of the *A. jandaei* L-*allo*-TA Tyr 89 SSM library, extended screening revealed that the Y89D mutation actually gave some of the best diatereoselectivites and overall conversions. Therefore, the poor diastereoselectivity observed for *P. putida* L-TA must be due to additional factors beyond the residue at position 89.

Conclusion

Three SSM libraries were constructed and screened against a wide range of aldehyde acceptors. The complete collection of mutants were tested with three representative aldehydes (**3**, **9** and **11**). Interesting variants were then tested against a broader range of aldehydes to uncover their effects on substrate tolerance and diastereoselectivity. Mutations at His 85 left the enzyme completely inactive, indicating that this amino acid was absolutely crucial, perhaps because of cofactor stabilization or because it acts as the catalytic base. Substitutions for His 128 increased diastereoselectivity (Asn or Ile), particularly for branched aldehyde acceptors. Reversed diastereoselectivity was observed for branched, aliphatic aldehyde acceptors and pyridinium aldehyde acceptors when Tyr 89 was mutated. The Y89P variant was among the most interesting mutation in this series: this single change increased diastereoselectivity for aldehyde **9** while reversing diastereoselectivity for aldehyde **11**. In conclusion, we have benefitted from SSM strategies and solved the diastereoselectivity problem for at least some of the substrates.

Experimental Procedures

General. LB medium contained 10 g/L Bacto-Tryptone, 5 g/L Bacto-Yeast Extract and 10 g/L NaCl; 15 g/L agar was added for plates. PCR amplifications were performed with Phusion Hot Start II DNA polymerase using the manufacturer's protocols. Electroporation was carried out with a BioRad GenePulser apparatus using

0.2 cm cuvettes. Promega Wizard kits and CsCl buoyant density ultracentrifugation [244] were used for small- and large-scale plasmid purifications, respectively. Fluorescent Sanger DNA sequencing was performed by the University of Florida ICBR. GC/MS analysis employed a 30 m × 0.25 mm Beta Dex™ 225 column and ionization by EI at 70 eV. The temperature program involved an initial hold at 95 ºC for 5 min, an initial increase of 5 ºC/min to 138 ºC followed by an increase of 10 ºC/min to 180 ºC, then a final increase of 2 ºC/min to 200 ºC and a hold at that temperature for 10 min.

Plasmid construction. The gene encoding L-*allo*-TA from *A. jandaei* (accession number D87890) was synthesized by GenScript and ligated into a pUC57 with flanking *Nde*I and *Xho*I restriction sites at the 5'- and 3'-ends, respectively. The TA gene was excised by digesting with these restriction enzymes and ligated with *Nde*I, *Xho*I-cut pET15b (Novagen). After transformation into *E. coli* ElectroTen-Blue, plasmid DNA from a randomly-chosen colony was isolated, restriction mapped and then sequenced to verify the desired structure. The resulting plasmid (designated pSF3) was used to transform *E. coli* BL21-Gold(DE3) strain for protein overexpression.

Site saturation mutagenesis. Each mutation was accomplished by PCR with individual primer sets using pSF3 as the template DNA and the corresponding forward and reverse primers for each mutation (Table 5-8). These primer sets introduced a specific mutation at a specific site, using the most frequent codon usage for *E. coli* (underlined in Table 5-8). After purification, the PCR product was digested with *Dpn*I to cut the template DNA (pSF3). After transformation into *E. coli* ElectroTen-Blue, plasmid DNA from a randomly-chosen colony was isolated and sequenced to verify the desired

mutation. The resulting plasmid with mutation was used to transform *E. coli* BL21-Gold(DE3) strain for protein overexpression.

Table 5-8. Forward and reverse primer sets for site saturation mutagenesis

Mutation of pSF3	Forward Primer	Reverse Primer
H85G	5’ – GCAGCCGGCATCTAT CGCTATGAGGCG – 3’	5’ – ATAGATGCCGGCTGC CGAGCC – 3’
H85A	5’ – GCAGCCGCGATCTAT CGCTATGAGGCGC – 3’	5’ – ATAGATCGCGGCTGC CGAGC – 3’
H85V	5’ – GCAGCCGTGATCTAT CGCTATGAGGCGCAG – 3’	5’ – ATAGATCACGGCTGC CGAGCC – 3’
H85I	5’ – GCAGCCATTATCTAT CGCTATGAGGCGCAGG – 3’	5’ – ATAGATAATGGCTGC CGAGCCC – 3’
H85L	5’ – GCAGCCCTGATCTAT CGCTATGAGGCGCAG – 3’	5’ – ATAGATCAGGGCTGC CGAGCC – 3’
H85P	5’ – GCAGCCCCGATCTAT CGCTATGAGGCGCAG – 3’	5’ – ATAGATCGGGGCTGC CGAGC – 3’
H85M	5’ – GCAGCCATGATCTAT CGCTATGAGGCGCAG – 3’	5’ – ATAGATCATGGCTGC CGAGCCC – 3’
H85F	5’ – GCAGCCTTTATCTAT CGCTATGAGGCGCAGG– 3’	5’ – ATAGATAAAGGCTGC CGAGCCCAG – 3’
H85Y	5’ – GCAGCCTATATCTAT CGCTATGAGGCGCAGG – 3’	5’ – ATAGATATAGGCTGC CGAGCCCAG – 3’
H85W	5’ – GCAGCCTGGATCTAT CGCTATGAGGCGC – 3’	5’ – ATAGATCCAGGCTGC CGAGCC – 3’
H85S	5’ – GCAGCCAGCATCTAT CGCTATGAGGCGCA – 3’	5’ – ATAGATGCTGGCTGC CGAGCCCA – 3’
H85C	5’ – GCAGCCTGCATCTAT CGCTATGAGGCGC – 3’	5’ – ATAGATGCAGGCTGC CGAGCCCA – 3’
H85T	5’ – GCAGCCACCATCTAT CGCTATGAGGCGCA – 3’	5’ – ATAGATGGTGGCTGC CGAGCCCA – 3’
H85N	5’ – GCAGCCAACATCTAT CGCTATGAGGCGCAG – 3’	5’ – ATAGATGTTGGCTGC CGAGCCCA – 3’
H85Q	5’ – GCAGCCCAGATCTAT CGCTATGAGGCGCAG – 3’	5’ – ATAGATCTGGGCTGC CGAGCC – 3’
H85R	5’ – GCAGCCCGTATCTAT CGCTATGAGGCGCAGG – 3’	5’ – ATAGATACGGGCTGC CGAGCC – 3’
H85K	5’ – GCAGCCAAAATCTAT CGCTATGAGGCGCAG – 3’	5’ – ATAGATTTTGGCTGC CGAGCCC – 3’
H85D	5’ – GCAGCCGATATCTAT CGCTATGAGGCGCAGG – 3’	5’ – ATAGATATCGGCTGC CGAGCCC – 3’
H85E	5’ – GCAGCCGAAATCTAT CGCTATGAGGCGCAG – 3’	5’ – ATAGATTTCGGCTGC CGAGCC – 3’
Y89G	5’ – TATCGCGGCGAGGCG CAGGGTT – 3’	5’ – CGCCTCGCCGCGATA GATGTGGGCT – 3’
Y89A	5’ – TATCGCGCGGAGGCG CAGGGTT – 3’	5’ – CGCCTCCGCGCGATA GATGTGGGCTGC – 3’
Y89V	5’ – TATCGCGTGGAGGCG CAGGGTTCT – 3’	5’ – CGCCTCCACGCGATA GATGTGGGC – 3’
Y89I	5’ – TATCGCATTGAGGCG CAGGGTTCTG – 3’	5’ – CGCCTCAATGCGATA GATGTGGGCTG – 3’

Table 5-8. Continued

Mutation of pSF3	Forward Primer	Reverse Primer
Y89L	5’ – TATCGCCTGGAGGCG CAGGGTTCTG – 3’	5’ – CGCCTCCAGGCGATA GATGTGGGCTGC – 3’
Y89P	5’ – TATCGCCCGGAGGCG CAGGGTT – 3’	5’ – CGCCTCCGGGCGATA GATGTGGGCT – 3’
Y89M	5’ – TATCGCATGGAGGCG CAGGGTTCTG – 3’	5’ – CGCCTCCATGCGATA GATGTGGGCTGC – 3’
Y89H	5’ – TATCGCCATGAGGCG CAGGGTTCTG – 3’	5’ – CGCCTCATGGCGATA GATGTGGGCTGC – 3’
Y89F	5’ – TATCGCTTTGAGGCG CAGGGTTCTG – 3’	5’ – CGCCTCAAAGCGATA GATGTGGGCTGCC – 3’
Y89W	5’ – TATCGCTGGGAGGCG CAGGGTTCTG – 3’	5’ – CGCCTCCCAGCGATA GATGTGGGCTGC – 3’
Y89S	5’ – TATCGCAGCGAGGCG CAGGGTTCT – 3’	5’ – CGCCTCGCTGCGATA GATGTGGGCTGC – 3’
Y89C	5’ – TATCGCTGCGAGGCG CAGGGTTCT – 3’	5’ – CGCCTCGCAGCGATA GATGTGGGCTGC – 3’
Y89T	5’ – TATCGCACCGAGGCG CAGGGTTCT – 3’	5’ – CGCCTCGGTGCGATA GATGTGGGCTGC – 3’
Y89N	5’ – TATCGCAACGAGGCG CAGGGTTCTG – 3’	5’ – CGCCTCGTTGCGATA GATGTGGGCTGC – 3’
Y89Q	5’ – TATCGCCAGGAGGCG CAGGGTTCTG – 3’	5’ – CGCCTCCTGGCGATA GATGTGGGCTGC – 3’
Y89R	5’ – TATCGCCGTGAGGCG CAGGGTTCT – 3’	5’ – CGCCTCACGGCGATA GATGTGGGCTG – 3’
Y89K	5’ – TATCGCAAAGAGGCG CAGGGTTCTGCT – 3’	5’ – CGCCTCTTTGCGATA GATGTGGGCTGC – 3’
Y89D	5’ – TATCGCGATGAGGCG CAGGGTTCTG – 3’	5’ – CGCCTCATCGCGATA GATGTGGGCTGC – 3’
Y89E	5’ – TATCGCGAAGAGGCG CAGGGTTCTG – 3’	5’ – CGCCTCTTCGCGATA GATGTGGGCTG – 3’
H128G	5’ – GCCCCTGACGATGTC GGCTTTACCCCGACTCGC – 3’	3’ – GCGAGTCGGGGTAAA GCCGACATCGTCAGGGG – 3’
H128A	5’ – GCCCCTGACGATGTC GCGTTTACCCCGACTCGC – 3’	5’ – GCGAGTCGGGGTAAA CGCGACATCGTCAGGGG– 3’
H128V	5’ – GCCCCTGACGATGTCGTG TTTACCCCGACTCGCCTC – 3’	5’ – GCGAGTCGGGGTAAA CACGACATCGTCAGGGGC – 3’
H128I	5’ – GCCCCTGACGATGTCATT TTTACCCCGACTCGCCTCGT – 3’	5’ – GCGAGTCGGGGTAAAAAT GACATCGTCAGGGGCGATG – 3’
H128L	5’ – GCCCCTGACGATGTCCTG TTTACCCCGACTCGCCT – 3’	5’ – GCGAGTCGGGGTAAA CAGGACATCGTCAGGGGC – 3’
H128P	5’ – GCCCCTGACGATGTCCCG TTTACCCCGACTCGCCT – 3’	5’ – GCGAGTCGGGGTAAA CGGGACATCGTCAGGGG – 3’
H128M	5’ – GCCCCTGACGATGTCATG TTTACCCCGACTCGCCTCG – 3’	5’ – GCGAGTCGGGGTAAACAT GACATCGTCAGGGGCGAT – 3’
H128F	5’ – GCCCCTGACGATGTCTTT TTTACCCCGACTCGCCTCG – 3’	5’ – GCGAGTCGGGGTAAAAAA GACATCGTCAGGGGCGATG – 3’
H128Y	5’ – GCCCCTGACGATGTCTATTTT ACCCCGACTCGCCTCGTCT – 3’	5’ – GCGAGTCGGGGTAAAATA GACATCGTCAGGGGCGATG – 3’
H128W	5’ – GCCCCTGACGATGTC TGGTTTACCCCGACTCGCC – 3’	5’ – GCGAGTCGGGGTAAA CCAGACATCGTCAGGGGC – 3’
H128S	5’ – GCCCCTGACGATGTCAGC TTTACCCCGACTCGCCTC – 3’	5’ – GCGAGTCGGGGTAAA GCTGACATCGTCAGGGGC – 3’

Table 5-8. Continued

Mutation of pSF3	Forward Primer	Reverse Primer
H128C	5' – GCCCCTGACGATGTC TGCTTTACCCCGACTCGC – 3'	5' – GCGAGTCGGGGTAAA GCAGACATCGTCAGGGGC – 3'
H128T	5' – GCCCCTGACGATGTC ACCTTTACCCCGACTCGCC – 3'	5' – GCGAGTCGGGGTAAA GGTGACATCGTCAGGGGC – 3'
H128N	5' – GCCCCTGACGATGTC AACTTTACCCCGACTCGCCTC – 3'	5' – GCGAGTCGGGGTAAA GTTGACATCGTCAGGGGCG – 3'
H128Q	5' – GCCCCTGACGATGTC CAGTTTACCCCGACTCGCCTC – 3'	5' – GCGAGTCGGGGTAAA CTGGACATCGTCAGGGGC – 3'
H128R	5' – GCCCCTGACGATGTCCGT TTTACCCCGACTCGCCTCT – 3'	5' – GCGAGTCGGGGTAAA ACGGACATCGTCAGGGGC – 3'
H128K	5' – GCCCCTGACGATGTCAAA TTTACCCCGACTCGCCTCT – 3'	5' – GCGAGTCGGGGTAAATTT GACATCGTCAGGGGC – 3'
H128D	5' – GCCCCTGACGATGTCGAT TTTACCCCGACTCGCCTCTC – 3'	5' – GCGAGTCGGGGTAAAATC GACATCGTCAGGGGCG – 3'
H128E	5' – GCCCCTGACGATGTCGAA TTTACCCCGACTCGCCTC – 3'	5' – GCGAGTCGGGGTAAATTC GACATCGTCAGGGGC – 3'

Note: Mutation is underlined in each primer.

Protein overexpression. A single colony of the appropriate strain was used to inoculate 25 mL of LB medium supplemented with 100 μg/mL ampicillin. After shaking overnight at 37 ºC, a 10 mL portion of the preculture was added to 1 L of LB medium supplemented with 100 μg/mL ampicillin. The culture was grown at 37 ºC with shaking at 250 rpm until the $O.D._{600}$ reached 0.5 – 0.6. Protein overexpression was induced by adding 0.4 mL of 0.16 M IPTG (to yield a final concentration of 0.4 mM). After 3 hr, the cells were harvested by centrifuging at 6,300 × *g* for 15 min at 4 ºC, resuspended in 50 mM KP_i, pH 8.0 (1 mL buffer per gram wcw), then lysed by a French pressure cell at 17,000 psi. Insoluble debris was pelleted by centrifuging at 39,000 × *g* for 1 hr at 4 ºC and the yellow supernatant was used for TA-catalyzed reactions. Glycerol was added to a final concentration of 20% and the protein was stored in aliquots at -80 ºC.

Amino acid derivatization. Reaction mixtures were dried completely under reduced pressure for 30 min by a Savant SpeedVac SVC100, then the residue was taken up in pyridine (1 μL) and MSTFA (50 μL). After shaking at 37 ºC for 30 min, the mixtures were analyzed by GC/MS.

Enzyme assays. The activity of each L-TA mutant was measured by mixing 0.1 mmol acetaldehyde, 1.0 mmol glycine, 10 nmol PLP and 20 µL of enzyme solution in 50 mM KPi, pH 8.0 (total volume of 1 mL). The mixture was gently rotated at room temperature and 5 µL aliquots were removed after 20 hr. Samples were derivatized with MSTFA and analyzed by GC/MS. The temperature program involved an initial hold at 95 ºC for 5 min, an initial increase of 5 ºC / min to 120 ºC followed by an increase of 2 ºC / min to 138 ºC, then a final increase of 10 ºC / min to 200 ºC and a hold at that temperature for 5 min.

General procedure for screening aldehyde acceptors. Reactions contained 0.1 mmol of aldehyde, 0.5 mmol of glycine, 10 nmol of PLP and 20 µL of enzyme lysate in 50 mM Tris base, pH 9.7 (total volume of 1 mL). These were gently rotated overnight at 37 ºC and sampled after 20 hr for MSTFA derivatization and GC/MS analysis.

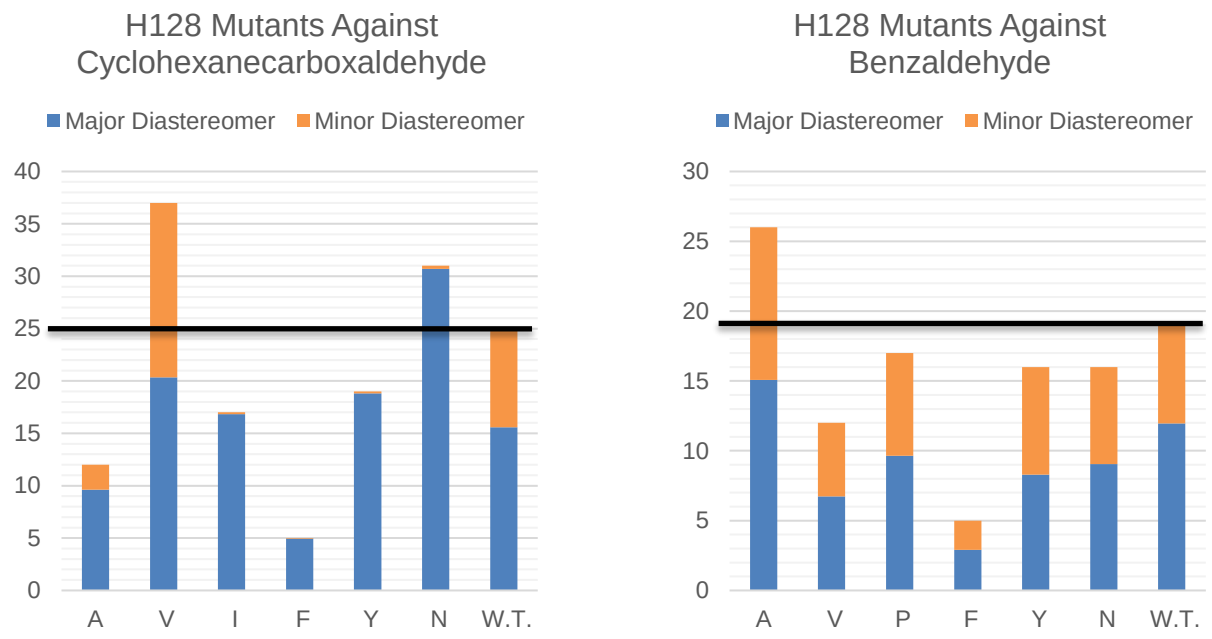

Figure 5-1. Initial screening of H128 mutants against the three aldehydes: (*a*) cyclohexanecarboxaldehyde, (*b*) benzaldehyde, and (*c*) 3-pyridinecarboxaldehyde. Each mutation was represented by its one letter abbreviation. W.T. stands for the wild type enzyme for comparison. All 20 amino acids were put through this initial screening, however if a conversion of <5% was observed, it was excluded from the graph. The magnitude of the each chart represents the % conversion with major (blue) and minor (orange) diastereomers noted. Reaction conditions are as follows: Reaction mixtures contained 500 mM glycine, 100 mM aldehyde, 0.05 mM PLP, 20% ethanol, and 10 µL of enzyme lysate in 1 mL of 50 mM Tris Base, pH 9.7. Reactions were incubated at 37 ºC.

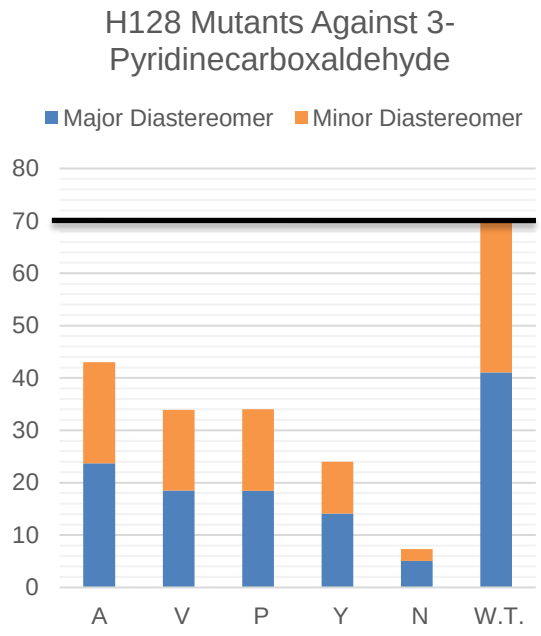

(*c*)

Figure 5-1. Continued

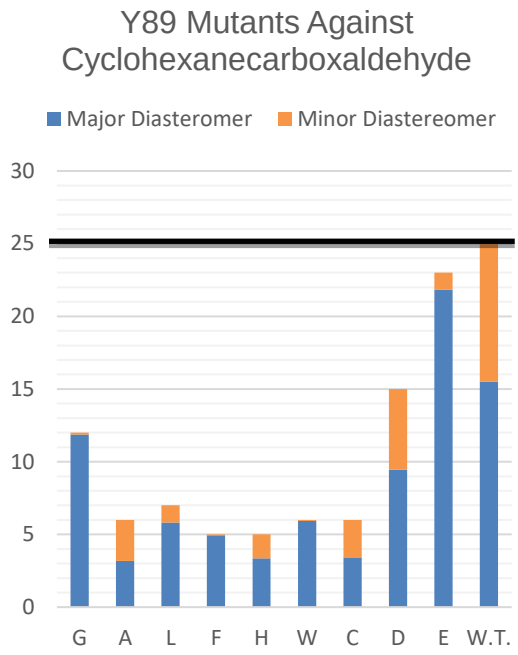

(*a*)

Figure 5-2. Initial screening of Y89 mutants against the three aldehydes: (*a*) cyclohexanecarboxaldehyde, (*b*) benzaldehyde, and (*c*) 3-pyridinecarboxaldehyde. Each mutation was represented by its one letter abbreviation. W.T. stands for the wild type enzyme for comparison. All 20 amino acids were put through this initial screening, however if a conversion of <5% was observed, it was excluded from the graph. The magnitude of the each chart represents the % conversion with “major” (blue) and “minor” (orange) diastereomers noted. In some cases diastereoselectivity was reversed, indicated the original diastereomer in blue. Reaction conditions are as follows: Reaction mixtures contained 500 mM glycine, 100 mM aldehyde, 0.05 mM PLP, 20% ethanol, and 10 µL of enzyme lysate in 1 mL of 50 mM Tris Base, pH 9.7. Reactions were incubated at 37 ºC.

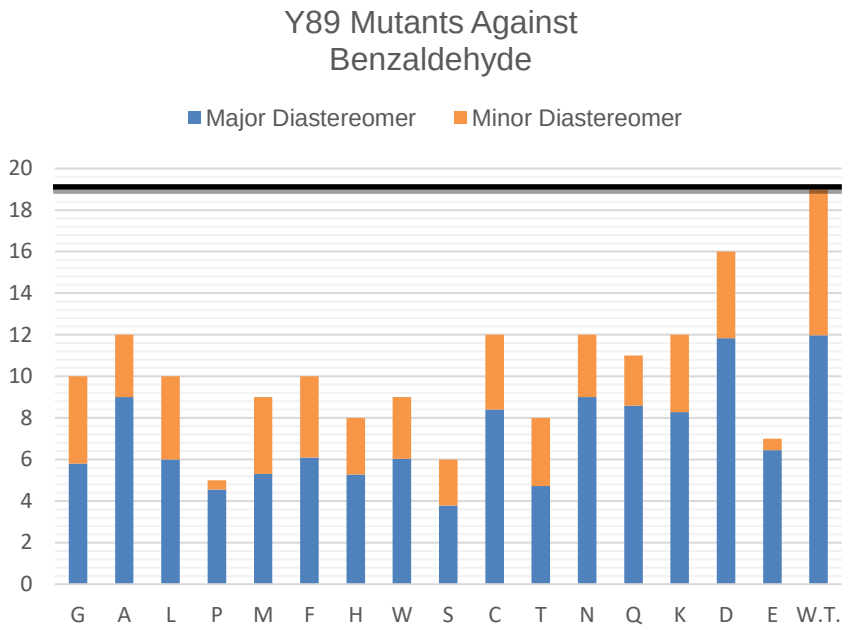

(*b*)

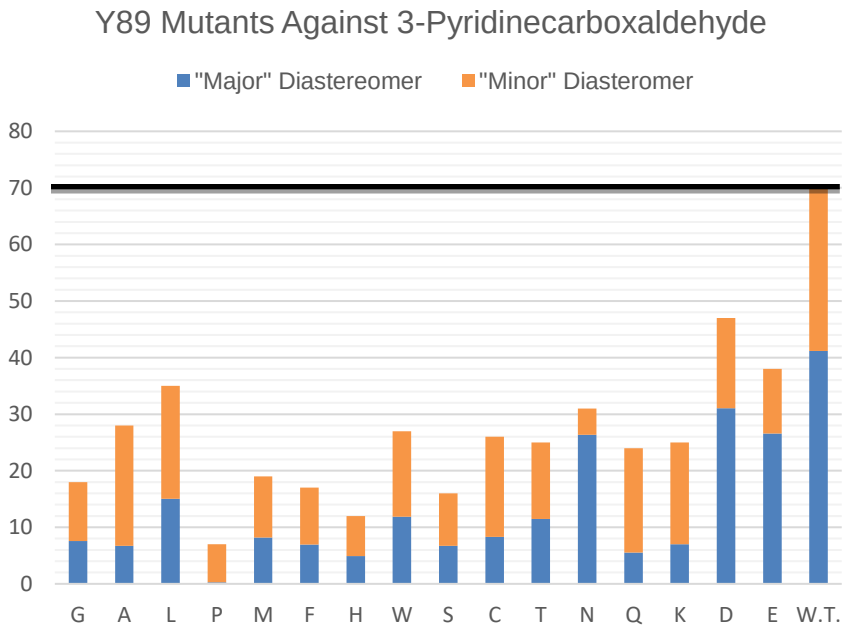

(*c*)

Figure 5-2. Continued

CHAPTER 6
BIOCATALYTIC SYNTHESIS OF TERTIARY β-METHYL-FLUORINATED β-HYDROXY-α-AMINO ACIDS BY THREONINE ALDOLASE

Introduction

β-Hydroxy-α-amino acids have been valuable precursors for wide variety of pharmaceuticals.[263-266] Zhou, Toone and coworkers discovered LPC-058, (difluoromethyl-*allo*-threonyl hydroxamate) a broad spectrum antibiotic.[153, 157] LPC-058 inhibits the enzyme UDP-3-O-(R-3-hydroxymyristoyl)-*N*-acetylglucosamine deacetylase (LpxC), which catalyzes the irreversible first step in the biosynthesis of lipid A.[155, 156] Zhou, Toone, and coworkers initially reported a 10-step total synthesis,[153] which was later shortened to 8 steps[157] by modifying the synthesis of the difluoromethylthreonine methyl ester.

Threonine aldolases (TAs) are pyridoxal phosphate (PLP) dependent enzymes that yield β-hydroxy-α-amino acids by a one-step aldol condensation between glycine and an aldehyde acceptor. TAs have been shown to accept a wide variety of aldehyde partners, ranging from long chain aliphatic chains to complex aromatic side chains.[184] The Griengl group also identified a handful of TAs that accepted more complex amino acids such as D-Ala, D-Ser, and D-Cys, increasing the utility of these enzymes.[184, 188, 198] However, to the best of our knowledge, no TA has catalyzed an aldol reaction between an amino acids and a ketone acceptor. Here, we report the first example of such a reaction (Figure 6-1).

Results and Discussion

Screening of Fluorinated Acetones

Gene cloning, protein overexpression, and optimized reaction conditions were completed as previously described (Chapters 3 – 5). The following L-TAs were

investigated for their tolerance toward four fluorinated acetones **40** – **43**: L-*allo*-TA from *A. jandaei*, H128N L-*allo*-TA from *A. jandaei*, Y89D L-*allo*-TA from *A. jandaei*, Y89P L-*allo*-TA from *A. jandaei*, and L-TA from *P. putida* (Table 6-1). As expected, no aldol condensation was observed when the enzymes were tested with glycine and trifluoroacetone **43**, as >99% of this ketone is in the hydrate form.[267] While ketones **40**, **41** and **42** all gave measurable aldol products, yields were below 10%. Interestingly for ketone **40**, both that Y89D and Y89P variants of *A. jandaei* L-*allo*-TA favored the opposite diastereomer *versus* that afforded by the wild type enzyme (Table 6-1, entry 1). The symmetry of ketone **41** is advantageous since only one chiral center was formed upon aldol condensation by an L-TA. These enzymes generally exert virtually complete control over the configuration at the α-carbon, all e.e. values were >99%. Screening reactions used a ten-fold molar excess of glycine *versus* the ketone acceptor to afford maximum conversions, although the standard five-fold molar excess gave similar results. Thus while the overall conversions were poor, our goal in this phase was to determine whether these five enzymes could tolerate a ketone acceptor.

Table 6-1. L-TA-catalyzed aldol condensation of fluorinated acetones

Entry	Fluorinated Acetone	Product	Enzyme	Reaction Time (hr)	Conversion[a] (%)	d.e.[a] (%)
1	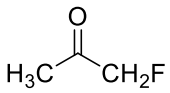 **40**	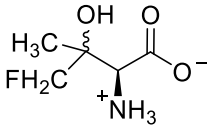	*A. jandaei* L-*allo*-TA	4	3	--[b]
				20	4	--[b]
			H128N *A. jandaei* L-*allo*-TA	4	2	--[b]
				20	4	--[b]
			Y89D *A. jandaei* L-*allo*-TA	4	<1	--[b,d]
				20	<1	--[b,d]
			Y89P *A. jandaei* L-*allo*-TA	4	<1	--[b,d]
				20	<1	--[b,d]
			P. putida L-TA	4	3	--[b]
				20	3	--[b]

Table 6-1. Continued

Entry	Fluorinated Acetone	Product	Enzyme	Reaction Time (hr)	Conversion[a] (%)	d.e.[a] (%)
2	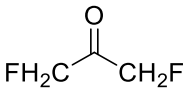 **41**	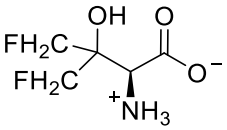	*A. jandaei* L-*allo*-TA	4	5	99[c]
				20	7	99[c]
			H128N *A. jandaei* L-*allo*-TA	4	5	99[c]
				20	6	99[c]
			Y89D *A. jandaei* L-*allo*-TA	4	<1	--[b]
				20	1	--[b]
			Y89P *A. jandaei* L-*allo*-TA	4	2	--[b]
				20	2	--[b]
			P. putida L-TA	4	4	--[b]
				20	6	99[c]
3	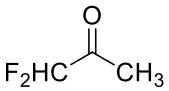 **42**	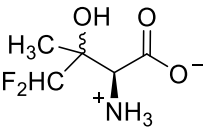	*A. jandaei* L-*allo*-TA	4	8	30
				20	10	23
			H128N *A. jandaei* L-*allo*-TA	4	5	32
				20	5	1
			Y89D *A. jandaei* L-*allo*-TA	4	<1	--[b]
				20	<1	--[b]
			Y89P *A. jandaei* L-*allo*-TA	4	1	--[b]
				20	2	--[b]
			P. putida L-TA	4	6	36
				20	10	2
4	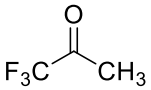 **43**	--	*A. jandaei* L-*allo*-TA	4	--	--
				20	--	--
			H128N *A. jandaei* L-*allo*-TA	4	--	--
				20	--	--
			Y89D *A. jandaei* L-*allo*-TA	4	--	--
				20	--	--
			Y89P *A. jandaei* L-*allo*-TA	4	--	--
				20	--	--
			P. putida L-TA	4	--	--
				20	--	--

Note: Reaction mixtures contained 1 M glycine, 100 mM acetone, 0.05 mM PLP, 20% ethanol, and 20 µL of enzyme lysate in 1 mL of buffer. Reactions with *A. jandaei* L-*allo*-TA and its mutants were in 50 mM Tris base, pH 9.7 and were incubated at 37 ºC. Reactions with *P. putida* L-TA were in 50 mM KP_i, pH 8 and were incubated at room temperature.

[a] Conversion and diastereomeric excess values were determined by GC/MS after MSTFA derivatization. Reactions with 1 – 5% conversions are listed as "<5%" and no values for diastereomeric purity are provided since the small peak sizes preclude accurate integration.

[b] Accurate values for conversion and diastereomeric excess could not be determined due to the very low peak areas.

[c] This value was enantiomeric excess as a result of the symmetrical ketone.

[d] Reverse diastereoselectivity was observed.

Preparative Conversions

Since the overall conversions were very low for all of these ketone substrates, we scaled up the reactions to provide sufficient amounts of products to allow ^{1}H NMR analysis. All preparative conversions were accomplished with wild type enzymes, as they provided best overall conversions. Screening reaction conditions were scaled-up ten-fold. After the 20 hr, any unreacted aldehyde was removed by extracting with Et_2O, then the water was removed by lyophilization. The solid was extracted with two portions of methanol, which left most unreacted glycine and buffer salts undissolved. After evaporating the methanol, the residue was dissolved in buffer at pH 8.0 and glycine oxidase was added to decompose any remaining glycine. An anion-exchange resin eluted with 0.5% aqueous acetic acid was used for final purification prior to final lyophilization the afforded the aldol products.

The low yields were mainly due to poor conversions by the enzymes, rather than to losses during isolation. While yields were disappointing, enough material was isolated for MS and NMR analysis (Figures A-10 and A-11 – 13). We first confirmed product formation MS analysis of the product from ketone **42**.[i] The theoretical $[M-H]^-$ = 168.0478 was observed as 168.0473, confirming the aldol condensation with ketone **42** (Figure A-10). Both ^{1}H and ^{19}F NMR also confirmed the aldol product (Figure A-11 and 12) resulting in the first known example of threonine aldolases in the synthesis of β-trisubstituted amino acids. Both ketones **40** and **41** were also scaled up ten-fold; however, yields for ketone **41** were too low for NMR analysis. Both ^{1}H and ^{19}F NMR confirmed the aldol product from ketone **40** (Figure A-13).

[i] Nominal mass spectrometry was determined by the UF Mass Spectrometry Lab.

Conclusion

In summary, four fluorinated acetones were tested as substrates for the L-TA from *P. putida* and *A. jandaei* and a few mutations of *A. jandaei*. Three of the four ketones were tolerated (albeit poorly). The product from ketones **40** and **42** was isolated on a sufficient scale to allow MS and NMR analysis, which confirmed its structure. This represents the first example of a ketone acceptor for a threonine aldolase.

Experimental Procedures

General. LB medium contained 10 g/L Bacto-Tryptone, 5 g/L Bacto-Yeast Extract and 10 g/L NaCl; 15 g/L agar was added for plates. PCR amplifications were performed with Phusion Hot Start II DNA polymerase using the manufacturer's protocols. Electroporation was carried out with a BioRad GenePulser apparatus using 0.2 cm cuvettes. Promega Wizard kits and CsCl buoyant density ultracentrifugation[244] were used for small- and large-scale plasmid purifications, respectively. Fluorescent Sanger DNA sequencing was performed by the University of Florida ICBR. GC/MS analysis employed a 30 m × 0.25 mm Beta Dex™ 225 column and ionization by EI at 70 eV. The temperature program involved an initial hold at 95 ºC for 5 min, an initial increase of 5 ºC/min to 138 ºC followed by an increase of 10 ºC/min to 180 ºC, then a final increase of 2 ºC/min to 200 ºC and a hold at that temperature for 10 min.

Cloning of *A. jandaei* L-*allo*-TA. The gene encoding L-*allo*-TA from *A. jandaei* (accession number D87890) was synthesized by GenScript and ligated into a pUC57 with flanking *Nde*I and *Xho*I restriction sites at the 5'- and 3'-ends, respectively. The TA gene was excised by digesting with these restriction enzymes and ligated with *Nde*I, *Xho*I-cut pET15b (Novagen). After transformation into *E. coli* ElectroTen-Blue, plasmid

DNA from a randomly-chosen colony was isolated, restriction mapped and then sequenced to verify the desired structure. The resulting plasmid (designated pSF3) was used to transform *E. coli* BL21-Gold(DE3) strain for protein overexpression.

Cloning of *P. putida* L-TA. The L-TA gene from *P. putida* (accession number AP013070) was isolated and amplified from a *P. putida* strain purchased from Carolina Biological Company by colony PCR[229] using 5' – CGTTCACAGGACCGTCATATGACA GATAAGAGCCAACAATTCGCC – 3' and 5' – CTGGCTTGCCGGCGATTGGGGATCC TCAGGCGGTGATGATGCTGCGGATA – 3' as forward and reverse primers, respectively. These primers also introduced flanking *Nde*I and *Bam*HI restriction sites (underlined). After purification, the PCR product was digested sequentially with *Nde*I and *Bam*HI, then ligated with *Nde*I, *Bam*HI-digested pET-15b. After transformation into *E. coli* ElectroTen-Blue, plasmid DNA from a randomly-chosen colony was isolated, restriction mapped and then sequenced to verify the desired structure. The resulting plasmid (designated pSF6) was used to transform *E. coli* BL21-Gold(DE3) strain for protein overexpression.

Cloning of *B. subtilis* glycine oxidase. The complete coding sequence for *B. subtilis* glycine oxidase (accession number NC000964) was synthesized by GenScript and ligated into pUC57 with flanking *Nde*I and *Bam*HI restriction sites at the 5'- and 3'-ends, respectively. Silent mutations were introduced to the coding region to remove internal *Nde*I and *Bam*HI sites that occur in the native sequence. The gene was subcloned as an *Nde*I, *Bam*HI fragment between these sites into pET-15b. After transforming *E. coli* ElectroTen-Blue, plasmid DNA was isolated from a randomly-chosen colony, restriction mapped and sequenced to verify that the desired plasmid had

been prepared (designated pSF9). This was used to transform *E. coli* BL21-Gold(DE3) for protein overexpression.

Mutagenesis of *A. jandaei* L-*allo*-TA. Each mutation was accomplished by PCR with individual primer sets using pSF3 as the template DNA and the corresponding forward and reverse primers for each mutation. These primer sets introduced a specific mutation at a specific site, using the most frequent codon usage for *E. coli* (underlined in Table 6-2). After purification, the PCR product was digested with *Dpn*I to cut the template DNA (pSF3). After transformation into *E. coli* ElectroTen-Blue, plasmid DNA from a randomly-chosen colony was isolated and sequenced to verify the desired mutation. The resulting plasmid with mutation was used to transform *E. coli* BL21-Gold(DE3) strain for protein overexpression.

Table 6-2. Forward and reverse primer sets for mutagenesis

Mutation of pSF3	Forward Primer	Reverse Primer
Y89P	5' – TATCGCCCGGAGGCG CAGGGTT – 3'	5' – CGCCTCCGGGCGATA GATGTGGGCT – 3'
Y89D	5' – TATCGCGATGAGGCG CAGGGTTCTG – 3'	5' – CGCCTCATCGCGATA GATGTGGGCTGC – 3'
H128N	5' – GCCCCTGACGATGTCAAC TTTACCCCGACTCGCCTC – 3'	5' – GCGAGTCGGGGTAAAGTT GACATCGTCAGGGGCG – 3'

Note: Mutation is underlined in each primer.

Protein overexpression. A single colony of the appropriate strain was used to inoculate 50 mL of LB medium supplemented with 100 µg/mL ampicillin. After shaking overnight at 37 ºC, a 40 mL portion of the preculture was added to 4 L of LB medium supplemented with 100 µg/mL ampicillin, 80 mL of 20% glucose, and 1.5 mL of Sigma Antifoam 204 in a New Brunswick M19 fermenter. The culture was grown at 37 ºC with stirring at 400 rpm and an air flow of 1 vvm until the O.D.600 reached 0.5 – 0.6. Protein overexpression was induced by adding 10 mL of 0.16 M IPTG (to yield a final concentration of 0.4 mM) and adjusting the temperature to 30 ºC and shaking. After 3

hr, the cells were harvested by centrifuging at 6,300 × g for 15 min at 4 ºC, resuspended in 50 mM KP_i, pH 8.0 (1 mL buffer per gram wcw), then lysed by a French pressure cell at 17,000 psi. Insoluble debris was pelleted by centrifuging at 39,000 × g for 1 hr at 4 ºC and the yellow supernatant was used for TA-catalyzed reactions.

Affinity purification of *B. subtilis* glycine oxidase. A crude extract containing glucose oxidase was prepared as described above, then the sample was applied to a 5 mL HiTrap Chelating HP column (GE Healthcare Life Sciences) that had been equilibrated with binding buffer (20 M NaP_i, 500 mM NaCl, 20 mM imidazole, pH 7.4). After washing with 50 mL of binding buffer, the desired protein was eluted by elution buffer (20 mM NaPi, 500 mM NaCl, 500 mM imidazole, pH 7.4). A flow rate of 2 mL/min was employed throughout. The eluate was concentrated by ultrafiltration (Amicon Ultra), then diluted with 50 mM KPi, pH 8.0 and re-concentrated. This was repeated two more times. The final glycine oxidase sample was diluted with the same buffer to 5 mg / mL, then glycerol was added to a final concentration of 10% and the protein was stored in aliquots at -80 ºC.

Enzyme assays for threonine aldolase. The activity of L-TAs was measured by mixing 0.1 mmol acetaldehyde, 1.0 mmol glycine, 10 nmol PLP and 20 µL of enzyme solution in 50 mM KPi, pH 8.0 (total volume of 1 mL). The mixture was gently rotated at room temperature and 5 µL aliquots were removed after 0.5 hr, 1.5 hr, 4 hr, and overnight. Samples were derivatized with MSTFA and analyzed by GC/MS. The temperature program involved an initial hold at 95 ºC for 5 min, an initial increase of 5 ºC/min to 120 ºC followed by an increase of 2 ºC/min to 138 ºC, then a final increase of 10 ºC/min to 200 ºC and a hold at that temperature for 5 min.

Enzyme assay for glycine oxidase. Glycine oxidase activity was measured by monitoring the formation of H_2O_2 by UV -Vis spectroscopy at 500 nm using a coupled HRP assay.[228] Reaction mixtures containing 10 mM glycine and 0.25 mg glycine oxidase (in 50 µL of 50 mM KPi, pH 8.0) were added to 1.5 mM 4-aminoantipyrine, 2 mM phenol, and 5 U HRP in 50 mM KPi, pH 8.0 (total volume of 1000 µL). After incubating at 37 ºC for 10 min, the A^{500} value was used to calculate units glycine oxidase activity.[228]

Derivatization of amino acids by MSTFA. Reaction mixtures were dried completely under reduced pressure for 30 min by a Savant SpeedVac SVC100, then the residue was taken up in pyridine (1 µL) and MSTFA (50 µL). After shaking at 37 ºC for 30 min, the mixtures were analyzed by GC/MS.

General procedure for screening fluorinated acetone acceptors. Reactions contained 0.1 mmol of fluorinated acetone, 1 mmol of glycine, 10 nmol of PLP and 10 µL of enzyme lysate in buffer (total volume of 1 mL). These were gently rotated overnight at room temperature and sampled after 4 hr and overnight for MSTFA derivatization and GC/MS analysis.

Preparative synthesis of β-hydroxy-α-amino acids. Reaction mixtures contained 2.0 mmol of aldehyde, 10 mmol glycine, 100 nmol PLP and 200 µL of enzyme lysate in 20 mL 50 mM Tris, pH 9.7 and 2% (v/v) ethanol. After gently rotating at 37 ºC (if using *A. jandaei* L-*allo*-TA) or 25 ºC (if using *P. putida* L-TA) for 20 hr, the unreacted aldehyde was removed by extraction with Et_2O (2 × 30 mL) and the aqueous layer was lyophilized. The solid residue was mixed thoroughly with 30 mL of MeOH and the solution was filtered and evaporated under reduced pressure. This procedure was

repeated to remove additional unreacted glycine. The crude product was resuspended in 10 mL of 50 mM KP_i, pH 8.0, then 1 mg of purified glycine oxidase was added and the mixture was gently rotated at 37 ºC for 8 hr. An additional of 1 mg portion of purified glycine oxidase was then added and incubation at 37 ºC was continued for an additional 20 hr. The reaction mixture was lyophilized. The residue was stirred with MeOH, leaving most phosphate undissolved. After evaporating the solvent, the crude product was dissolved in water and applied to an 11 × 1.5 cm DOWEX, 1 × 2 (HO^- form) column. The column was washed with 100 mL of deionized water, then the desired product was eluted by washing with 50 mL of 0.5% acetic acid. The solvent was removed using a SpeedVac to afford the final product.

2-Amino-4,4-difluoro-3-hydroxy-3-methylbutanoic acid (synthesized by *P. putida* L-TA). White solid 30 mg, 8.8% yield, 0% d.e., ^{1}H NMR (300 MHz, D_2O) δ 6.34 – 5.79 (1H, q), 3.88 – 3.78 (1H, d), 1.48 – 1.27 (3H, d) ppm. ^{19}F NMR (300 MHz, D_2O) δ -129.49 – -132.24 (dq), -132.39 – -136.37 (dq) ppm (Figure A-11).

2-Amino-4,4-difluoro-3-hydroxy-3-methylbutanoic acid (synthesized by *A. jandaei* L-*allo*-TA). White solid 12.9 mg, 7.2% yield, 37% d.e., ^{1}H NMR (300 MHz, D_2O) δ 6.34 – 5.79 (1H, q), 3.88 – 3.78 (1H, d), 1.48 – 1.28 (3H, d) ppm. ^{19}F NMR (300 MHz, D_2O) δ -129.50 – -132.22 (dq), -132.38 – -136.37 (dq) ppm (Figure A-12).

2-Amino-4-fluoro-3-hydroxy-3-methylbutanoic acid (synthesized by *A. jandaei* L-*allo*-TA). White solid 13 mg, 8% yield, 6% d.e., ^{1}H NMR (300 MHz, D_2O) δ 4.63 – 4.33 (2H, m), 3.86 – 3.72 (1H, d), 1.40 – 1.16 (3H, d) ppm. ^{19}F NMR (300 MHz, D_2O) δ 3.83 – 3.53 (t), 2.49 – 2.15 (t) ppm (Figure A-13).

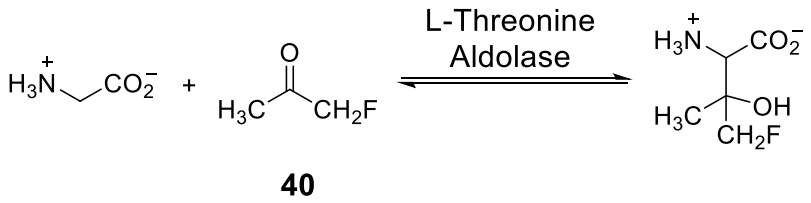

40

Figure 6-1. Tertiary β-methylfluoro threonine analogues by threonine aldolase

CHAPTER 7
CONCLUSIONS AND FUTURE WORK

Wild Type L-Threonine Aldolase

The L-TAs from *A. jandaei*, *E. coli*, *T. maritima*, and *P. putida* were successfully isolated and screened against a variety of aldehyde and ketone acceptors using glycine as the amino donor. Among these L-TAs, the L-*allo*-TA from *A. jandaei* proved superior at synthesizing β-hydroxy-α-amino acids with moderate conversions and diastereoselectivities. Since a simple isolation and purification protocol for the products had not been established prior to our work, one was devised and six aldehyde acceptors were scaled up moderately. The aldol products were isolated from the reaction mixtures using glycine oxidase to simplify downstream processing by removing excess glycine from the reaction mixture.

Mutant L-Threonine Aldolase

One of the major limitations of these enzymes was the reversibility of the reactions and the unfavorable thermodynamic equilibrium. Because of this reversibility, diastereoselectivity degraded over time, resulting in a mixture of diastereomers. It had been shown previously that shortened reaction times would prevent this erosion of diastereoselectivity; however, in most cases, fractional conversion had to be significantly sacrificed. In order for TAs to be synthetically relevant in an industrial setting, this issue had to be addressed. Therefore, site saturation mutagenesis was carried out on the L-*allo*-TA from *A. jandaei* at three active site residues, His 128, His 85, and Tyr 89. Each mutant was initially screened using glycine and three aldehyde acceptors (one aliphatic aldehyde and two aromatic aldehydes) in order to minimize screening efforts while still sketching the broad picture of the substrate selectivity of the

mutants. His 128 and Tyr 89 mutants gave increased diastereoselectivity for some aldehyde acceptors; however, mutations at the 85 position rendered the enzyme completely inactive. In summary, we can definitively say that by targeting active site residues and using SSM strategies the diastereoselectivity problem for at least some of the substrates was solved and specific results are summarized in the following paragraphs.

Histidine 128 Mutants

Histidine 128 was selected for mutagenesis because it hydrogen bonds with the hydroxyl group of L-*allo*-Thr. Qin *et al.* revealed some mutations at this position increased activity (8.4-fold) for the retro-aldol cleavage of L-Thr; however, the aldol condensation of glycine with aldehyde acceptors was never tested with these variants.[207] In this study, the His 128 mutants that displayed the best overall results in the initial screening were the Ile and Asn variants. More extensive screening of these variants was carried out on a variety of aliphatic aldehydes, *i.e*. straight chain, cyclic, branched, and unsaturated aldehydes and a few aromatic aldehydes. The Ile mutant showed >90% d.e. across all aliphatic aldehydes screened, although conversions were uniformly low (<20%). On the other hand, the Asn mutant gave comparable diastereoselectivities (>85%) along with reasonable conversions for some substrates.

Tyrosine 89 Mutants

Tyrosine 89 was targeted because it is located in the hydrophobic pocket where the methyl group of L-*allo*-Thr rests when it is bound as an external aldimine with PLP. The initial screening of these mutations revealed not only increased diastereoselectivity with some variants (Gly, Pro, Asp, Glu, and Trp), but also *reversed* diastereoselectivity (Ala, Pro, Gln and Lys). The best variants in this library were the Pro (Y89P) and Asp

(Y89D) mutants. The Y89P mutant increased the wild type diastereoselectivity (to 81% d.e.) with benzaldehyde **9**, but gave almost complete reversed selectivity for 3-pyridinecarboxaldehyde **11** (to 91% d.e.), despite the very similar sizes of the aldehydes. Y89D revealed reversed diastereoselectivity for non-cyclic, branched aldehyde acceptors. For example, the overall conversion of pivaldehyde **28** was increased seven-fold and completely reversed the diastereoselectivity (99% d.e.) with this single mutation. Isobutryaldehyde **31** presented similar results: a 2.7-fold increase in conversion (73%) as well as 99% d.e. for the opposite diastereomer. Surprisingly, cyclic aliphatic aldehydes did not show reversed diastereoselectivity. In conclusion, the diastereoselectivity problem for at least some of the substrates was solved.

Structure of L-Threonine Aldolases

The L-TA from *P. putida* was studied for its broad substrate range in producing β-hydroxy-α-amino acids. Although other L-TAs displayed tolerance in the synthesis of a variety amino acids, the diastereoselectivity of *P. putida* L-TA was found to be rather poor compared to the other L-TAs; however, in most cases, conversions were generally high for this of enzyme. We hoped to identify the problem by determining the crystal structure of this enzyme. After careful optimization of crystallogenesis conditions, the structure of *P. putida* L-TA was determined at a 2.27 Å resolution. The active site lysine was determined to be Lys 207 and other highly conserved amino acid residues included Ser 10, His 89, His 133, Arg 177, and Arg 321.

A comparison with the other L-TA structures revealed two main differences. First, the loop located near the active site was slightly longer in *P. putida* L-TA than in the others (by approximately 4 – 7 amino acids). This was thought to distort the folding of the preceding α-helix as the electron density was poor. Second, the amino acid

residue at position 93 differed from those of other L-TAs. In *P. putida* L-TA, it was Asp; in other L-TAs, the residue at the analogous position was a large aromatic residue (Tyr or Phe). The poor diastereoselectivity of *P. putida* L-TA might therefore be due to the extended loop, the acidic residue at position 93, or to other, more subtle factors. Interestingly, our mutagenesis studies of the equivalent position (93) in *A. jandaei* L-*allo*-TA revealed that an Asp at this position actually *increased* diastereoselectivity in that enzyme. It is therefore likely that the poor diastereoselectivity observed for *P. putida* L-TA was due to additional factors beyond the nature of the residue at position 93.

Future Work

Double Mutations

The double mutations H128N/Y89P and H128N/Y89D of L-*allo*-TA from *A. jandaei* should be isolated, overexpressed in *E. coli* and screened against aldehyde and ketone acceptors. Since both single mutations had an augmented effect on diastereoselectivity, the double mutants might provide even higher stereoselectivities. If the screening yields desirable outcomes, scaled up reactions should be preformed followed by isolation of aldol products.

Additional Mutations

One goal of this project was to increase the diastereoselectivity of *A. jandaei* L-*allo*-TA by manipulating the residues that interact with the hydroxyl and side-chain of the product. The next step in this project would be to mutate the amino acid residues that interact with the carboxylate group of the starting material and product to allow for different amino donors with interesting functional groups (*i.e.* sulfonate and phosphonate). The active site of L-TAs contain five conserved residues. These include

Ser 10, Arg 177, and Arg 321, which hydrogen bond with the carboxyl group of Gly and L-Thr. The most probable solution to help stabilize the extra charge from a phosphonate or sulfonate amino donor would be to mutate the Ser 10 to an Arg or Lys variant. This would produce a more positively charged environment that might allow for electrostatic interactions between the negatively charge phosphonate/sulfonate and the guanidinium group of Arg or the protonated amine of Lys.

Structure of Mutant L-Threonine Aldolase

H128N, Y89P and Y89D variants of *A. jandaei* L-*allo*-TA have proven useful at solving the diastereoselectivity problem for some aldehyde acceptors and, in some cases, reversing the diastereoselectivity completely. Crystallographic studies on these mutations should be carried out to help understand how these changes affected the active site. Since Qin *et al.* solved the crystal structure of both the wild type and the H128Y/S292R variant, these efforts should be fairly straight forward. Molecular replacement with the native L-*allo*-TA should allow for simple structure determination.

APPENDIX

SUPPORTING INFORMATION

Table A-1. Assignment of ^{1}H and ^{13}C chemical shifts in diastereomers M and m in D_2O (or methanol-d4, a), at 25 ºC

Compound		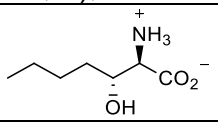		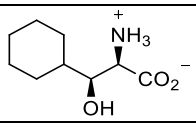		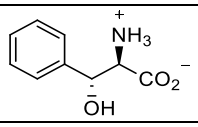	
Position	δ, ppm	M	m	M	m	M	m
1	C	171.6	172.8	172.1	170.7	171.8	170.9
2	C	57.4	57.1	56.0	56.9	60.7	60.3
2	H	3.75	3.55	3.65	3.72	3.84	4.00
3	C	69.4	69.6	3.6	74.5	71.2	71.1
3	H	4.00	3.97	3.78	3.57	5.21	5.26
4	C	30.5	32.8	40.1	39.7	139.0	136.8
4	H	1.40	1.49	1.47	*nm*	-	-
5	C	27.4	27.1	*nm*	*nm*	125.8	126.3
5	H	1.37, 1.25	1.35, 1.25	*nm*	*nm*	7.37	7.30
6	C	21.6	21.6	*nm*	*nm*	129.0	129.0
6	H	1.25	1.25	*nm*	*nm*	7.37	7.35
7	C	13.1	13.2	*nm*	*nm*	128.6	128.6
7	H	0.78	0.79	*nm*	*nm*	7.30	7.31

Compound		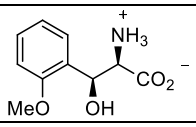		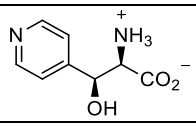		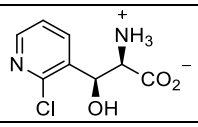	
Position	δ, ppm	M	m	M	m	M	m
1	C	169.0	*nm*	171.2	169.9	171.3	170.0
2	C	56.7	*nm*	60.0	59.6	57.8	56.9
2	H	4.25	4.01	3.88	4.08	4.01	4.02
3	C	65.8	*nm*	70.0	69.9	67.6	68.2
3	H	5.61	5.44	5.29	5.33	5.47	5.29
4	C	126.9	*nm*	153.2	153.6	134.1	134.3
5	C	156.1	*nm*	122.6	122.6	148.0	147.1
5	H	*nm*	*nm*	7.60	7.60	-	-
6	C	110.2	*nm*	146.7	145.4	-	-
6	H	7.03	6.98	8.50	8.49	-	-
7	C	129.4	*nm*	-	-	148.8	148.6
7	H	7.36	7.31	-	-	8.20	8.17
8	C	120.5	*nm*	-	-	123.8	123.3
8	H	7.04	6.99	-	-	7.39	7.33
9	C	126.6	*nm*	-	-	138.0	138.6
9	H	7.59	7.52	-	-	8.00	7.90
10	C	54.5	*nm*	-	-	-	-
10	H	3.90	3.85	-	-	-	-

Table A-2. *ΔR-ΔS* sign resulting from disubstitution with MPA

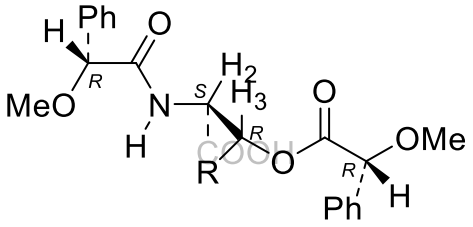

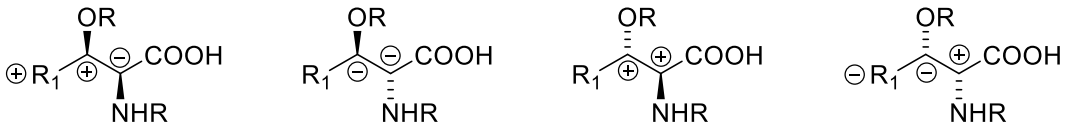

2-*S*, 3-*R* 2-*R*, 3-*R* 2-*S*, 3-*S* 2-*R*, 3-*S*

2-amino-3-hydroxy acid	2-*R*, 3-*R*	2-*R*, 3-*S*	2-*S*, 3-*R*	2-*S*, 3-*S*
H2	0-	0+	0-	0+
H3	-0	-0	+0	+0
R	-+	--	++	+-

Table A-3. Chemical shifts and *ΔR-ΔS* sign in double MPA derivatives of the *n*-butyl and cyclohexyl compounds

R1	CD	δR (ppm)	δH3 (ppm)	δH2 (ppm)
n-Butyl (OH) (M)	R,R	0.68	5.14	4.81
anti	S,S	0.80	5.02	4.73
2-*S*,3-*S*	$\Delta\delta_{RS}$	-0.18	0.12	0.08
n-Butyl (m)	R,R	0.86	5.40	4.71
syn	S,S	0.56	5.32	4.77
2-*S*,3-*R*	$\Delta\delta_{RS}$	0.30	0.08	-0.06
Cyclohexyl (OMe) (M)	R,R	1.56	5.23	4.86
syn	S,S	1.10	5.11	4.90
2-*S*,3-*R*	$\Delta\delta_{RS}$	0.46	0.12	-0.04
Cyclohexyl (m)	R,R	1.63	4.97	4.89
anti	S,S	1.50	5.11	4.87
2-*R*,3-*R*	$\Delta\delta_{RS}$	0.13	-0.14	0.02[a]

[a] Of the two possible configurations with $\Delta\delta_{RS}$ at H2<0, the one which allows for a $\Delta\delta_{RS}$ at R>0 was chosen, because of the absolute values of $\Delta\delta_{RS}$.

Table A-4. Chemical shifts in the methyl ester of 3-phenyl-2-amino-3-hydroxypropanoic acids and its amides with MPA.

R	MPA	δH5 (ppm)	δMeO1 (ppm)
Ph (M)	N/A	7.78	3.60
syn	R	7.78	3.54
2-*S*, 3-*S*	S	7.70	3.65
Ph (m)	N/A	7.91	3.67
anti	R	7.79	3.63
2-*R*, 3-*S*	S	*nm*	*nm*[a]

[a] For the minor, the shielding of H5 in the *R*-MPA was compared to the one in the amine.

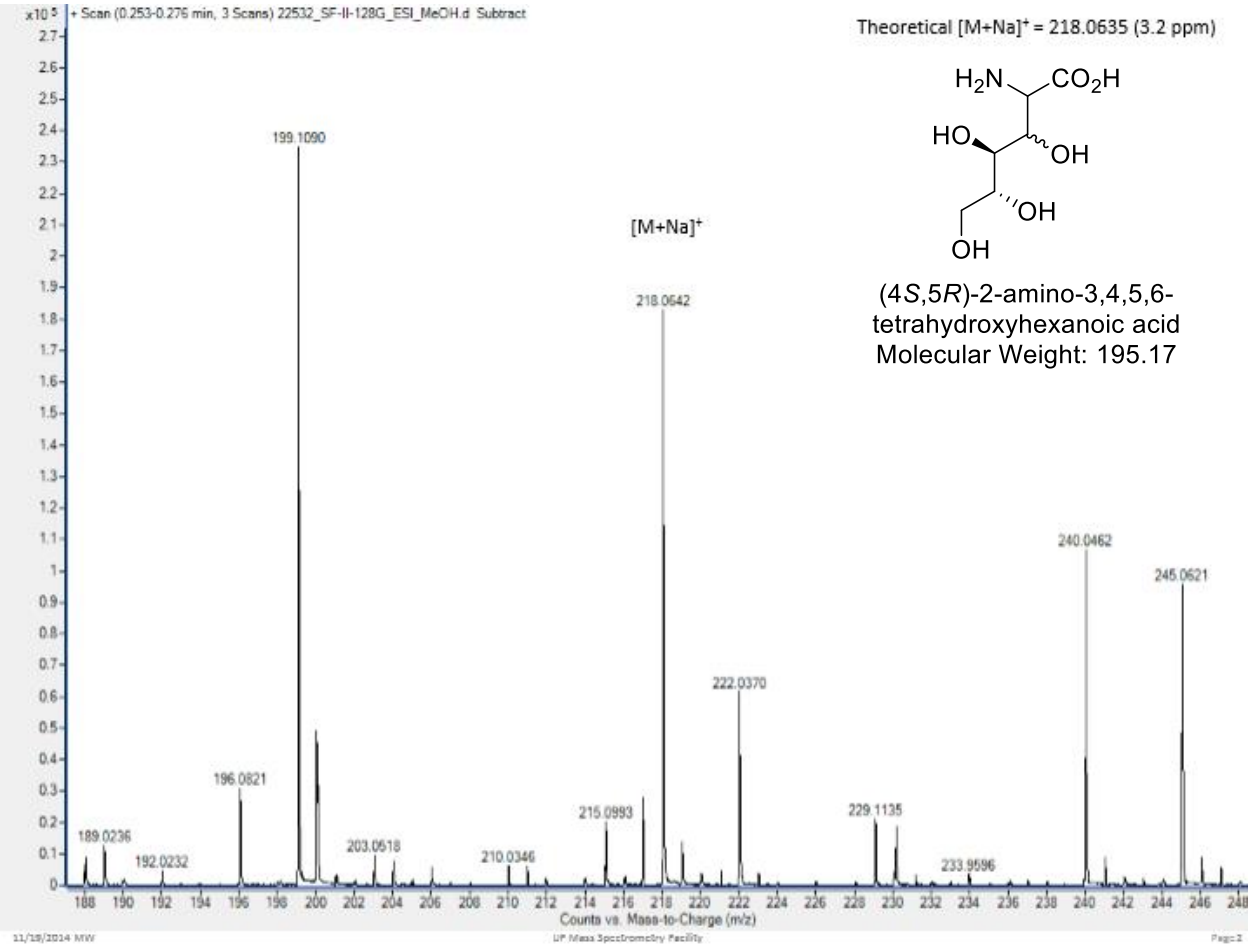

(*a*)

Figure A-1. Mass spectrum of (4*S*,5*R*)-2-amino-3,4,5,6-tetrahydroxyhexanoic acid

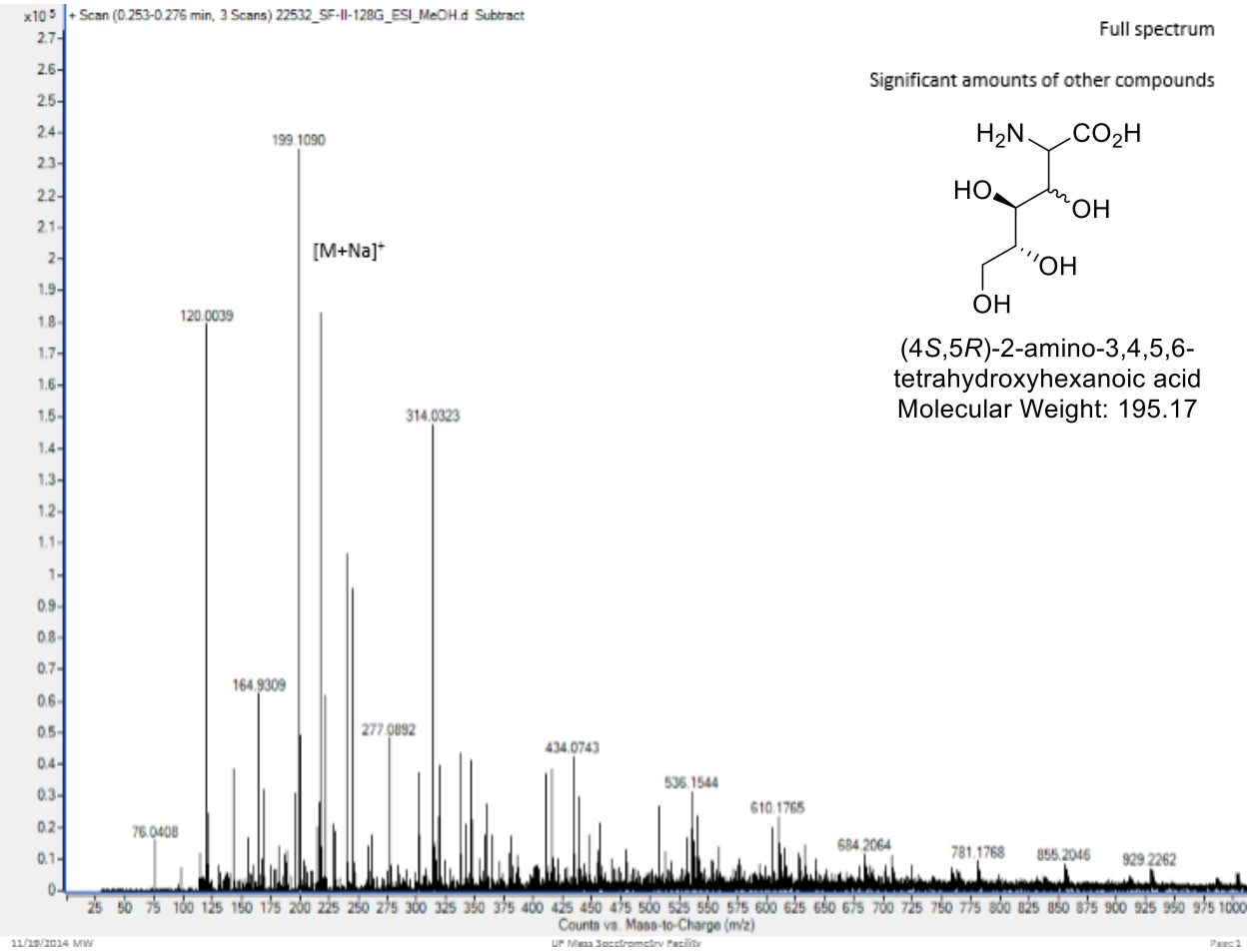

(*b*)

Figure A-1. Continued

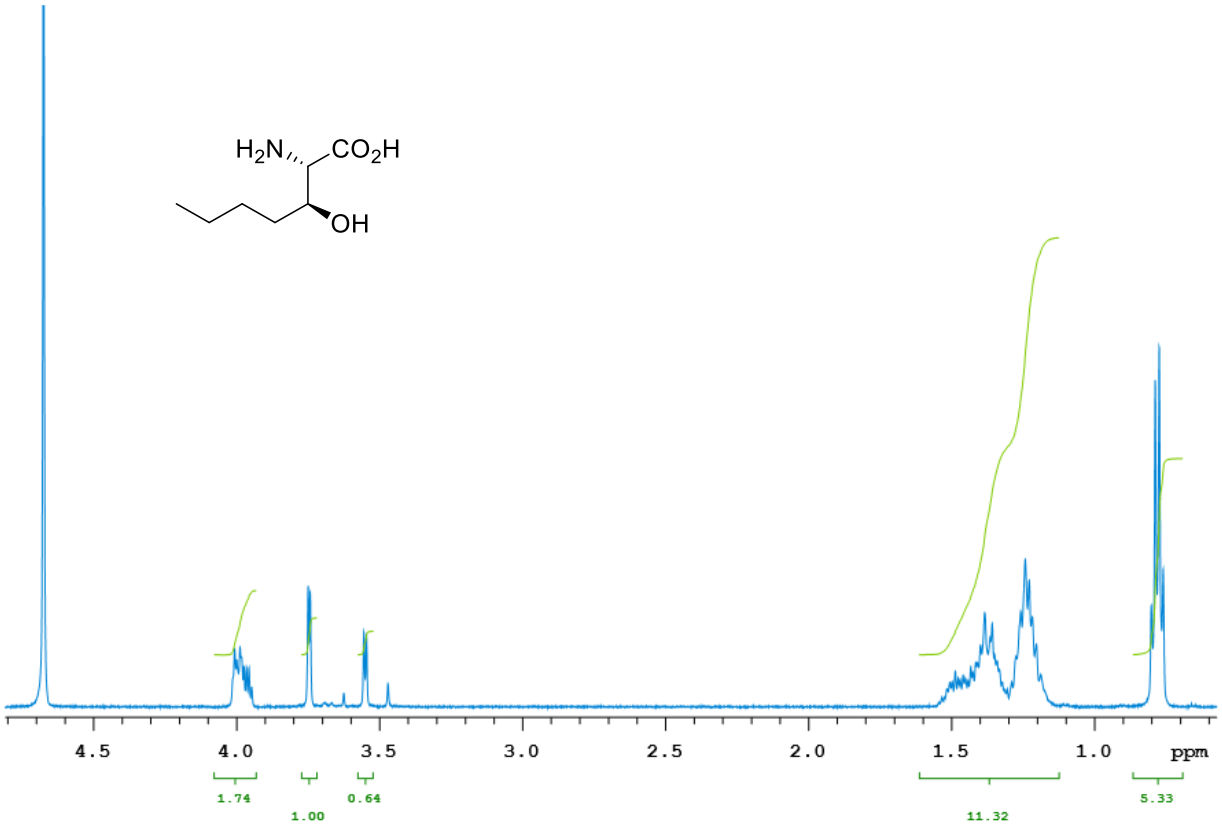

(*a*)

Figure A-2. NMR spectra of (2*S*,3*S*)-2-amino-3-hydroxyheptanoic acid

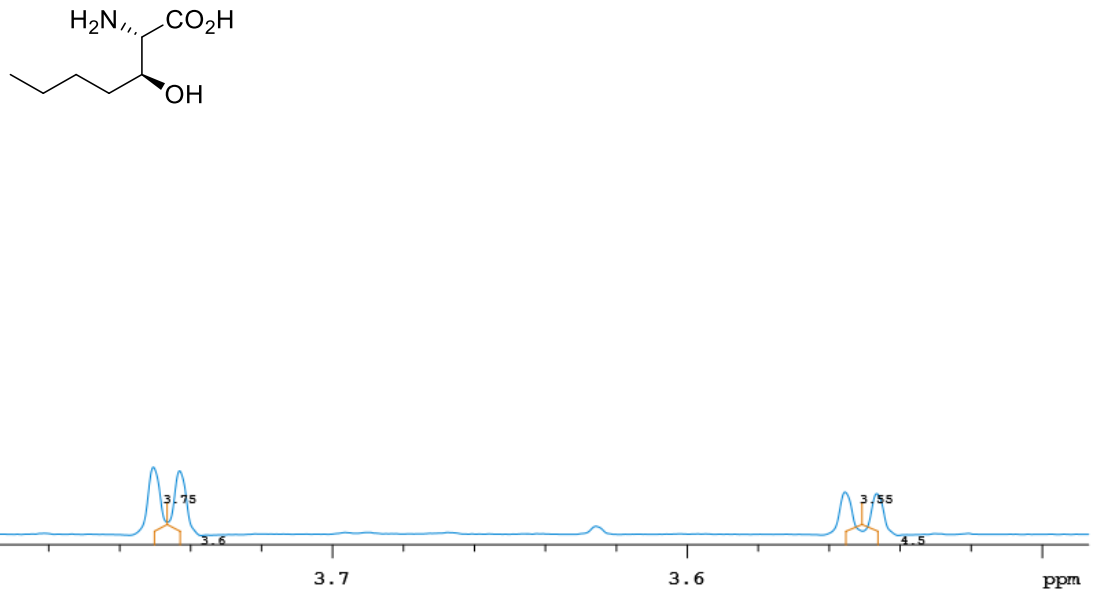

(*b*)

Figure A-2. Continued

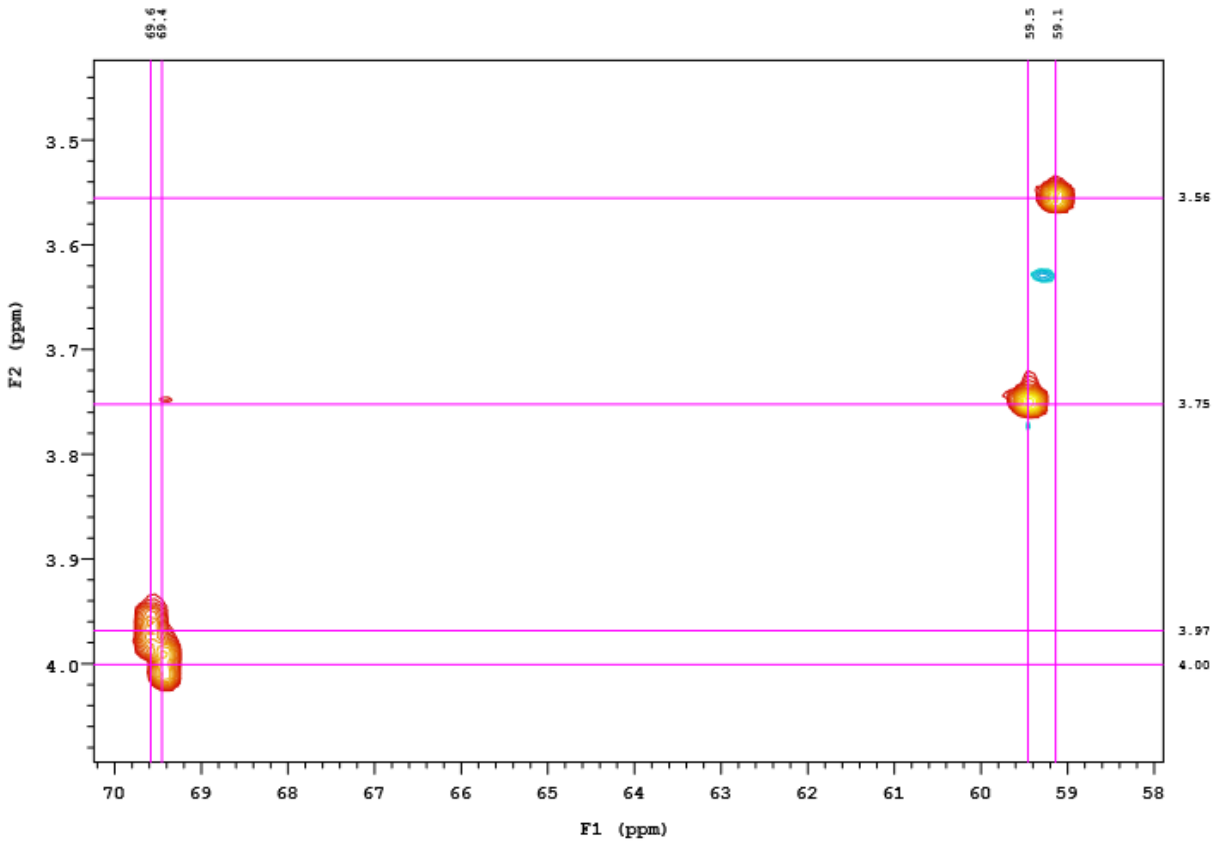

(*c*)

Figure A-2. Continued

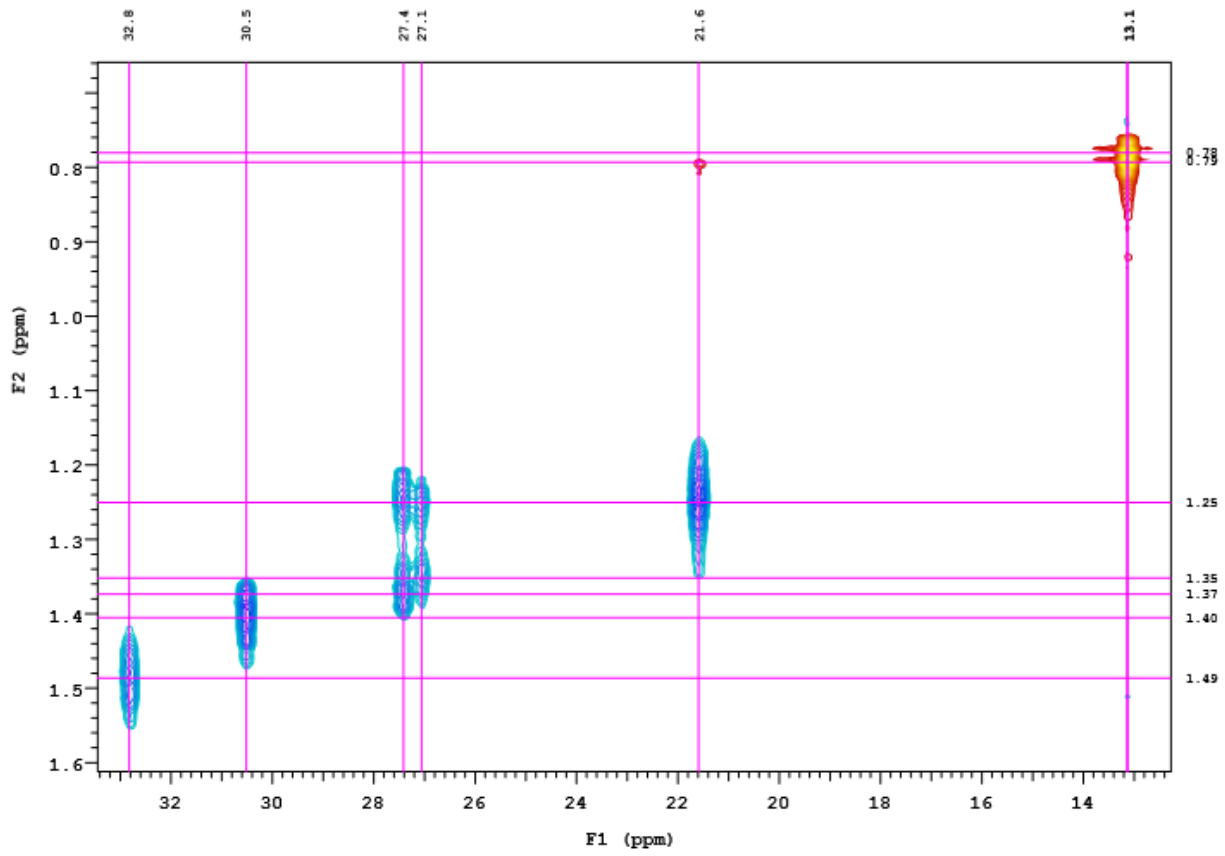

(*d*)

Figure A-2. Continued

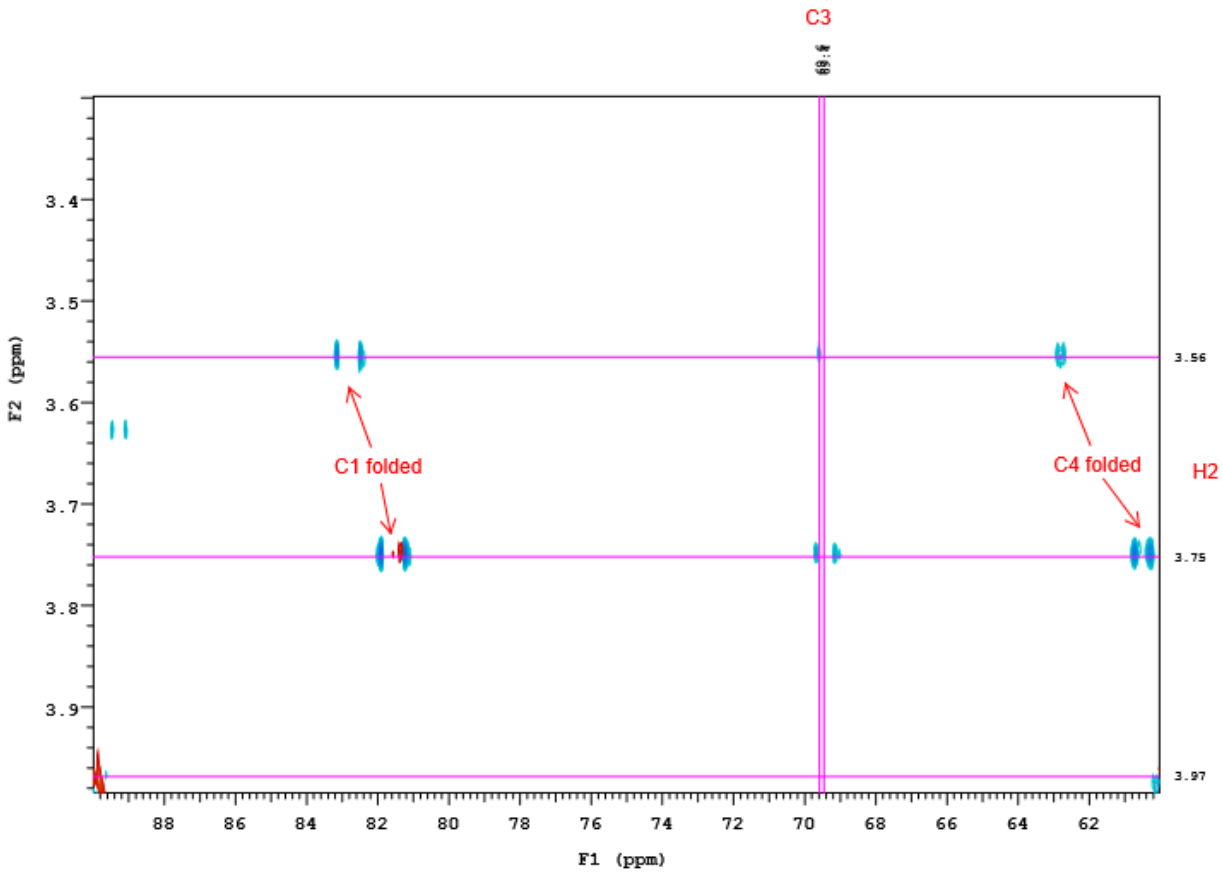

(*e*)

Figure A-2. Continued

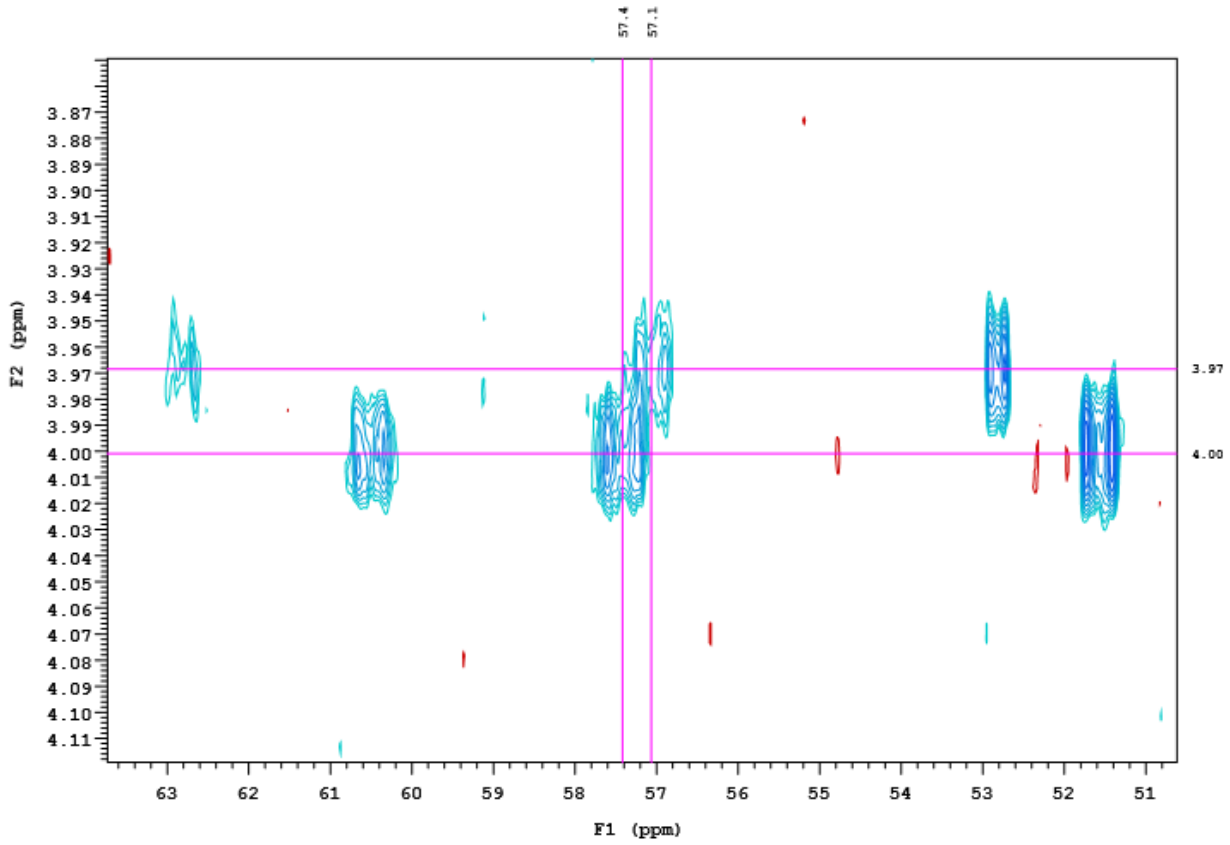

(*f*)

Figure A-2. Continued

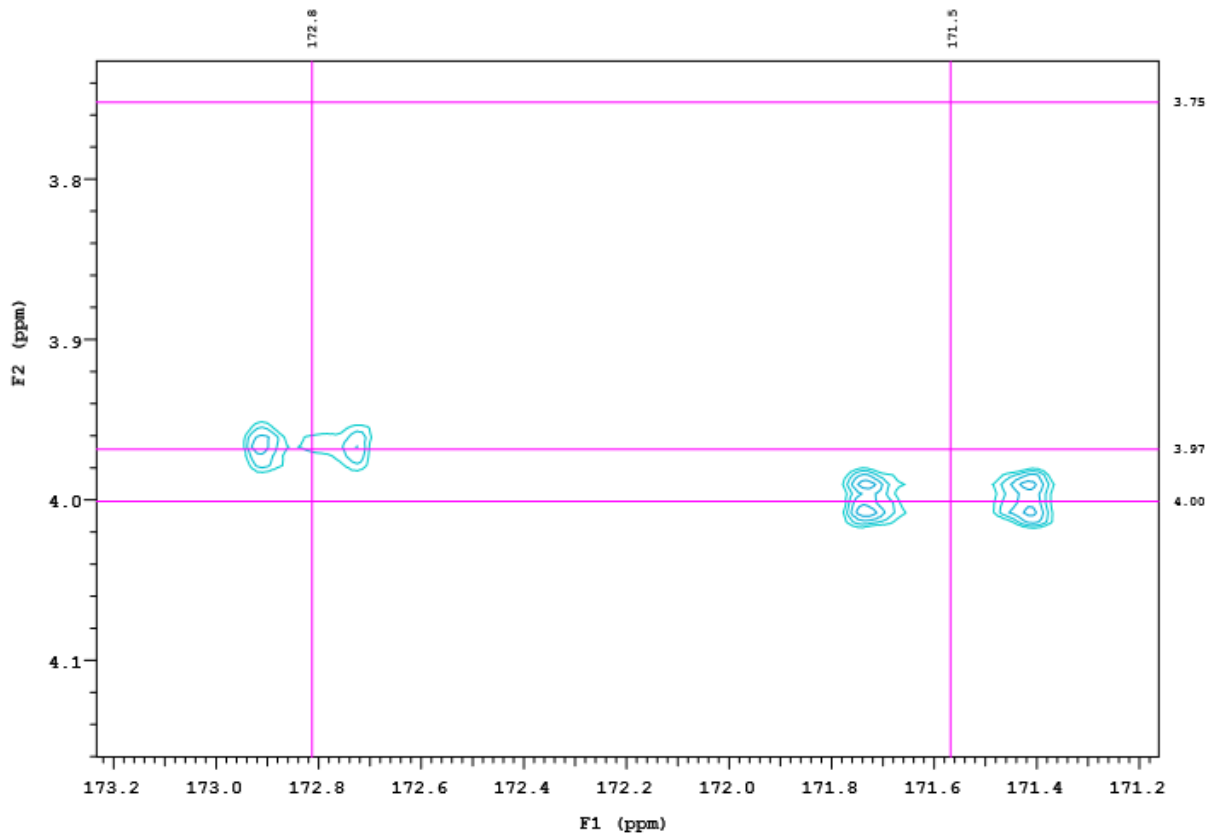

(*g*)

Figure A-2. Continued

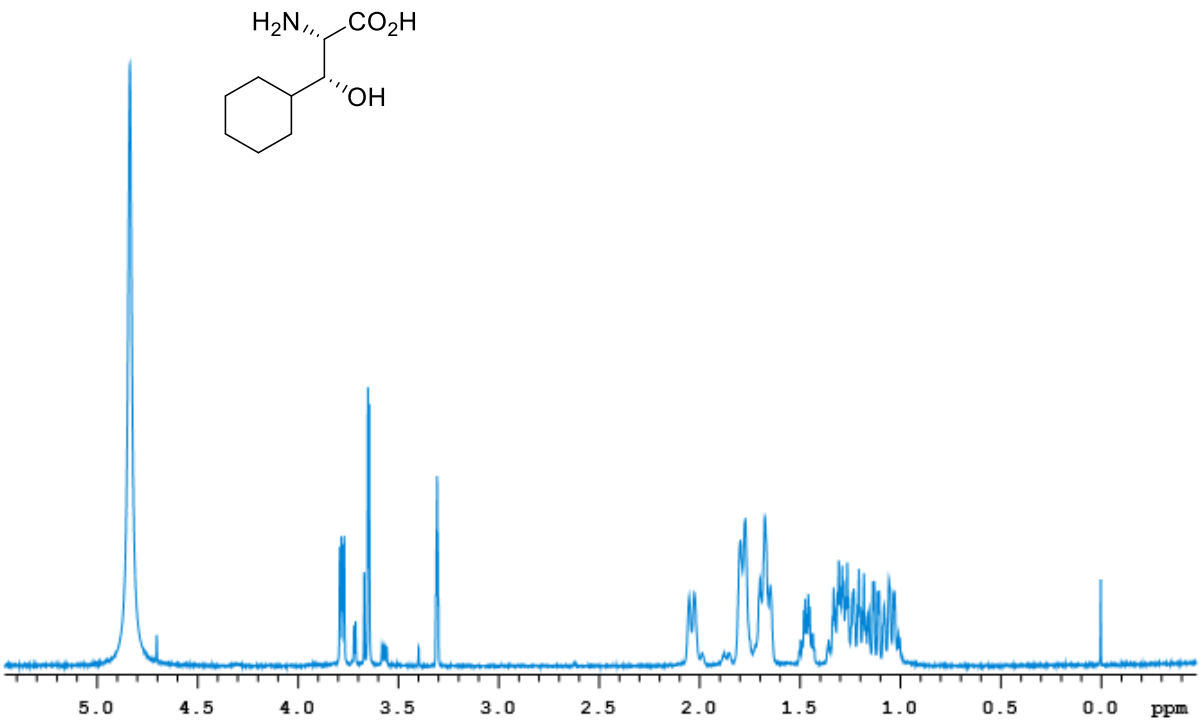

(*a*)

Figure A-3. NMR spectra of (2*S*,3*R*)-2-amino-3-hydroxycyclohexanepropanoic acid

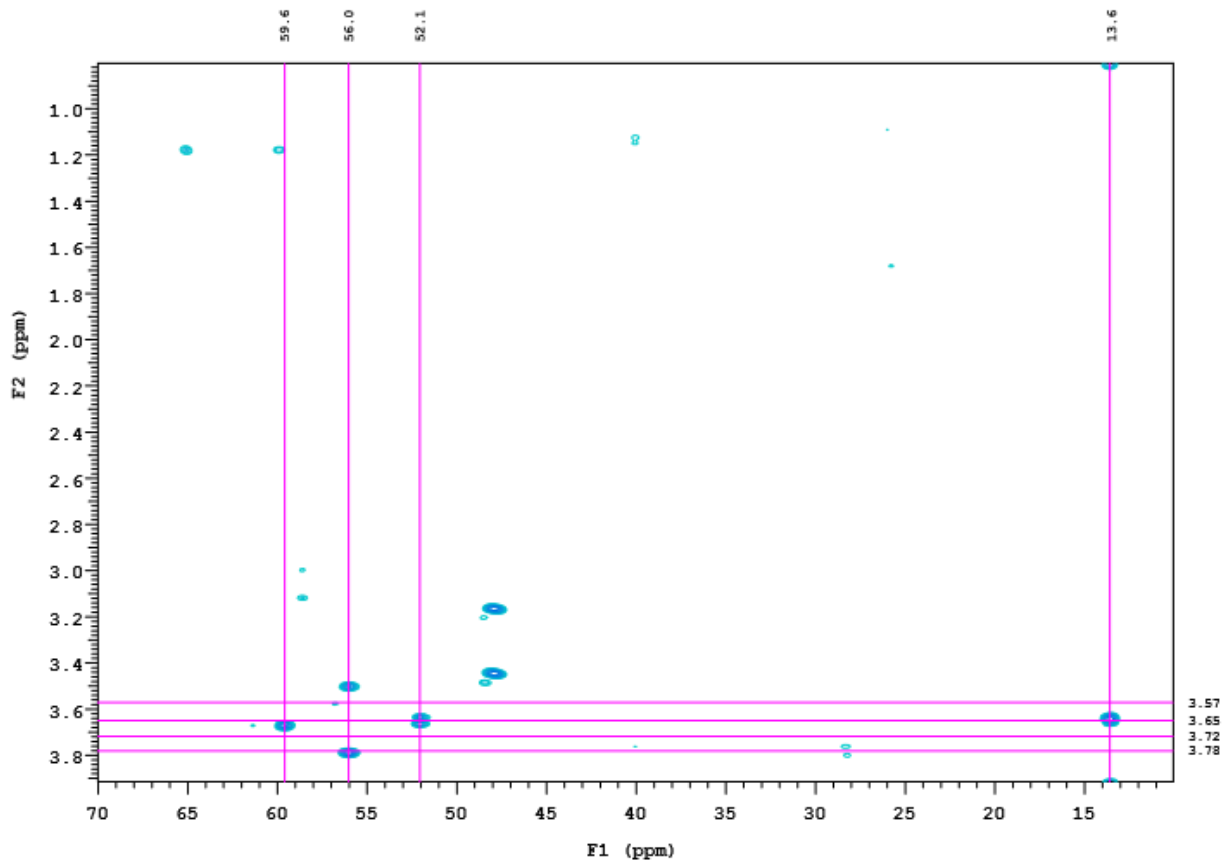

(*b*)

Figure A-3. Continued

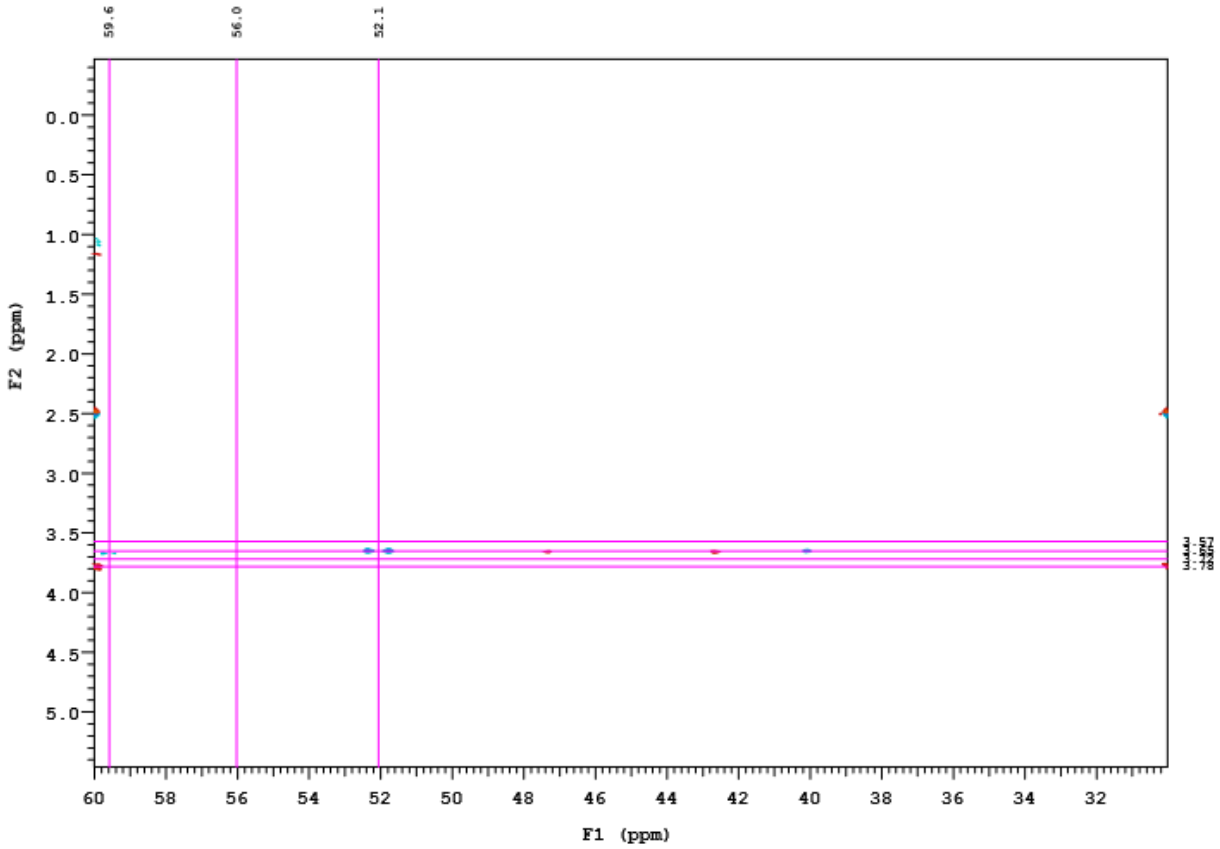

(*c*)

Figure A-3. Continued

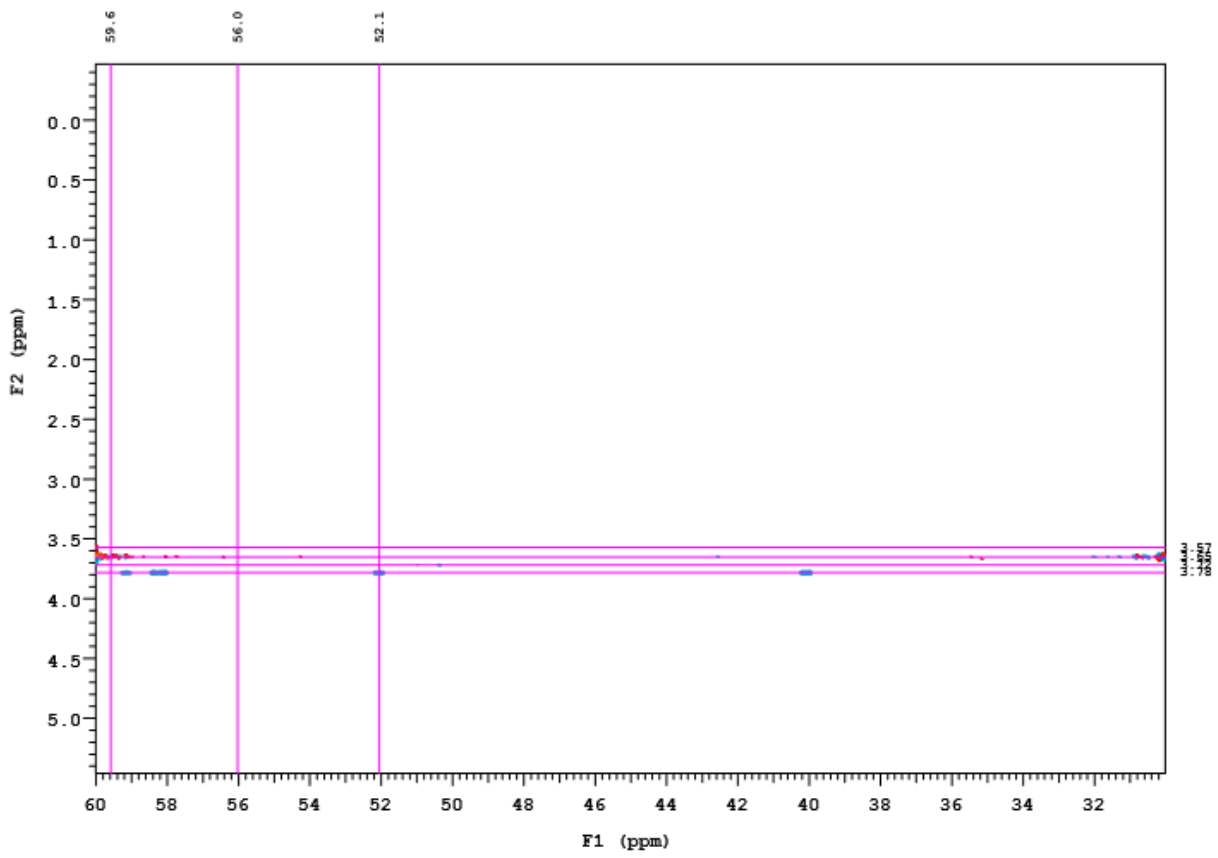

(*d*)

Figure A-3. Continued

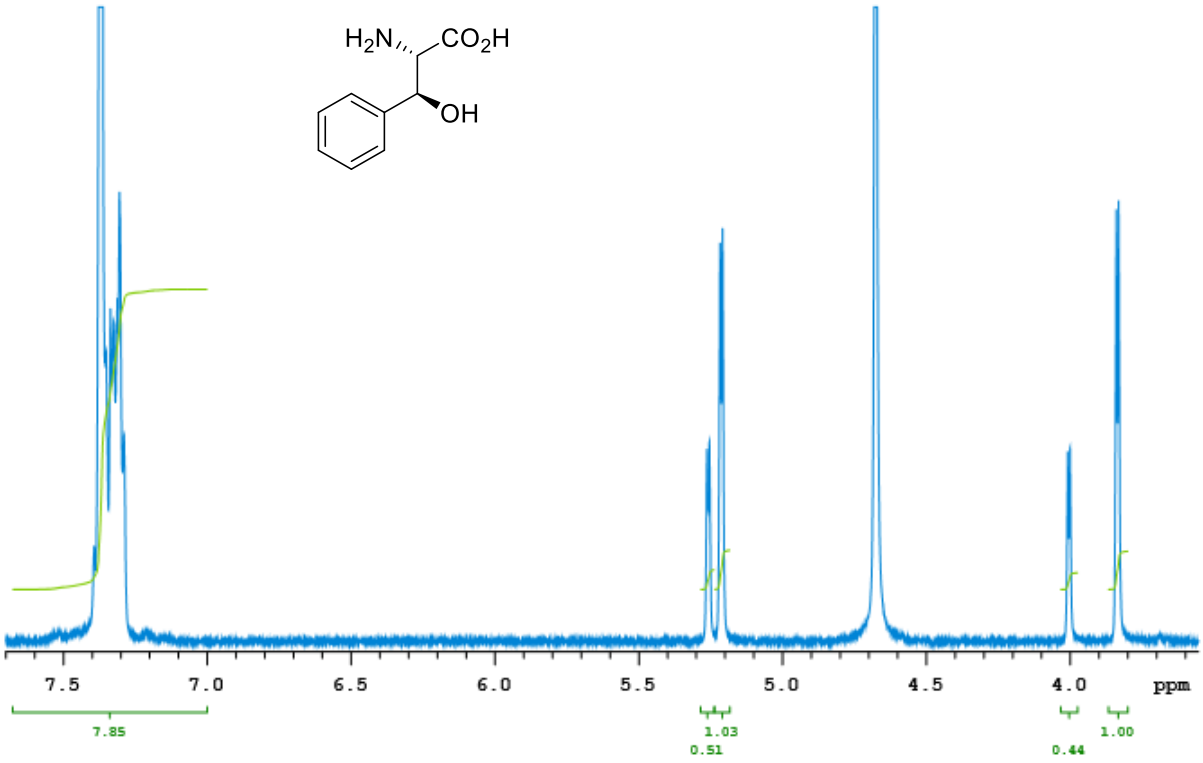

(*a*)

Figure A-4. NMR spectra of (2*S*,3*S*)-3-hydroxyphenylalanine

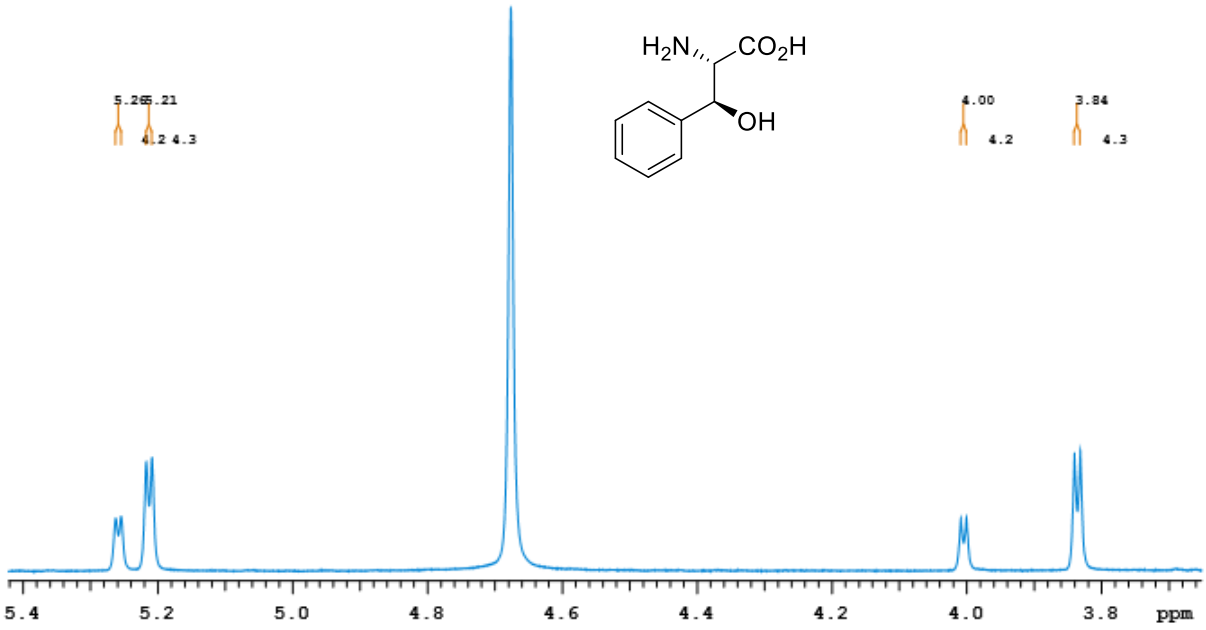

(*b*)

Figure A-4. Continued

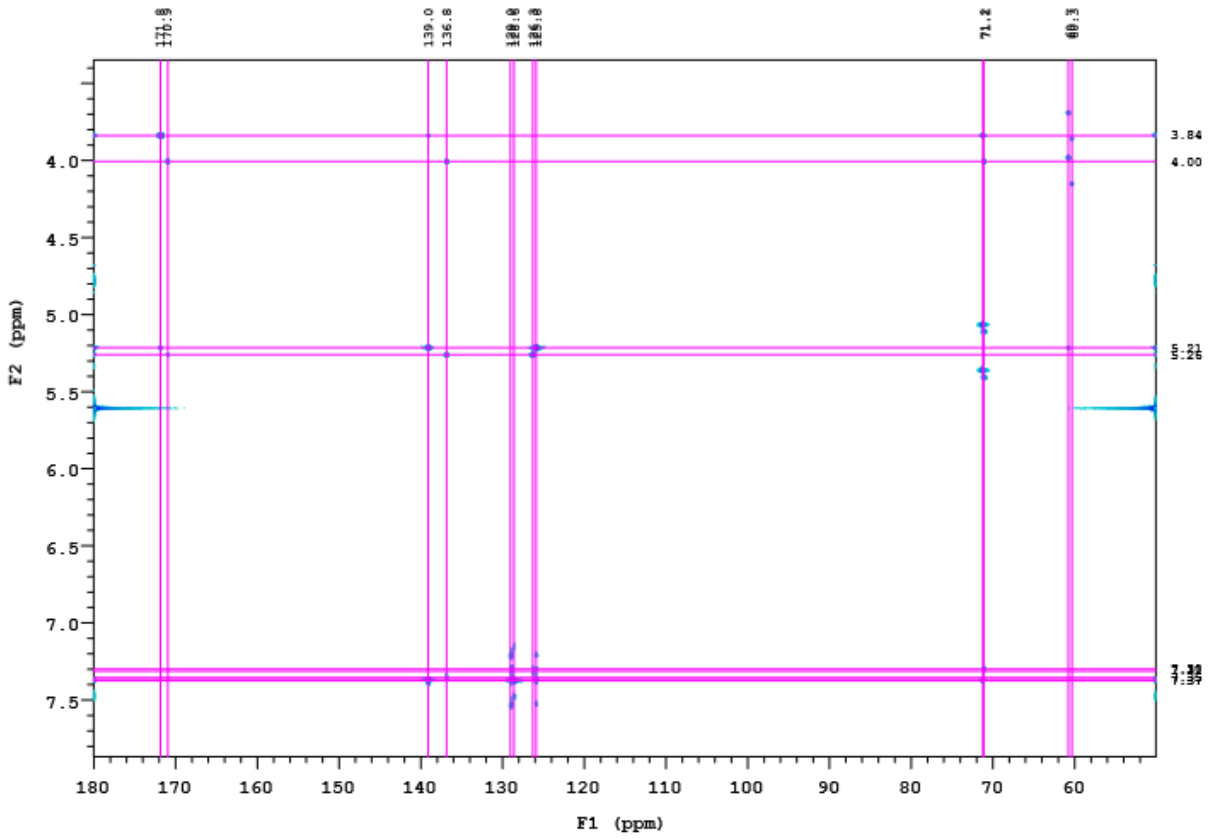

(*c*)

Figure A-4. Continued

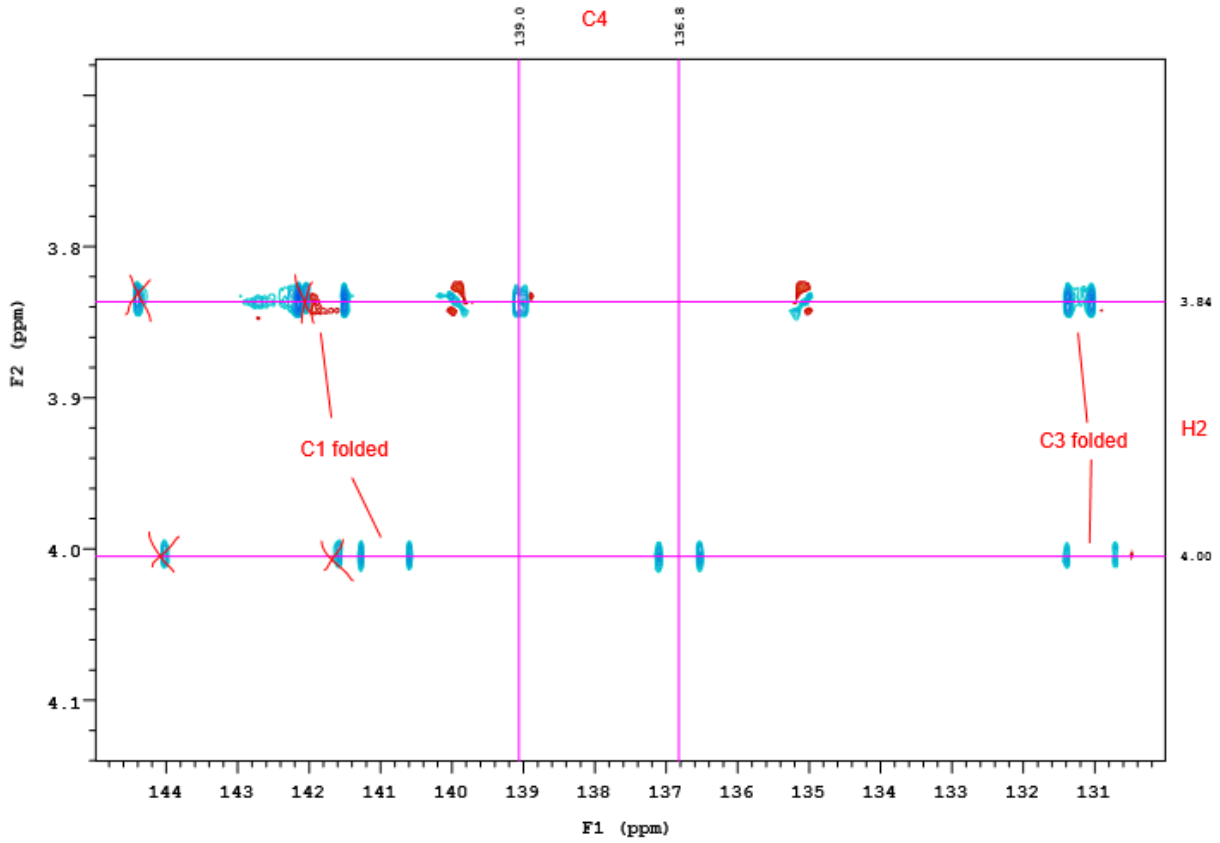

(*d*)

Figure A-4. Continued

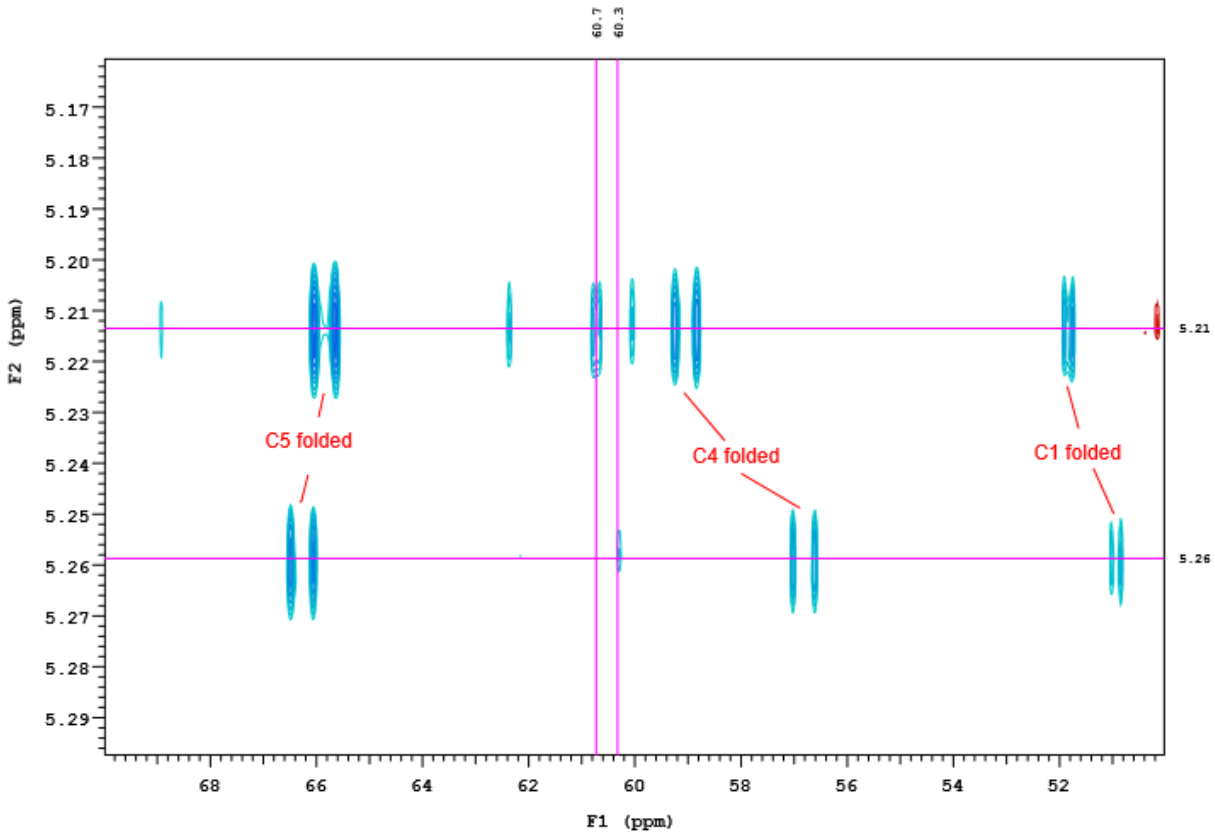

(*e*)

Figure A-4. Continued

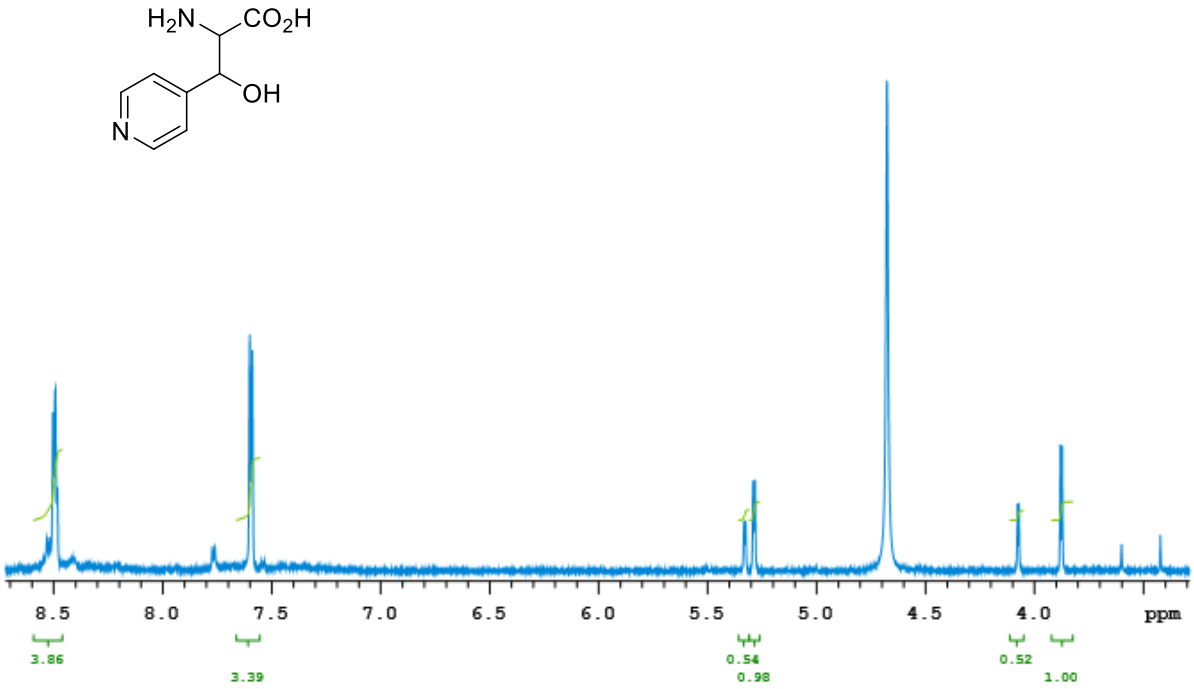

(*a*)

Figure A-5. NMR spectra of 2-amino-3-hydroxy-4-pyridinepropanoic acid

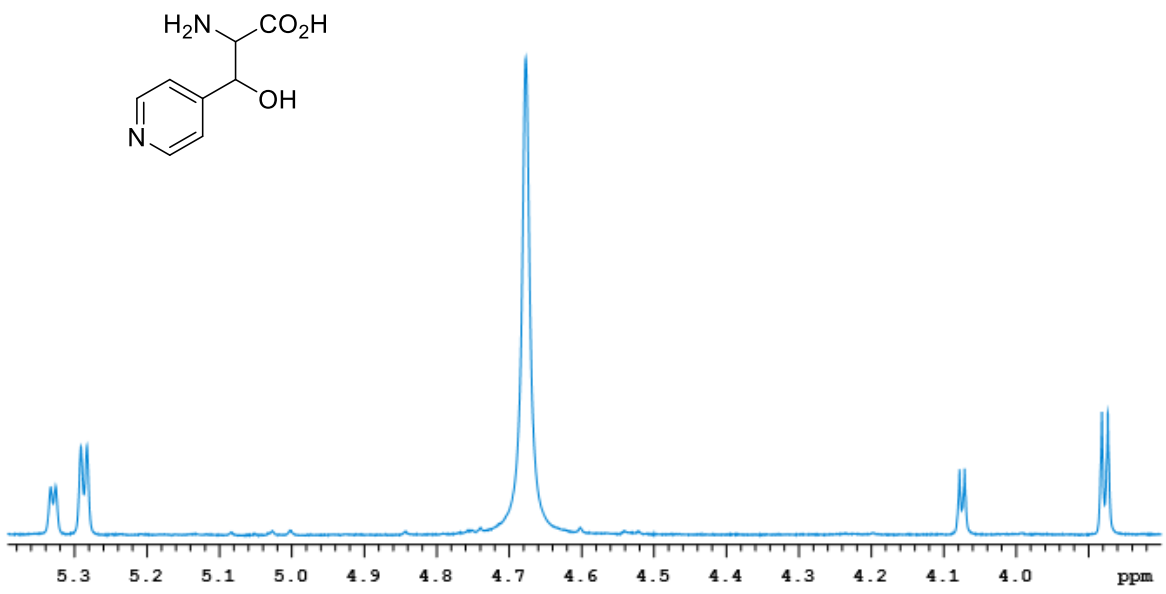

(*b*)

Figure A-5. Continued

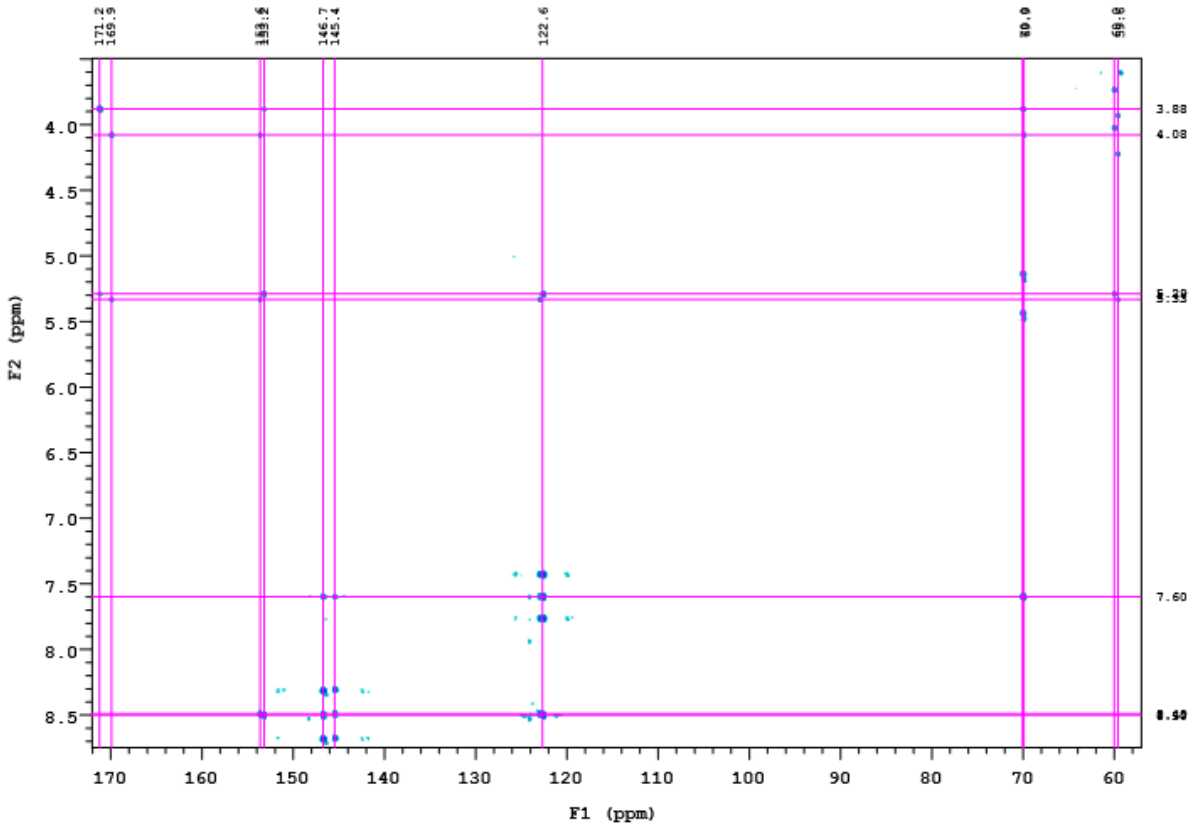

(*c*)

Figure A-5. Continued

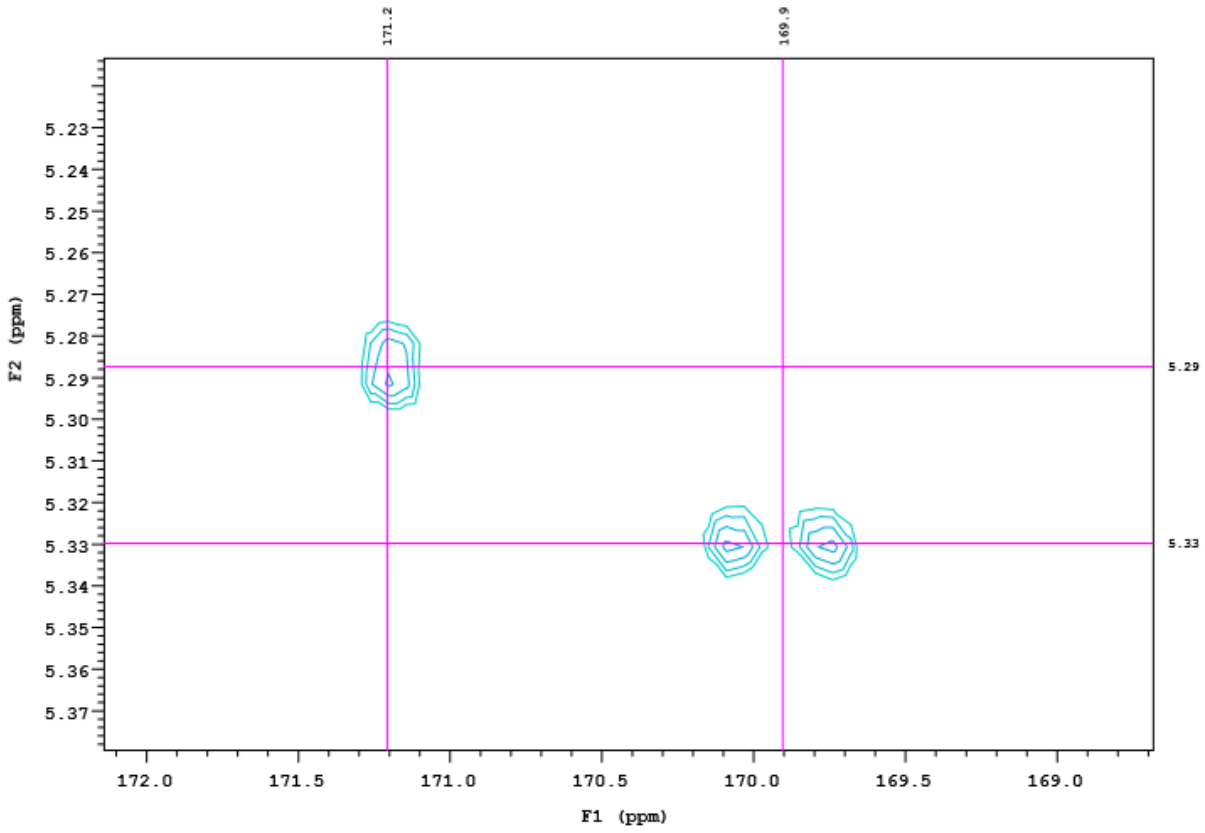

(*d*)

Figure A-5. Continued

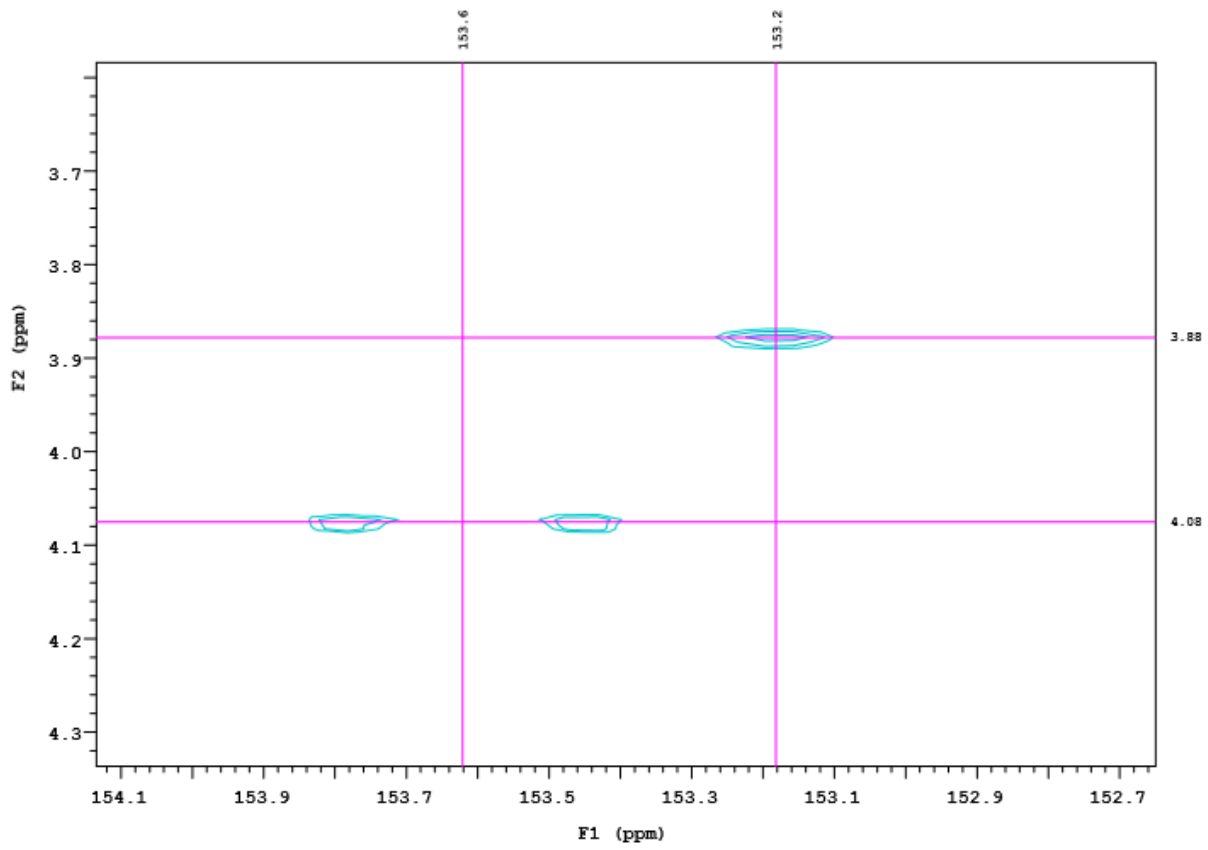

(*e*)

Figure A-5. Continued

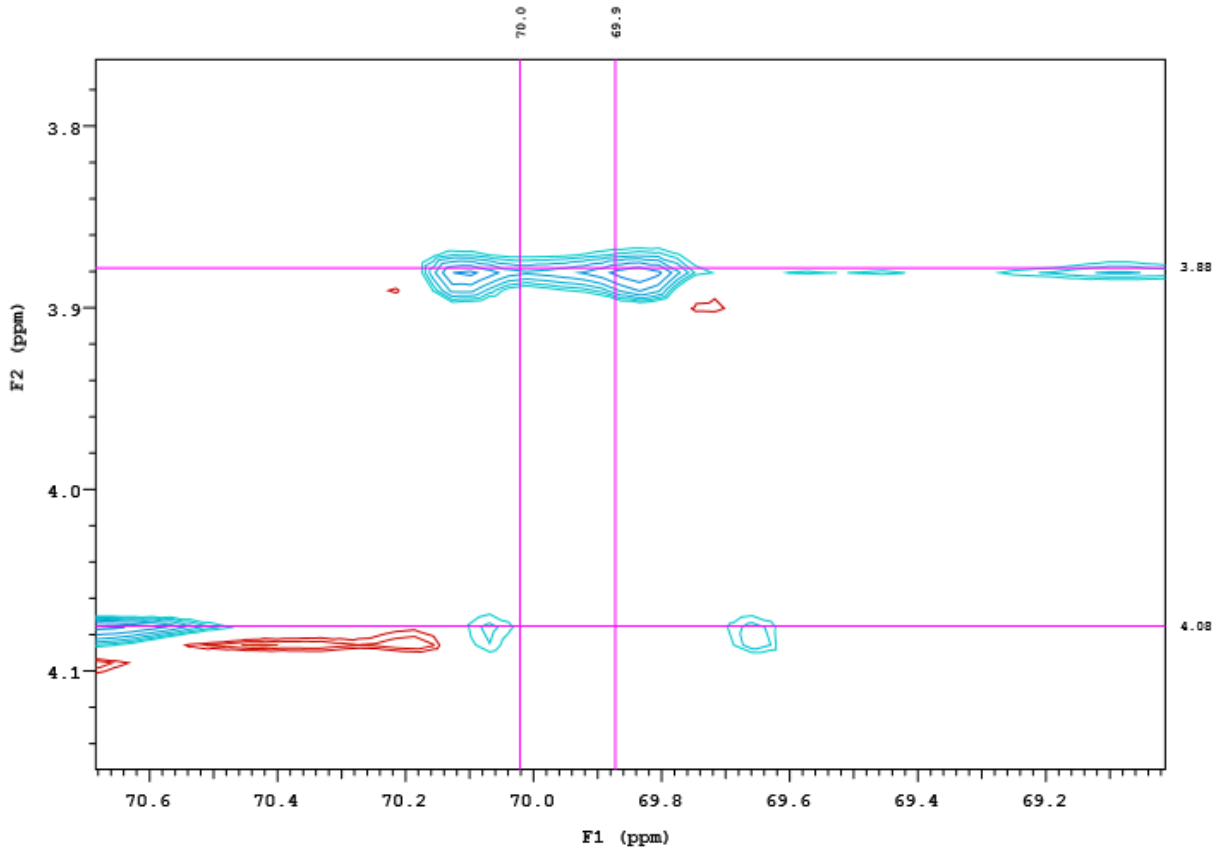

(*f*)

Figure A-5. Continued

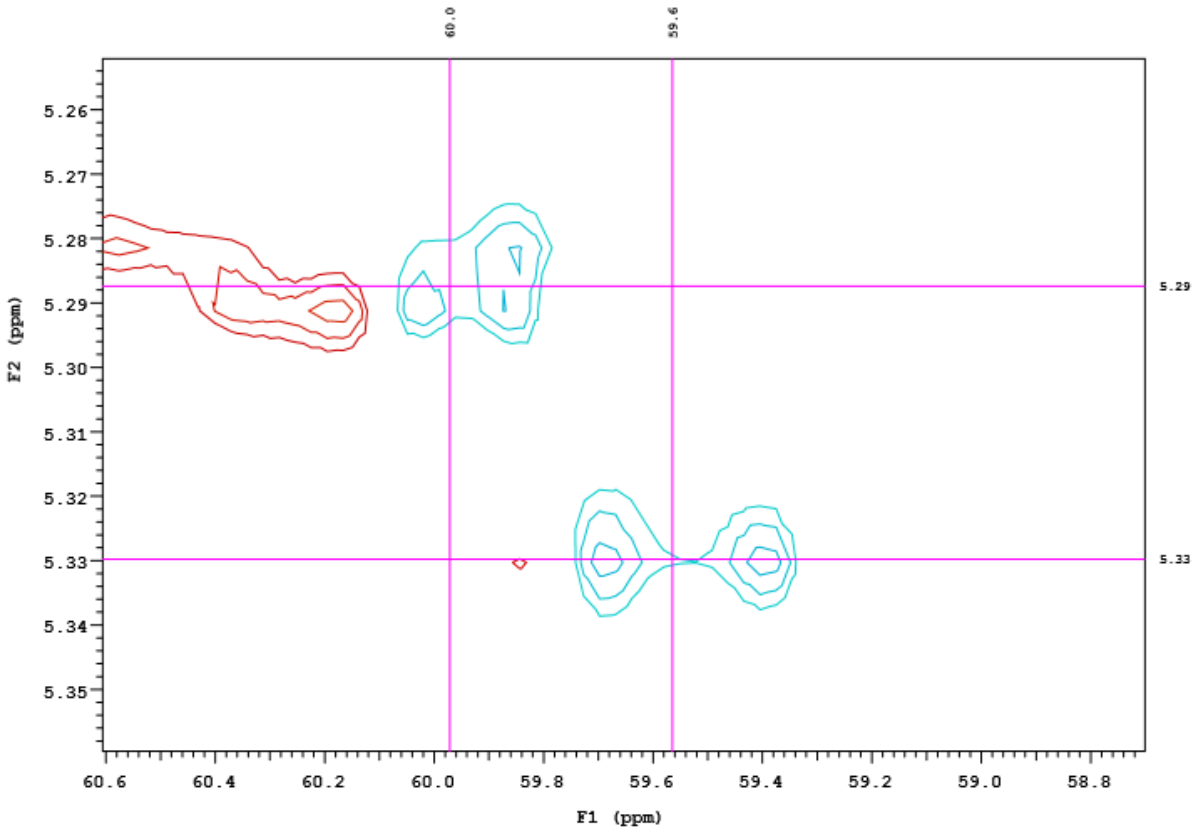

(*g*)

Figure A-5. Continued

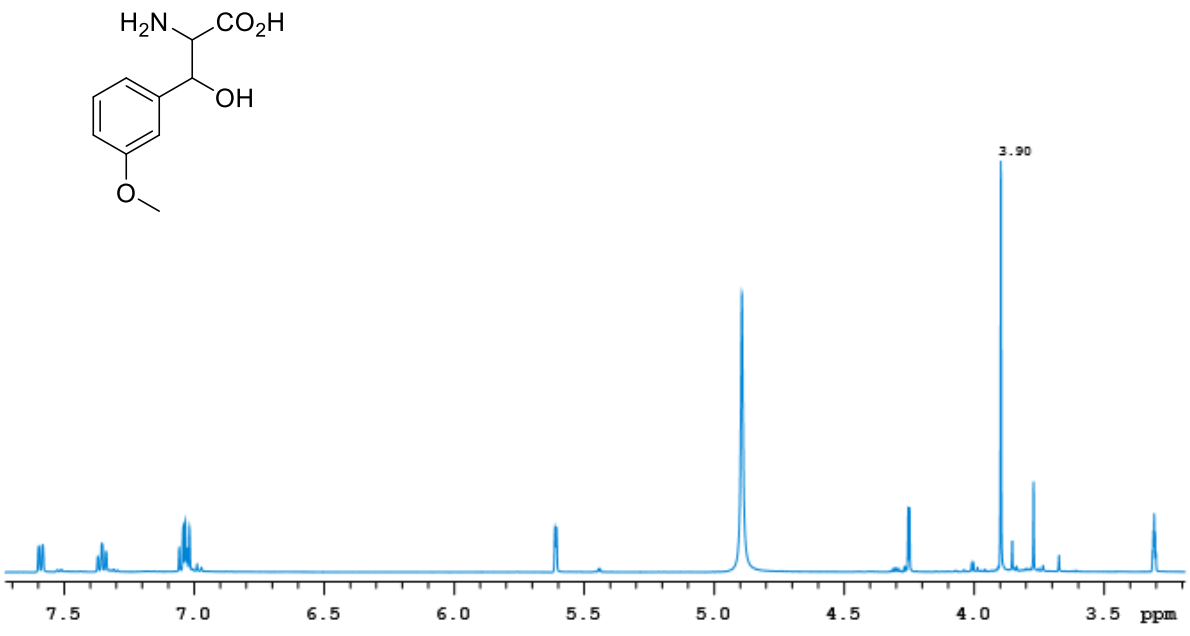

(*a*)

Figure A-6. NMR spectra of 3-hydroxy-2-methoxy-phenylalanine

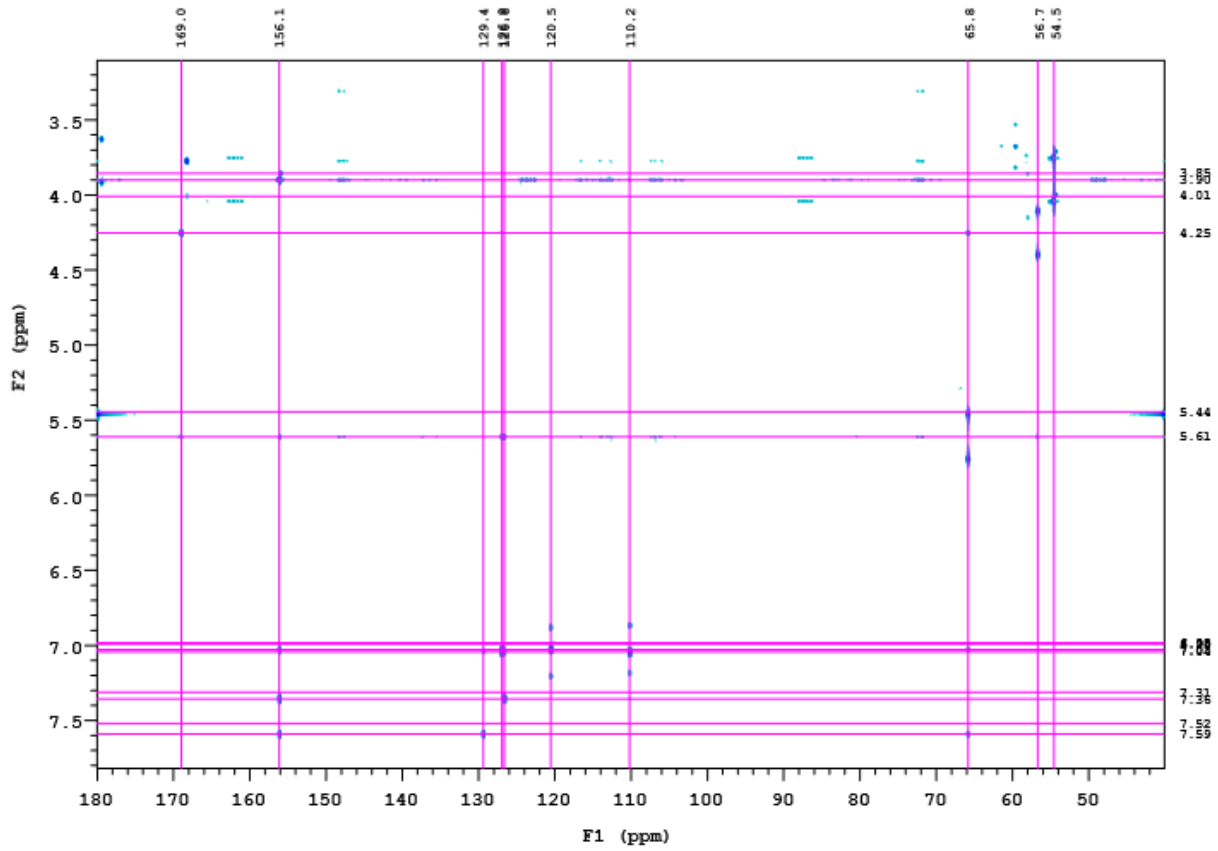

(*b*)

Figure A-6. Continued

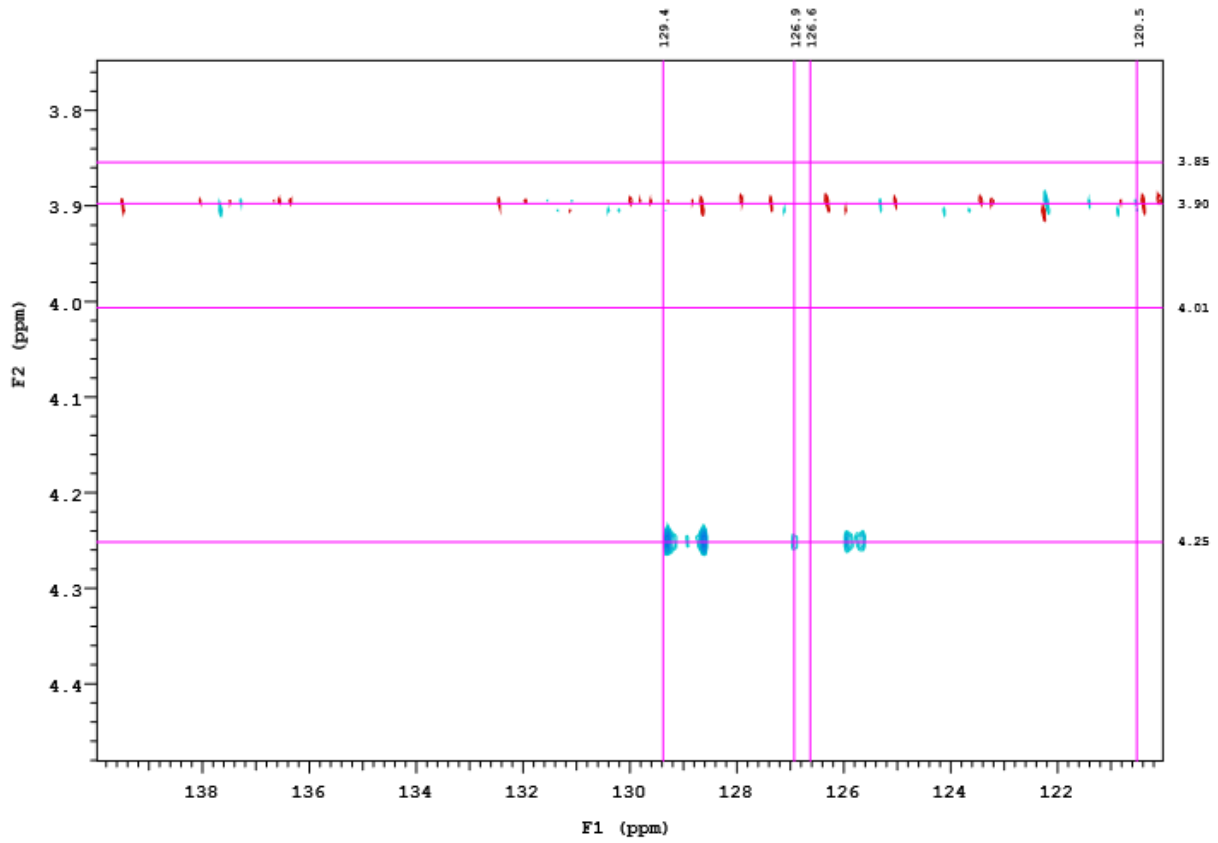

(*c*)

Figure A-6. Continued

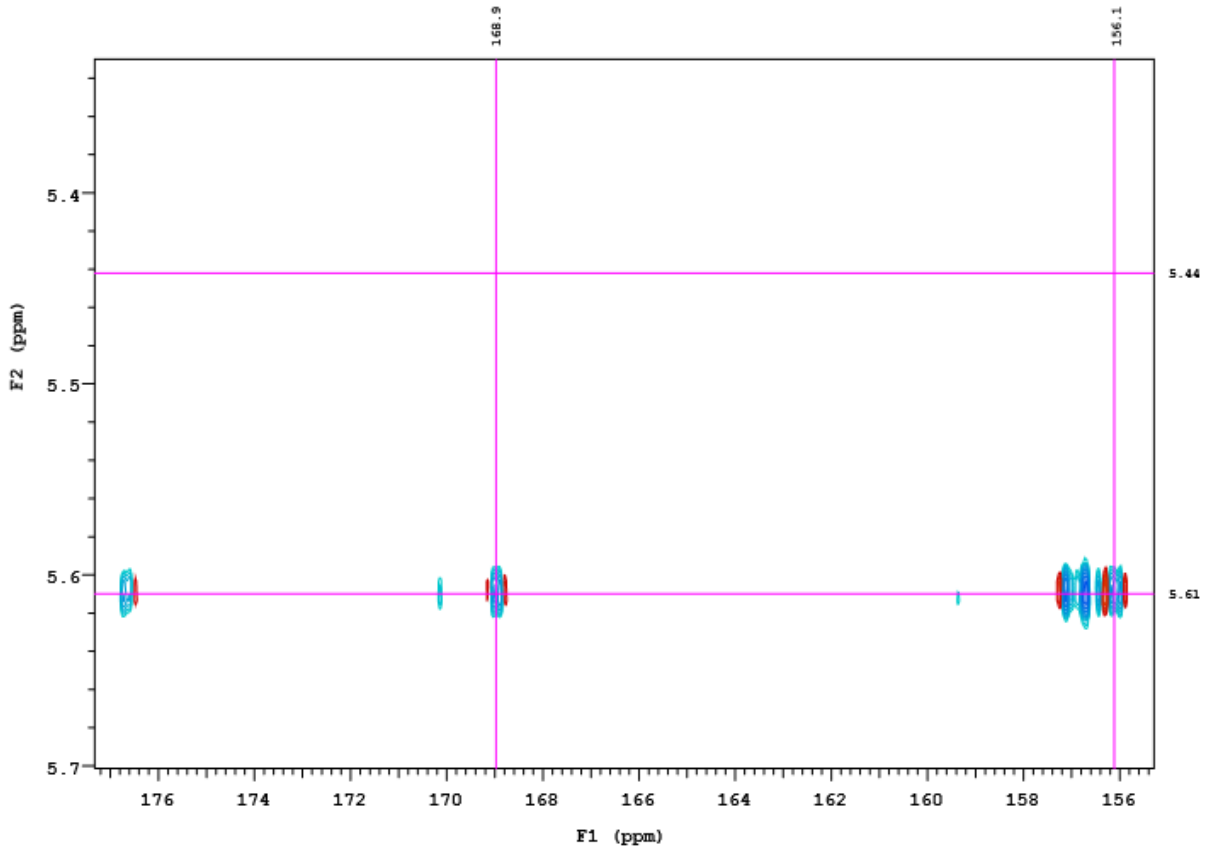

(*d*)

Figure A-6. Continued

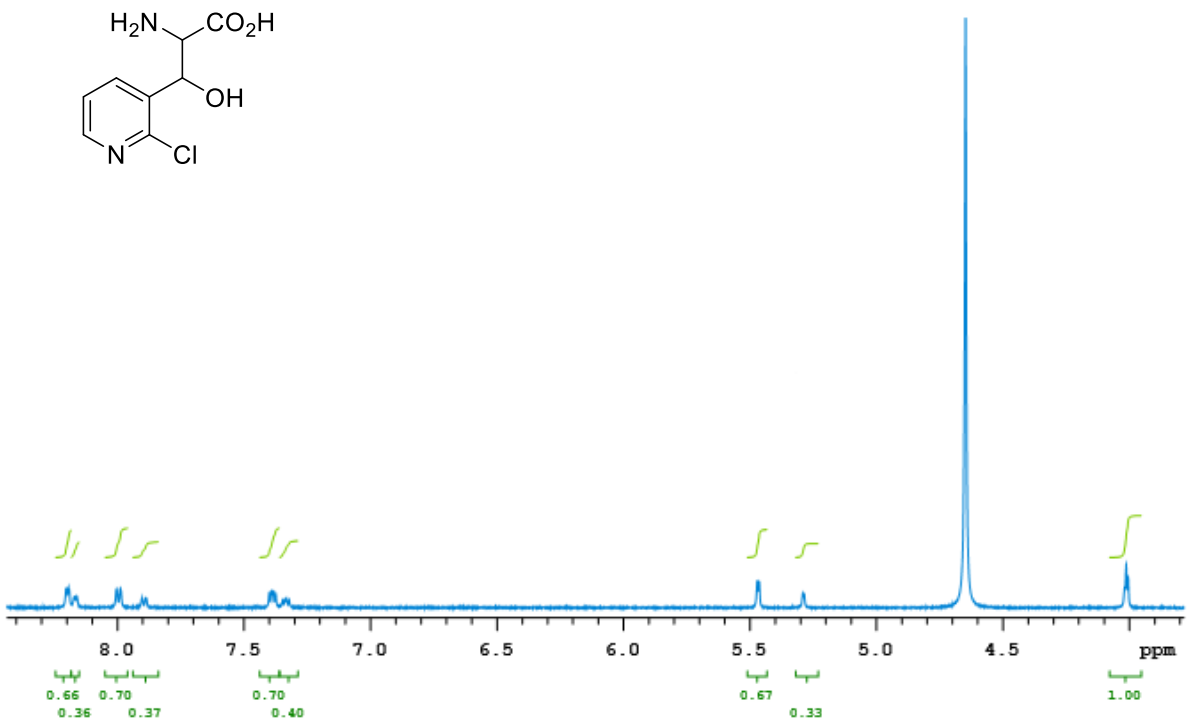

(*a*)

Figure A-7. NMR spectra of 2-amino-3-(2-chloro-3-pyridine)-3-hydroxypropanoic acid

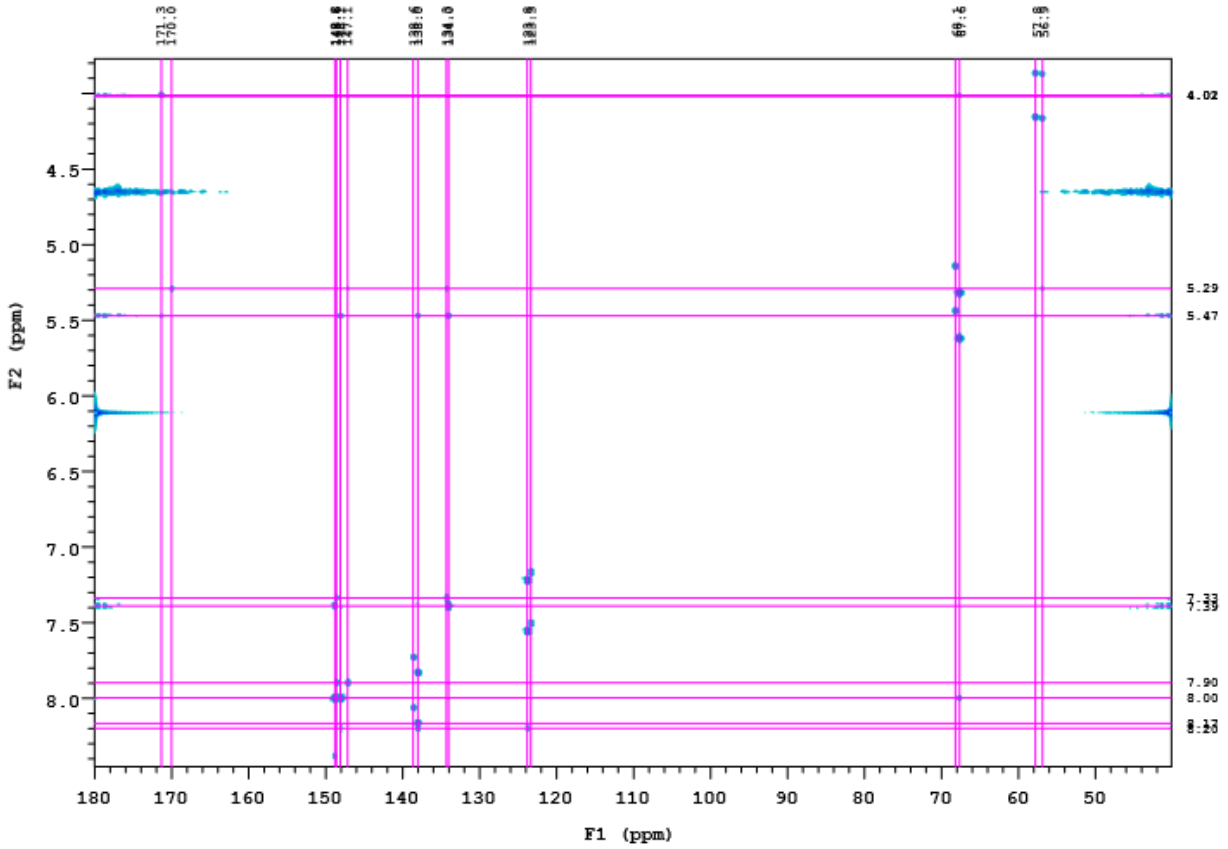

(*b*)

Figure A-7. Continued

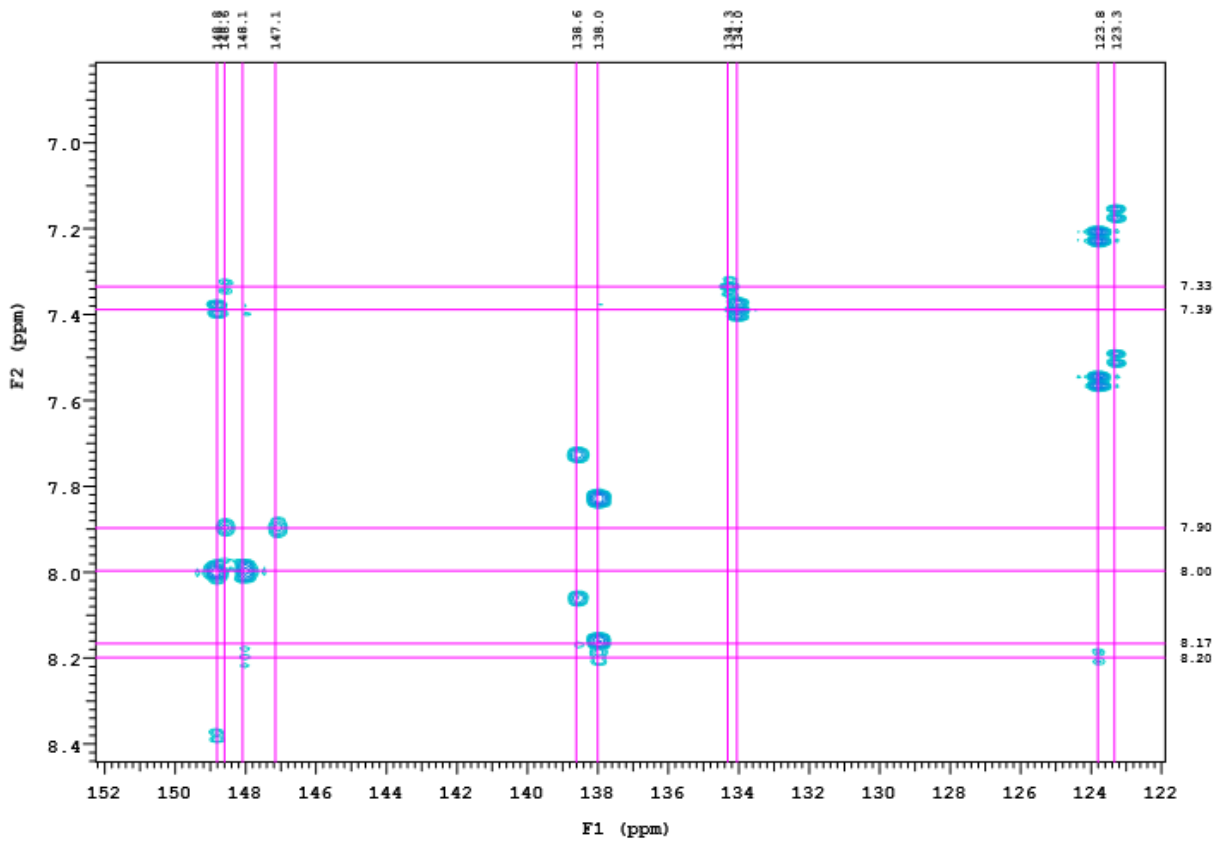

(*c*)

Figure A-7. Continued

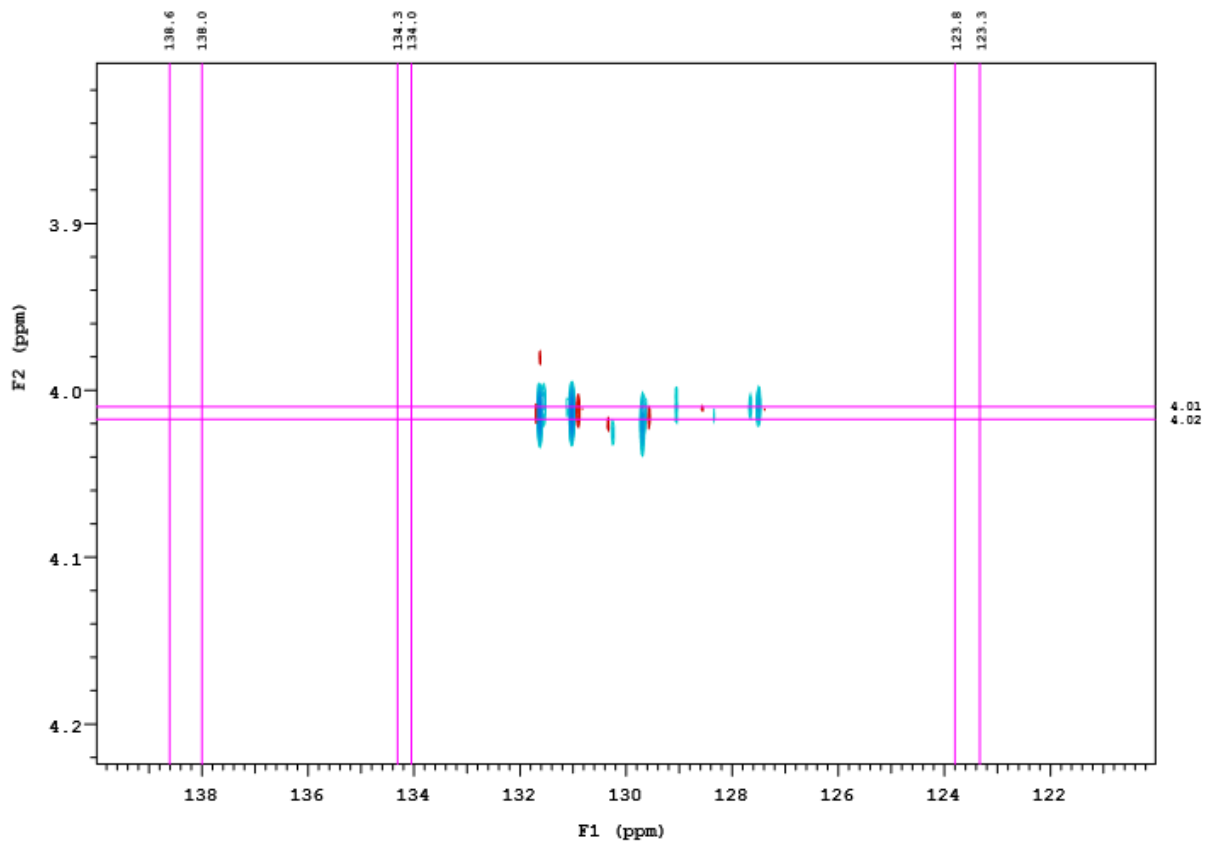

(*d*)

Figure A-7. Continued

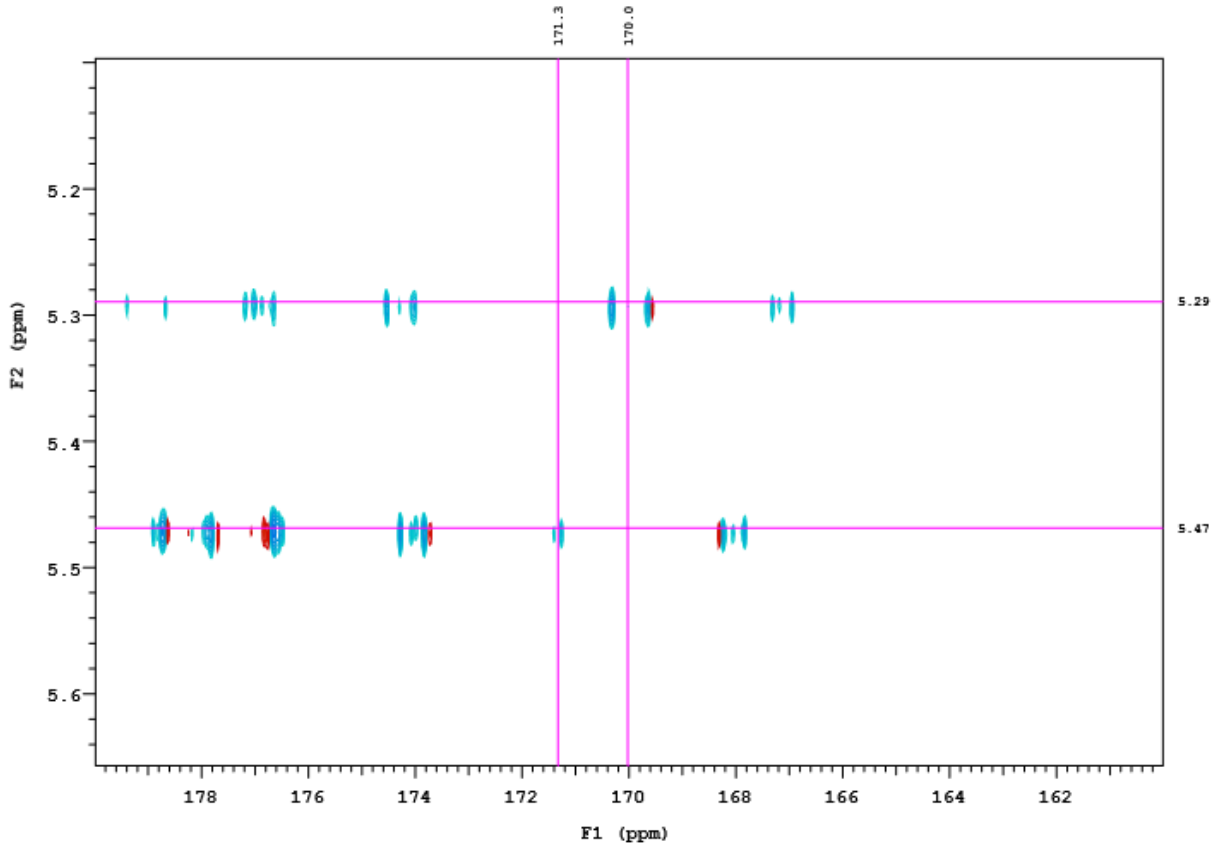

(*e*)

Figure A-7. Continued

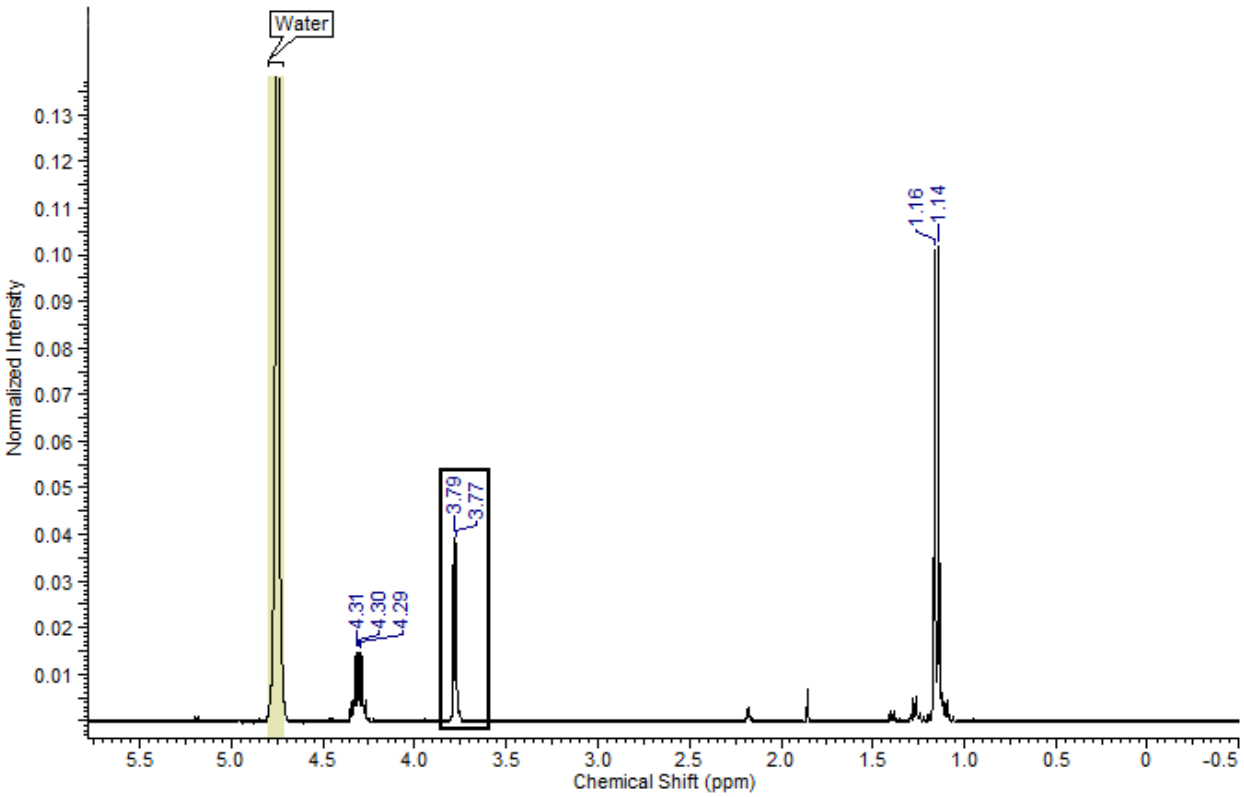

(*a*)

Figure A-8. ^{1}H NMR for thermodynamic reversibility of L-*allo*-threonine aldolase. Negative control at (*a*) zero hours and (*b*) 24 hours. L-allo-Thr and acetaldehyde-d4 in the presence of L-*allo*-TA at (*c*) zero hours, (*d*) 1 hour, (*e*) 3 hours, (*f*) 6 hours and (*g*) 24 hours.

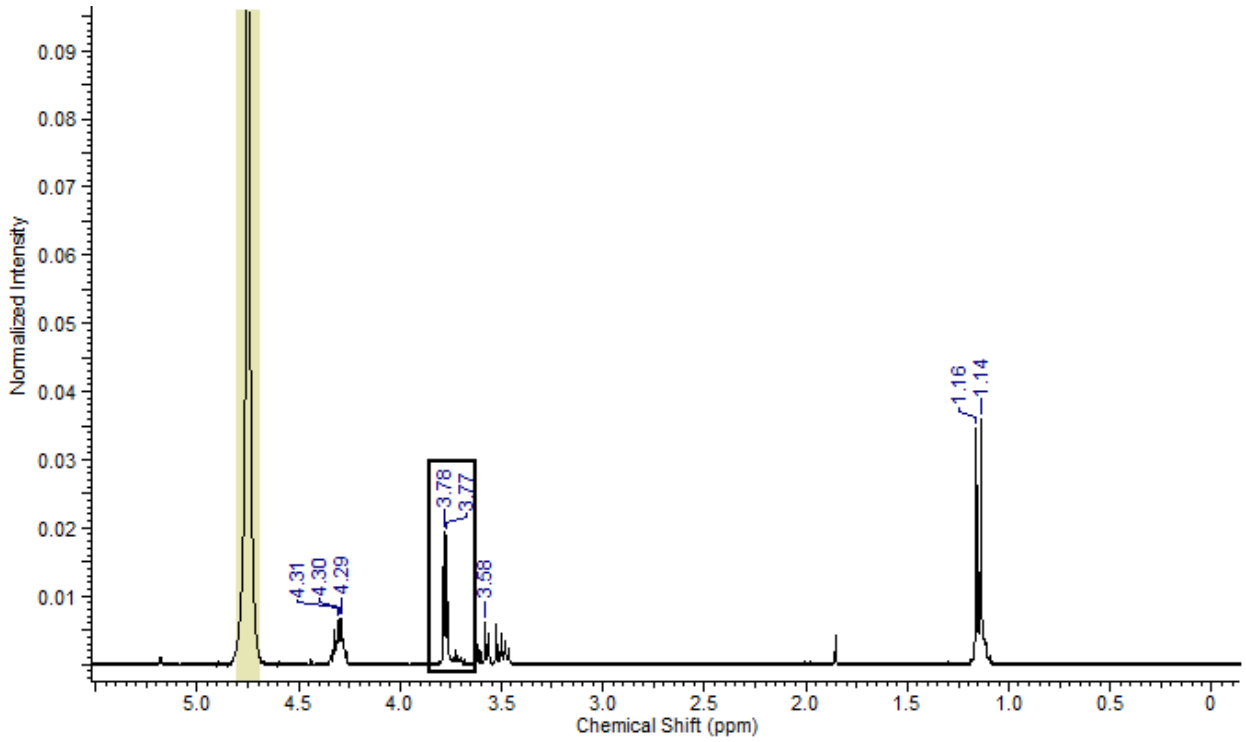

(*b*)

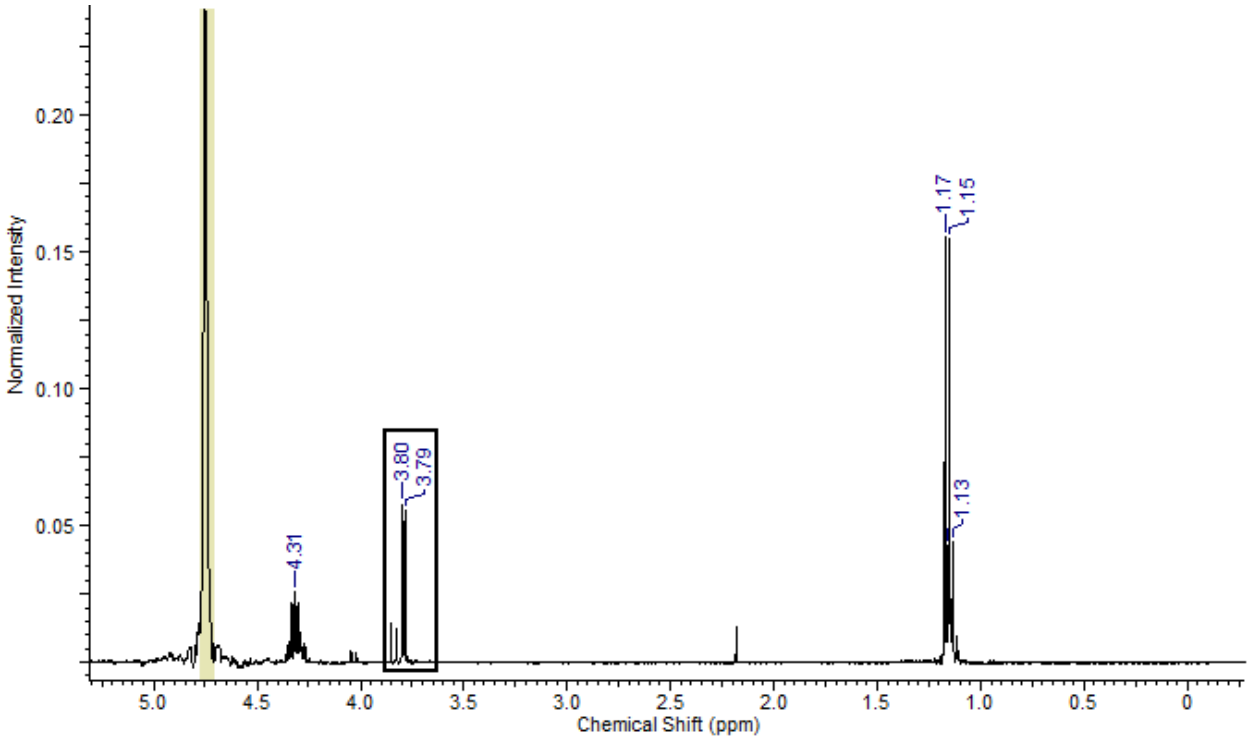

(*c*)

Figure A-8. Continued

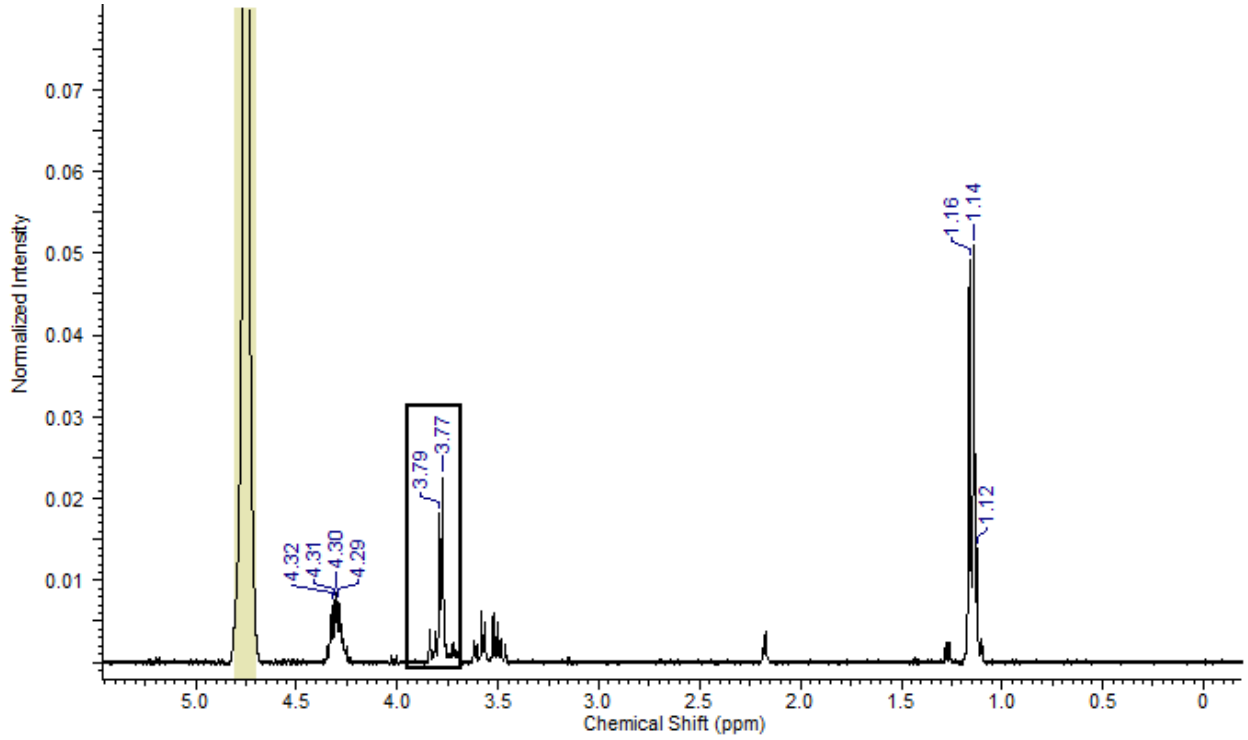

(*d*)

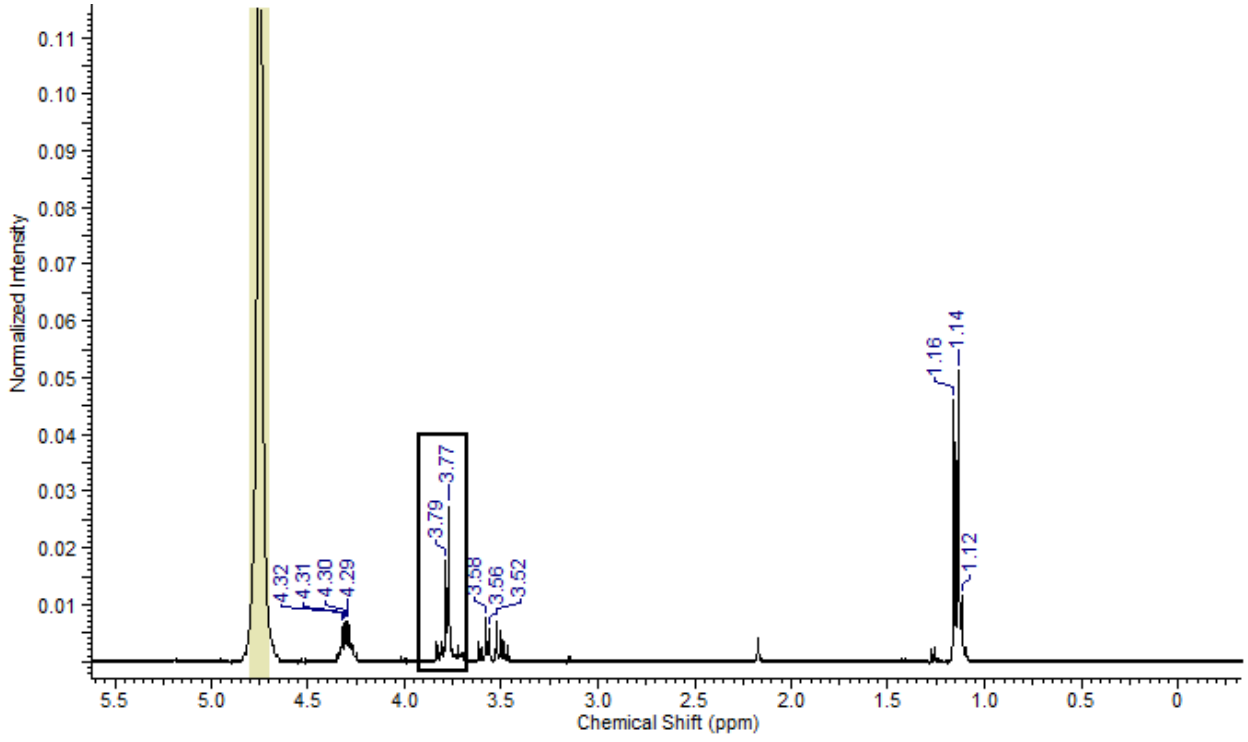

(*e*)

Figure A-8. Continued

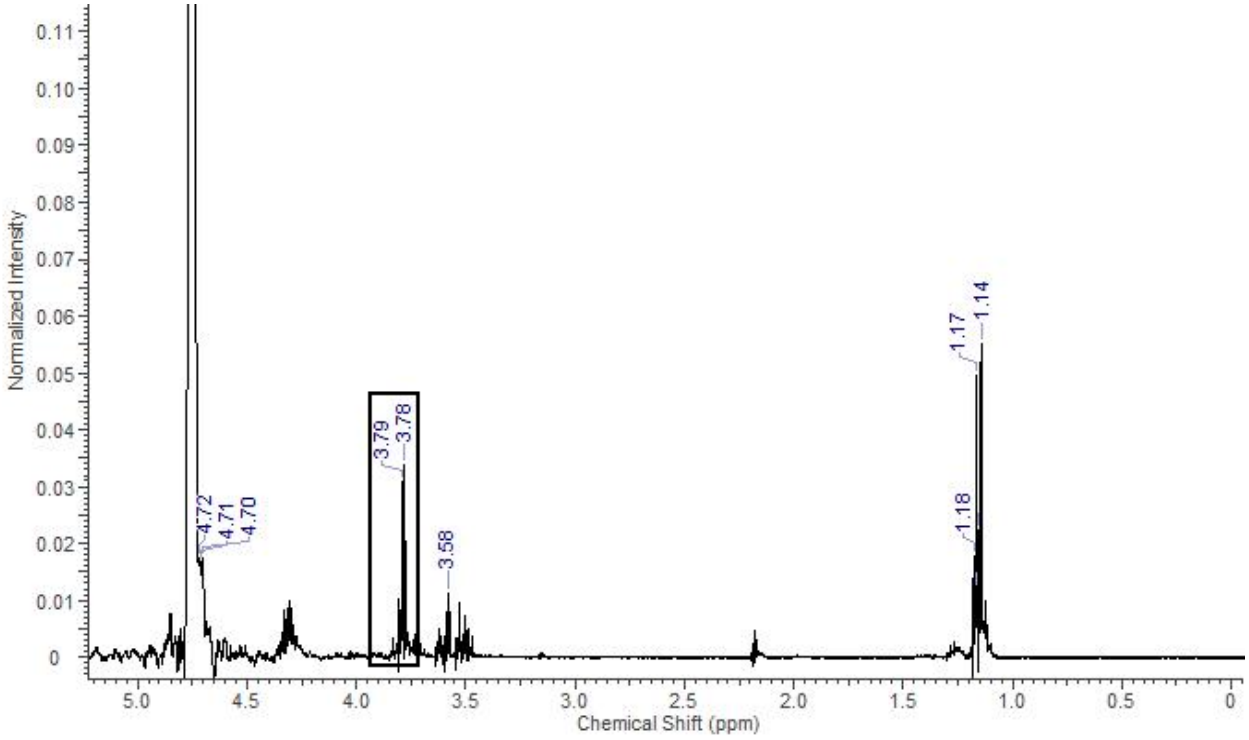

(*f*)

Figure A-8. Continued

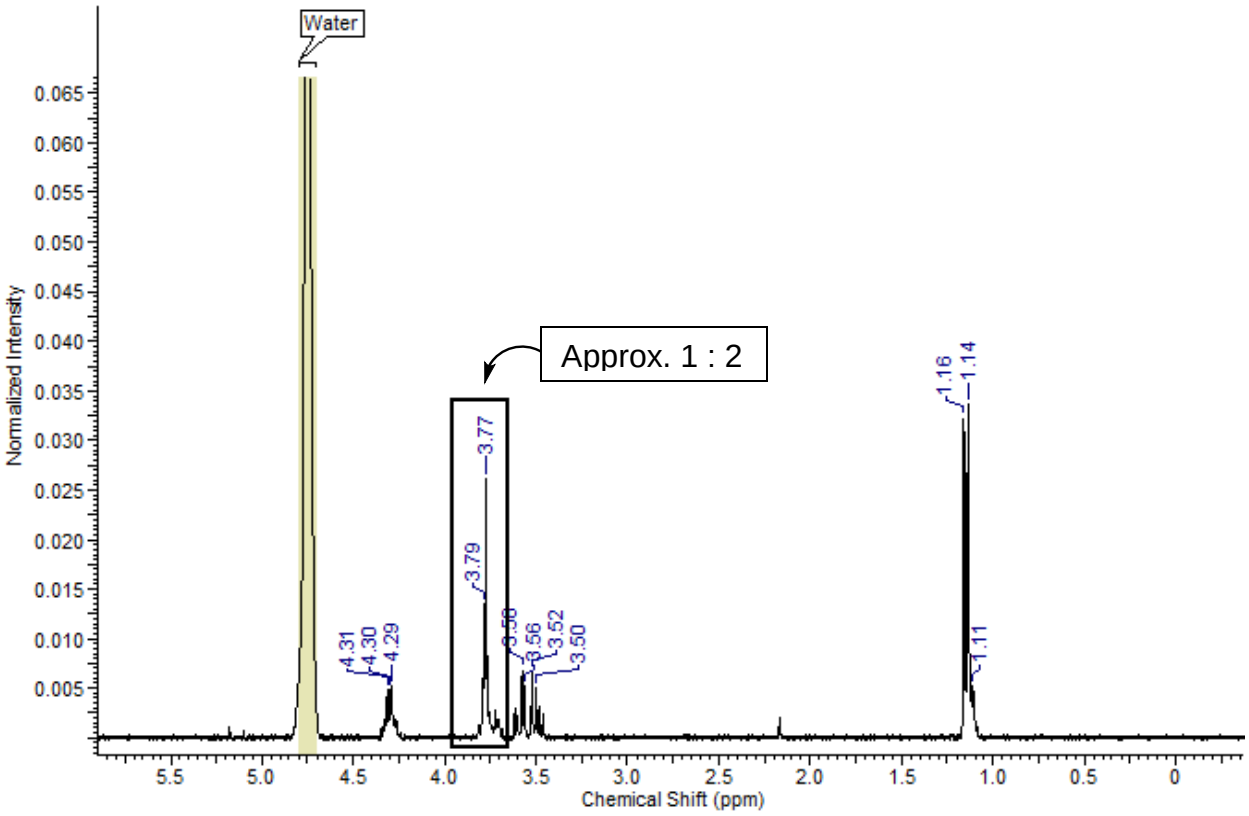

(*g*)

Figure A-8. Continued

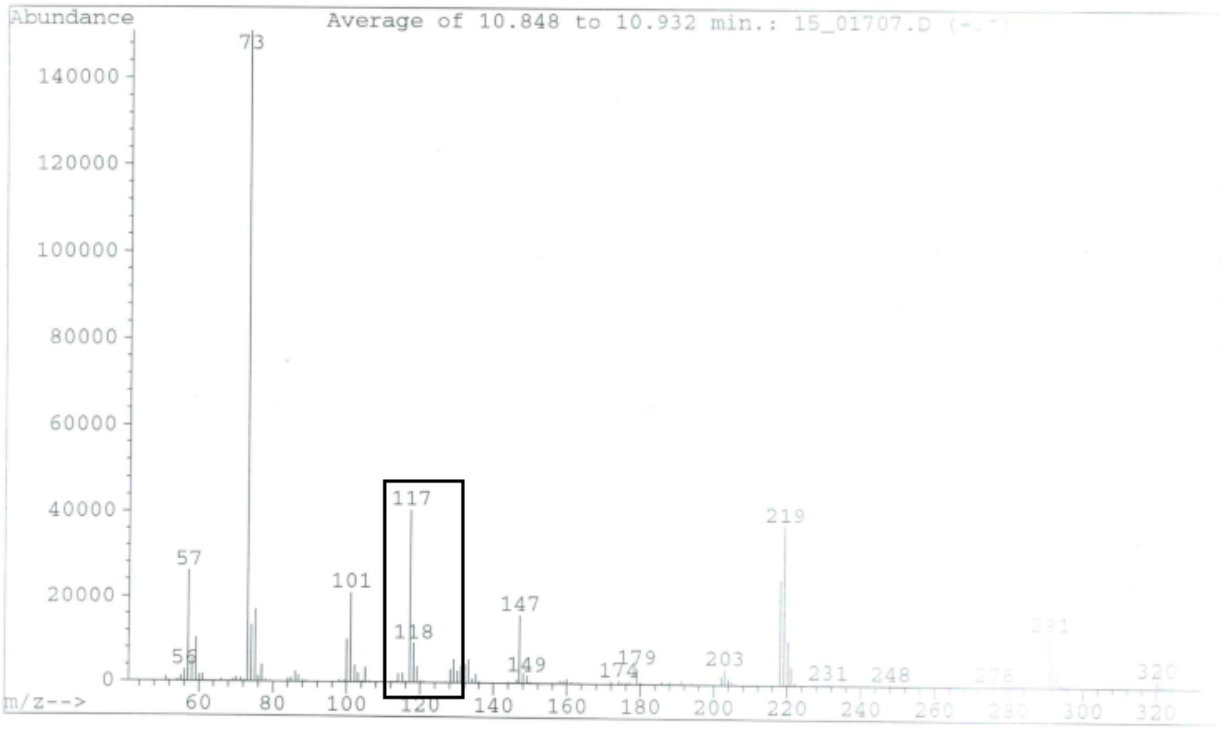

(*a*)

Figure A-9. MS for thermodynamic reversibility of L-*allo*-threonine aldolase. Negative control at (*a*) 1 hour and (*b*) 24 hours. L-allo-Thr and acetaldehyde-d4 in the presence of L-*allo*-TA at (*c*) 1 hour, (*d*) 3 hours, (*e*) 5 hours and (*f*) 24 hours.

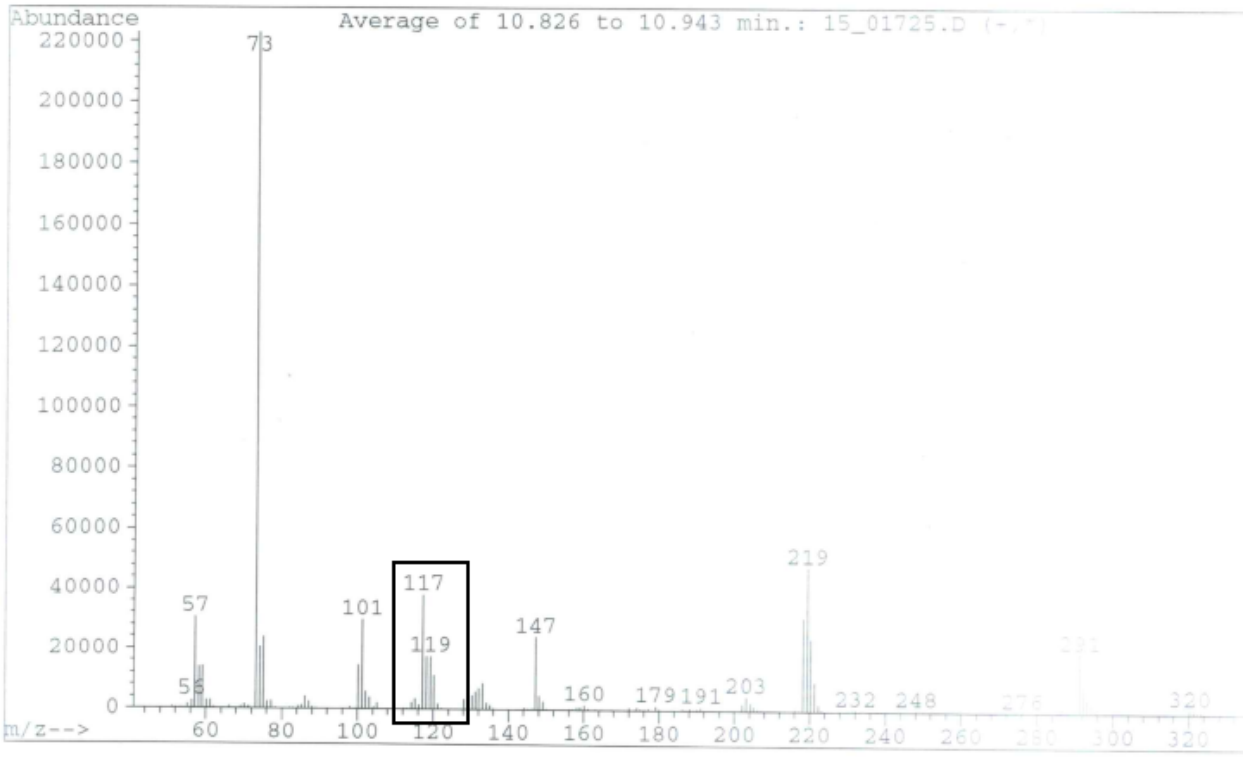

(*b*)

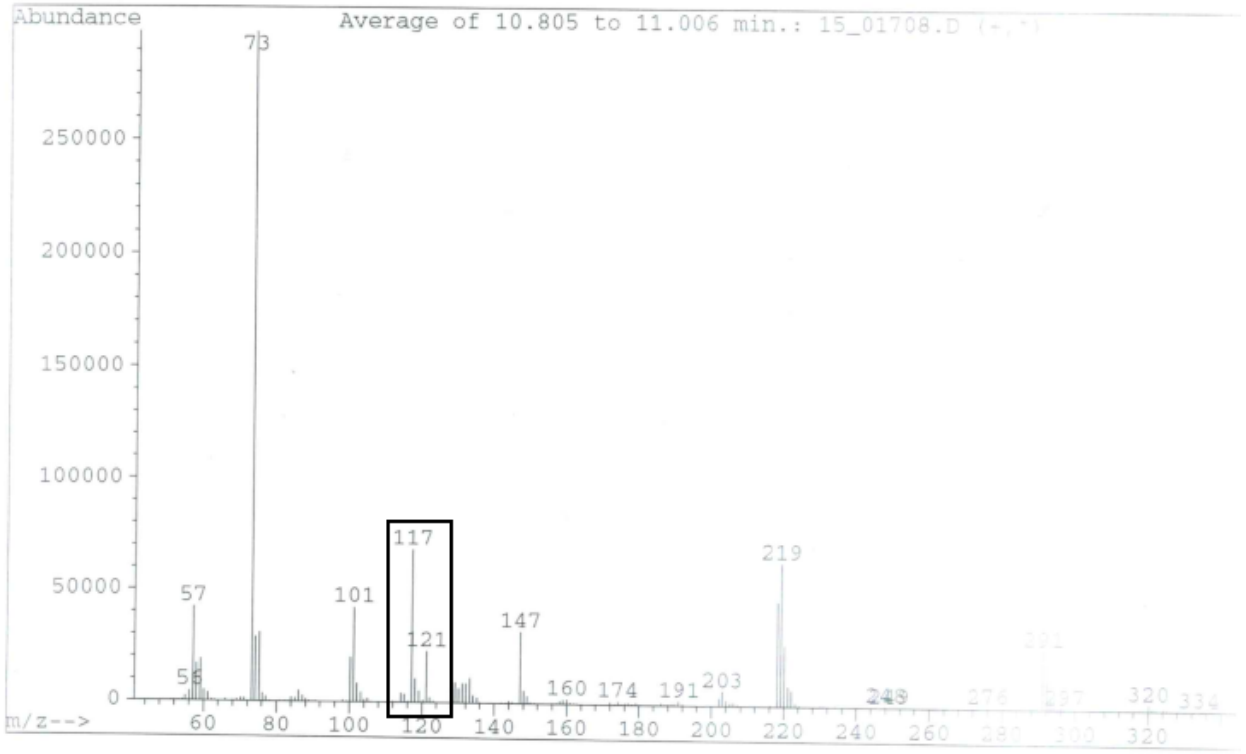

(*c*)

Figure A-9. Continued

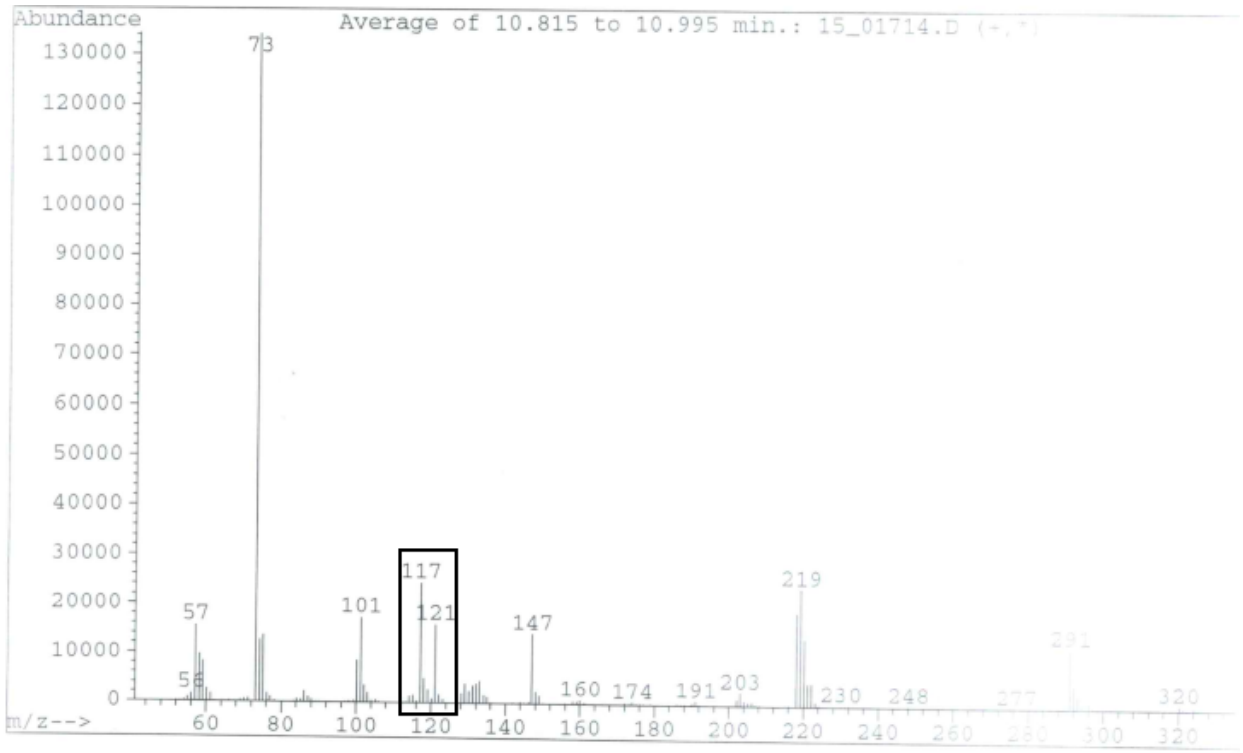

(*d*)

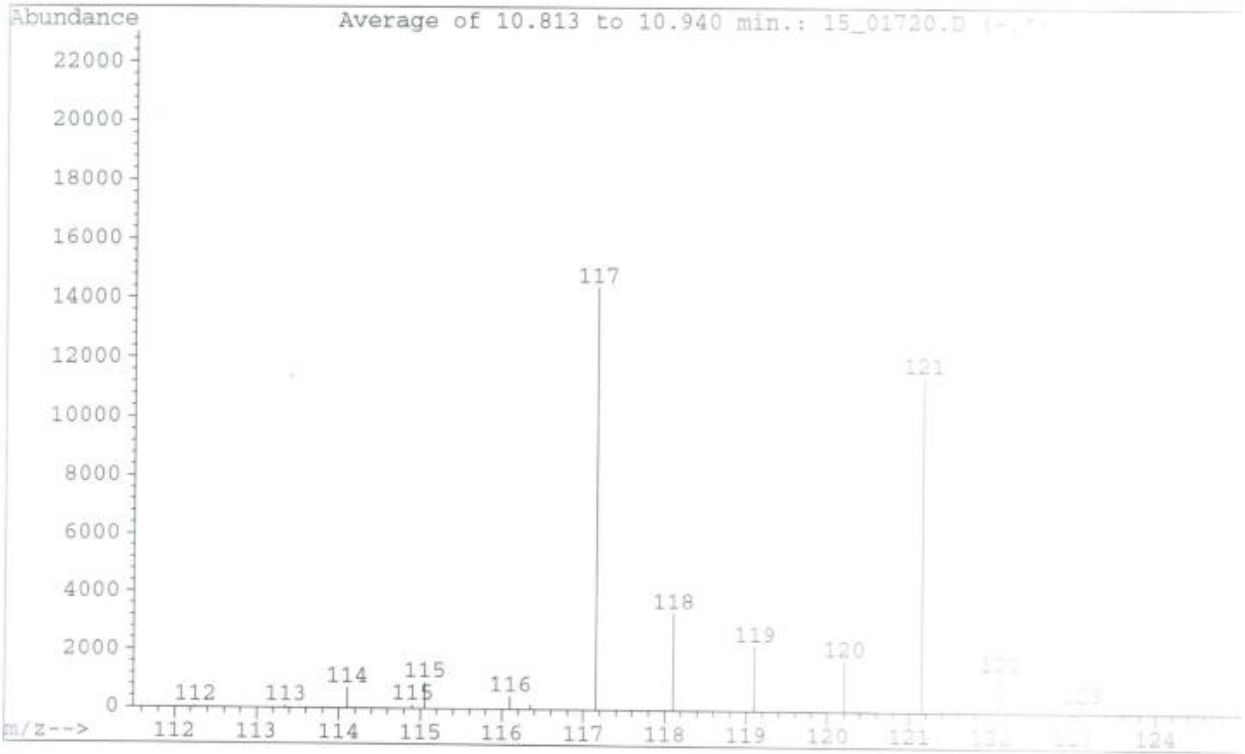

(*e*)

Figure A-9. Continued

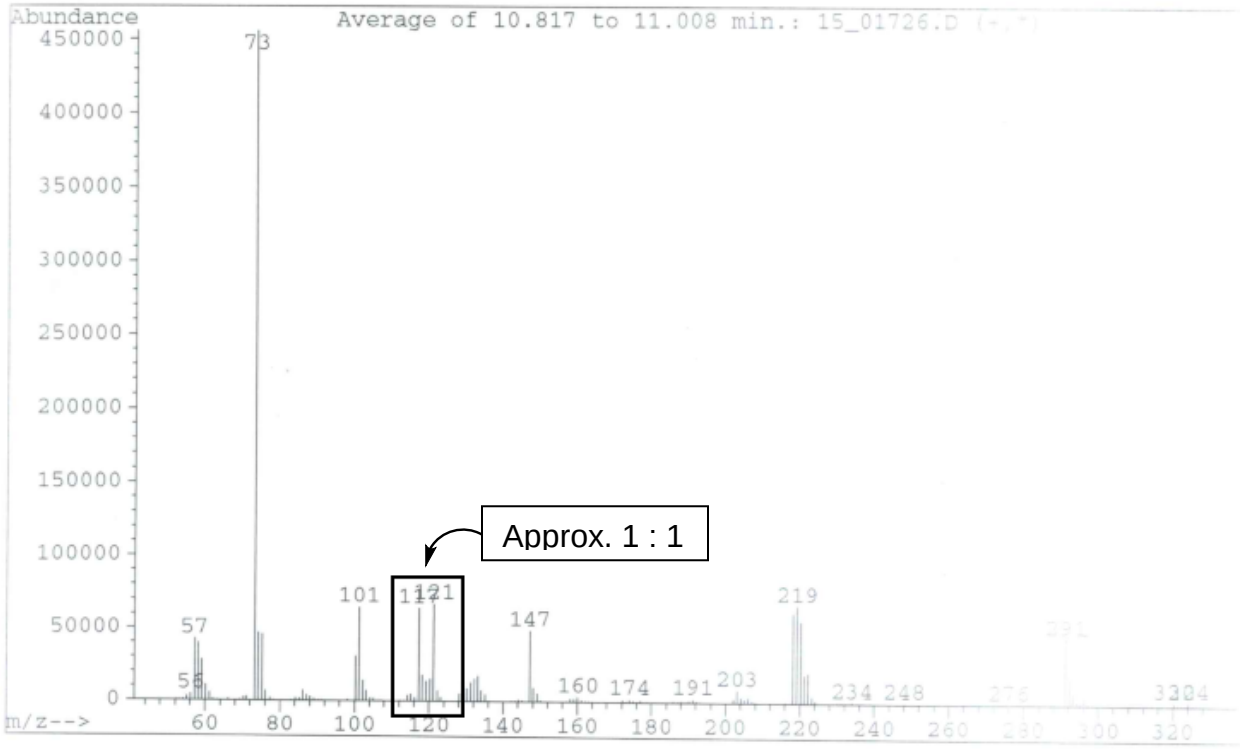

(*f*)

Figure A-9. Continued

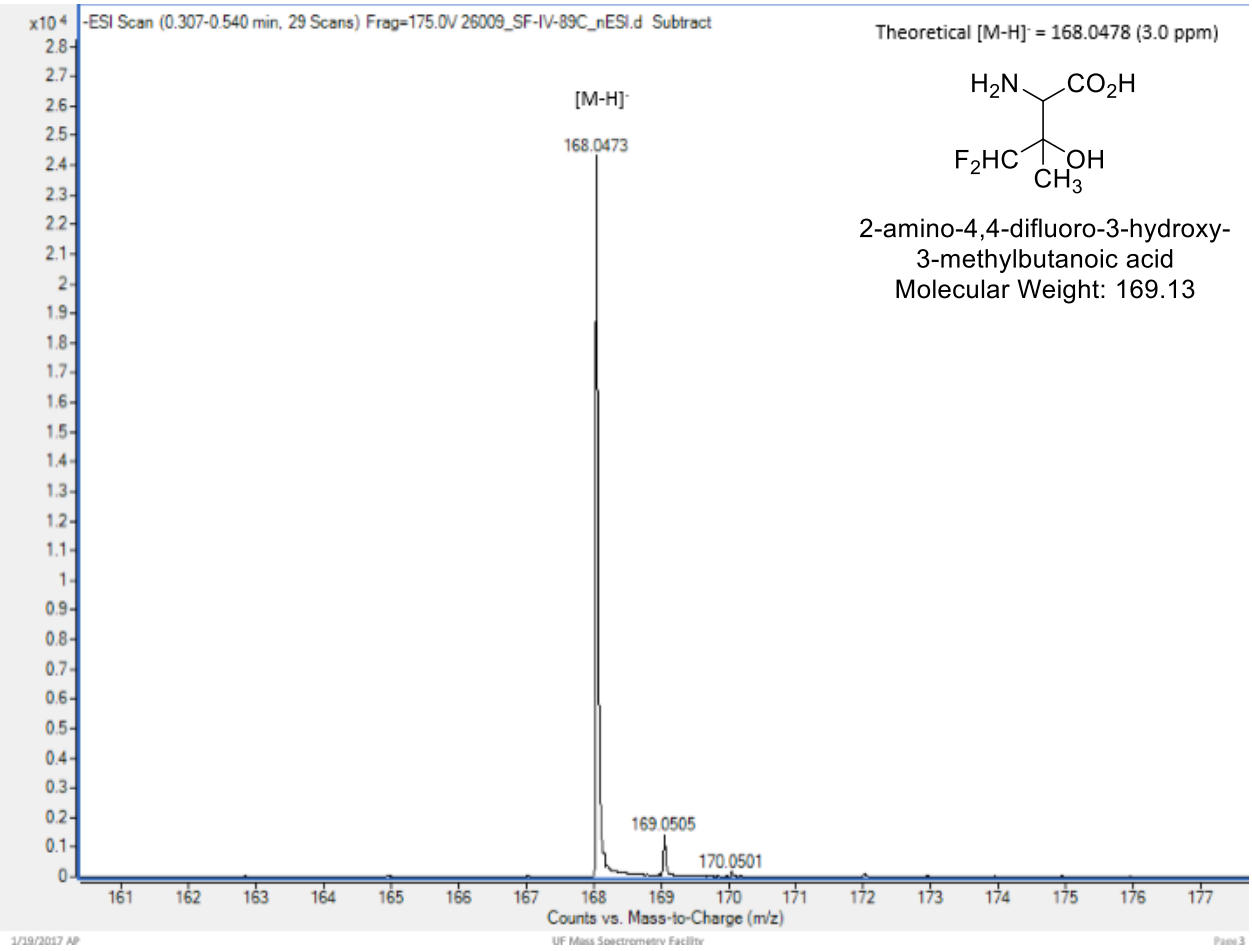

(*a*)

Figure A-10. Mass spectrum of 2-amino-4,4-difluoro-3-hydroxy-3-methylbutanoic acid

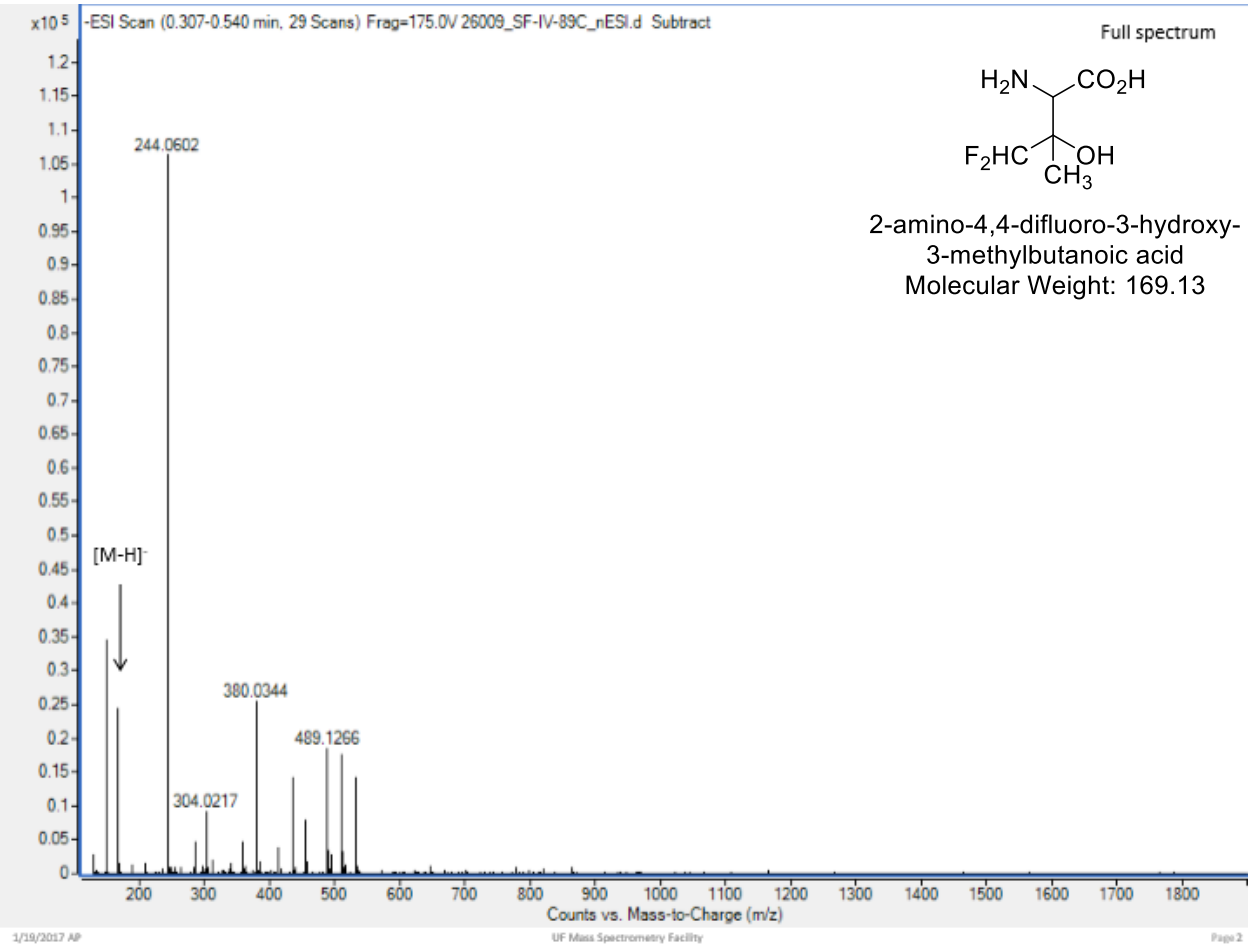

(*b*)

Figure A-10. Continued

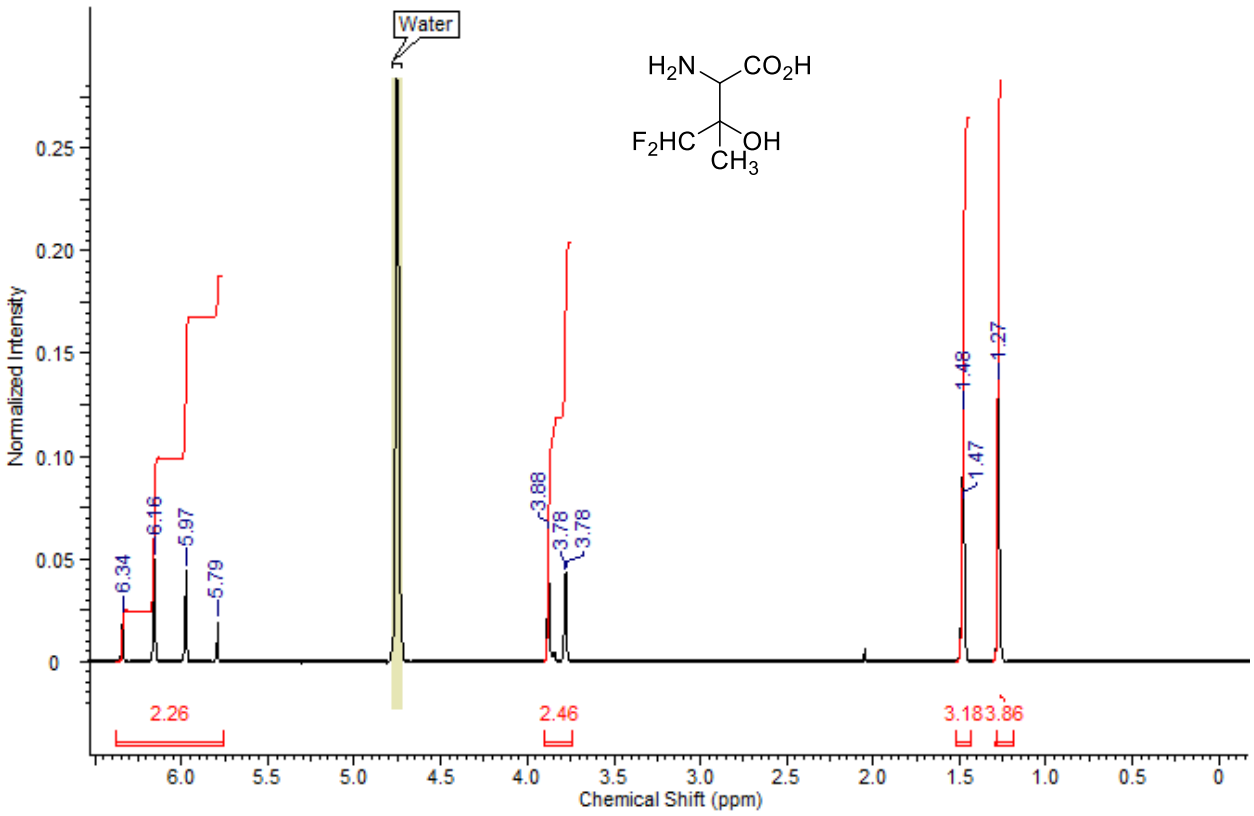

(*a*)

Figure A-11. Proton and fluorine NMR spectra of 2-amino-4,4-difluoro-3-hydroxy-3-methylbutanoic acid synthesized by *P. putida* L-TA

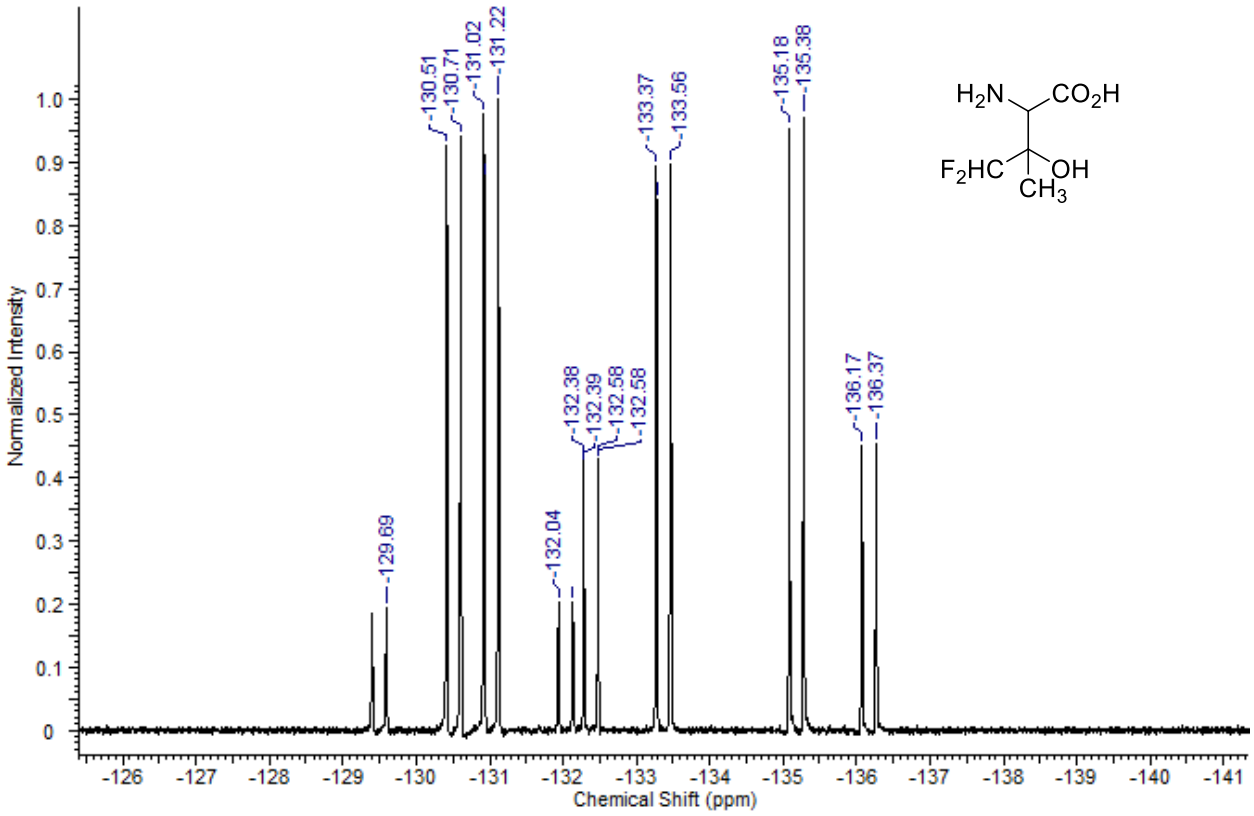

(*b*)

Figure A-11. Continued

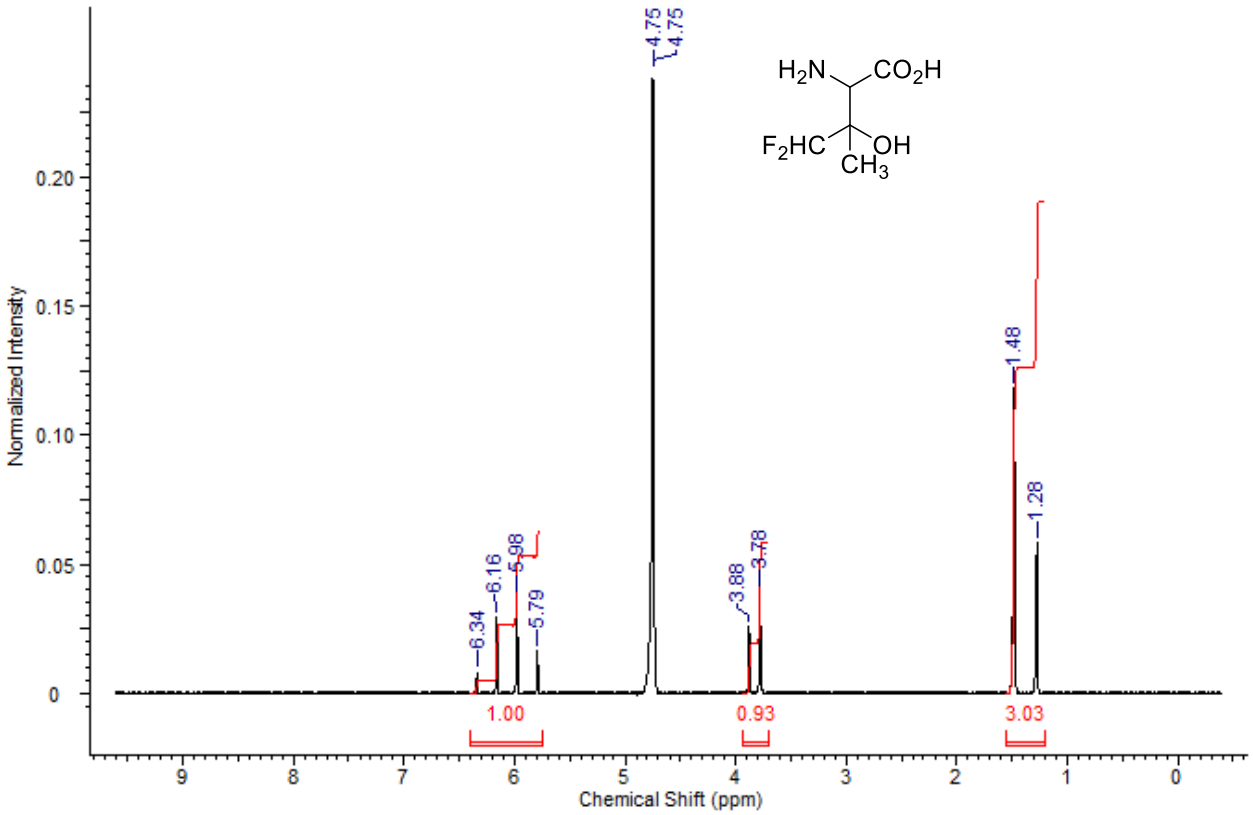

(*a*)

Figure A-12. Proton and fluorine NMR spectra of 2-amino-4,4-difluoro-3-hydroxy-3-methylbutanoic acid synthesized by *A. jandaei* L-*allo*-TA

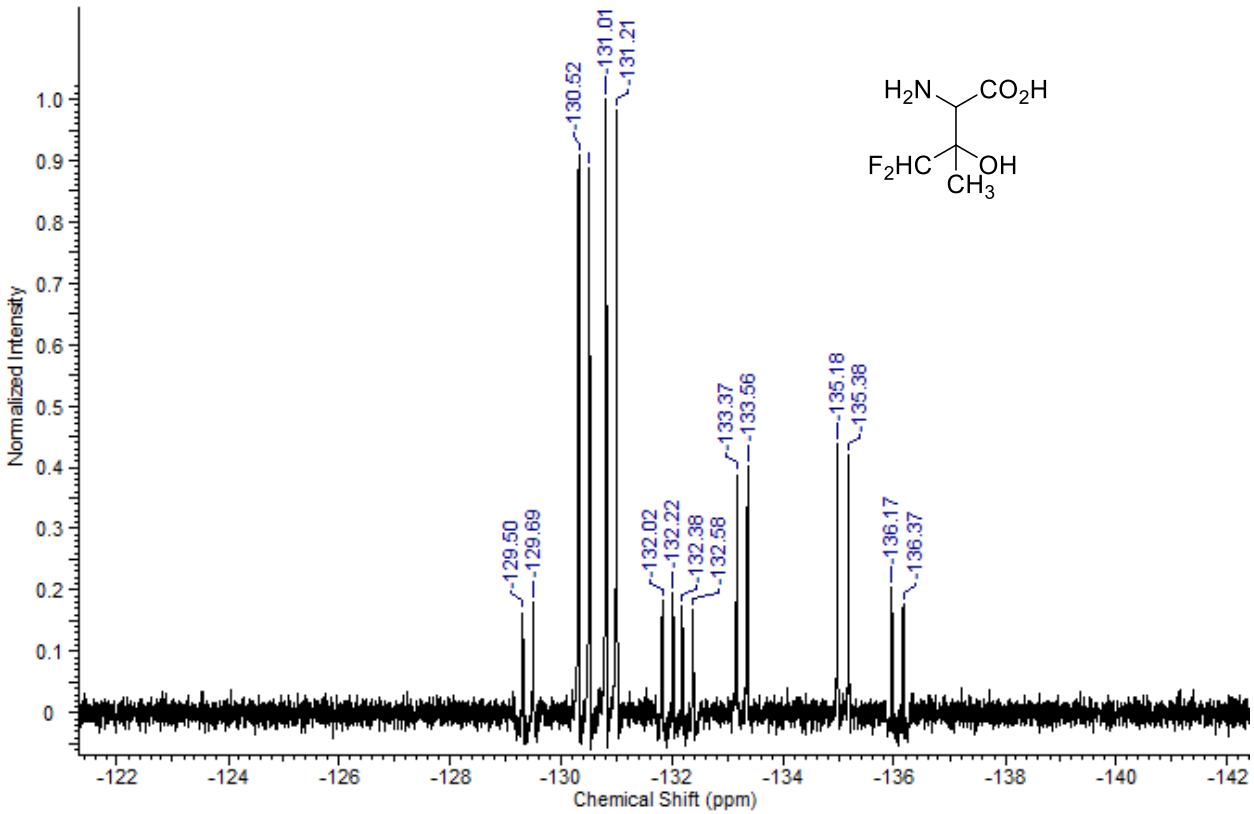

(*b*)

Figure A-12. Continued

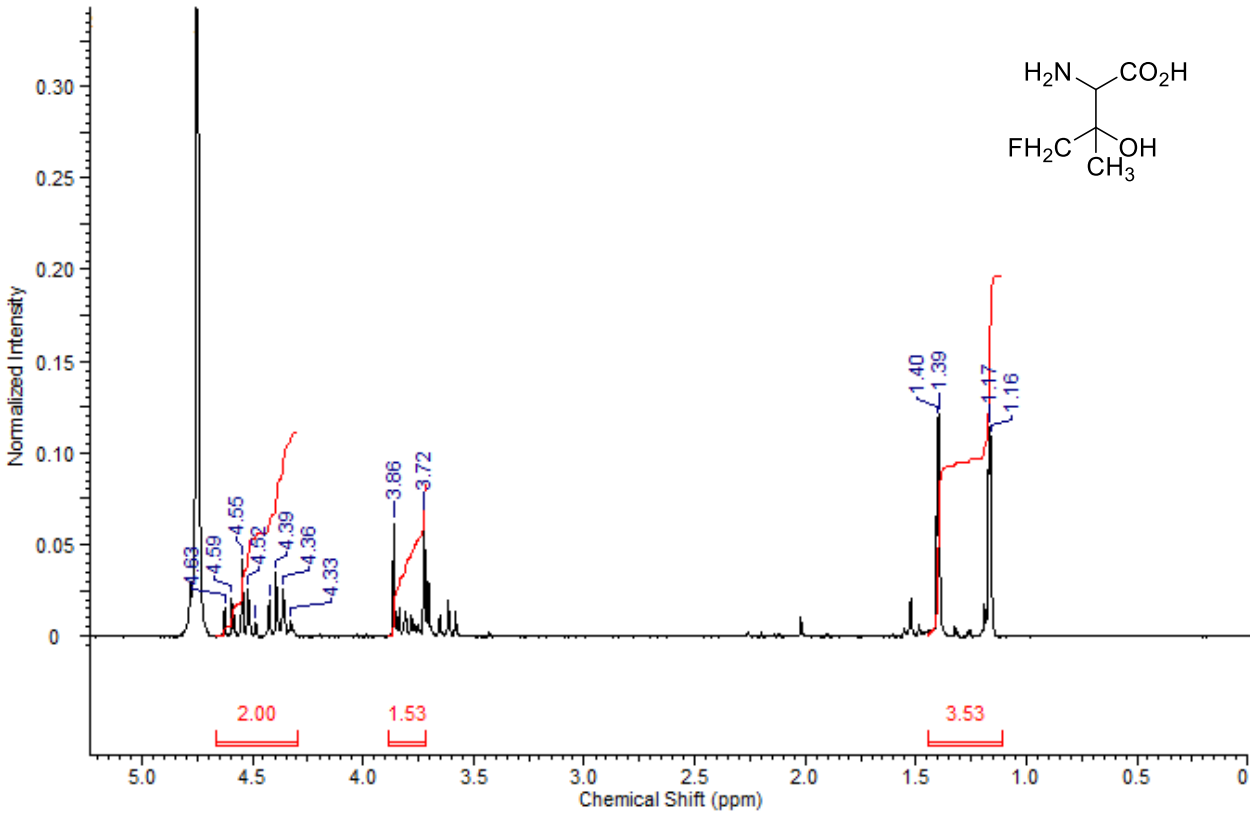

(*a*)

Figure A-13. Proton and fluorine NMR spectra of 2-amino-4-fluoro-3-hydroxy-3-methylbutanoic acid synthesized by *A. jandaei* L-*allo*-TA.

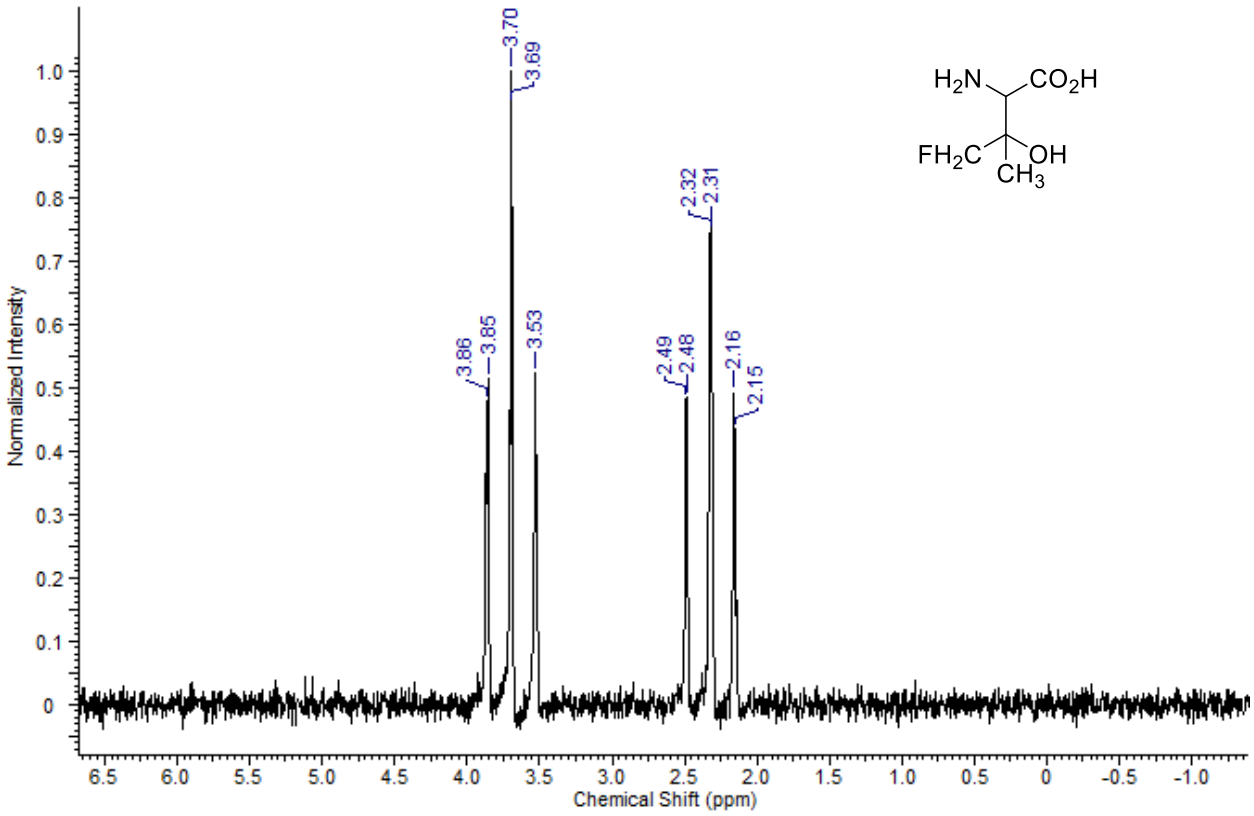

(*b*)

Figure A-13. Continued

LIST OF REFERENCES

1. Yim, G.; Thaker, M. N.; Koteva, K.; Wright, G., *Journal of Antibiotics* **2014,** *67* (1), 31-41.

2. Suzuki, S.; Isono, K.; Nagatsu, J.; Mizutani, T.; Kawashim.Y; Mizuno, T., *Journal of Antibiotics* **1965,** *18* (3), 131.

3. Miyake, Y.; Kozutsumi, Y.; Nakamura, S.; Fujita, T.; Kawasaki, T., *Biochemical and Biophysical Research Communications* **1995,** *211* (2), 396-403.

4. Kang, S. H.; Kang, S. Y.; Lee, H.-S.; Buglass, A. J., *Chemical Reviews* **2005,** *105* (12), 4537-4558.

5. Ohfune, Y.; Shinada, T., *European Journal of Organic Chemistry* **2005,** *2005* (24), 5127-5143.

6. Pirrung, M. C.; Nunn, D. S.; McPhail, A. T.; Mitchell, R. E., *Bioorganic and Medicinal Chemistry Letters* **1993,** *3* (10), 2095-2098.

7. Liu, J. Q.; Odani, M.; Yasuoka, T.; Dairi, T.; Itoh, N.; Kataoka, M.; Shimizu, S.; Yamada, H., *Applied Microbiology and Biotechnology* **2000,** *54* (1), 44-51.

8. Baik, S. H.; Yoshioka, H.; Yukawa, H.; Harayama, S., *Journal of Microbiology and Biotechnology* **2007,** *17* (5), 721-727.

9. Wenger, R. M., *Helvetica Chimica Acta* **1983,** *66* (7), 2308-2321.

10. Kaufmann, H.; Saadia, D.; Voustianiouk, A.; Goldstein, D. S.; Holmes, C.; Yahr, M. D.; Nardin, R.; Freeman, R., *Circulation* **2003,** *108* (6), 724-728.

11. Mitsubishi; Co., G. C. Glucosaminic Acid Production by Aeromonas. 1982.

12. Gu, W. X.; Xia, W. S., *Journal of Carbohydrate Chemistry* **2006,** *25* (4), 297-301.

13. Varela, O.; Nin, A. P.; Delederkremer, R. M., *Tetrahedron Letters* **1994,** *35* (50), 9359-9362.

14. Evans, D. A.; Weber, A. E., *Journal of the American Chemical Society* **1986,** *108* (21), 6757-6761.

15. Alonso, M.; Riera, A., *Tetrahedron-Asymmetry* **2005,** *16* (23), 3908-3912.

16. Nagamitsu, T.; Sunazuka, T.; Tanaka, H.; Omura, S.; Sprengeler, P. A.; Smith, A. B., *Journal of the American Chemical Society* **1996,** *118* (15), 3584-3590.

17. Kim, I. H.; Kirk, K. L., *Tetrahedron Letters* **2001,** *42* (48), 8401-8403.

18. Fanning, K. N.; Jamieson, A. G.; Sutherland, A., *Organic and Biomolecular Chemistry* **2005,** *3* (20), 3749-3756.

19. Willis, M. C.; Piccio, V. J. D., *Synlett* **2002,** *2002* (10), 1625-1628.

20. Willis, M. C.; Cutting, G. A.; Piccio, V. J. D.; Durbin, M. J.; John, M. P., *Angewandte Chemie-International Edition* **2005,** *44* (10), 1543-1545.

21. Thayumanavan, R.; Tanaka, F.; Barbas, C. F., *Organic Letters* **2004,** *6* (20), 3541-3544.

22. Belokon, Y. N.; Bulychev, A. G.; Vitt, S. V.; Struchkov, Y. T.; Batsanov, A. S.; Timofeeva, T. V.; Tsyryapkin, V. A.; Ryzhov, M. G.; Lysova, L. A., *Journal of the American Chemical Society* **1985,** *107* (14), 4252-4259.

23. Genet, J. P.; Pinel, C.; Mallart, S.; Juge, S.; Thorimbert, S.; Laffitte, J. A., *Tetrahedron-Asymmetry* **1991,** *2* (7), 555-567.

24. Mordant, C.; Dunkelmann, P.; Ratovelomanana-Vidal, V.; Genet, J. P., *European Journal of Organic Chemistry* **2004,** (14), 3017-3026.

25. Makino, K.; Goto, T.; Hiroki, Y.; Hamada, Y., *Angewandte Chemie-International Edition* **2004,** *43* (7), 882-884.

26. Makino, K.; Hiroki, Y.; Hamada, Y., *Journal of the American Chemical Society* **2005,** *127* (16), 5784-5785.

27. Makino, K.; Fujii, T.; Hamada, Y., *Tetrahedron-Asymmetry* **2006,** *17* (4), 481-485.

28. Noyori, R.; Ikeda, T.; Ohkuma, T.; Widhalm, M.; Kitamura, M.; Takaya, H.; Akutagawa, S.; Sayo, N.; Saito, T.; Taketomi, T.; Kumobayashi, H., *Journal of the American Chemical Society* **1989,** *111* (25), 9134-9135.

29. Genêt, J. P.; Pinel, C.; Mallart, S.; Juge, S.; Thorimbert, S.; Laffitte, J. A., *Tetrahedron-Asymmetry* **1991,** *2* (7), 555-567.

30. Ratovelomanana-Vidal, V.; Genêt, J.-P., *Canadian Journal of Chemistry* **2000,** *78*, 846 - 851.

31. Li, G. G.; Chang, H. T.; Sharpless, K. B., *Angewandte Chemie-International Edition in English* **1996,** *35* (4), 451-454.

32. Loncaric, C.; Wulff, W. D., *Organic Letters* **2001,** *3* (23), 3675-3678.

33. Wang, Y. H.; Chen, Z. Y.; Mi, A. Q.; Hu, W. H., *Chemical Communications* **2004,** (21), 2486-2487.

34. Mettath, S.; Srikanth, G. S. C.; Dangerfield, B. S.; Castle, S. L., *The Journal of Organic Chemistry* **2004,** *69* (19), 6489-6492.

35. Ooi, T.; Taniguchi, M.; Doda, K.; Maruoka, K., *Advanced Synthesis and Catalysis* **2004,** *346* (9-10), 1073-1076.

36. Li, L.; Klauber, E. G.; Seidel, D., *Journal of the American Chemical Society* **2008,** *130* (37), 12248.

37. Chen, X. H.; Zhu, Y.; Qiao, Z.; Xie, M. S.; Lin, L. L.; Liu, X. H.; Feng, X. M., *Chemistry-a European Journal* **2010,** *16* (33), 10124-10129.

38. Chelucci, G.; Murineddu, G.; Pinna, G. A., *Tetrahedron: Asymmetry* **2004,** *15* (9), 1373-1389.

39. Malkov, A. V.; Kočovský, P., *European Journal of Organic Chemistry* **2007,** *2007* (1), 29-36.

40. Yu, Z.; Liu, X.; Dong, Z.; Xie, M.; Feng, X., *Angewandte Chemie* **2008,** *120* (7), 1328-1331.

41. Shang, D.; Xin, J.; Liu, Y.; Zhou, X.; Liu, X.; Feng, X., *The Journal of Organic Chemistry* **2008,** *73* (2), 630-637.

42. Itoh, K.; Kanemasa, S., *Journal of the American Chemical Society* **2002,** *124* (45), 13394-13395.

43. Itoh, K.; Hasegawa, M.; Tanaka, J.; Kanemasa, S., *Organic Letters* **2005,** *7* (6), 979-981.

44. Evans, D. A.; Seidel, D., *Journal of the American Chemical Society* **2005,** *127* (28), 9958-9959.

45. Evans, D. A.; Thomson, R. J.; Franco, F., *Journal of the American Chemical Society* **2005,** *127* (31), 10816-10817.

46. Heine, H. W., *Angewandte Chemie International Edition in English* **1962,** *1* (10), 528-532.

47. Padwa, A.; Woolhouse, A. D., 5.04 - Aziridines, Azirines and Fused-ring Derivatives A2 - Katritzky, Alan R. In *Comprehensive Heterocyclic Chemistry*, Rees, C. W., Ed. Pergamon: Oxford, 1984; pp 47-93.

48. Tanner, D., *Angewandte Chemie International Edition in English* **1994,** *33* (6), 599-619.

49. Pellissier, H., *Tetrahedron* **2010,** *66* (8), 1509-1555.

50. Zhang, Y.; Lu, Z.; Wulff, W. D., *Synlett* **2009,** *2009* (17), 2715-2739.

51. Gabriel, S.; Stelzner, R., *Berichte der Deutschen Chemischen Gesellschaft* **1895,** *28*.

52. Huang, L.; Wulff, W. D., *Journal of the American Chemical Society* **2011,** *133* (23), 8892-8895.

53. Hashimoto, T.; Nakatsu, H.; Yamamoto, K.; Watanabe, S.; Maruoka, K., *Chemistry-an Asian Journal* **2011,** *6* (2), 607-613.

54. Danielsson, J.; Toom, L.; Somfai, P., *European Journal of Organic Chemistry* **2011,** *2011* (3), 607-613.

55. Cativiela, C.; Díaz-de-Villegas, M. D., *Tetrahedron: Asymmetry* **2007,** *18* (5), 569-623.

56. Nakatsuka, T.; Miwa, T.; Mukaiyama, T., *Chemistry Letters* **1981,** *10* (2), 279-282.

57. Mukaiyama, T.; Miwa, T.; Nakatsuka, T., *Chemistry Letters* **1982,** (2), 145-148.

58. Mukaiyama, T.; Hayashi, H.; Miwa, T.; Narasaka, K., *Chemistry Letters* **1982,** (10), 1637-1640.

59. Mukaiyama, T., *Pure and Applied Chemistry* **1982,** *54* (12), 2455-2464.

60. Evans, D. A.; Bartroli, J.; Shih, T. L., *Journal of the American Chemical Society* **1981,** *103* (8), 2127-2129.

61. Volkmann, R. A.; Davis, J. T.; Meltz, C. N., *Journal of the American Chemical Society* **1983,** *105* (18), 5946-5948.

62. Rich, D. H.; Sun, C. Q.; Guillaume, D.; Dunlap, B.; Evans, D. A.; Weber, A. E., *Journal of Medicinal Chemistry* **1989,** *32* (8), 1982-1987.

63. Tung, R. D.; Rich, D. H., *Tetrahedron Letters* **1987,** *28* (11), 1139-1142.

64. Schmidt, U.; Siegel, W., *Tetrahedron Letters* **1987,** *28* (25), 2849-2852.

65. Aebi, J. D.; Dhaon, M. K.; Rich, D. H., *Journal of Organic Chemistry* **1987,** *52* (13), 2881-2886.

66. El Achqar, A.; Boumzebra, M.; Roumestant, M.-L.; Viallefont, P., *Tetrahedron* **1988,** *44* (17), 5319-5332.

67. Evans, D. A.; Britton, T. C.; Ellman, J. A.; Dorow, R. L., *Journal of the American Chemical Society* **1990,** *112* (10), 4011-4030.

68. Caddick, S.; Parr, N. J.; Pritchard, M. C., *Tetrahedron* **2001,** *57* (30), 6615-6626.

69. Evans, D. A.; Chapman, K. T.; Bisaha, J., *Journal of the American Chemical Society* **1988,** *110* (4), 1238-1256.

70. Evans, D. A.; Weber, A. E., *Journal of the American Chemical Society* **1987,** *109* (23), 7151-7157.

71. Caddick, S.; Parr, N. J.; Pritchard, M. C., *Tetrahedron Letters* **2000,** *41* (31), 5963-5966.

72. Caddick, S.; Jenkins, K., *Chemical Society Reviews* **1996,** *25* (6), 447.

73. Caddick, S.; Jenkins, K.; Treweeke, N.; Candeias, S. X.; Afonso, C. A. M., *Tetrahedron Letters* **1998,** *39* (15), 2203-2206.

74. Iwanowicz, E. J.; Blomgren, P.; Cheng, P. T. W.; Smith, K.; Lau, W. F.; Pan, Y. Y.; Gu, H. H.; Malley, M. F.; Gougoutas, J. Z., *Synlett* **1998,** *1998* (06), 664-666.

75. Overman, L. E., *Journal of the American Chemical Society* **1974,** *96* (2), 597-599.

76. Overman, L. E., *Journal of the American Chemical Society* **1976,** *98* (10), 2901-2910.

77. Overman, L. E., *Accounts of Chemical Research* **1980,** *13* (7), 218-224.

78. Ikariya, T.; Ishikawa, Y.; Hirai, K.; Yoshikawa, S., *Chemistry Letters* **1982,** (11), 1815-1818.

79. Overman, L. E., *Angewandte Chemie-International Edition in English* **1984,** *23* (8), 579-586.

80. Overman, L. E.; Knoll, F. M., *Tetrahedron Letters* **1979,** (4), 321-324.

81. Fanning, K. N.; Jamieson, A. G.; Sutherland, A., *Organic and Biomolecular Chemistry* **2005,** *3* (20), 3749-3756.

82. Zhang, Y. F.; Farrants, H.; Li, X. C., *Chemistry-an Asian Journal* **2014,** *9* (7), 1752-1764.

83. Schenck, T. G.; Bosnich, B., *Journal of the American Chemical Society* **1985,** *107* (7), 2058-2066.

84. Calter, M.; Hollis, T. K.; Overman, L. E.; Ziller, J.; Zipp, G. G., *Journal of Organic Chemistry* **1997,** *62* (5), 1449-1456.

85. Hollis, T. K.; Overman, L. E., *Tetrahedron Letters* **1997,** *38* (51), 8837-8840.

86. Jamieson, A. G.; Sutherland, A., *Organic and Biomolecular Chemistry* **2006,** *4* (15), 2932-2937.

87. Jaunzeme, I.; Jirgensons, A., *Synlett* **2005,** (19), 2984-2986.

88. Jaunzeme, I.; Jirgensons, A., *Tetrahedron* **2008,** *64* (24), 5794-5799.

89. Anderson, C. E.; Overman, L. E., *Journal of the American Chemical Society* **2003,** *125* (41), 12412-12413.

90. Jamieson, A. G.; Sutherland, A., *Organic Letters* **2007,** *9* (8), 1609-1611.

91. Swift, M. D.; Sutherland, A., *Tetrahedron Letters* **2007,** *48* (22), 3771-3773.

92. Zaed, A. M.; Sutherland, A., *Organic and Biomolecular Chemistry* **2010,** *8* (19), 4394-4399.

93. Zaed, A. M.; Sutherland, A., *Organic and Biomolecular Chemistry* **2011,** *9* (23), 8030-8037.

94. Ahmad, S.; Swift, M. D.; Farrugia, L. J.; Senn, H. M.; Sutherland, A., *Organic and Biomolecular Chemistry* **2012,** *10* (19), 3937-3945.

95. Calder, E. D. D.; Zaed, A. M.; Sutherland, A., *Journal of Organic Chemistry* **2013,** *78* (14), 7223-7233.

96. Overman, L. E.; Owen, C. E.; Pavan, M. M.; Richards, C. J., *Organic Letters* **2003,** *5* (11), 1809-1812.

97. Watson, M. P.; Overman, L. E.; Bergman, R. G., *Journal of the American Chemical Society* **2007,** *129* (16), 5031-5044.

98. Swift, M. D.; Sutherland, A., *Tetrahedron* **2008,** *64* (40), 9521-9527.

99. Genêt, J. P.; Mallart, S.; Jugé, S. Improvement in the Manufacture of Chiral Catalysts Based on Ruthenium and Phosphocomplexes. 1989.

100. Kagan, H. B.; Fiaud, J. C., Kinetic Resolution. In *Topics in Stereochemistry*, Eliel, E. L., Ed. John Wiley and Sons, Inc.: 1988; Vol. 18, p 249.

101. Noyori, R.; Ohkuma, T.; Kitamura, M.; Takaya, H.; Sayo, N.; Kumobayashi, H.; Akutagawa, S., *Journal of the American Chemical Society* **1987,** *109* (19), 5856-5858.

102. Genêt, J. P.; Pinel, C.; Ratovelomananavidal, V.; Mallart, S.; Pfister, X.; Deandrade, M. C. C.; Laffitte, J. A., *Tetrahedron-Asymmetry* **1994,** *5* (4), 665-674.

103. Genêt, J. P.; Pinel, C.; Ratovelomananavidal, V.; Mallart, S.; Pfister, X.; Bischoff, L.; Deandrade, M. C. C.; Darses, S.; Galopin, C.; Laffitte, J. A., *Tetrahedron-Asymmetry* **1994,** *5* (4), 675-690.

104. Genêt, J. P.; Ratovelomananavidal, V.; Deandrade, M. C. C.; Pfister, X.; Guerreiro, P.; Lenoir, J. Y., *Tetrahedron Letters* **1995,** *36* (27), 4801-4804.

105. Pellissier, H., *Tetrahedron* **2003,** *59* (42), 8291-8327.

106. Pellissier, H., *Tetrahedron* **2008,** *64* (8), 1563-1601.

107. Noyori, R.; Tokunaga, M.; Kitamura, M., *Bulletin of the Chemical Society of Japan* **1995,** *68* (1), 36-55.

108. Ward, R. S., *Tetrahedron: Asymmetry* **1995,** *6* (7), 1475 - 1490.

109. Pellissier, H., *Advanced Synthesis and Catalysis* **2011,** *353* (5), 659-676.

110. Li, P.; Hu, X. Q.; Dong, X. Q.; Zhang, X. M., *Molecules* **2016,** *21* (10).

111. Girard, A.; Greck, C.; Ferroud, D.; Genêt, J. P., *Tetrahedron Letters* **1996,** *37* (44), 7967-7970.

112. Nishi, T.; Kitamura, M.; Ohkuma, T.; Noyori, R., *Tetrahedron Letters* **1988,** *29* (48), 6327-6330.

113. Schmidt, U.; Meyer, R.; Leitenberger, V.; Griesser, H.; Lieberknecht, A., *Synthesis-Stuttgart* **1992,** (10), 1025-1030.

114. Phansavath, P.; de Paule, S. D.; Ratovelomanana-Vidal, V.; Genet, J. P., *European Journal of Organic Chemistry* **2000,** (23), 3903-3907.

115. Mashima, K.; Matsumura, Y.; Kusano, K.; Kumobayashi, H.; Sayo, N.; Hori, Y.; Ishizaki, T.; Akutagawa, S.; Takaya, H., *Journal of the Chemical Society-Chemical Communications* **1991,** (9), 609-610.

116. Coulon, E.; Cristina, M.; de Andrade, C.; Ratovelomanana-Vidal, V.; Genêt, J. P., *Tetrahedron Letters* **1998,** *39* (36), 6467-6470.

117. Sun, G. D.; Zhou, Z. H.; Luo, Z. H.; Wang, H. L.; Chen, L.; Xu, Y. B.; Li, S.; Jian, W. L.; Zeng, J. B.; Hu, B. Q.; Han, X. D.; Lin, Y. C.; Wang, Z. Q., *Organic Letters* **2017,** *19* (16), 4339-4342.

118. Tone, H.; Buchotte, M.; Mordant, C.; Guittet, E.; Ayad, T.; Ratovelomanana-Vidal, V., *Organic Letters* **2009,** *11* (9), 1995-1997.

119. Mohar, B.; Valleix, A.; Desmurs, J. R.; Felemez, M.; Wagner, A.; Mioskowski, C., *Chemical Communications* **2001,** (24), 2572-2573.

120. Mordant, C.; Dunkelmann, P.; Ratovelomanana-Vidal, V.; Genet, J. P., *Chemical Communications* **2004,** (11), 1296-1297.

121. de Paule, S. D.; Jeulin, S.; Ratovelomanana-Vidal, V.; Genet, J. P.; Champion, N.; Dellis, P., *European Journal of Organic Chemistry* **2003,** (10), 1931-1941.

122. Labeeuw, O.; Phansavath, P.; Genet, J. P., *Tetrahedron-Asymmetry* **2004,** *15* (12), 1899-1908.

123. Makino, K.; Goto, T.; Hiroki, Y.; Hamada, Y., *Tetrahedron: Asymmetry* **2008,** *19* (24), 2816-2828.

124. Mordant, C.; Reymond, S.; Ratovelomanana-Vidal, V.; Genet, J. P., *Tetrahedron* **2004,** *60* (43), 9715-9723.

125. Spector, S.; Sjoerdsm, A.; Udenfrie, S., *Journal of Pharmacology and Experimental Therapeutics* **1965,** *147* (1), 86.

126. Creveling, C. R.; Daly, J.; Tokuyama, T.; Witkop, B., *Biochemical Pharmacology* **1968,** *17* (1), 65.

127. Bartholini, G.; Constantinidis, J.; Tissot, R.; Pletscher, A., *Biochemical Pharmacology* **1971,** *20* (6), 1243-1247.

128. Porter, C. C.; Torchiana, M. L.; Stone, C. A., *Life Sciences* **1972,** *11* (16, Part 1), 787-795.

129. Bartholini, J.; Constantinidis, J.; Puig, M.; Tissot, R.; Pletscher, A., *Journal of Pharmacology and Experimental Therapeutics* **1975,** *193* (2), 523-532.

130. Inagaki, C.; Fujiwara, H.; Tanaka, C., *The Japanese Journal of Pharmacology* **1976,** *26* (3), 380-382.

131. Chiyoko, I.; Chikako, T., *Biochemical Pharmacology* **1978,** *27* (7), 1081-1086.

132. Belcher, G.; Ryall, R. W.; Schaffner, R., *Brain Research* **1978,** *151* (2), 307-321.

133. Kawabata, A.; Kasamatsu, K.; Umeda, N.; Takagi, H., *British Journal of Pharmacology* **1994,** *111* (2), 503-508.

134. Narabayashi, H.; Nakanishi, T., *Clinical Evaluation* **1987,** *15*, 423-457.

135. Carvalho, M. J.; van den Meiracker, A. H.; Boomsma, F.; Man in 't Veld, A. J.; Freitas, J.; Costa, O.; Falcao de Freitas, A., *Journal of the Autonomic Nervous System* **1997,** *62* (1–2), 63-71.

136. Mathias, C. J.; Senard, J. M.; Braune, S.; Watson, L.; Aragishi, A.; Keeling, J. E. A.; Taylor, M. D., *Clinical Autonomic Research* **2001,** *11* (4), 235-242.

137. Kaufmann, H., *Clinical Autonomic Research* **2008,** *18*, 19-24.

138. Knosalla, M.; Weis, J.; Isenmann, S.; Haensch, C. A., *Klinische Neurophysiologie* **2011,** *42* (2), 103-109.

139. Perez-Lloret, S.; Rey, M. V.; Traon, A. P. L.; Rascol, O., *Expert Opinion on Emerging Drugs* **2013,** *18* (1), 39-53.

140. Biaggioni, I.; Freeman, R.; Mathias, C. J.; Low, P.; Hewitt, L. A.; Kaufmann, H.; Behalf Droxidopa, I., *Hypertension* **2015,** *65* (1), 101.

141. Isaacson, S.; Shill, H. A.; Vernino, S.; Ziemann, A.; Rowse, G. J., *Journal of Parkinsons Disease* **2016,** *6* (4), 751-759.

142. Kalinin, S.; Polak, P. E.; Lin, S. X.; Sakharkar, A. J.; Pandey, S. C.; Feinstein, D. L., *Neurobiology of Aging* **2012,** *33* (8), 1651-1663.

143. Phillips, C.; Fahimi, A.; Das, D.; Mojabi, F. S.; Ponnusamy, R.; Salehi, A., *Current Alzheimer Research* **2015,** *13* (1), 68-83.

144. Heneka, M. T.; Nadrigny, F.; Regen, T.; Martinez-Hernandez, A.; Dumitrescu-Ozimek, L.; Terwel, D.; Jardanhazi-Kurutz, D.; Walter, J.; Kirchhoff, F.; Hanisch, U. K.; Kummer, M. P., *Proc Natl Acad Sci U S A* **2010,** *107* (13), 6058-63.

145. Coll, M.; Rodriguez, S.; Raurell, I.; Ezkurdia, N.; Brull, A.; Augustin, S.; Guardia, J.; Esteban, R.; Martell, M.; Genesca, J., *Hepatology* **2012,** *56* (5), 1849-1860.

146. Rodriguez, S.; Raurell, I.; Ezkurdia, N.; Augustin, S.; Esteban, R.; Genesca, J.; Martell, M., *Liver International* **2015,** *35* (2), 326-334.

147. Wecht, J. M.; Rosado-Rivera, D.; Weir, J. P.; Ivan, A.; Yen, C.; Bauman, W. A., *Archives of Physical Medicine and Rehabilitation* **2013,** *94* (10), 2006-2012.

148. Mathias, C. J., *Clinical Autonomic Research* **2008,** *18*, 25-29.

149. George, S.; Narina, S. V.; Sudalai, A., *Tetrahedron Letters* **2007,** *48* (8), 1375-1378.

150. Herbert, B.; Kim, I. H.; Kirk, K. L., *The Journal of Organic Chemistry* **2001,** *66* (14), 4892-4897.

151. Hegedüs, B.; Krassó, A. F.; Noack, K.; Zeller, P., *Helvetica Chimica Acta* **1975,** *58* (1), 147-162.

152. Guan, Y. Q.; Gao, M.; Deng, X.; Lv, H.; Zhang, X. M., *Chemical Communications* **2017,** *53* (58), 8136-8139.

153. Lee, C.-J.; Liang, X.; Wu, Q.; Najeeb, J.; Zhao, J.; Gopalaswamy, R.; Titecat, M.; Sebbane, F.; Lemaitre, N.; Toone, E. J.; Zhou, P., **2016,** *7*, 10638.

154. Titecat, M.; Liang, X. F.; Lee, C. J.; Charlet, A.; Hocquet, D.; Lambert, T.; Pages, J. M.; Courcol, R.; Sebbane, F.; Toone, E. J.; Zhou, P.; Lemaitre, N., *Journal of Antimicrobial Chemotherapy* **2016,** *71* (10), 2874-2882.

155. Raetz, C. R.; Whitfield, C., *Annu Rev Biochem* **2002,** *71*, 635-700.

156. Pei Zhou and Adam, W. B., *Current Pharmaceutical Biotechnology* **2008,** *9* (1), 9-15.

157. Liang, X.; Gopalaswamy, R.; Navas, F.; Toone, E. J.; Zhou, P., *The Journal of Organic Chemistry* **2016,** *81* (10), 4393-4398.

158. Owens, L. D.; Wright, D. A., *Plant Physiology* **1965,** *40* (5), 927.

159. Owens, L. D.; Lieberman, M.; Kunishi, A., *Plant Physiology* **1970,** *46*, 32.

160. Giovanelli, J.; Owens, L. D.; Mudd, S. H., *Biochimica Et Biophysica Acta* **1971,** *227* (3), 671.

161. Owens, L. D.; Guggenheim, S.; Hilton, J. L., *Biochimica Et Biophysica Acta* **1968,** *158* (2), 219.

162. Keith, D. D.; Debernardo, S.; Weigele, M., *Tetrahedron* **1975,** *31* (20), 2629-2632.

163. Keith, D. D.; Tortora, J. A.; Ineichen, K.; Leimgruber, W., *Tetrahedron* **1975,** *31* (20), 2633-2636.

164. Owens, L. D., *Weed Science* **1973,** *21* (1), 63-66.

165. Wang, C. Y.; Mellenthin, W. M., *Plant Physiology* **1977,** *59* (4), 546-549.

166. Baker, J. E.; Anderson, J. D.; Lieberman, M.; Apelbaum, A., *Plant Physiology* **1979,** *63* (5), 91-91.

167. Mitchell, R. E.; Frey, E. J.; Benn, M. H., *Phytochemistry* **1986,** *25* (12), 2711-2715.

168. Mitchell, R. E.; Frey, E. J., *Physiological and Molecular Plant Pathology* **1988,** *32* (2), 335-341.

169. Mitchell, R. E., *Phytochemistry* **1989,** *28* (6), 1617-1620.

170. Mitchell, R. E.; Coddington, J. M., *Phytochemistry* **1991,** *30* (6), 1809-1814.

171. Duodu, S.; Bhuvaneswari, T. V.; Stokkermans, T. J. W.; Peters, N. K., *Molecular Plant-Microbe Interactions* **1999,** *12* (12), 1082-1089.

172. Mills, J.; Masur, H., *Scientific American* **1990,** *263* (2), 50-57.

173. Mukhopadhyay, R.; Roy, K.; Coutinho, L.; Rupp, R. H.; Ganguli, B. N.; Fehlhaber, H. W., *The Journal of Antibiotics* **1987,** *40* (7), 1050 - 1052.

174. Vanmiddlesworth, F.; Dufresne, C.; Wincott, F. E.; Mosley, R. T.; Wilson, K. E., *Tetrahedron Letters* **1992,** *33* (3), 297-300.

175. Vanmiddlesworth, F.; Giacobbe, R. A.; Lopez, M.; Garrity, G.; Bland, J. A.; Bartizal, K.; Fromtling, R. A.; Polishook, J.; Zweerink, M.; Edison, A. M.; Rozdilsky, W.; Wilson, K. E.; Monaghan, R. L., *Journal of Antibiotics* **1992,** *45* (6), 861-867.

176. Horn, W. S.; Smith, J. L.; Bills, G. F.; Raghoobar, S. L.; Helms, G. L.; Kurtz, M. B.; Marrinan, J. A.; Frommer, B. R.; Thornton, R. A.; Mandala, S. M., *J Antibiot (Tokyo)* **1992,** *45* (10), 1692-6.

177. Zweerink, M. M.; Edison, A. M.; Wells, G. B.; Pinto, W.; Lester, R. L., *Journal of Biological Chemistry* **1992,** *267* (35), 25032-25038.

178. Mori, K.; Otaka, K., *Tetrahedron Letters* **1994,** *35* (49), 9207-9210.

179. Otaka, K.; Mori, K., *European Journal of Organic Chemistry* **1999,** (8), 1795-1802.

180. Kobayashi, S.; Furuta, T.; Hayashi, T.; Nishijima, M.; Hanada, K., *Journal of the American Chemical Society* **1998,** *120* (5), 908-919.

181. Kobayashi, S.; Furuta, T., *Tetrahedron* **1998,** *54* (35), 10275-10294.

182. Trost, B. M.; Lee, C. B., *Journal of the American Chemical Society* **2001,** *123* (49), 12191-12201.

183. Trost, B. M., *Chemical and Pharmaceutical Bulletin* **2002,** *50* (1), 1-14.

184. Franz, S. E.; Stewart, J. D., Chapter Three - Threonine Aldolases. In *Advances in Applied Microbiology*, Sima Sariaslani and Geoffrey Michael, G., Ed. Academic Press: 2014; Vol. Volume 88, pp 57-101.

185. Wong, C. H.; Whitesides, G. M., *Journal of Organic Chemistry* **1983,** *48* (19), 3199-3205.

186. Brovetto, M.; Gamenara, D.; Mendez, P. S.; Seoane, G. A., *Chemical Reviews* **2011,** *111* (7), 4346-4403.

187. Clapes, P.; Fessner, W. D.; Sprenger, G. A.; Samland, A. K., *Current Opinion in Chemical Biology* **2010,** *14* (2), 154-167.

188. Fesko, K.; Uhl, M.; Steinreiber, J.; Gruber, K.; Griengl, H., *Angewandte Chemie-International Edition* **2010,** *49* (1), 121-124.

189. Liu, J. Q.; Dairi, T.; Kataoka, M.; Shimizu, S.; Yamada, H., *Journal of Bacteriology* **1997,** *179* (11), 3555-3560.

190. Vassilev, V. P.; Uchiyama, T.; Kajimoto, T.; Wong, C. H., *Tetrahedron Letters* **1995,** *36* (23), 4081-4084.

191. Steinreiber, J.; Fesko, K.; Mayer, C.; Reisinger, C.; Schurmann, M.; Griengl, H., *Tetrahedron* **2007,** *63* (34), 8088-8093.

192. Steinreiber, J.; Fesko, K.; Reisinger, C.; Schürmann, M.; van Assema, F.; Wolberg, M.; Mink, D.; Griengl, H., *Tetrahedron* **2007,** *63* (4), 918-926.

193. Gwon, H. J.; Baik, S. H., *Biotechnology Letters* **2010,** *32* (1), 143-149.

194. Gutierrez, M. L.; Garrabou, X.; Agosta, E.; Servi, S.; Parella, T.; Joglar, J.; Clapes, P., *Chemistry-a European Journal* **2008,** *14* (15), 4647-4656.

195. Gwon, H. J.; Yoshioka, H.; Song, N. E.; Kim, J. H.; Song, Y. R.; Jeong, D. Y.; Baik, S. H., *Preparative Biochemistry and Biotechnology* **2012,** *42* (2), 143-154.

196. Kimura, T.; Vassilev, V. P.; Shen, G. J.; Wong, C. H., *Journal of the American Chemical Society* **1997,** *119* (49), 11734-11742.

197. Sagui, F.; Conti, P.; Roda, G.; Contestabile, R.; Riva, S., *Tetrahedron* **2008,** *64* (22), 5079-5084.

198. Fesko, K.; Strohmeier, G. A.; Breinbauer, R., *Applied Microbiology and Biotechnology* **2015,** *99* (22), 9651-9661.

199. Liu, J. Q.; Dairi, T.; Itoh, N.; Kataoka, M.; Shimizu, S.; Yamada, H., *Journal of Molecular Catalysis B-Enzymatic* **2000,** *10* (1-3), 107-115.

200. Goldberg, S. L.; Goswami, A.; Guo, Z. W.; Chan, Y.; Lo, E. T.; Lee, A.; Truc, V. C.; Natalie, K. J.; Hang, C.; Rossano, L. T.; Schmidt, M. A., *Organic Process Research and Development* **2015,** *19* (9), 1308-1316.

201. Liu, J. Q.; Odani, M.; Dairi, T.; Itoh, N.; Shimizu, S.; Yamada, H., *Applied Microbiology and Biotechnology* **1999,** *51* (5), 586-591.

202. Fesko, K.; Giger, L.; Hilvert, D., *Bioorganic and Medicinal Chemistry Letters* **2008,** *18* (22), 5987-5990.

203. Toscano, M. D.; Muller, M. M.; Hilvert, D., *Angewandte Chemie-International Edition* **2007,** *46* (24), 4468-4470.

204. Fesko, K.; Reisinger, C.; Steinreiber, J.; Weber, H.; Schurmann, M.; Griengl, H., *Journal of Molecular Catalysis B-Enzymatic* **2008,** *52-53*, 19-26.

205. Kielkopf, C. L.; Burley, S. K., *Biochemistry* **2002,** *41* (39), 11711-11720.

206. di Salvo, M. L.; Remesh, S. G.; Vivoli, M.; Ghatge, M. S.; Paiardini, A.; D'Aguanno, S.; Safo, M. K.; Contestabile, R., *Febs Journal* **2014,** *281* (1), 129-145.

207. Qin, H. M.; Imai, F. L.; Miyakawa, T.; Kataoka, M.; Kitamura, N.; Urano, N.; Mori, K.; Kawabata, H.; Okai, M.; Ohtsuka, J.; Hou, F.; Nagata, K.; Shimizu, S.; Tanokura, M., *Acta Crystallographica Section D-Biological Crystallography* **2014,** *70*, 1695-1703.

208. Uhl, M. K.; Oberdorfer, G.; Steinkellner, G.; Riegler-Berket, L.; Mink, D.; van Assema, F.; Schurmann, M.; Gruber, K., *Plos One* **2015,** *10* (4).

209. Rayment, I., *Macromolecular Crystallography, Pt A* **1997,** *276*, 171-179.

210. Paiardini, A.; Contestabile, R.; D'Aguanno, S.; Pascarella, S.; Bossa, F., *Biochimica et Biophysica Acta (BBA) - Proteins and Proteomics* **2003,** *1647* (1–2), 214-219.

211. Liu, J. Q.; Dairi, T.; Itoh, N.; Kataoka, M.; Shimizu, S.; Yamada, H., *Journal of Biological Chemistry* **1998,** *273* (27), 16678-16685.

212. Mugford, P. F.; Wagner, U. G.; Jiang, Y.; Faber, K.; Kazlauskas, R. J., *Angewandte Chemie-International Edition* **2008,** *47* (46), 8782-8793.

213. Hirato, Y.; Goto, M.; Tokuhisa, M.; Tanigawa, M.; Nishimura, K., *Acta Crystallographica Section F-Structural Biology Communications* **2017,** *73*, 86-89.

214. Bougioukou, D. J.; Kille, S.; Taglieber, A.; Reetz, M. T., *Advanced Synthesis and Catalysis* **2009,** *351* (18), 3287-3305.

215. Lee, S. J.; Kang, H. Y.; Lee, Y., *Journal of Molecular Catalysis B-Enzymatic* **2003,** *26* (3-6), 265-272.

216. Giger, L.; Toscano, M. D.; Bouzon, M.; Marliere, P.; Hilvert, D., *Tetrahedron* **2012,** *68* (37), 7549-7557.

217. Wieteska, L.; Ionov, M.; Szemraj, J.; Feller, C.; Kolinski, A.; Gront, D., *Journal of Biotechnology* **2015,** *199*, 69-76.

218. Seebeck, F. P.; Hilvert, D., *Journal of the American Chemical Society* **2003,** *125* (34), 10158-10159.

219. Seebeck, F. P.; Guainazzi, A.; Amoreira, C.; Baldridge, K. K.; Hilvert, D., *Angewandte Chemie-International Edition* **2006,** *45* (41), 6824-6826.

220. Tufvesson, P.; Lima-Ramos, J.; Jensen, J. S.; Al-Haque, N.; Neto, W.; Woodley, J. M., *Biotechnology and Bioengineering* **2011,** *108* (7), 1479-1493.

221. Tominaga, M.; Nagashima, M.; Taniguchi, I., *Electrochem. Commun.* **2007,** *9*, 911-914.

222. Dückers, N.; Baer, K.; Simon, S.; Groger, H.; Hummel, W., *Applied Microbiology and Biotechnology* **2010,** *88* (2), 409-424.

223. Fesko, K., *Applied Microbiology and Biotechnology* **2016,** *100* (6), 2579-2590.

224. Goldberg, S. L.; Goswami, A.; Guo, Z. W.; Chan, Y.; Lo, E. T.; Lee, A.; Truc, V. C.; Natalie, K. J.; Hang, C.; Rossano, L. T.; Schmidt, M. A., *Organic Process Research and Development* **2015,** *19* (9), 1308-1316.

225. Yao, P.; Lin, Y. J.; Wu, G. B.; Lu, Y. L.; Zhan, T.; Kumar, A.; Zhang, L. L.; Liu, Z. D., *International Journal of Biological Macromolecules* **2015,** *79*, 965-970.

226. Zhang, K.; Guo, Y. M.; Yao, P.; Lin, Y. J.; Kumar, A.; Liu, Z. D.; Wu, G. B.; Zhang, L. L., *Enzyme and Microbial Technology* **2016,** *85*, 12-18.

227. Nishiya, Y.; Imanaka, T., *Febs Letters* **1998,** *438* (3), 263-266.

228. Job, V.; Marcone, G. L.; Pilone, M. S.; Pollegioni, L., *Journal of Biological Chemistry* **2002,** *277* (9), 6985-6993.

229. Packeiser, H.; Lim, C.; Balagurunathan, B.; Wu, J.; Zhao, H., *Applied Biochemistry and Biotechnology* **2013,** *169* (2), 695-700.

230. Khuhawar, M. Y.; Majidano, S. A., *Chromatographia* **2011,** *73* (7-8), 701-708.

231. Zuman, P., *Chemical Reviews* **2004,** *104* (7), 3217-3238.

232. Vasanits, A.; Kutlan, D.; Sass, P.; Molnar-Perl, I., *Journal of Chromatography A* **2000,** *870* (1-2), 271-287.

233. Nimura, N.; Kinoshita, T., *Journal of Chromatography* **1986,** *352*, 169-177.

234. Donike, M., *Journal of Chromatography* **1969,** *42*, 103.

235. Yoon, H. R., *Archives of Pharmacal Research* **2013,** *36* (3), 366-373.

236. Schummer, C.; Delhomme, O.; Appenzeller, B. M. R.; Wennig, R.; Millet, M., *Talanta* **2009,** *77* (4), 1473-1482.

237. Steinreiber, J.; Schuermann, M.; van Assema, F.; Wolberg, M.; Fesko, K.; Reisinger, C.; Mink, D.; Griengl, H., *Advanced Synthesis and Catalysis* **2007,** *349* (8-9), 1379-1386.

238. Gwon, H. J.; Yoshioka, H.; Song, N. E.; Kim, J. H.; Song, Y. R.; Jeong, D. Y.; Baik, S. H., *Preparative Biochemistry and Biotechnology* **2012,** *42* (2), 143-154.

239. Matsumori, N.; Kaneno, D.; Murata, M.; Nakamura, H.; Tachibana, K., *Journal of Organic Chemistry* **1999,** *64* (3), 866-876.

240. Krishnamurthy, V. V., *Journal of Magnetic Resonance Series A* **1996,** *121* (1), 33-41.

241. Seco, J. M.; Quiñoá, E.; Riguera, R., *Chemical Reviews* **2012,** *112*, 4603–4641.

242. Ghiviriga, I., *Journal of Organic Chemistry* **2012,** *77* (8), 3978–3985.

243. Schirch, D.; Dellefratte, S.; Iurescia, S.; Angelaccio, S.; Contestabile, R.; Bossa, F.; Schirch, V., *Journal of Biological Chemistry* **1993,** *268* (31), 23132-23138.

244. Sambrook, J.; Fritsch, E. F.; Maniatis, T., *Molecular Cloning. A Laboratory Manual.* Second ed.; Cold Spring Harbor Laboratory Press: Cold Spring Harbor, New York, 1989.

245. Blaskovch, M. A.; Evindar, G.; Rose, N. G. W.; Wilkinson, S.; Luo, Y.; Lajoie, G. A., *J. Org. Chem.* **1998,** *63*, 3631-3646.

246. Looker, J. H.; Thatcher, D. N., *J. Org. Chem.* **1957,** *22*, 1233-1237.

247. Steinreiber, J.; Schuermann, M.; van Assema, F.; Wolberg, M.; Fesko, K.; Reisinger, C.; Mink, D.; Griengl, H., *Advanced Synthesis and Catalysis* **2007,** *349* (8-9), 1379-1386.

248. Winn, M. D.; Ballard, C. C.; Cowtan, K. D.; Dodson, E. J.; Emsley, P.; Evans, P. R.; Keegan, R. M.; Krissinel, E. B.; Leslie, A. G. W.; McCoy, A.; McNicholas, S. J.; Murshudov, G. N.; Pannu, N. S.; Potterton, E. A.; Powell, H. R.; Read, R. J.; Vagin, A.; Wilson, K. S., *Acta Crystallographica Section D-Biological Crystallography* **2011,** *67*, 235-242.

249. Adams, P. D.; Afonine, P. V.; Bunkoczi, G.; Chen, V. B.; Davis, I. W.; Echols, N.; Headd, J. J.; Hung, L. W.; Kapral, G. J.; Grosse-Kunstleve, R. W.; McCoy, A. J.; Moriarty, N. W.; Oeffner, R.; Read, R. J.; Richardson, D. C.; Richardson, J. S.; Terwilliger, T. C.; Zwart, P. H., *Acta Crystallographica Section D-Biological Crystallography* **2010,** *66*, 213-221.

250. Emsley, P.; Lohkamp, B.; Scott, W. G.; Cowtan, K., *Acta Crystallographica Section D-Biological Crystallography* **2010,** *66*, 486-501.

251. Afonine, P. V.; Grosse-Kunstleve, R. W.; Echols, N.; Headd, J. J.; Moriarty, N. W.; Mustyakimov, M.; Terwilliger, T. C.; Urzhumtsev, A.; Zwart, P. H.; Adams, P. D., *Acta Crystallographica Section D-Biological Crystallography* **2012,** *68*, 352-367.

252. Robert, X.; Gouet, P., *Nucleic Acids Research* **2014,** *42* (1), 320-324.

253. Reetz, M. T., *Journal of Organic Chemistry* **2009,** *74* (16), 5767-5778.

254. Reetz, M. T.; Krebs, G. P. L., *Comptes Rendus Chimie* **2011,** *14* (9), 811-818.

255. Patterson-Orazem, A.; Sullivan, B.; Stewart, J. D., *Bioorganic and Medicinal Chemistry* **2014,** *22* (20), 5628-5632.

256. Liu, Z. Q.; Zhang, X. H.; Xue, Y. P.; Xu, M.; Zheng, Y. G., *Journal of Agricultural and Food Chemistry* **2014,** *62* (20), 4685-4694.

257. Lutz, S., *Current Opinion in Biotechnology* **2010,** *21* (6), 734-743.

258. Sullivan, B.; Walton, A. Z.; Stewart, J. D., *Enzyme and Microbial Technology* **2013,** *53* (1), 70-77.

259. Chica, R. A.; Doucet, N.; Pelletier, J. N., *Current Opinion in Biotechnology* **2005,** *16* (4), 378-384.

260. Morley, K. L.; Kazlauskas, R. J., *Trends in Biotechnology* **2005,** *23* (5), 231-237.

261. Ozaki, S. I.; Demontellano, P. R. O., *Journal of the American Chemical Society* **1994,** *116* (10), 4487-4488.

262. Reetz, M. T.; Wilensek, S.; Zha, D. X.; Jaeger, K. E., *Angewandte Chemie-International Edition* **2001,** *40* (19), 3589.

263. Breuer, M.; Ditrich, K.; Habicher, T.; Hauer, B.; Keßeler, M.; Stürmer, R.; Zelinski, T., *Angewandte Chemie International Edition* **2004,** *43* (7), 788-824.

264. Panke, S.; Wubbolts, M., *Current Opinion in Chemical Biology* **2005,** *9* (2), 188-194.

265. Sun, H.; Zhang, H.; Ang, E. L.; Zhao, H., *Bioorganic and Medicinal Chemistry* **2017**.

266. Patel, R. N., *Bioorganic and Medicinal Chemistry* **2017**.

267. Guthrie, J. P., *Canadian Journal of Chemistry* **1975,** *53* (6), 898-906.

BIOGRAPHICAL SKETCH

Sarah Franz Beaudoin was born in Dunedin, Florida in 1989. Shortly thereafter her family moved to Savannah, Georgia where she attended Savannah Christian Prepatory School. After completing her coursework in 2008, she entered Armstrong Atlantic State University in Savannah, Georgia. She began undergraduate level research in the lab of Dr. Brent Feske in the summer of 2010. She published a first author paper in *Synthesis* for her work on chiral γ-lactones. While attending Armstrong Atlantic State University, Sarah received several prestigious rewards including the Robert Kolodney Scholarship and the Department of Chemistry and Physics' biochemistry award. She received her Bachelor of Science in chemistry from Armstrong Atlantic State University in December 2012.

Sarah followed her passion for biocatalysis and attended the University of Florida in the summer 2013. She began her graduate studies in the lab of Dr. Jon Stewart where she launched her project on threonine aldolases. In 2014, she published a book chapter with Dr. Jon Stewart titled, "Chapter 3: Threonine Aldolases" in *Advances in Applied Microbiology*. While attending the University of Florida, she received the University's Graduate School Fellowship for her first four years. Sarah received her Doctor of Philosophy in chemistry from the University of Florida in December 2017.